Fahrtbericht

Cruise Report

BMBF-Forschungsvorhaben 03G0139A

SONNE-Fahrt SO-139

Geowissenschaftliche Untersuchungen an der aktiven Konvergenzzone zwischen der ost-eurasischen und der indisch-australischen Platte im Bereich Indonesiens
Geologie, Geochemie, Geothermik und Biologie

SONNE Cruise SO-139

Geoscientific investigations at the active convergence zone between the Eastern Eurasian and Indo-Australian Plates off Indonesia
Geology, Geochemistry, Geothermics, and Biology

GINCO 3

Jakarta (30.01.99) – Jakarta (27.02.99)

BGR Bundesanstalt für Geowissenschaften und Rohstoffe

BUNDESANSTALT FÜR GEOWISSENSCHAFTEN UND ROHSTOFFE (BGR), HANNOVER

Fahrtbericht

BMBF-Forschungsvorhaben 03G0139A + 03G0139B
SONNE-Fahrt SO-139

Geowissenschaftliche Untersuchungen an der aktiven Konvergenzzone zwischen der ost-eurasischen und indisch-australischen Platte im Bereich Indonesiens

Geologie, Geochemie, Geothermik und Biologie

Cruise Report

SONNE Cruise SO-139

Geoscientific investigations at the active convergence zone between the eastern Eurasian and Indo-Australian Plates off Indonesia

Geology, Geochemistry, Geothermics, and Biology

GINCO 3

Jakarta (30.01.99) – Jakarta (27.02.99)

Sachbearbeiter: H. Beiersdorf (Projektleiter) mit Beiträgen von
H. Andruleit, B. Bannert, Safri Burhanuddin, G. Delisle, E. Faber, B. Harazim, Syarif Hidayat, U. Jürgens, H.S. Koesnadi, Ibrahim Lakoni, V. Marchig, N. v. Mirbach, Haryadi Permada, J. Poggenburg, H. Sahling, Salahuddin, S.T., W. Stahl, D. Steinmann, Eko Triarso, Udrekh, W. Weiss, M. Wiedicke-Hombach, M. Zeibig

Auftraggeber: Bundesministerium für Bildung und Forschung (BMBF)
(FV 03G0139A)

Datum: Juni 1999

Archiv-Nr.: 118.878

CONTENTS

ZUSAMMENFASSUNG
SUMMARY

List of Figures:

List of Tables:

Zusammenfassung

Die Forschungsfahrt SO-139 GINCO 3 des deutschen Forschungsschiffes SONNE wurde von der BGR (Hannover, Deutschland) innerhalb der "Vereinbarung zur Zusammenarbeit auf dem Gebiet der Wissenschaft und Technologie zwischen der Republik Indonesien und der Bundesrepublik Deutschland" organisiert und geleitet. Kooperationspartner auf indonesischer Seite war BPP Teknologi (Jakarta, Indonesien) und auf deutscher Seite das GEOMAR Forschungszentrum für marine Geowissenschaften (Kiel, Deutschland). Die Arbeit basierte im wesentlichen auf den unmittelbar zuvor durchgeführten geophysikalischen Forschungsfahrten SO-137 und SO-138 und konzentrierte sich auf geologische und biologische Probenahme, auf Meeresbodenbeobachtung, Wärmestrommessungen und Sammlung hydroakustischer Daten in verschiedenen geologischen Situationen des Kontinentalrandes südwestlich von Süd-Sumatra und südlich von West-Java. Das Ziel dieser Arbeit war die Kalibrierung reflexionsseismischer Bilder, das Studium des thermischen Regimes im "Forearc"-Bereich in Beziehung zu tektonischen und fluidalen Prozessen sowie die Suche nach Fluidaustritten im Zusammenhang mit Methan-Bildung und tektonischen Kräften.

Ein Wärmestrom von 64 mW/m^2 wurde in pelagischen Sedimenten an einer ozeanischen Referenzlokation vor Sumatra bestimmt. In Übereinstimmung mit anderen Altersmodellen zeigt er an, daß kretazische ozeanische Kruste an der Subduktionszone des Sunda-Bogen vor Süd-Sumatra angelangt ist. Der Wärmestrom über den Akkretionskomplexen vor Süd-Sumatra und West-Java variiert zwischen 35 und 64 mW/m^2. Der Akkretionskeil vor Sumatra scheint etwas kühler zu sein. Dies gilt auch für die "Forearc"-Becken: Das Bengkulu-Becken (22 - 49 mW/m^2) ist kühler als das Süd-Java-Becken (30 - 153 mW/m^2). Der unterschiedliche Wärmestrom scheint mit dem Unterschied zwischen der höheren Subduktionsrate am Java-"Forearc"-Komplex im Vergleich zu dem vor Süd-Sumatra zusammenzuhängen.

Ausstoß von methanbeladenen Flüssigkeiten scheint in beiden "Forearc"-Becken weitverbreitet zu sein, wie mehrere Methan-Anomalien in der Wassersäule sowie hohe Methankonzentrationen in den meeresbodennahen Sedimenten andeuten. Ein aktives Fluidaustrittsfeld mit einer typischen Quell-Fauna (*Acharax sp.* und Röhrenwürmer) sowie Karbonatablagerungen wurde am Scheitel einer Antiklinalstruktur im Süd-Java-Becken entdeckt. Es ist das erste Feld seiner Art, welches je in einem rein sedimentären "Forearc"-Becken gefunden wurde.

Anzeichen für Methan-Austritte wurden außerdem noch in der meerwärtigen Verlängerung des Semangka-Grabens (Sumatra) am Südausgang der Sunda-Straße gefunden mit hohen Wärmestromwerten (83 - 104 mW/m^2) und einem Exemplar des "Quellen-Röhrenwurms" *Vestimentifera sp.*. Hier wurden außerdem zum ersten Mal kontinentale Gesteine gedredscht (paläogen-miozäner kalkhaltiger Siltstein, Grünstein, Andesit, Quarzit), die zeigen, daß der akustische Sockel am Südausgang der Sunda-Straße durch kontinentale Gesteine gebildet wird. Schwache Methananomalien wurden auch an der Deformationsfront und in einem der Kontinentalhang-Becken gefunden.

Pliozäne bis rezente Sedimente wurden an verschiedenen Stellen gewonnen. Sie bilden nicht nur die obersten Abschnitte der Füllungen der "Forearc"- und Kontinentalhang-Becken, sondern bilden auch die relativ dünne Sedimentdecke, die die Schuppen des Akkretions-Komplexes abdeckt. Es sind hemipelagische olivgraue Schlämme mit eingeschalteten Turbidit- und vulkanischen Aschen-Lagen. Die Turbidite weisen auf dynamische Ablagerungsverhältnisse hin, während die vulkanischen Aschen mit Sicherheit vom Vulkanismus des Sunda-Bogens herrühren. Beprobung von Ausbissen der Schuppen des Akkretions-Komplexes ergab, daß diese zum Teil aus geklüfteten und an einigen Stellen tektonisierten grauen Tonsteinen bestehen. Die Sedimente der jüngsten Schuppen-Einheit sind graue steife siltige und glimmerhaltige Schlämme und Tonsteine, vermutlich Material, welches vom Bengal-Fächer stammt und vermischt wurde mit lokalem

hemipelagischen Material, welches auf dem Hang des Sunda-Bogens und im Sunda-Graben abgelagert wurde.

Summary

Cruise SO-139 GINCO 3 of the German Research Vessel SONNE was organized and conducted by BGR (Hannover, Germany) under the scope of the "Agreement on Cooperation in Science and Technology between The Republic of Indonesia and The Federal Republic of Germany". Co-operating partners were BPP Teknologi (Jakarta, Indonesia) and GEOMAR Research Center for Marine Geosciences (Kiel, Germany). The work followed immediately after the preceding geophysical research cruises SO-137 and SO-138 and concentrated on geological and biological sampling, on seafloor observation, heat flow measurements, and collecting hydro-acoustic data in different geological settings of the continental margin southwest of southern Sumatra and south of West Java. Aim of this work was calibrating reflection seismic features, studying the forearc geothermal regime in relation to tectonic and fluidal processes, and searching for fluid expulsions in conjunction with methane generation and tectonic forcing.

A heat flow of 64 mW/m^2 was determined in pelagic sediments at an oceanic reference site off Sumatra. In concurrence with other age models it is indicative of Cretaceous oceanic crust arriving at the Sunda Arc subduction zone of southern Sumatra. Heat flow across the accretionary complexes off southern Sumatra and western Java varies between 35 and 64 mW/m^2. The accretionary wedge off Sumatra seems to be slightly cooler. This difference applies also to the forearc basins: The Bengkulu Basin (22 - 49 mW/m^2) is cooler than the South Java Basin (30 - 153 mW/m^2). The different heat flow regimes seem to be related to the difference between a higher subduction rate at the Java forearc complex in comparison to that off southern Sumatra.

Expulsion of methane-laden fluids seems to be very common in both forearc basins as indicated by several methane plumes discovered in the water column as well as by high methane concentrations in sediments near the seafloor. One active vent field with a typical vent fauna (*Acharax sp.* and tubeworms) and carbonate precipitates was discovered at the crest of an anticline structure in the South Java Basin. It is the first of its kind found in an exclusively sedimentary forearc basin.

Signs of methane venting were also detected at the offshore extension of the Semangka Graben (Sumatra) at the southern approaches of the Sunda Strait with high heat flow values (83 - 104 mW/m^2) and a specimen of the "vent tubeworm" *Vestimentifera sp.*. Here also continental rocks (Paleogene to Miocene calcareous siltstone, greenstone, andesite, quarzite) were dredged for the first time, proving that the acoustic basement of the southern approaches of the Sunda Strait is represented by continental rocks.

Weak methane anomalies were also found at the deformation front and in one of the intra-slope basins.

Pliocene to Recent sediments were sampled at various locations. The sediments not only form the uppermost sections of the sedimentary forearc basin and intra-slope basin fills, but also form the relatively thin sedimentary veneer covering the thrust blocks of the accretionary complex. They are hemipelagic olive gray muds with frequent intercalated turbidite and volcanic ash layers. The turbidites hint at a dynamic depositional environment, while the volcanic ashes certainly resulted from the Sunda Arc volcanism. Sampling of outcropping thrust blocks revealed that they in part consist of cleaved, and tectonized grayish mudstones. The sediments of the youngest thrust unit are gray stiff silty micaceous muds and mudstone, possibly representing material derived from the Bengal Fan which was mixed with the local hemipelagic material deposited on the Sunda Arc slope and in the Sunda Trench.

Acharax sp.

Vent fauna recovered from the forearc basin off Java during cruise SO-139.
Living specimen of specialised clam Acharax sp. (at right) and tube worm Vestimentifera sp. (below).

Vestimentifera sp.

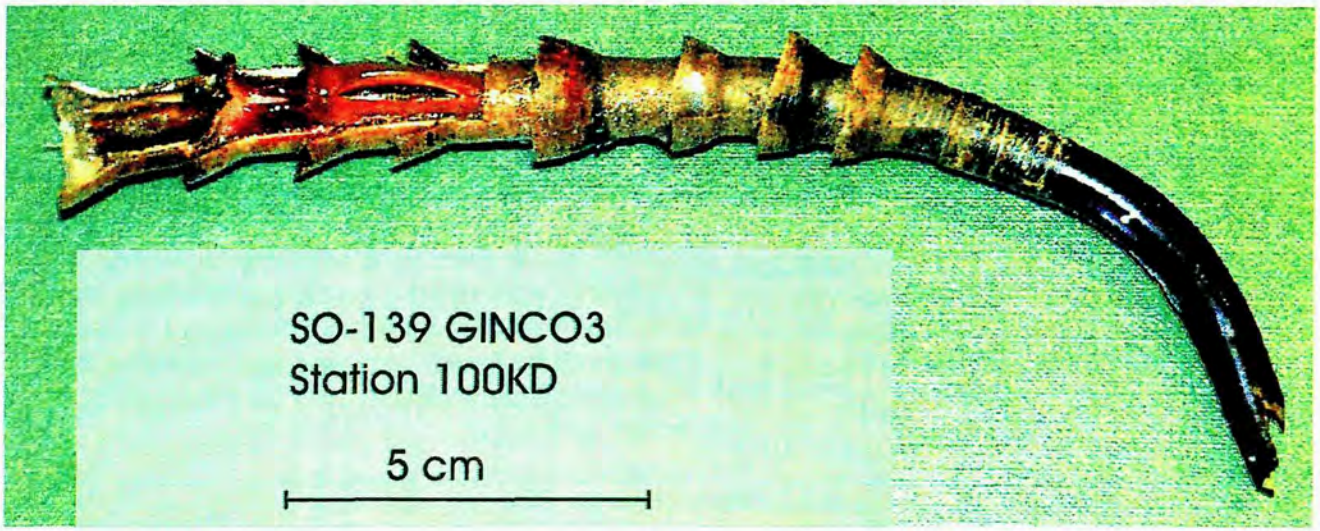

1. Introduction

H. Beiersdorf

GINCO is the acronym for Joint Indonesian-German "***G***eoscientific ***In***vestigations along the ***Co***nvergence Zone between the Eastern Eurasian and Indo-Australian Plates off Indonesia". The project is jointly carried out by the Agency for the Assessment and Application of Technology (BPP Teknologi), Jakarta (Republic of Indonesia) and the Bundesanstalt fuer Geowissenschaften und Rohstoffe (BGR), Hannover (Germany) and focuses on the accretionary and neo-tectonic processes of the subduction zone south of West Java and southern Sumatra.

The area of work is part of the Sunda Arc subduction zone (Fig. 1.1). Although the structural inventory of the subduction zone is fairly well known through hydrocarbon exploration and other studies (e.g. HAMILTON, 1979, HOFFMANN-ROTHE, 1994), the area was chosen because here a transition from normal (frontal) to oblique subduction occurs. Therefore, the consequences of the different subduction processes with regard to deformational style can be studied here in detail.

The Sunda Arc belongs to an arc system which stretches over 5000 km between the Arakan collision belt in the northwest and the Banda Arc in the east. At this arc system the Indo-Australian Plate is being subducted under the Eurasian Plate. While the subduction under East Java is normal, it is oblique from West Java to the northern tip of Sumatra. Therefore the subduction rates range from 60mm/yr off Sumatra to 78 mm/yr at the easternmost part of the arc . The depth of the Benioff zone reaches 300 km only under Sumatra, but 700 km under Java (GHOSE et al. 1990). The forearc complex has a well developed accretionary wedge and forearc basin. The oblique subduction under southern Sumatra and West Java causes transpressional deformations with dextral strike-slip faults and grabens in the forearc and arc systems (PRAMUMIJOYO & SEBRIER, 1991; McCAFFREY, 1991). The structural expressions of these are the Sumatra strike slip fault system on Sumatra and the Mentawai fault system in the Bengkulu (forearc) Basin. In the South Java Basin off West Java the strike slip fault system (here called South Java Basin Fault) can still be recognised in the reflection seismic records. The complexity of the forearc system is further increased south of the Sunda Strait where the Sumatra Fault (or Semangka Fault System) joins the extension of the Cimandiri Graben in West Java. Microseismicity analyses in the Sunda Strait by HARJONO et al. (1990) suggest crustal stretching and the existence of two magma chambers underneath the Krakatau (Krakatoa) volcano.

The Indo-Australian Plate is separated from the Sunda forearc complex by the up to 7450m deep Sunda Trench. The trench shallows towards the northwest, caused by a thickening of the graben fill as a consequence of increased sediment supply by the Bengal Fan system, because some of the suspended sediment shed from Ganges and Brahmaputra bypasses the Ninety East Ridge and enters the Sunda Graben.

The Indo-Australian Plate just in front of the subduction zone south of Sumatra and West Java is of Cretaceous age as proven by drilling through the sedimentary section into the basalt of the oceanic crust by the Deep Sea Drilling Project (Site 211). K-Ar dating on the basalt provided an age of 71 ma (Hamilton, 1979). The basalt is overlain by Maestrichtian and Early Campanian nannofossil ooze and clay.

Fig. 1.1 Tectonic setting of survey area SO-139

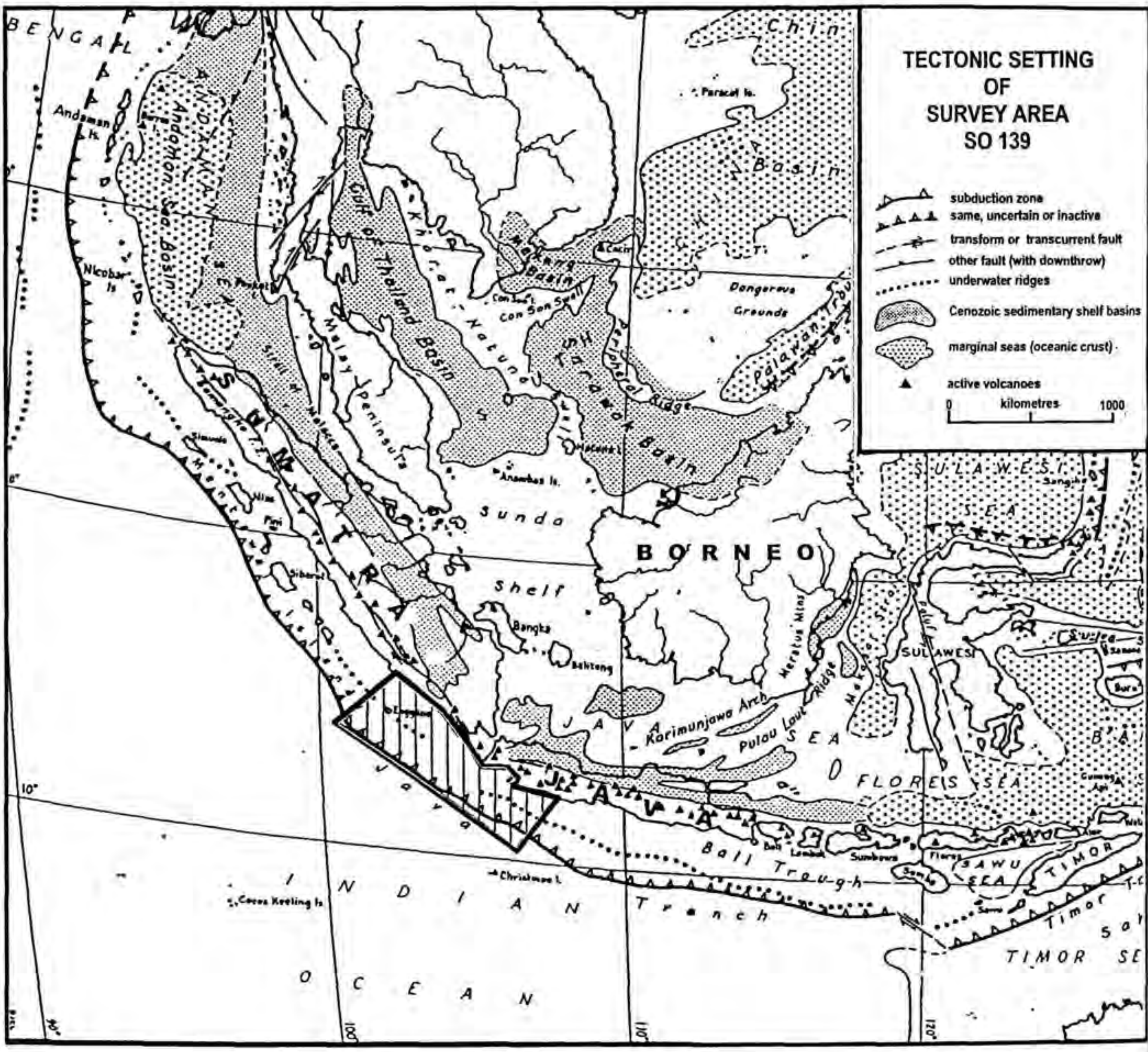

Numerous thrust and normal faults can be seen in reflection seismic profiles from the forearc region, thus supporting the hypothesis that conduits are provided for upward migration of fluids which eventually leads to fluid venting at the seafloor. Though gas hydrates were not reported from the forearc region, they were expected to occur when the plan of work for the GINCO project was discussed.

Taking into account the information available on the subduction zone of southern Sumatra and West Java the individual goals of the project GINCO were:

- Studying the structure and composition of a reference area on the Indo-Australian Plate juxtaposing the Sunda Trench.
- Studying the structure and composition of the subducting complex and of the overriding plate including the accretionary complex.
- Searching for splinters of oceanic crust which have been thrusted into the accretionary prism.
- Deciphering the tectonic mechanisms which have led to the structural inventory of the convergence zone, in particular placing emphasis on the structural difference between areas of oblique versus areas with frontal subduction.
- Studying the heat flow and fluid flow regimes at the deformation front and within the accretionary complex.
- Searching for bottom simulating reflectors as indicators for the occurrence of gas hydrates.
- Searching for active venting of methane in fault settings and studying biota associated with the venting.

For the work at sea, which started on 30 November 1998 in Cilacap (Java, Indonesia), the German Reseach Vessel SONNE of Reedereigemeinschaft Forschungsschiffahrt, Bremen (Germany) was chartered by BGR and by GEOMAR Forschungszentrum fuer marine Geowissenschaften, Kiel using funds provided by the Federal Ministry of Science and Research (BMBF), Germany.

Three consecutive cruises were carried out:

- SO-137 GINCO 1 (21 Nov - 28 Dec 1998) aiming at the assessment of the structural inventory of the subduction complexes off western Java and southern Sumatra using the BGR multi-channel reflection seismic system, the *HYDROSWEEP* swath mapping system and the high resolution subbottom profiling system *PARASOUND* of SONNE, as well as the BGR gradient magnetometer and the BGR gravimeter (Reichert et al., 1999).
- SO-138 GINCO 2 (29 Dec 1998 - 21 Jan 1999) with its main goal to carry out refraction seismic work using GEOMAR ocean bottom hydrophones and ocean bottom seismometers in order to delineate deep structures of the continental margin and to assess their seismic velocities. Additional bathymetric, reflection seismic, magnetic and gravimetric profiling was performed in order to expand the geophysical data base of the previous cruise (Flueh et al., 1999).
- SO-139 GINCO 3 (30 Jan - 27 Feb 1999) aimed at sampling of sediments, rocks and seafloor biota, making TV seafloor observations as well as heat flow measurements in the study area of cruises SO-137 and -138 in order to verify the interpretation of geophysical data and to study heat flow and fluid migration systems of various forearc realms. Particular emphasis was placed on search for methane vent systems and associated biota.

Cruises SO-137 and -139 were led by BGR, Cruise SO-138 by GEOMAR Forschungszentrum fuer marine Geowissenschaften, Kiel (Germany). The research teams of the three cruises were joined by scientists from Indonesia, coming from BPP Teknologi and various universities and research institutes.

Like the preceding two cruises, Cruise SO139 was split into two Legs. This provided an opportunity to increase the number of Indonesian scientists to become acquainted with the research methods used on SONNE by having a mid-cruise exchange of personnel.

REFERENCES

FLUEH, E., SCHRECKENBERGER, B., BIALAS, J., and Cruise Participants, 1999: FS SONNE CRUISE REPORT SO-138 GINCO 2 "Geoscientific Investigations on the Active Convergence Zone between the East Eurasian and Indo-Australian Plates along Indonesia. GEOMAR Rpt. 81, Kiel (Germany)

GHOSE, R., YOSHIOKA, S., and OIKE, K., 1990:Three-dimensional numerical simulation of the subduction dynamics in the Sunda arc region, Southeast Asia. Tectonophysics, 181, 223-255

HAMILTON, W.B., 1979: Tectonics of the Indonesian Region. USGS Professional Paper, 1078

HARJONO, H., DIAMENT, M., and LASSAL, O., 1990: Tectonics of the Sunda Strait: A new constraint from geological data.- In: Geologi Kuarter dan Pengempangan Wilayah. Pusat Penelitian dan Pengempangan Geologi. Publikasi khusus Pulat Penelitian da Pengempangan Geologi, 10, 118-122

HOFFMANN-ROTHE, J., 1994: Indonesien.- In: Kulke, H. (Ed.): Regional petroleum geology of the world, Part 1, 747-794, Borntraeger, Stuttgart

McCAFFREY, R., 1991: Slip vectors and stretching of the Sumatran forearc. Geology, 19, 881-884

PRAMUNJOYO, S. and SEBRIER, M., 1991: Neogene and Quaternary fault kinematics around the Sunda Strait, Indonesia. J. SE Asian Earth Science, 6, 2, 137-145

REICHERT, Ch. and Cruise Participants, 1999: CRUISE REPORT SO-137 GINCO 1 "Geoscientific Investigations on the Active Convergence Zone between the East Eurasian and Indo-Australian Plates along Indonesia. BGR Rpt. Archive No. 118.844

2. Implementation of Cruise SO-139

H. Beiersdorf

On January 30, 1999, 11:30 hrs local time the SONNE was clear of the pier at Tanjung Priok, Jakarta (Republic of Indonesia) and set course for the Sunda Strait with 25 scientific cruise participants (Table 2.1) and 30 crew members (Table 2.2) on board. The scientific work at sea started on January 31, 1999, 00:03 hrs with HYDROSWEEP and PARA-SOUND profiling in the southern Sunda Strait in order to fill gaps in the coverage by the swath mapping of the Sumatra Fault System from the preceding cruises SO-137 and -138. This goal was achieved 06:55 hrs the same day and the SONNE set course for the area of detailed work of the first Leg, which was carried out on and around geophysical profiles BGR 137-01 and 03 south of West Java. The transit to this area was used for additional swath mapping and sub-bottom profiling. Emphasis was put on adding more bathymetric information to the area of the deformation front off West Java. The Sunda Trench was reached at 9°13,37'S, 106°17,66'E, where the water depth is 6483m. In order to avoid later instrument failures, components of the underwater-TV system OFOS and of the BGR heat flow probe were lowered to 6410m to undergo a pressure test. All components resisted the hydrostatic pressure at this depth. All further work is listed in Table 2.3. An overview of the sampling and probing tools used during the cruise is given in Fig. 2.1. Profiles and sampling /probing stations are shown in Figs. 2.2 - 2.4.

On February 13, 1999, 17:55 hrs station work was finished on Leg1 with a successful deployment of the TV grab sampler at 7°57,45'S, 106°17,71'E (water depth 2908m) recovering the first specimens of vent fauna in a forearc basin environment. 18:44 hrs SONNE set course for the Sunda Strait and the transit was used for swath mapping and sub-bottom profiling again. At the anchorage of Ciwandan an exchange of Indonesian scientists was performed on February 13, 1999, 11:45 hrs. Four scientists left the SONNE and were replaced by three others (Tab. 2.2). 21:35 hrs the same day we started profiling with HYDROSWEEP and PARASOUND around the northern part of reflection seismic profile BGR 137-06 aimed at obtaining detailed information about a major fault system in the Bengkulu Basin south of Sumatra. Most of the work during Leg 2 concentrated on seismic Lines BGR 137-06 and 06A. On this composite profile the only heat flow measurement on the Indo-Australian Plate was performed. Low methane concentrations in the water column at the deformation front led to the decision to leave the area and save time for additional work in the Bengkulu (forearc) Basin, where a methane plume was discovered at the southern boundary fault. Before heading back to this location on February 18, 1999, 11:45 hrs, we tried to recover GEOMAR OBH No. 06 and two transponders which were lost during Cruise SO-138 at 6°34,40'S, 102°17,65'E in a water depth of around 3880m. After eight hours and two unsuccessful drag anchor hauls we abandoned the attempt and headed for the Enggano Ridge site on seismic profile BGR 137-09A for small-scale bathymetric mapping and sub-bottom profiling as well as for undertaking heat flow measurements, coring and dredging. On February 20, 1999, 06:47 hrs we resumed sampling, seafloor observation, heat flow measurements and multiprobe deployment in the methane plume area of the Bengkulu Basin. The area was left on February 22, 17:00 hrs without finding a vent system despite of high methane concentrations found in the water column and in the sediments. We went on with swath mapping and sub-bottom profiling across the southern end of the Sumatra Fault.

Work was resumed on February 22, 08:46 hrs in the vent area on seismic profile BGR 137-01. Here work centered around the vent area with several deployments of the multiprobe, heat flow probe, gravity corer, chain bag dredge, underwater-TV system OFOS, and TV grab sampler. Sediment particle plumes produced by the preceding sampling in the vent area prevented a deployment of the vent sampler VESP.

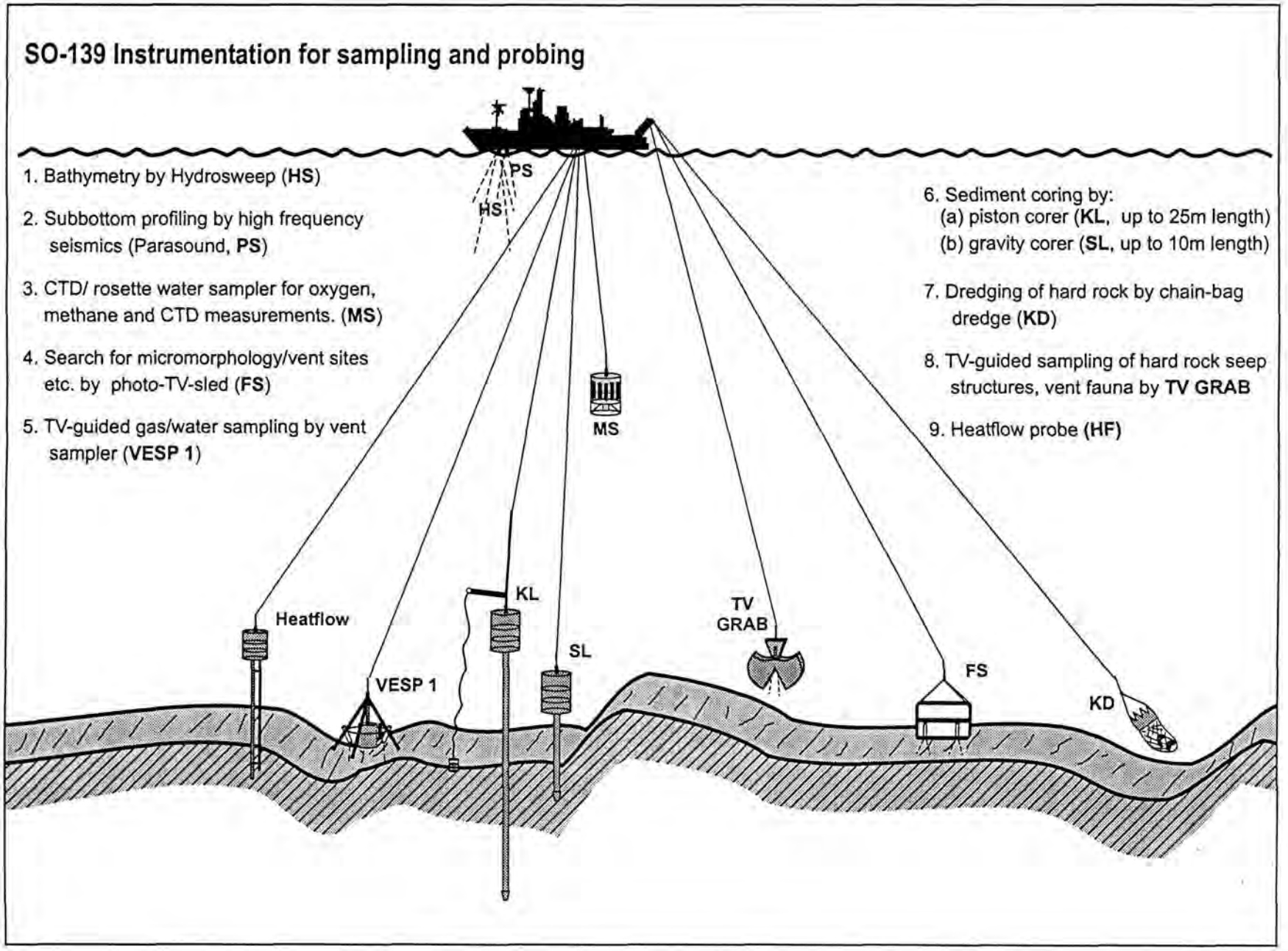

Fig. 2.1 SO-139 Instrumentation for sampling and probing

Figure 2.2: Cruise track of expedition SO-139

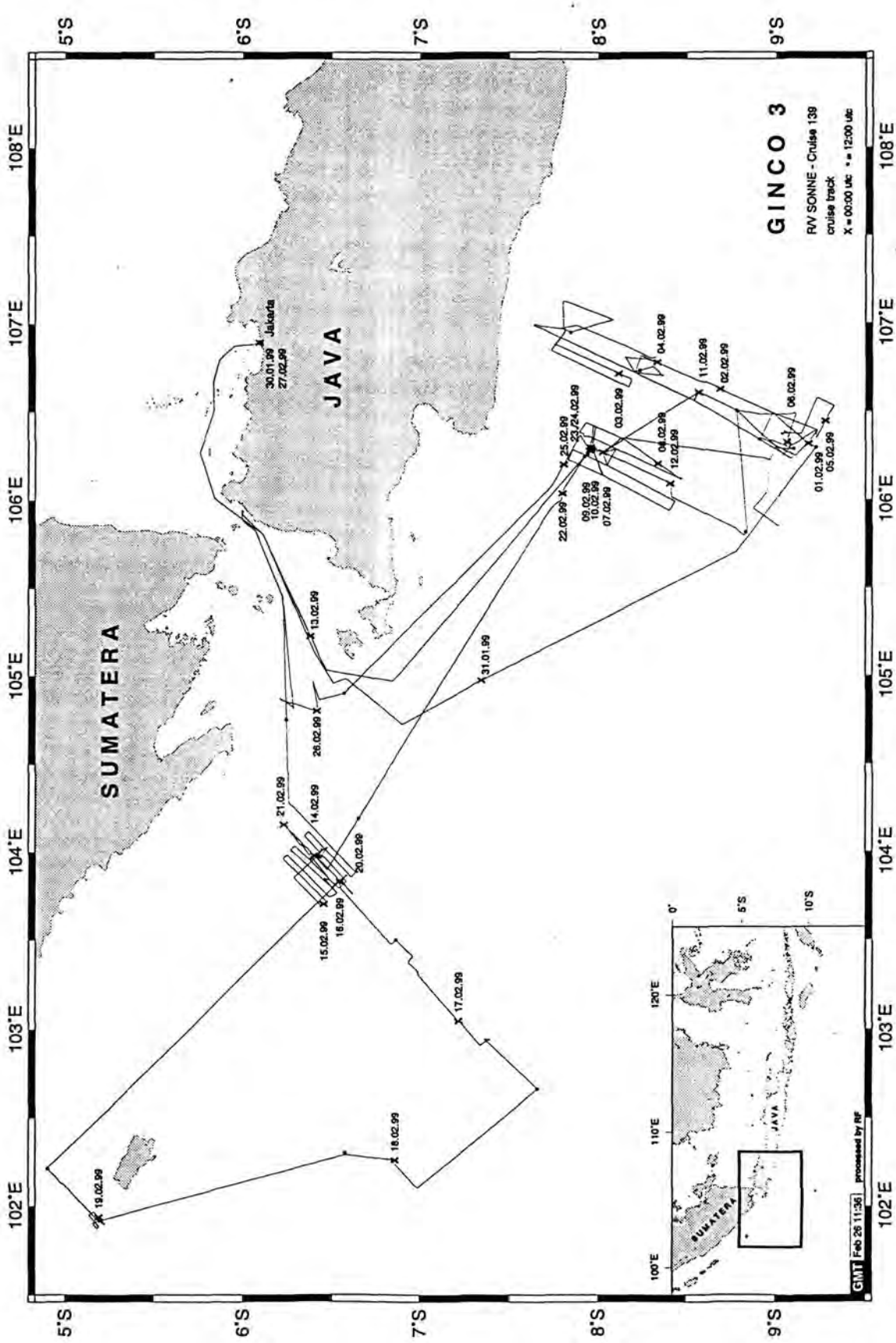

Figure 2.3: Sampling and probing stations of cruise SO-139 south of Java

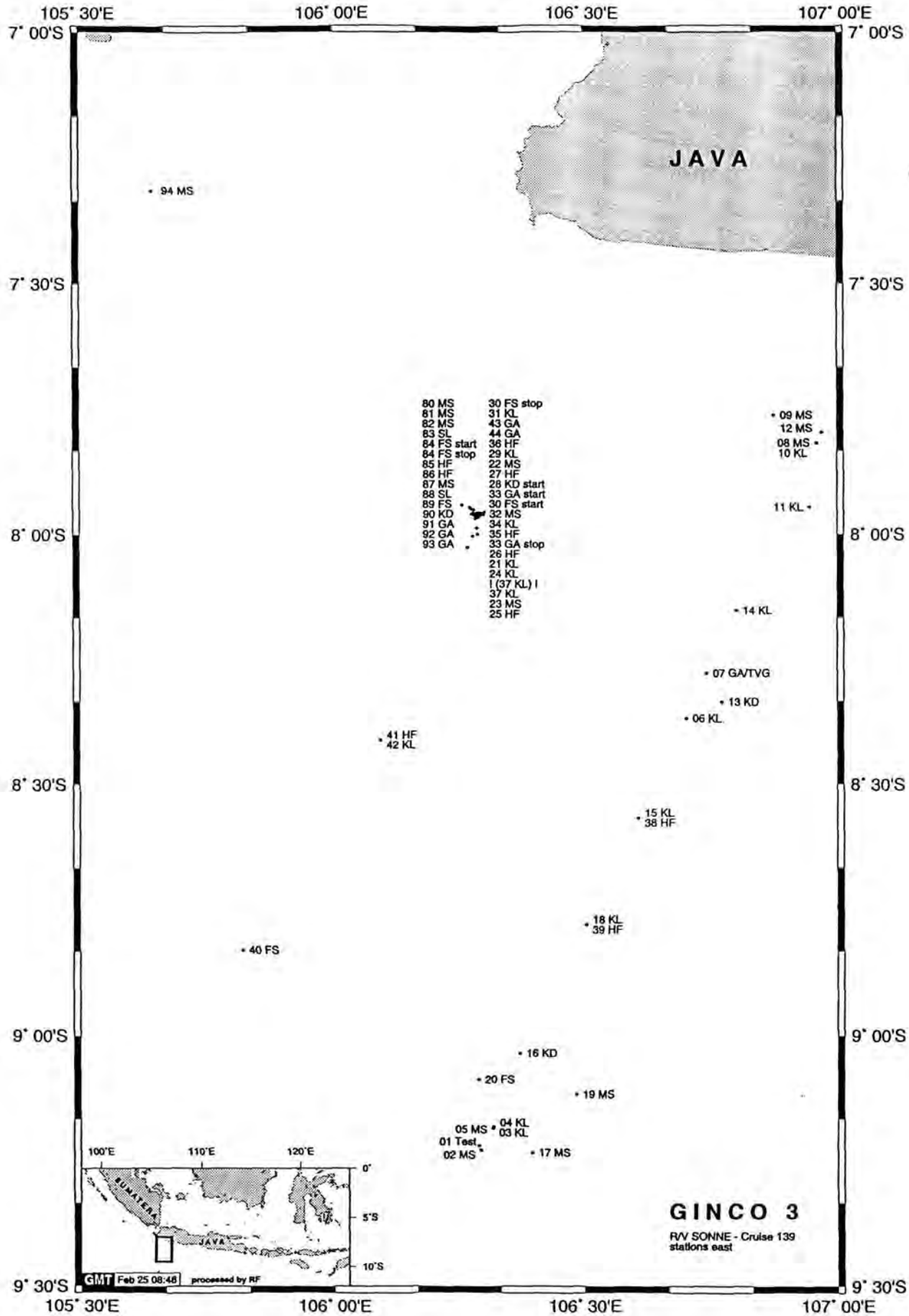

Figure 2.4: Sampling and probing stations of cruise SO-139 south of Sumatra

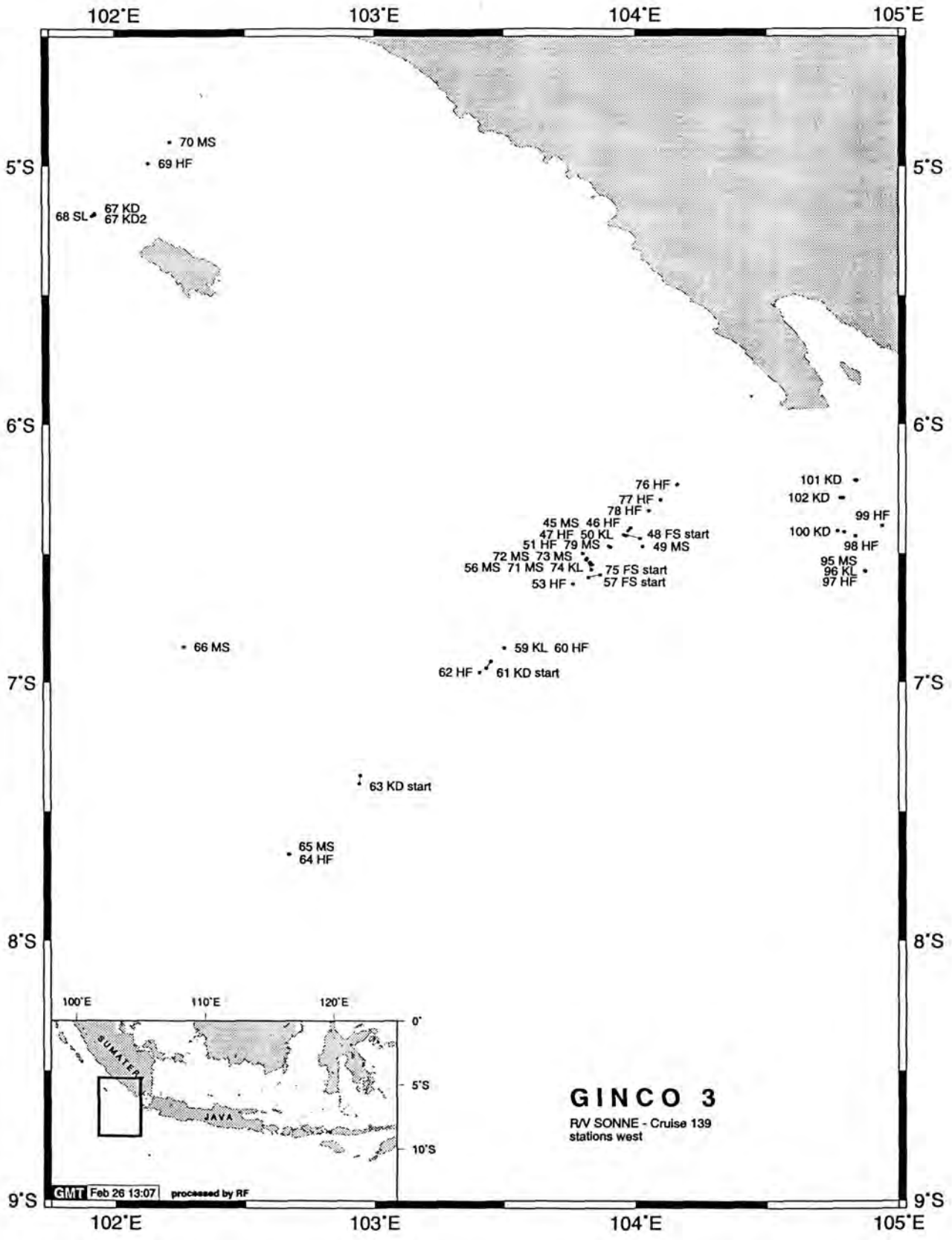

We left the area on February 25, 05:15 hrs. SONNE set course for the Sunda Strait. The transit was interrupted at 7°18,79'S, 105°38,94'E for plankton sampling in the upper 200m of the water column. The ship arrived at the first location in the Sunda Strait on 25 February, 17:09 hrs, and station work started with another plankton sampling in the uppermost 200m of the water column, followed by piston coring, heat flow measurements, and dredging. Coring and heat flow measurements were carried out on the floor of the Semangka Graben, while dredging took place at both walls of the graben. Station work of Cruise SO-139 GINCO 3 was finished 26 February 1999, 18:15 hrs, and SONNE prepared for transit to Jakarta. All lines were tight at Tanjung Priok on February 27,12:10 hrs. The event times for transit, profiling, and station work are listed in Tab. 2.3.

Port activities following the cruise included off-loading of scientific equipment on February 28, 1999, a reception on board SONNE on March 1, 1999, and an "Open Ship" to the public on March 2, 1999. The latter included a press conference on board SONNE held by Dr. Eitner, Deputy Director for International Affairs at the Federal Ministry for Education and Research (Bonn, Germany), Mr. Yusuf Djajadihardja (BPP Teknologi, Jakarta), Professor Dr. Beiersdorf; Chief Scientist Cruise SO-139 (BGR Hannover), and Cpt. Papenhagen, Master of R/V SONNE (see Appendix B). The reception was held to celebrate the participation of SONNE at the TECHNOGERMA '99 and the successful cruises of the research vessel in Indonesian waters from 28 November 1998 to 28 February 1999, and was generously hosted by RF Reedereigemeinschaft Forschungsschiffahrt GmbH (Bremen, Germany). The invitation to the reception was jointly issued by Dr. Eitner, Prof. Dr. Beiersdorf, and Cpt. Papenhagen. It was opened with adresses from Cpt. Papenhagen, State Minister for Research and Technology of the Republic of Indonesia Prof. Zuhal, Dr. Eitner and Prof. Beiersdorf.

Table 2.1

Members of the Shipboard Scientific Part for Cruise SO139 Leg1

Andruleit, Harald	Geology	BGR
Beiersdorf, Helmut	Chief Scientist	BGR
Bannert, Bernhard	Geochemsitry	GEOMAR
Bruns, Angelika	Geology	BGR
Delisle, Georg	Geothermics	BGR
Faber, Eckhard	Geochemistry	BGR
Goergens, Rainer	Geology	BGR
Harazim, Bodo	Geochemistry	BGR
Haryadi Permada	Geology	LIPI
Ibrahim Lakoni	Liaison Officer	TNI-AL
Jürgens, Udo	Geology	BGR
Kawohl, Helmut	Geology	BGR
Kothe, Jürgen	Geology	BGR
Marchig, Vesna	Geology	BGR
von Mirbach, Nikolaus	Biology	GEOMAR
Poggenburg, Jürgen	Geochemistry	BGR
Safri Burhanuddin	Geology	UH
Sahling, Jens Heiko	Biology	GEOMAR
Salahuddin, S.T.	Geology	GMU
Stahl, Wolfgang	Geochestry	BGR
Steinmann, Dieter	Geology, Geothermics	BGR
Syarif Hidayat	Geology	GRD
Weiss, Wolfgang	Geology	BGR

Wiedicke-Hombach, Michael	Geology	BGR
Zeibig, Michael	Geothermics	BGR

Members of the Shipboard Scientific Part for Cruise SO139 Leg 2

Andruleit, Harald	Geology	BGR
Beiersdorf, Helmut	Chief Scientist	BGR
Bannert, Bernhard	Geochemsitry	GEOMAR
Bruns, Angelika	Geology	BGR
Delisle, Georg	Geothermics	BGR
Eko Triarso	Geophysics	BPPT
Faber, Eckhard	Geochemistry	BGR
Goergens, Rainer	Geology	BGR
Harazim, Bodo	Geochemistry	BGR
Ibrahim Lakoni	Liaison Officer	TNI-AL
Jürgens, Udo	Geology	BGR
Kawohl, Helmut	Geology	BGR
Koesnadi H.S.	Geology	MGI
Kothe, Jürgen	Geology	BGR
Marchig, Vesna	Geology	BGR
von Mirbach, Nikolaus	Biology	GEOMAR
Poggenburg, Jürgen	Geochemistry	BGR
Sahling, Jens Heiko	Biology	GEOMAR
Stahl, Wolfgang	Geochestry	BGR
Steinmann, Dieter	Geology, Geothermics	BGR
Udrekh	Geophysics	BPPT
Weiss, Wolfgang	Geology	BGR
Wiedicke-Hombach, Michael	Geology	BGR
Zeibig, Michael	Geothermics	BGR

BGR	Bundesanstalt für Geowissenschaften und Rohstoffe, Hannover, Germany
BPPT	Agency for the Assessment and Aplication of Technology, Jakarta, Indonesia
GEOMAR	GEOMAR Forschungszentrum für marine Geowissenschaften, Kiel, Germany
GMU	Gadjah Mada University, Yogyakarta, Indonesia
GRD	Geological Research & Development Centre, Ministry of Mines & Energy, Bandung, Indonesia
LIPI	R & D Centre for Geotechnology, LIPI, Bandung, Indonesia
MGI	Marine Geological Institute, Bandung, Indonesia
TNI-AL	Dishidros TNI-AL, Jakarta, Indonesia
UH	Universitas Hasanuddin, Ujung Padang, Indonesia

Table 2.2 Crew-List of RV SONNE
(all of Reedereigemeinschaft Forschungsschiffahrt GmbH, Bremen, Germany)

Papenhagen, Henning	Master
Becker, Wolfgang	Ch. Offc.
Bendin, Axel	1st Offc.
Osterhues, Wilfried	Rdo.Offc.
Walther, Anke	Surgeon
Martin, Andreas	Ch. Eng.
Guzman, Werner	2nd Eng.
Bochnik, Eberhard	2nd Eng.
Rehberg, Burkhard	Electrician
Hoffmann, Hilmar	Ch. Electron.
Vöhrs, Helmut	Electron.
Klein, Andreas	Sys. Manag.
Angermann, Rudolf	Sys. Manag.
Tscharntke, Rudolf	Fitter
Koch, Michael	Motorman
Blohm, Volker	Motorman
Arronet, Johannes	Motorman
Prinz, Udo	Motorman
Tiemann, Frank	Ch. Cook
Cwienk, Adolf	2nd Cook
Bronn, Johann	Ch. Steward
Grübe, gerlinde	Stewardess
Hoppe, Jan	2nd Steward
Lohmueller, Karl-Heinz	Boatswain
Becker, Siegfried	A.B.
Schober, Peter	A.B.
Neitzsch, Bernd	A.B.
Ventz, Günther	A.B.
Roepti, Hermann	A.B.
Tamm, Stefan	A.B.

Table 2.3: Time table for Transit, Profiling, Work on Station and other Events

Time (local)	Profile, Station etc.	Koordinates, Water depth Cable length
30 Jan 1999		
11:30 h	All lines off	Pier 214 Jakarta
12:00	Start Cruise SO139	
31 Jan 1999		
00:03	Start Scientific Work Start Profile 139-01 HS,PS	6°24.00'S, 105°08.00'E
01:16	End Profile 139-01 and Start Profile 139-02	6°30.50'S, 104°57.50'E
01:48	End Profile 139-02 and Start Profile 139-03	6°34.80'S, 104°59.00'E
04:02	End Profile 139-03 and Start Profile 139-04	6°55.10'S, 104°43.30'E
06:55	End Profile 139-04 and Start Profile 139-05	7°20.00'S, 104°58.00'E
15:11	End Profile 139-05 and Start Profile 139-06	8°46.50'S. 105°42.20'E
18:52	End Profile 139-06	9°13,37'S, 106°17,66'E
19:00	Beginn pressure test HF and OFOS components	9°13,37'S, 106°17,66'E WD 6463m
22:00	Maximum WD reached	CL 6410m
1 Feb 1999		
00:40	HF & OFOS components on deck	
00:56	Beginn 2MS	9°13,17'S, 106°17,60'E
03:16	Bottom contact 2MS	9°13,17'S, 106°17,60'E WD 6460m, CL 6467m
06:30	End 2MS	
06:30	Begin Profile 139-07	9°13,70'S, 106°17,60'E
06:50	End Profile 139-07	9°11,10'S, 106°19,00'E
07:15	Start Station 3KL	
09:34	Bottom contact 3KL	9°11,1'S, 106°19,000'E Waterdepth 6338m Cable length 6296m
12:32	End Station 3KL	
12:32	Start Profile 139-08	
13:02	End Profile 139-08, Start Profile 139-09	9°14,20'S, 106°23,50'E
14:27	End Profile 139-09, Start Profile 139-10	8°59,85'S, 106°29,50E
15:19	End Profile 139-10, Start Profile 139-11	8°55,00'S, 106°21,00'E
16:32	End Profile 139-11, Start Profile 139-12	9°06,80'S, 106°14,80'E
17:13	End Profile 139-12	9°10,89'S, 106°19,11'E
17:18	Start Station 4KL	
19:26	Bottom contact	9°10,17'S, 106°19,10'E Cable length 6260m, Water depth 6238m
22:24	End Station 4KL	

22:45	Start Station 5MS	9°11,13'S, 106°19,03'E Water depth 6372m
2 Feb 1999		
00:47	Maximum depth 5MS reached	9°11,09'S, 106°19,03'E Water depth 6332m Cable length 6739m
03:50	End Station 5MS	
03:50	Start Profile 139-13	9°01,40'S, 106°27,4'E
05:18	End Profile 139-13 and Start Profile 139-14	8°59,30'S, 106°29,5'E
09:30	End Profile 139-14 and Start Profile 139-15	9°14,60'S, 106°48,80'E
10:08	End Profile 139-15 and Start 139-16	8°12,50'S, 106°43,00'E
11:00	End Profile 139-16	8°22,03'S, 106°42,13'E
11:08	Start Station 6KL	
12:20	Bottom contact 6KL	8°22,03'S, 106°42,13'E Water depth 2139m Cable length 2111m
13:26	End Station 6KL	
14:38	Start Station 7TVG	
15:31	First bottom view 7TVG	8°17,90'S, 106°45,02'E Water depth 2527m Cable length 2500m
17:18	Sample taken at 7TVG	8°16,66'S, 106°44,55'E Water depth3024m Cable length 2954m
18:25	End Station 7TVG	
18:43	Start Profile 139-17	8°16,55'S, 106°44,48'E
19:12	End Profile 139-17 and Start Profile 139-18	8°12,50'S, 106°44,46'E
22:41	End Profile 139-18	7°39,00'S, 106°59,00'E
22:48	Start Profile 139-19	7°38,90'S, 106°59,50'E
23:45	End Profile 139-19	7°48,48'S, 106°57,90'E
23:53	Start Station 8MS	
3 Feb 1999		
01:17	Maximum depth 8MS reached	7°49,07'S, 106°57,52'E Water depth 2730m Cable length 2733m
02:55	End Station 8MS and Start Profile 139-20	7°49,10'S, 106°57,10'E
03:35	End Profile 139 -20	7°45,75'S, 106°52,60'E
04:10	Start Station 9MS	
04:30	Maximum depth 9MS reached	7°45,77'S, 106°52,60'E Water depth 2666m Cable length 200m
4:54	End Station 9MS and Start Profile 139-21	7°45,73'S, 106°52,60'E
07:23	End Profile 139-21 and Start Profile 139-22	8°10,20'S, 106°40,80'E
07:43	End Profile 139-22 and Start Profile 139-23	8°10,20'S, 106°38,20'E
10:12	End Profile 139-23	7°44,60'S, 106°50,50'E
11:05	Start Station 10KL	

12:12	Bottom contact 10KL	7°49,15'S, 106°57,61'E Water depth 2727m Cable length 2700m
13:39	End Station 10KL	
13:45	Start Profile 139-24	7°49,15'S, 106°57,50'E
14:37	End Profile 139-24 and Start Profile 139-25	/°48,25'S, 107°07,70'E
16:45	End Profile 135-25	8°04,86'S, 107°01,26'E
17:50	Start Station 11KL	
19:08	Bottom contact 11KL	7°50,85'S, 106°56,78E Water depth 2793m Cable length 2771m
20:45	End Station 11KL	
21:25	Start Station 12MS	
22:36	Maximum depth 12MS reached	7°47,88'S, 106°58,27E Water depth 2641m Cable length 2617m
4 Feb 1999		
00:15	End Station 12MS	
00:47	Start Profile 139-26	7°52,80'S, 106°59,10'E
02:17	End Profile 139-26 and Start Profile 139-27	8°08,08'S, 106°52,7=='E
03:17	End Profile 139-27	8°18,20'S, 106°47,80'E
03:32	Start Station 13KD	
04:34	Bottom contact, start dredging	8°20°02'S, 106°47,20'E Water depth 2952m
05:50	Start hoisting	8°20,10'S, 106°46,40'E Water depth 2936m Cable length 3178m
07:15	End Station 13KD	
08:21	Start Station 14KL	
09:38	Bottom contact 14KL	8°09,14'S, 106°48,14'E Water depth 3000m Cable length 2970m
11:06	End Station 14KL	
11:48	Start Profil 139-28	8°12,5'S, 106°43,00'E
13:40	End Profile 139-28	8°24,4'S, 106°37,40'E
14:14	Start Station 15KL	
15:15	Bottom contact 15KL	8°34,00'S 106°36,46'E Water depth 2245m Cable length 2213m
16:19	End Station 15KL	
16:42	Begin Profile 139-29	8°32,45'S, 106°33,70'E
20:10	Start Station 16KD	
22:25	Bottom contact 16KD	9°03,00'S, 106°23,09'E Water depth 4862m Cable length 5300m
5 Feb 1999		
03:38	End Station 16KD	
04:45	Start Profil 139-30	9°09,00'S, 106°22,30'E
05:55	End Profile 139-30 and Start Profile 139-31	9°14,00'S, 106°34,50'E
06:25	End Profile 139-31 and Start Profile 139-32	9°19,55'S, 106°34,80'E

08:02	Beginn Station 17MS	
10:20	Maximum cable length 17MS	9°13,99'S, 106°23,71'E Waterdepth 6404m Cable length 6371m
13:50	End Station 17MS	
18:59	Start Station 18KL	
20:21	Bottom contact 18KL	8°46,79'S, 106°30,26'E Water depth 3374m Cable length 3359m
22:00	End Station 18KL	
6 Feb 1999		
00:10	Start Station 19MS	
02:26	Maximum cable length 19MS	9°07,0'S, 106°29,01S Water depth 5531m Cable length 5542m
07:28	Start Profile 139-33	9°02,4'S, 106°14,6'E
09:43	End Profile 139-33 and Start Profile 139-34	9°01,0'S, 105°51,0'E
10:36	End Profile 139-34 and Start Profile 139-35	8°52,5'S, 105°57,0'E
11:13	End Profile 139-35 and Start Profile 139-36	8°57,8'S, 106°02,4'E
12:38:	End Profile 139-36	
14:15	Begin Station 20OFOS	9°04,60'S, 106°17,60'E Water depth 4802m
15:53	Start bottom observation	9°04,62'S, 106°17,58'E Water depth 4807m Cable length 4823m
16:47	End bottom observation	9°05,28'S, 106°17,28'E Water depth 4913m Cable length 4760m
18:30	End Station 20OFOS	
20:25	Start Profile 139-37	8°58,23'S, 106°13,60'E
7 Feb 1999		
01:30	End Profile 139-37 and Start Profile 139-38	8°08,0'S, 106°21,0'E
02:55	End Profile 139-38 and Start Profile 139-39	7°56,0'S, 106°26,0'E
03:35	End Profile 139-39 and Start Profile 139-40	7°54,0'S, 106°23,0'E
05:25	End Profile 139-40 and Start Profile 139-41	8°06,0'S, 106°14,2'E
06:00	End Profile 139-40	8°02,1'S, 106°16,1'E
06:10	Start Station 21KL	
07:37	Bottom contact 21KL	8°01,59'S, 106°16,12'E Water depth 2991m Cable length 2958m
09:10	End Station 21KL	
09:11	Start Profile 139-42	8°01,16'S, 106°16,65'E
09:54	End Profile 139-42 and Start Profile 139-43	8°03,0'S, 106°11,7'E
11:15	End Profile 139-43 and Start Profile 139-44	7°51,5'S, 106°17,0'E
11:45	End Profile 139-44 and	

	Start Profile 139-45	7°50,0'S, 106°13,5'E
1305	End Profile 139-45	8°o1,5'S, 106°o8,4'E
14:41	Start Station 22MS	
18:05	Maximum cable length 22MS reached	7°57,67'S, 106°18.0'E Water depth 2994m Cable length 2985m
20:03	End Station 22MS	
21:28	Start Profile 139-46	8°01,5'S, 106°08,4'E
8 Feb 1999		
00:13	End Profile 139-46 and Start Profile 139-47	8°24,5'S, 105°56,2'E
00:34	End Profile 139-47 and Start Profile 139-48	8°26,2'S, 105°59,5'E
03:02	End Profile 139-48 and Start Profile 139-49	8°03,0'S, 106°11,7'E
03:32	End Profile 139-49 and Start profile 139-50	8°06,0'S, 106°17,2'E
06:00	End Profile 139-50	8°27,8'S, 106°07,2'E
06:10	Start Profile 139-51	8°27,8'S, 106°07,2'E
08:53	End Profile 139-51	8°08,0'S, 106°21,0'E
09:24	Start Station 23MS	8°01,61'S, 106°16,53'E
10:51	Maximum cable length 23MS reached	8°01,6'S, 106°16,11'E Water depth 2990m Cable length 2980m
12:40	End Station 23MS	
12:47	Start Station 24KL	
14:06	Bottom contact 24KL	8°01,6'S, 106°16,1'E Water depth 2989m Cable length 2954m
15:35	End Station 24KL	
16:15	Start Station 25HF	
17:26	Bottom contact 25HF	8°01,6'S, 106°16,1'S Water depth 2990m Cable length 3017m
18:46	End Station 25HF	
19:37	Start Station 26HF	
20:41	Bottom contact 26HF	8°00,289'S, 106°16,74'E Water depth 3039m Cable length 3054m
22:01	End Station 26HF	
22:25	Start Station 27HF	
23:32	Bottom contact 27HF	07°66'S, 106°19,99'E Water depth 2996m Cable length 3011m
9 Feb 1999		
00:55	End Station 27HF and Start Profile 139-52	7°57,7'S, 106°18,0'E
01:25	End Profile 139-52 and Start Profile 139-53	7°56,43'S, 106°14,76'E
01:30	End Profile 139-53 and Start Profile 139-54	7°55,86'S, 106°15,04'E
02:15	End Profile 139-54 and Start Profile 139-55	7°58,17'S, 106°21,02'E

02;45	End Profile 139-55 and Start Profile 139-56	7°58,4'S, 106°25,1'E
02:53	End Profile 139-56 and Start Profile 139-57	7°59,21'S, 106°24,79'E
03:23	End Profile 139-57 and Start Profile 139-58	7°58,65'S, 106°20,77'E
03:50	End Profile 139-58	7°57,67'S, 106°17,98'E
03:58	Start Station 28KD	
04:58	Bottom contact 28 KD	7°57,68'S, 106°18,00'E Water depth 2997m Cable length 2900m
05:33	Maximum cable length	7°57,50'S, 106°17,56'E Water depth 2953m Cable length 3805m
10:01	End Station 28KD	
10:28	Start Station 29KL	
11:44	Bottom contact 29KL	7°57,55'S, 106°17,99'E Water depth 2997m Cable length 2957m
13:15	End Station 29KL	
13:35	Start Station 30FS	
15:11	Start bottom observation 30FS	7°58,24'S, 106°17,34'S Water depth 2993m Cable length 2993m
18:50	End bottom observation 30FS	7°56,50'S, 106°15,54'E Water depth 2946m
19:58	End Station 30FS	
21:02	Start Station 31KL	
22:25	Bottom contact 31KL	7°57,00'S, 106°16,56'E Water depth 2949m Cable length 2918m
10 Feb 1999		
00:03	End Station 31KL	
00:25	Start Station 32MS	
01:47	Maximum cable length 32MS reached	7°58,15'S, 106°17,0'E Water depth 3004m Cable length 2995m
04:12	End Station 32MS	
04:50	Start Station 33GA	
05:54	Start bottom Observation 33GA	7°57,95'S, 106°17,30'E Water depth 2985m Cable length 2960m
06:13	Sample taken by 33GA	7°57,52'S, 106°17,20'E Water depth 2969m
07:18	End Station 33GA	
08:10	Start Station 34KL	
09:30	Bottom contact 34KL	7°59,26'S, 106°17,22'E Water depth 3023m Cable length 2983m
11:34	End Station 34KL	
12:35	Start Station 35HF	
13:28	Bottom contact 35HF	7°59,26'S, 106°17,2'E Water depth 3022m Cable length 3035m
14:47	End Station 35HF	

15:14	Start Station 36HF	
16:18	Bottom contact 36HF	7°56,996'S, 106°16,558'E Water depth 2950m Cable length 2964m
17:45	End Station 36HF	
18:30	Start Station 37KL	
18:55	Lost piston corer, start assembling replacement corer	
22:34	Re-start 37KL with new corer	
23:42	Bottom contact 37KL	8°01,6'S, 106°16,09'E Water depth 2989m Cable length 2949m
11 Feb 1999		
02:00	End Station 37KL and Start Profile 139-59	8°10,7'S, 106°21,9'E
05:27	End Profile 139-59	8°34,0S, 106°36,46'E
05:40	Start Station 38HF	
06:38	Bottom contact 38HF	8°34,0'S, 106°26,47'E Water depth 2249m Cable length 2264m
07:40	End Station 38HF	
09:08	Start Station 39HF	
10:14	Bottom contact 39HF	8°46,8'S, 106°30,24'E Water depth 3367m Cable length 3389m
11:35	End Station 39HF	
11:38	Start Profile 139-60	8°46,78'S, 106°46,78'E
15:35	End Profile 139-60	8°50,2'S, 105°50,2'E
15:50	Start Station 40FS	
17:10	Start bottom observation 40FS	8°50,25'S, 105°50,19'E Water depth 4848m Cable length 4711m
18:24	End bottom observation	8°49,81'S, 105°49,15'E Water depth 4988m
19:58	End Station 40FS	
20:26	Start Profile 139-61	8°47,98'S, 105°48,65'E
12 Feb 1999		
00:32	End Profile 139-61	8°25,0'S, 160°01,0'E
01:10	Start Station 41HF	
02:10	Bottom contact 41HF	8°24,64'S, 106°05,65'E Water depth 3181m Cable length 3196m
03:36	End Station 41HF	
04:20	Start Station 42KL	
05:49	Bottom contact 42KL	8°24,64'S, 106°05,65'E Water depth 3181m Cable length 3142m
07:12	End Station 42KL	8°24,67'S, 106°05,64'E
10:07	Start Station 43GA	7°57,45'S, 106°16,05'E
11:08	Start bottom observation 43GA	7°57,43'S, 106°18,03'E Water depth 2997m Cable length 2983m
12:16	Sample taken 43GA	7°57,45'S, 106°17,60'E

		Water depth 2947m Cable length 2914m
13:21	End Station 43GA	
14:23	Start Station 44GA	
16:40	Sample taken 44GA	7°57,45'S, 106°17,71'E Water depth 2938m Cable length 2908m
17:55	End Station 44GA	
18:44	Start Profile 139-62	7°57,15'S, 106°16,78'E
13 Feb 1999		
04:10	End Profile 139-62	6°51,0'S, 104°58,0'E
11:45	Exchange of 4 vs 3 Indonesia Scientists at anchorage Cindawan/Merak	
12:06	Start transit to work area off Sumatra	
21:35	Start Profile 139-63	6°15,5'S, 104°17,0'E
14 Feb 1999		
00:35	End Profile 139-63 and Start Profile 139-64	6°38,05'S, 103°53,0'E
00:47	End Profile 139-64 and Start Profile 139-65	6°36,5'S,103°51,5'E
02:32	End Profile 139-65 and Start Profile 139-66	6°22,1'S, 104°07,0'E
02:44	End Profile 139-66 and Start Profile 139-67	6°20,8'S, 104°05,5'E
04:39	End Profile 139-67 and Start Profile 139-68	6°34,8'S, 103°50,0'E
04:59	End Profile 139-68 and Start Profile 139-69	6°32,3'S, 103°47,6'E
06:05	End Profile 139-69 and Start Profile 139-70	6°22,5'S, 103°57,2'E
06:25	End Profile 139-70	6°24,11'S, 103°58,91'E
06:28	Start Station 45MS	
07:26	Maximum cable length 45MS	6°24,13'S, 103°58,87'E Water depth 2002m Cable length 1997m
08:50	End Station 45MS and Start Station 46HF	
09:49	Bottom contact 46HF	6°24,095'S, 103°58,922'E Water depth 2008m Cable length 2026m
10:45	Start Station 47HF	
11:50	Bottom contact 47HF	6°25,56'S, 103°57,40'E Water depth 1997m Cable length 1995m
12:47	End Station 47HF	
14:25	Start Station 48FS	
15:13	Start bottom observation 48FS	6°26,55'S, 104°01,12'E Water depth 1872m Cable length 1858m
20:25	End Station 48FS	
21:00	Start Station 49MS	
22:02	Maximum cable length 49MS	6°28,39'S, 104°01,69'E Water depth 2024m Cable length 2015m

23:20	End Station 49MS	
15 Feb 1999		
00:03	Start Profile 139-71	6°22,5'S, 103°57,2'E
00.38	End Profile 139-71 and Start Profile 139-72	6°17,6'S, 104°02,1'E
00:50	End Profile 139-72 and Start Profile 139-73	6°16,1'S, 104°00,8'E
02:52	End Profile 139-73 and Start Profile 139-74	6°31,8'S, 103°46,0'E
03:06	End Profile 139-74 and Start Profile 139-75	6°29,1'S, 103°44,6'E
04:52	End Profile 139-75 and Start Profile 139-76	6°14,9'S, 103°59,2'E
05:02	End Profile 139-76 and Start Profile 139-77	6°13,5'S, 103°57,9'E
06:52	End Profile 139-77 and Start Profile 139-78	6°28,0'S, 103°23,2'E
07:04	End Profile 139-78 and Start Profile 139-79	6°26,5'S, 103°41,6'E
08:11	End Profile 139-79 and Start Profile 139-80	6°17,2'S, 103°51,2'E
09:07	End Profile 139-80	6°24,6'S, 103°58,39'E
09:15	Start Station 50KL	
10:09	Bottom contact 50KL	6°24,63'S, 103°58,39'E Water depth 1874m Cable length 1840m
11:12	End Station 50KL	
12:04	Start Station 51HF	
12:59	Bottom contact 51HF	6°28,49'S, 103°54,41'E Water depth 1910m Cable length 1927m
13:55	End Station 51HF	
14:37	Start Station 52HF	
15:20	Bottom contact 52HF	6°32,65'S, 103°50,12'E Water depth 1691m Cable length 1717m
15:11	End Station 52HF	
16:50	Start Station 53HF	
17:23	Bottom contact 53HF	6°56,03'S, 103°45,77'E Water depth 1119m Cable length 1141m
18:03	End Station 53HF	
18:45	Start Station 54KL	
19:43	Bottom contact 54KL	6°32,64'S, 103°50,12'E Water depth 1692m Cable length 1657m
20:40	End Station 54KL	
21:20	Start Station 55MS	
22:18	Maximum cable length 55MS	6°32,57'S, 103°50,03'E Water depth 1691m Cable length 1687m
23:23	End Station 55MS	
16 Feb 1999		
01:12	Start Station 56MS	

01:25	56 MS plankton sample 250m	6°32,03'S, 103°49,68'E
01:50	End Station 56MS	
02:23	Start Station 57FS	
03:05	Start bottom observation 57FS	6°34,98'S, 103°52,02'E Water depth 1569m Cable length 1558m
08:16	End bottom observation 57FS	6°32,57'S, 103°49,31'E Water depth 1592m Cable length 1640m
08:53	End Station 57FS	
09:25	Start Station 58KL	
10:57	Bottom contact 58KL	6°32,58'S, 103°50,02'E Water depth 1697m Cable length 1660m
12:03	End Station 58KL	
12:20	Start Profile 139-81	6°33,0'S, 103°47,5'E
14:40	End Profile 139-81	6°50,1'S, 103°28,6'E
14:58	Start Station 59KL	6°51,89'S, 103°30,10'E
16:20	Bottom contact 59KL	6°51,87'S, 103°30,08'E Water depth 2654m Cable length 2622m
18:07	End Station 59KL	
18:28	Start Station 60HF	
19:25	Bottom contact 60HF	6°51,87'S. 103°31,07'E Water depth 2655m Cable length 2676m
20:29	End Station 60HF	
21:08	Start Station 61KD	
22:22	Start dredge haul 61KD	6°55,83'S, 103°26,0'E Water depth 2746m Cable length 3400m
00:10	End haul 61KD	6°54,97'S, 103°26,0'E Water depth 2512m Cable length 2940m
01:27	End Station 61KD	
02:00	Start Station 62HF	
02:58	Bottom contact 62HF	6°57,48'S, 103°24,28'E Water depth 2954m Cable length 2975m
04:16	End Station 62HF	
04:33	Start Profile 139-82	6°56,0'S, 103°22,4'E
08:02	End Profile 139-82	7°20,0'S, 102°54,6'E
08:22	Start Station 63KD	
10:34	Bottom contact 63KD	7°23,44'S, 102°56,45'E Water depth 5885m Cable length 6405m
15:42	End Station 63KD	
18:07	Start Station 64HF	
19:55	Bottom contact 64HF	7°39,86'S, 102°40,06'E Water depth 5946m Cable length 5997m
21:56	End Station 64HF	
22:10	Start Station 65MS	
22:20	Plankton sample taken	7°39,87'S, 102°39,91'E Water depth 5946m Cable length 200m

22:38	End Station 65MS	
22:46	Start Profile 139-83	7°39,86'S, 102°40,05'E
18 Feb 1999		
03:24	End Profile 139-83 and Start Profile 139-84	6°59,4'S, 102°06,2'E
04:28	End Profile 139-84	6°50,5'S, 102°15,7'E
04:44	Start 66MS	
07:13	Maximum cable length 66MS	6°51,66'S, 102°15,75'S Water depth 6149m Cable length 6177m
10:05	End Station 66MS	
11:45	Start first attempt for recovery of lost GEOMAR OBH 06	
13:38	Bottom contact drag anchor	6°34,40'S, 102°17,65'E Water depth 3886m Cable length 3888m
15:28	End first attempt	
15:55	Start second attemt	
16:58	Bottom contact drag anchor	6°33,89'S, 102°17,80'E Water depth 3882m Cable length 3902m
20:15	End unsuccessful attempt Start transit to next location west of Pulau Enggano	
03:59	Start small scale survey of Station 67KD	5°11,43'S, 101°55,04'E
0:7:35	End small scale survey	
08:04	Start Station 67KD1	
08:19	Bottom contact 67KD1	5°10,94'S, 101°55,51'E Water depth 699m Cable length 705m
09:33	End Station 67KD1	
09:49	Start Station 67KD2	
10:04	Bottom contact 67KD2	5°10,96'S, 101°55,55'E Water depth 683m Cable length 693m
11:35	End Station 67KD2	
13:10	Start Station 68SL	
13:37	Bottom contact 68SL	5°11,61'S, 101°54,88'E Water depth 699m Cable length 693m
14:06	End Station 68SL	
16:17	Start Station 69HF	
17:03	Bottom contact 69HF	4°59,27'S, 102°07,59'E Water depth 1571m Cable length 1592m
17:45	End Station 69HF	
18:33	Start Station 70MS	
18:44	Plankton sampling 70MS	4°54,26'S, 102°12,74'E Cable length 200m
19:02	End Station 69HF	
19:08	Start Profile 139-85	4°54,23'S, 102°12,70'E
20 Feb 1999		
06:40	End Profile 139-85	6°32,6'S,, 103°50,1E

06:47	Start Station 71MS	
07:50	Maximum cable length 71MS	6°32,47'S, 103°49,85'E Water depth 1697m Cable length 1687m
08:41	End Station 71MS	
09:11	Start Station 72MS	
10:16	Maximum cable lengt 72MS	6°30,00'S, 103°47,999'E Water depth 1741m Cable length 1730m
11:20	End Station 72MS	
11:25	Start HYDROSWEEP test	
13:12	End HYDROSWEEP test	
13:46	Start Station 73MS	
14:45	Maximum cable length 73MS	6°31,16'S, 103°48,96'E Water depth 1734m Cable length 1723m
16:03	End Station 73MS	
16:52	Start Station 74KL	
17:47	Bottom contact 74KL	6°32,58'S, 103°50,02'E Water depth 1691m Cable length 1654m
19:20	End Station 74KL	
19:35	Start Station 75FS	
20:15	Start bottom obsevation 75FS	6°33,79'S, 103°50,05'E Water depth 1509m Cable length 1500m
21 Feb 1999		
01:57	End bottom observation 75FS	6°31,5'S, 103°48,73'E Water depth 1675m Cable length 1678
03:00	End Station 75FS	
06:15	Start Station 76HF	
07:02	Bottom contact 76HF	6°13,92'S, 104°05,82'E Water depth 2199m Cable length 2217m
07:58	End Station 76HF	
08:40	Start Station 77HF	
09:26	Bottom contact 77HF	6°17,43'S, 104°05,78'E Water depth 2187m Cable length 2197m
10:24	End Station 77HF	
11:02	Start Station 78HF	
11:49	Bottom contact 78HF	6°19,97'S, 104°03,01'E Water depth 2171m Cable length 2185m
12:45	End Station 78HF	
14:18	Start Station 79MS	
15:20	Maximum cable length 79MS	6°28,25'S, 103°53,99'E Water depth 1894m Cable length 1880m
17:00	End Station 79MS	
17:08	Start Profile 139-86	6°28,5'S, 103°54,4'E
22 Feb 1999		
03:10	End Profile 139-86 and Start Transit	7°25,0'S, 105°26,5'E

08:40	End Transit	7°57,5'S, 106°17,7°E
08:46	Start Station 80MS	
10:39	Maximum cable length 80MS	7°57,0'S, 106°17,23'E Water depth 2954m Cable length 2950m
12:30	End Station 80MS	
13:20	Start Station 81MS	
14:52	Maximum cable length 81MS	7°57,37'S, 106°18,51'E Water depth 2989m Cable length 2975m
16:42	End Station 81MS	
17:35	Start Station 82MS	
20:05	Maximum cable length 82MS	7°57,51'S, 106°17,78'E Water depth 2946m Cable length 2923m
21:47	End Station 82MS	
22:02	Start Station 83SL	
23:14	Bottom contact 83SL	7°57,44'S, 106°17,67'E Water depth 2944m Cable length 2938m
23 Feb 1999		
00:22	End Station 83SL	
01:05	Start Station 84FS	
02:14	Start bottom observation 84FS	7°57,82'S, 106°17,98'E Water depth 2990m Cable length 3009m
04:28	End bottom observation 84FS	7°56,98'S. 106°16,79'E Water depth 2954m Cable length 3004m
05:33	End Station 64FS	
06:17	Start small scale HS7PS mapping Profile 139-87	7°57,45'S, 106°16,10'E
07:58	End Profile 139-87	7°52,65'S, 106°17,65'E
08:43	Start Station 85HF	
09:49	Bottom contact 85HF	7°57,72'S, 106°17,22'E Water depth 2968m Cable length 2984m
10:56	End Station 85HF	
11:13	Start Station 86HF	
12:12	Bottom contact 86HF	7°57,51'S, 106°17,80'E Water depth 2937m Cable length 2956m
13:25	End Station 86HF	
14:10	Start Station FS	
15:45	End Station FS, optic fibre broken	
16:22	Start Station 87MS	
17:55	Maximum cable length 87MS	7°57,42'S, 106°17,59'E Water depth 2940m Cable length 2934m
19:37	End Station 87MS	
19:50	Start Station 88SL	
21:06	Bottom contact 88SL	7°57,42'S, 106°17,64'E Water depth 2939m Cable length 2937m
22:15	End Station 88SL	

24 Feb 1999		
00:38	Start Station 89FS	
01:39	Start bottom observation 89FS	7°57,46'S, 106°17,73'E Water depth 2939m Cable length 2951m
03::23	End bottom observation 89FS	7°57,38'S, 106°17,23'E Cable length 2944m
04:35	End Station 89FS	
05:14	Start Station 90KD	
06:11	Bottom contact 90KD	7°57,24'S, 106°17,91'E Water depth 2969m Cable length 2800m
06:49	Maximum cable length 90KD	7°57,47'S, 106°17,74'E Water depth 2938m Cable length 3450m
08:33	End Station 90KD	
10:02	Start Station 91GA	
15:24	Sample taken by 91GA	7°57,397'S, 106°17,91'E Water depth 2965m Cable length 2919m
17:00	End Station 91GA	
18:14	Start Station 92GA	
23:34	Sample taken by 92GA	7°57,44'S, 106°17,80'E Water depth 2943m Cable length 2920m
25 Feb 1999		
01:10	End Station 92GA	
02:10	Start Station 93GA	
03:57	Sample taken by 93GA	7°57,43'S, 106°17,58'E Water depth 2942m Cable length 2927m
05:15	End Station 93GA Start Transit to Station 94MS	
10:15	Start Station 94MS	
11:03	Maximum cable length 94MS	7°18,79'S, 105°38'94'E Water depth 2310m Cable length 200m
11:21	End Station 94MS and transit to Sunda Strait resumed	
17:09	Start Station 95MS	
17:20	Maximum cable length 95MS	6°34,02'S, 104°53,98'E Water depth 1891m Cable length 200m
17:39	End Station 95MS	
17:50	Start Station 96KL	
18:56	Bottom contact 96KL	6°34,09'S, 104°54,08'E Water depth 1890m Cable length 1854m
20:04	End Station 96KL	
20:36	Start Station 97HF	
21:18	Bottom contact 97HF	6°34,00'S, 104°53,98'E Water depth 1893m Cable length 1908m
22:16	End Station 97HF	

23:17	Start Station 98HF	
23:58	Bottom contact 98HF	6°25,77'S, 104°51,89'E Water depth 1841m Cable length 1848m
26 Feb 1999		
00:41	End Station 98HF	
01:30	Start Station 99HF	
02:10	Bottom contact 99HF	6°23,55'S, 104°57,97'E Water depth 1396m Cable length 1412m
02:57	End Station 99HF	
03:53	Start Station 100KD	
04:48	Bottom contact 100KD	6°24,91'S, 104°49,24'E Water depth 1573m Cable length 1602m
08:41	End Station 100KD	
10:40	Start Station 101KD	
12:10	Bottom contact 101KD	6°12,98'S, 104°51,78'E Water depth 1512m Cable length 1946m
14:35	End Station 101KD	
15:27	Start Station 102KD	
16:00	Bottom contact 102KD	6°16,99'S, 10449,06'E Water depth 1458m Cable length 1510m
18:15	End Station 102KD End sampling and profiling of Cruise SO139	

Table 2.4: Sampling and Probing statistics

Station Nr.:	Date	Time (UTC) from:	Time (UTC) to:	Position Latitude:	Longitude:	Water depth	Remarks
1 Test	31.01.99	12:00	17:40	9°13,170 S	106°17,360 E	6465 m	
2 MS	31.01.99	20:40		9°13,700 S	106°17,600 E	6467 m	
3 KL	01.02.99	02:39		9°11,100 S	106°19,006 E	6338 m	L = 542 cm
4 KL	01.02.99	12:27		9°10,880 S	106°19,100 E	6238 m	L = 80 cm
5 MS	01.02.99	17:49		9°11,095 S	106°19,037 E	6326 m	
6 KL	02.02.99	05:21		8°22,038 S	106°42,117 E	2139 m	L = 685 cm
7 GA / TVG	02.02.99	10:19		8°16,664 S	106°44,536 E	2954 m	
8 MS	02.02.99	18:33		7°49,079 S	106°57,566 E	2732 m	
9 MS	02.02.99	21:30		7°45,772 S	106°52,587 E	2663 m	
10 KL	03.02.99	05:12		7°49,097 S	106°57,620 E	2726 m	L = 1240 cm
11 KL	03.02.99	12:08		7°50,750 S	106°56,750 E	2798 m	L = 1215 cm
12 MS	03.02.99	15:50		7°47,800 S	106°58,188 E	2649 m	
13 KD	03.02.99	22:50		8°20,074 S	106°46,387 E	2036 m	voll
14 KL	04.02.99	02:38		8°09,153 S	106°48,148 E	3000 m	L = 1319 cm
15 KL	04.02.99	08:15		8°34,000 S	106°36,480 E	2246 m	L = 1248 cm
16 KD	04.02.99	17:30		9°02,056 S	106°22,275 E	4572 m	leer

17 MS	05.02.99	03:20		9°13,988 S	106°23,708 E	6360 m	
18 KL	05.02.99	13:21		8°46,790 S	106°30.260 E	3274 m	L =1200 cm
19 MS	05.02.99	19:26		9°07,004 S	106°29,009 E	5531 m	
20 FS	06.02.99	09:44		9°05,240 S	106°17,310 E	4915 m	abgebrochen
21 KL	07.02.99	00:31		8°01,597 S	106°16,128 E	2994 m	
22 MS	07.02.99	11:10		7°57,668 S	106°17,990 E	3000 m	L = 1185 cm
23 MS	08.02.99	03:51		8°01,603 S	106°16,111 E	2991 m	
24 KL	08.02.99	07:07		8°01,600 S	106°16,090 E	2989 m	L = 1300 cm
25 HF	08.02.99	10:24	10:42	8°01,606 S	106°16,115 E	2998 m	
26 HF	08.02.99	13:40	14:00	8°00,242 S	106°16,732 E	3039 m	
27 HF	08.02.99	16:33	16:48	7°57,670 S	106°17,980 E	3000 m	
28 KD start	08.02.99	22:00		7°57,670 S	106°17,995 E	2946 m	
28 KD stop	09.02.99		00:50	7°56,748 S	106°16,109 E	2946 m	
29 KL	09.02.99	06:15		7°57,665 S	106°17,996 E	2995 m	L = 1312 cm
30 FS start	09.02.99	08:11		7°58,046 S	106°17°346 E	2992 m	
30 FS stop	09.02.99		11:50	7°56,502 S	106°15,446 E	2931 m	
31 KL	09.02.99	15:26		7°57,000 S	106°16,550 E	2952 m	L = 1200 cm
32 MS	09.02.99	18:55		7°58,154 S	106°17,002 E	3005 m	
33 GA start	09.02.99	22:54		7°59,995 S	106°17,306 E	2984 m	
33 GA stop	09.02.99		23:13	7°57,793 S	106°17,200 E	2989 m	
34 KL	10.02.99	02:30		7°59,254 S	106°17,222 E	3021 m	L = 1860 cm
35 HF	10.02.99	06:35		7°59,260 S	106°17,222 E	3021 m	
36 HF	10.02.99	09:24		7°57,600 S	106°16,560 E	2950 m	
(37 KL)	10.02.99	11:30		8°01,600 S	106°16,090 E	2989 m	Lot verloren
37 KL	10.02.99	16:42		8°01,600 S	106°16,090 E	2990 m	L = 1920 cm
38 HF	10.02.99	23:46		8°34,000 S	106°36,471 E	2241 m	
39 HF	11.02.99	03:13	03:30	8°46,800 S	106°30,236 E	3368 m	
40 FS	11.02.99	11:27		8°49,804 S	105°49,177 E	4768 m	
41 HF	11.02.99	19:17		8°24,649 S	106°05,646 E	3181 m	
42 KL	11.02.99	22:49		8°24,640 S	106°05,653 E	3182 m	L = 1764 cm
43 GA	12.02.99	05:16		7°57,449 S	106°17,619 E	2946 m	
44 GA	12.02.99	09:40		7°57,450 S	106°17,710 E	2941 m	
45 MS	14.02.99	01:14		6°24,635 S	103°58,963 E	2008 m	
46 HF	14.02.99	02:55		6°24,094 S	103°58,922 E	2007 m	
47 HF	14.02.99	04:57		6°25,566 S	103°57,401 E	1980 m	
48 FS start	14.02.99	08:15		6°26,500 S	104°01,100 E	1872 m	
48 FS stop	14.02.99		12:39	6°25,740 S	103°57,970 E	1983 m	
49 MS	14.02.99	15:02		6°28,390 S	104°01,680 E	2024 m	
50 KL	15.02.99	03:10		6°24,635 S	103°58,386 E	1875 m	L = 1255 cm
51 HF	15.02.99	06:06		6°28,490 S	103°54,410 E	1910 m	
52 HF	15.02.99	08:26		6°32,650 S	193°50,120 E	1691 m	
53 HF	15.02.99	10:21		6°37,030 S	103°47,770 E	1120 m	
54 KL	15.02.99	12:43		6°32,640 S	103°50,130 E	1692 m	L = 1770 cm
55 MS	15.02.99	15:52		6°32,570 S	103°49,940 E	1690 m	
56 MS	15.02.99	18:30		6°32,030 S	103°49,690 E	200 m	Plankton
57 FS start	15.02.99	20:05		6°34,985 S	103°52,020 E	1567 m	

57 FS stop	16.02.99		01:16	6°35,570 S	103°49,310 E	1590 m	
58 KL	16.02.99	03:56		6°32,581 S	103°50,022 E	1696 m	
59 KL	16.02.99	09:19		6°51,870 S	103°30,080 E	2655 m	L = 1790 cm
60 HF	16.02.99	12:30		6°51,870 S	103°30,080 E	2653 m	
61 KD start	16.02.99	15:10		6°55,967 S	103°25,837 E	2901 m	
61 KD stop	16.02.99		17:25	6°54,977 S	103°26,890 E	2514 m	
62 HF	16.02.99	20:04		6°57,483 S	103°24,288 E	2950 m	
63 KD start	17.02.99	03:38		7°23,437 S	102°56,472 E	6003 m	
63 KD stop	17.02.99		06:41	7°21,472 S	102°56,668 E	5522 m	
64 HF	17.02.99	12:54		7°39,860 S	102°40,060 E	5945 m	
65 MS	17.02.99	15:25		7°39,860 S	102°39,990 E	5946 m	
66 MS	18.02.99	00:13		6°51,667 S	102°15,751 E	6149 m	
67 KD start	19.02.99	01:19		5°10,934 S	101°55,488 E	699 m	
67 KD stop	19.02.99		02:20	5°11,330 S	101°55,500 E	627 m	
67 KD2start	19.02.99	03:04		5°11,021 S	101°55,474 E	683 m	
67 KD2stop	19.02.99		04:13	5°11,090 S	101°55,432 E	635 m	
68 SL	19.02.99	06:39		5°11,600 S	101°54,890 E	698 m	
69 HF	19.02.99	10:02	10:16	4°59,270 S	102°07,690 E	1569 m	
70 MS	19.02.99	11:33		4°54,300 S	102°12,670 E	1741 m	Plankton
71 MS	20.02.99	00:50		6°32,478 S	103°49,851 E	1696 m	
72 MS	20.02.99	03:16		6°30,006 S	103°47,995 E	1741 m	
73 MS	20.02.99	07:57		6°31,161 S	103°48,970 E	1734 m	
74 KL	20.02.99	10:47		6°32,580 S	103°50,020 E	1690 m	L = 1975 cm
75 FS start	20.02.99	13:15		6°33,791 S	103°50,007 E	1510 m	
75 FS stop	20.02.99		18:57	6°31,505 S	103°48,739 E	1675 m	
76 HF	21.02.99	00:02		6°13,932 S	104°09,505 E	2201 m	
77 HF	21.02.99	02:26		6°17,432 S	104°05;782 E	2187 m	
78 HF	21.02.99	04:48		6°19,967 S	104°03,018 E	2171 m	
79 MS	21.02.99	08:20		6°28,250 S	103°53,990 E	1893 m	
80 MS	22.02.99	03:30		7°57,028 S	106°17,254 E	2933 m	
81 MS	22.02.99	07:53		7°57,360 S	106°18,520 E	2990 m	
82 MS	22.02.99	11:40		7°57,480 S	106°17,750 E	2940 m	
83 SL	22.02.99	16:13		7°57,440 S	106°17,160 E	2945 m	L = 44 cm
84 FS start	22.02.99	19:14		7°57,820 S	106°17,980 E	2989 m	
84 FS stop	22.02.99		21:30	7°56,780 S	106°16,790 E	2956	
85 HF	23.02.99	02:46		7°57,720 S	106°17,223 E	2966	
86 HF	23.02.99	05:11		7°57,506 S	106°17,796 E	2935	
87 MS	23.02.99	10:56		7°57,430 S	106°17,590 E	2944	
88 SL	23.02.99	14:06		7°57,420 S	106°17,660 E	2939	L = 457 cm
89 FS start	23.02.99	18:42		7°57,470 S	106°17,710 E	2937	
89 FS stop	23.02.99		20:24	7°57,390 S	106°17,250 E	2937	
90 KD start	23.02.99	23:25		7°57,465 S	106°17,795 E	2954	
90 KD stop	24.02.99		00:20	7°57,630 S	106°17,450 E	2961	
91 GA	24.02.99	08:24		7°57,400 S	106°17,900 E	2963	
92 GA	24.02.99	16:35		7°57,450 S	106°17,810 E	2934	
93 GA	24.02.99	20:57		7°57,430 S	106°17,580 E	2952	
94 MS	25.02.99	04:05		7°57,824 S	105°38,973 E	2308	Plankton
95 MS	25.02.99	10:20		6°34,030 S	104°53,990 E	1892	Plankton

96 KL	25.02.99	11:56		6°34,090 S	104°54,080 E	1891	
97 HF	25.02.99	14:18		6°33,970 S	104°53,990 E	1892	
98 HF	25.02.99	16:58		6°25,870 S	104°51,860 E	1840	
99 HF	25.02.99	19:10		6°23,559 S	104°57,976 E	1398	
100 KD start	25.02.99	21:51		6°24,913 S	104°49,240 E	1557	
100 KS stop	26.02.99		01:17	6°24,733 S	104°47,752 E	1119	
101 KD start	26.02.99	04:42		6°12,910 S	104°51,780 E	1494	
101 KD stop	26.02.99		06:52	6°12,903 S	104°52,074 E	1156	
102 KD start	26.02.99	08:58		6°17,010 S	104°49,080 E	1471	
102 KD stop	26.02.99		10:47	6°16,992 S	104°48,461 E	1222	

Table 2.5: HYDROSWEEP & PARASOUND Profile statistics

Profile Nr.:	Date	Time (UTC) from:	to:	Position Latitude	Longitude	Water depth/m	Heading
PR001	30. Jan	17:01		S 6:23,8242	E 105:08,4798	303	250,3
			18:19	S 6:30,8298	E 104:57,6084	1380	157,2
PR002	30. Jan	18:20		S 6:31,0098	E 104:57,6786	1378	158,8
			18:41	S 6:34,9560	E 104:58,9530	1577	210,3
PR003	30. Jan	18:42		S 6:35,0898	E 104:58,8588	1590	216,0
			21:01	S 6:53,7672	E 104:43,5582	1891	220,5
PR004	30. Jan	21:02		S 6:53,9022	E 104:43,4484	1905	217,3
			23:56	S 7:19,9944	E 104:58,0986	2385	152,2
PR005	30. Jan	23:57		S 7:20,1432	E 104:58,1724	2391	154,4
	31. Jan		8:11	S 8:46,4676	E 105:42,1584	5203	154,9
PR006	31. Jan	8:12		S 8:46,5966	E 105:42,3018	5317	120,3
			11:53	S 9:13,6452	E 106:17,5182	6463	126,8
PR007	31. Jan	23:32		S 9:13,4988	E 106:17,7084	6460	33,0
			23:50	S 9:11,2182	E 106:18,9594	6371	26,9
PR008	1. Feb	5:39		S 9:11,3184	E 106:19,2600	6323	117,9
			6:04	S 9:14,0316	E 106:23,2422	6403	126,1
PR009	1. Feb	6:07		S 9:13,8900	E 106:23,6322	6385	9,5
			7:27	S 8:59,3712	E 106:29,3736	4102	20,2
PR010	1. Feb	7:28		S 8:59,1798	E 106:29,3910	4092	354,9
			8:19	S 8:54,9840	E 106:20,9832	4116	295,1
PR011	1. Feb	8:20		S 8:55,0164	E 106:20,8434	4139	222,8
			9:32	S 9:06,7434	E 106:14,8500	5661	208,3
PR012	1. Feb	9:33		S 9:06,9078	E 106:14,8254	5716	162,7
			10:03	S 9:10,8972	E 106:19,1220	6228	133,6

PR013	1. Feb	20:55		S 9:10,9722	E 106:19,1682	6247	39,2
			22:17	S 8:59,3460	E 106:29,1840	4132	40,7
PR014	1. Feb	22:18		S 8:59,1960	E 106:29,3142	4100	40,1
	2. Feb		2:30	S 8:14,6580	E 106:48,7656	3054	23,3
PR015	2. Feb	2:31		S 8:14,5176	E 106:48,7566	3035	322,4
			3:08	S 8:12,5208	E 106:43,0314	3071	277,6
PR016	2. Feb	3:10		S 8:12,7692	E 106:42,9396	3078	173,8
			4:00	S 8:22,0332	E 106:42,1404	2140	186,9
PR017	2. Feb	11:43		S 8:16,5384	E 106:44,4828	3037	338,0
			12:11	S 8:12,7068	E 106:43,2150	3073	325,3
PR018	2. Feb	12:13		S 8:12,4572	E 106:43,0920	3072,0	344,8
			15:41	S 7:39,2454	E 106:58,8366	2171	27,0
PR019	2. Feb	15:49		S 7:38,9148	E 106:59,5158	1952	205,8
			16:44	S 7:48,5226	E 106:57,9042	2683	187,8
PR020	2. Feb	20:01		S 7:49,1214	E 106:57,3924	2734	294,5
			20:35	S 7:45,8268	E 106:52,7034	2673	304,7
PR021	2. Feb	21:56		S 7:45,7398	E 106:52,5354	2658	202,7
	3. Feb		0:23	S 8:10,9554	E 106:41,0172	3062	203,6
PR022	3. Feb	0:24		S 8:11,1066	E 106:40,9164	3065	223,4
			0:39	S 8:10,5642	E 106:38,5164	3068	300,6
PR023	3. Feb	0:40		S 8:10,4766	E 106:38,3682	3069	301,3
			3:12	S 7:44,6394	E 106:50,4786	2569	22,6
PR024	3. Feb	6:45		S 7:48,7284	E 106:57,6318	2710	38,5
			7:36	S 7:48,1962	E 107:07,1850	2344	93,8
PR025	3. Feb	7:38		S 7:48,4032	E 107:07,4670	2330	160,6
			9:14	S 8:04,6812	E 107:01,3182	3086	200,6
PR026	3. Feb	17:47		S 7:52,5102	E 106:59,0688	2778	168,8
			19:18	S 8:08,0010	E 106:52,7094	3073	202,3
PR027	3. Feb	19:19		S 8:08,1726	E 106:52,6320	3072	207,4
			20:17	S 8:17,9226	E 106:47,9490	3195	204,8
PR028	4. Feb	4:48		S 8:12,4932	E 106:43,1028	3070	227,3
			6:49	S 8:32,3124	E 106:33,7428	2139	205,7
PR029	4. Feb	9:42		S 8:32,4726	E 106:33,6852	2087	217,1
			13:09	S 9:05,1642	E 106:13,9494	6018	214,0
PR030	4. Feb	21:45		S 9:08,7600	E 106:22,2540	4975	152,8
			22:50	S 9:13,7442	E 106:33,9090	5722	113,7
PR031	4. Feb	22:51		S 9:13,8174	E 106:34,0866	5757	111,8
			23:26	S 9:19,3206	E 106:31,9032	6348	203,4

PR032	4. Feb	23:27		S 9:19,4724	E 106:31,8162	6345	220,0
	5. Feb		0:34	S 9:14,2050	E 106:21,3870	6466	294,2
PR033	6. Feb	0:28		S 9:02,4642	E 106:14,7900	5249	289,7
			2:43	S 9:01,0128	E 105:51,1230	6437	271
PR034	6. Feb	2:44		S 9:00,9864	E 105:50,9496	6437	294,6
			3:36	S 8:52,7352	E 105:56,8242	5110	34,8
PR035	6. Feb	3:36		S 8:52,7352	E 105:56,8242	5110	34,8
			4:13	S 8:56,9430	E 106:02,3508	5685	133,5
PR036	6. Feb	4:14		S 8:57,0240	E 106:02,5218	5372	95,3
			5:38	S 8:57,9870	E 106:19,8114	4035	100,7
PR037	6. Feb	13:25		S 8:58,2336	E 106:13,6086	4568	289,1
			18:30	S 8:08,0832	E 106:20,9808	2323	16,6
PR038	6. Feb	18:31		S 8:07,9158	E 106:21,0336	2320	18
			19:56	S 7:56,0742	E 106:26,1084	3046	347,2
PR039	6. Feb	19:57		S 7:56,0166	E 106:26,0592	3051	308,6
			20:36	S 7:53,9190	E 106:23,0886	3026	306,9
PR040	6. Feb	20:37		S 7:53,8782	E 106:23,0298	3025	301,2
			22:23	S 8:05,6382	E 106:17,3874	2278	200,9
PR041	6. Feb	22:24		S 8:05,7720	E 106:17,3286	2273	205,8
			23:01	S 8:01,8132	E 106:16,2078	no data	353,7
PR042	7. Feb	2:11		S 8:01,1520	E 106:16,6596	no data	285,1
			2:54	S 8:02,9328	E 106:11,8806	2271	257,1
PR043	7. Feb	2:55		S 8:02,9364	E 106:11,7666	2274	293,6
			4:14	S 7:51,7002	E 106:16,8972	2969	28,9
PR044	7. Feb	4:15		S 7:51,5580	E 106:16,9686	2970	25
			4:43	S 7:50,0286	E 106:13,6146	2935	297,4
PR045	7. Feb	4:44		S 7:49,9854	E 106:13,4910	2939	278,4
			6:04	S 8:01,3968	E 106:08,4762	no data	203,5
PR046	7. Feb	14:29		S 8:01,5402	E 106:08,4924	6359	228,6
			17:13	S 8:24,0612	E 105:56,4948	3374	206,5
PR047	7. Feb	17:14		S 8:24,2064	E 105:56,4180	3400	208,1
			17:35	S 8:26,0640	E 105:59,5416	3305	33
PR048	7. Feb	17:36		S 8:25,9326	E 105:59,5992	3288	21,6
			20:00	S 8:03,3870	E 106:11,4864	2251	28,3
PR049	7. Feb	20:01		S 8:03,2274	E 106:11,5686	2242	29,2
			20:34	S 8:06,0528	E 106:17,1816	2268	178,2
PR050	7. Feb	20:35		S 8:06,1824	E 106:17,1450	2262	197,1
			22:59	S 8:27,5850	E 106:07,2894	3230	204,3

PR051	7. Feb	23:11		S 8:27,8628	E 106:07,2636	3223	356,8
	8. Feb		1:21	S 8:08,3094	E 106:20,7876	2314	34,3
PR052	8. Feb	17:56		S 7:57,6120	E 106:18,0966	2998	274,5
			18:24	S 7:56,5836	E 106:15,1422	2921	290,2
PR053	8. Feb	18:25		S 7:56,5380	E 106:15,0162	2922	289
			18:33	S 7:55,8186	E 106:15,1836	2946	97,3
PR054	8. Feb	18:34		S 7:55,8612	E 106:15,3084	2947	110,5
			19:14	S 7:57,9930	E 106:20,5980	2995	109,7
PR055	8. Feb	19:15		S 7:58,0464	E 106:20,7306	3014	112,8
			19:46	S 7:58,4352	E 106:25,0644	3043	110,7
PR056	8. Feb	19:47		S 7:58,5120	E 106:25,1676	3043	145,2
			19:54	S 7:59,1510	E 106:24,8172	3042	275,3
PR057	8. Feb	19:55		S 7:59,1486	E 106:24,7080	3041	265,5
			20:24	S 7:58,7094	E 106:21,0246	3009	279,9
PR058	8. Feb	20:25		S 7:58,6926	E 106:20,8914	3007	274,7
			20:54	S 7:57,5778	E 106:17,9910	2979	63,8
PR059	10. Feb	19:00		S 8:01,5924	E 106:16,2312	2995	228,8
			22:28	S 8:34,0428	E 106:36,5130	2246	146,6
PR060	11. Feb	4:39		S 8:46,7598	E 106:30,2490	3370	215,9
			8:35	S 8:50,2044	E 105:50,2146	4667	254,2
PR061	11. Feb	13:26		S 8:48,1284	E 105:48,5166	5697	40,4
			17:32	S 8:25,2816	E 106:00,8664	3258	28,2
PR062	12. Feb	11:44		S 7:57,2244	E 106:16,8216	2950	316
			21:02	S 6:50,9418	E 104:58,3272	1457	314,6
PR063	13. Feb	14:35		S 6:15,4824	E 104:17,1708	1746	270,7
			17:35	S 6:37,8774	E 103:53,1732	1570	231,6
PR064	13. Feb	17:36		S 6:37,8942	E 103:53,0154	1559	280,3
			17:47	S 6:36,5616	E 103:51,5796	1462	316
PR065	13. Feb	17:49		S 6:36,2616	E 103:51,6018	1468	45,7
			19:33	S 6:22,0050	E 104:06,8382	2177	313,7
PR066	13. Feb	19:34		S 6:21,9048	E 104:06,7176	2178	310,9
			19:43	S 6:20,8728	E 104:05,4828	2172	251,7
PR067	13. Feb	19:44		S 6:20,9634	E 104:05,3700	2176	231,8
			21:39	S 6:34,7484	E 103:50,0310	1393	257,9
PR068	13. Feb	21:40		S 6:34,6848	E 103:49,9044	1388	313,3
			21:58	S 6:32,4246	E 103:47,7102	1464	336,6
PR069	13. Feb	21:59		S 6:32,2674	E 103:47,7480	1483	29,3
			23:07	S 6:22,3614	E 103:57,3498	2000	54,5

PR070	13. Feb	23:09		S 6:22,3698	E 103:57,7014	2018	125,6
			23:25	S 6:24,0702	E 103:58,9356	2009	186,5
PR071	14. Feb	17:04		S 6:22,5702	E 103:57,2628	1985	357,8
			17:40	S 6:17,5800	E 104:02,0016	2174	353,5
PR072	14. Feb	17:41		S 6:17,4480	E 104:01,9140	2172	320,2
			17:50	S 6:16,2114	E 104:00,8268	2175	291,3
PR073	14. Feb	17:51		S 6:16,2456	E 104:00,6948	2172	229,2
			19:51	S 6:31,6302	E 103:46,1844	1420	223,6
PR074	14. Feb	19:52		S 6:31,7202	E 103:46,0440	1421	255,3
			20:09	S 6:29,1534	E 103:44,7030	1540	0
PR075	14. Feb	20:10		S 6:29,0232	E 103:44,8020	1579	32
			21:52	S 6:15,0492	E 103:59,0238	2168	33,9
PR076	14. Feb	21:53		S 6:14,8770	E 103:59,0178	2172	345,7
			22:02	S 6:13,5864	E 103:57,9108	2169	278,7
PR077	14. Feb	22:03		S 6:13,6416	E 103:57,7638	2169	228
			23:52	S 6:27,9114	E 103:43,3266	1569	225,7
PR078	14. Feb	23:53		S 6:28,0044	E 103:43,1742	1523	253,9
	15. Feb		0:04	S 6:26,6520	E 103:41,7630	1579	312,5
PR079	15. Feb	0:05		S 6:26,5290	E 103:41,6274	1589	317,3
			1:10	S 6:17,4696	E 103:50,9196	1934	45,8
PR080	15. Feb	1:11		S 6:17,3352	E 103:51,0588	1944	46,6
			2:07	S 6:24,5898	E 103:58,3416	1878	137,6
PR081	15. Feb	5:20		S 6:28,4862	E 103:54,4098	1911	255,7
			7:39	S 6:32,6616	E 103:50,1450	1692	296,2
PR082	16. Feb	21:34		S 6:56,2554	E 103:22,6878	2893	295,4
	17. Feb		1:02	S 7:20,0280	E 102:54,5616	5535	227,7
PR083	17. Feb	15:46		S 7:39,8874	E 102:40,2144	5953	9,4
			20:24	S 6:59,4606	E 102:06,3288	6050	355,3
PR084	17. Feb	20:25		S 6:59,3028	E 102:06,4098	6062	46,6
			21:28	S 6:50,6328	E 102:15,5526	6137	46,7
PR085 A	18. Feb	21:00		S 5:11,4372	E 101:55,0326	664	335,5
	19. Feb		0:35	S 5:13,4034	E 101:54,1290	739	229,2
PR085	19. Feb	12:08		S 4:54,2676	E 102:12,8322	1744	122,3
			23:41	S 6:32,4846	E 103:50,0034	1698	136,9
PR086	21. Feb	10:08		S 6:28,3614	E 103:54,2850	1903	122,5
			19:59	S 7:24,9516	E 105:26,4264	2344	121,7
PR087	23. Feb	0:05		S 7:57,5634	E 106:17,8974	2959	351,9
			1:10	S 7:57,6048	E 106:17,6298	2943	153,5

3. Navigation, bathymetry, and high-resolution acousto-stratigraphy

U. Jürgens, Ibrahim Lakoni, Eko Triarso, and Udrekh

In addition to the already existing data of the previous cruises SO-137 and SO-138 more than 3000 line kilometres on 87 profiles (Table 2.5 and Fig. 2.2) were obtained with HYDROSWEEP (HS) swath mapping and PARASOUND (PS) acousto-stratigraphic measurements.

3.1 Methods

3.1.1 Navigation

Onboard RV Sonne the differential GPS (DGPS) system SkyFix by RACAL SURVEY is installed. Data from several reference stations (Jakarta, Singapore and Darwin) are processed at an onshore based station and corrected values are broadcasted via INMARSAT satellites to the user. For calculations of DGPS positions on board the special software package MultiFix receives the signals from a special recorder and from the GPS receiver Trimble 4000 DS. Mean error for final positions is supposed to be less than 5 m.

All navigation data refer to the GPS antenna on the main mast of the vessel and are given in the WGS 84 co-ordinate system.

3.1.2 HYDROSWEEP swath mapping

For continuous bathymetric profiling the multibeam swath mapping HYDROSWEEP (HS) system made by KRUPP ATLAS ELEKTRONIK GmbH (Bremen) was used. It measures the water depth by using 59 preformed sound beams - one central vertical beam and 28 beams to each side - with a total opening angle of 90 degrees covering an area of about twice the water depth, i.e. at a water depth 5000 m a swath 10.000 m wide is mapped. The central beam measures depths up to 10.000 m with an error of 1% and the outer beams reaches depths up to 7000 m. The frequency is set to 15.5 kHz. The system compensates roll up to 20 degrees, pitch up to 10 degrees and heave up to plus/minus 5 m. At certain intervals the measurements are calibrated in longitudinal direction. Depth accuracy is about 0.3% i.e. at a water depth of 5000 m the depth is precise within 30 m.

The sound velocity in water was set first to 1500 m/s, making use of regular along track soundings for calibration to determine an average sound velocity profile. Later this sound profile was changed according to velocity measurements made during the first deep CTD sampling (Fig. 3.1).

The data are stored on magnetic tapes and on optical discs. For processing purposes of HS data the ATLAS HYDROMAP software is installed onboard. Merging navigational, depth, positions of the footprint of the beams and by removing artefacts and erroneous datapoints a digital terrain model (DTM) is generated.

3.1.3 PARASOUND acousto-stratigraphic profiling

For acousto-stratigraphic surveys FS SONNE is equipped with the low frequency echosounder system PARASOUND (PS), manufactured by KRUPP ATLAS ELEKTRONIK GmbH (Bremen).
The low frequency range of 2.5 to 5.5 kHz for this sub-bottom-profiler is generated by a so called parametric effect by emitting two higher primary frequencies of 18 and 23.5 kHz simultaneously.
The low frequency results in a deeper penetration and higher resolution than other echosounders. During this cruise the frequency was set to 4.0 kHz. The beam width is 4.5 degrees. Roll, pitch and heave are compensated. Depth range can be set to distinct recording ranges for example between 2000 and 5000 m water depth. Also the gain can be customised to prevailing reflectivity. The penetration and resolution of the upper-most sedimentary section depends largely on acoustic impedance differences and the morphology of the sea bottom. Penetration of up to 150 m can be recorded. If the inclination of the sea bottom is more than 2 (4) degrees no reflection signal will be recorded and limits therefore the applicability of this method.

The results are displayed on a colour screen as well as on paper of the two-channel recorder Atlas DESO. Ship's data, position and time are also included in the data set. To this unit a PARADIGMA display unit is connected, which displays the sea bottom and layers albeit with higher vertical exaggeration on a screen and on a colour printer.

Only in moderately inclined areas a sub-bottom signal was recorded that could be used to derive sub seafloor acousto-stratigraphic information. Therefore the application of PARASOUND was useful only in the flat-bottomed Java Trench and fore arc basins, and small slope basins within the accretionary wedge. Elsewhere the recording with the PARASOUND system was limited, partially non existent, especially the accretionary wedge and the margins of the fore arc basins remain almost not interpretable in this respect.

The PARASOUND records display a depth range of 200 m. Vertical exaggeration lies between 20 to 30 times.

3.2 Areas of hydro-acoustic surveys

In addition to the collection of hydroacoustic data for the filling of gaps left by the preceding cruises SO 137 and 138, detailed surveys with PS and HS were carried out in areas where venting of methane-laden fluids was expected according to the reflection seismic profiles. South of West Java detailed surveys focused on the accretionary wedge and the southern part of the South Java (forearc) Basin, including the anticline associated to the major strike-slip fault which runs parallel to the basin axis. South of Sumatra the survey targets were the outer arc high and the southern part of the Bengkulu (forearc) basin.Technical data of all profiles are given in Table 2.5.

3.3 Shipboard analysis of hydroacoustic data

HYDROSWEEP data were processed onboard with the installed MB software and conversion to depth was made by complete ray tracing through the different water layers using a sound velocity profile derived from CTD measurements (Fig. 3.1). Edited sweeps were assembled, gridded, and contoured. Data from cruise SO-137 and SO-138 were also incorporated. The scales of resulting maps range from 1:200.000 to 1:20.000. Mainly the

maps with scales of 1:50.000 or 1:100.000 were used for interpretation. Contour interval for detailed maps was set to 10 m, for reconnaissance maps to 50 or 100 m.
All maps are listed in Table 3. 1.

3.4 Preliminary results

The survey area of Cruise SO 139 is tectonically very active. Compressional stress prevails, **Forearc basins** (FAB's) are well developed, forming a mid-slope terrace south of West-Java and south of southeastern Sumatra. At the southern approaches to the Sunda Strait a typical forearc basin is missing, a complex fault system is seen instead. Basin widths vary and can reach as much as 100 km. Water depth in the FAB off Java is more than 3000 m and is around 2000 m off Sumatra. Both FAB's are filled with sediments up to 7 kilometres. The youngest sediments are of hemipelagic nature. Seafloor-parallel bedding can be discerned from the reflection seismic profiles. Few slump structures as well as sandwave and contourite structures can also be observed in these profiles.

In both areas of the FAB's a major strike-slip fault runs parallel to the basin axes. It is marked in the seismic profiles by a large anticline.

The **accretionary complex** (AW) is about 100 km wide. It culminates at water depths of less than 2000 m south of West Java and to less than 500 m south of southeastern Sumatra. This outer arc high (OAH) emerges in places to form an island chain. Its most southeasterly member is Enggano. In some places the northern slope of the OAH is steep, in other areas not very pronounced in the bathymetry. According to interpretations from the seismic profiles the OAH may be underlain by a splinter of oceanic crust and is covered by a thick sedimentary layer. Many sub-ridges and troughs are developed, more or less parallel to the crest of the OAB and extend for many kilometres. Further down the AW the sedimentary cover becomes thin or restricted to intra-slope basins. In some areas the upper part of this section is developed as a terrace with only minor differences in depth.

Another distinct section of the AW is the inner trench wall. Except for the few intra-slope basins this part is more or less devoid of sediments. Morphologically two parts can be distinguished, firstly the main descent and a frontal upthrusted ridge. Two bent coring barrels prove the lack of a soft sediment cover in that area (see Chapter 5).

The **Sunda Trench** (ST) marks the deepest part of the survey area. Water depths are more than 6500 m off Java and more than 6000 m off Sumatra. The trench is filled with sediments with thicknesses of only a couple of hundred meters. The trench stretches all the way from Java to Sumatra with an peculiar inward bending towards the islands in the area of the Sunda Strait, indicating inter alia a change in in the obliquity of the subduction.

The outer slope south of the trench is characterised by a structural high.

3.4.1 Forearc Basins

3.4.1.1 Forearc basin south of West Java (South Java Basin)

Of special interest was the southern part of the basin and especially the area immediately north of the comparatively steep slope of the outer arc high, which descends from a water depth of 2300 to more than 3000 m (Fig. 3.2 and Fig. 3.3). The slope is dissected by valleys. The irregular shape of the slope may be a result of faulting.

The floor of the basin lies in water depths around 3000 m and shows an undulating low relief with troughs and ridges. Some of them are associated with sand waves especially in the western part of the basin. Moderately inclined bedding seems to be typical in this area. In the southern part the floors of the troughs are more or less flat, and sediments have been deposited almost horizontally.

At the lower continental slope of Java the seafloor has a more pronounced relief formed by sand waves or contourite bodies. Further to the north the slope rises stepwise.

Fig. 3.4 shows a PARASOUND recording over a step of about 70 m height within the southern part of the basin. Below the flat-lying uppermost sediments of about 15 m thickness an old erosional surface can be seen in the northern part of this section. Below this surface irregular bedding prevails. In the southern, deeper part the beds are inclined to the south. At this part of seismic line SO137-03 the seismic recordings show a small reversal fault reaching the seafloor. This step in sea-bed morphology might be the expression of this subsurface fault.

3.4.1.2 Snails and Mussels Hill (SMH)

A special survey was carried out to define small-scale bathymetric features of an ENE-WSW trending asymmetric ridge about 10 km north of the OAH (Fig. 3.3). Its highest elevation is little less than 2940 below sea level. The ridge crest is undulating and rises about 50 to 60 meters above the surrounding seafloor. It is 1 to 3 km wide. At a depth of 2950 m the width is 900 m.

This ridge is underlain by a pronounced anticline which possibly started forming during the Late Miocene compressional phase when the accretionary wedge underwent considerable upthrust to the north and backstopping. The compression was continuous over a long time span as onlapping sedimentary layers on both flanks of the anticline suggest. Even the youngest sediments lap on to the anticline structure. The anticline seems to be slightly asymmetric, overturned to the north. In the reflection seismic profile the axial part of the anticline shows disturbed layering. This is obviously the result of transverse faulting. The conspicuous subsurface structure is named **Palung Java Fault (PJF).**

In the PARASOUND cross section (Fig. 3.5) the intense disturbance of the upper sedimentary layers by the fault is clearly visible. Along-strike the ridge seems to be portioned by north-south trending lows. The strike of the ridge axis varies from segment to segment.

3.4.1.3 Bengkulu (forearc) Basin off Sumatra

The greatest water depth of the Bengkulu (forearc) Basin is slightly more than 2000m. The basin is bounded in the south by the OAH, which rises from 1900 m at the basin floor to 1400 m waterdepth. A detailed HS and PS survey over the southern part of the basin and northern slope of the OAH was carried out close to reflection seismic line SO137-06. A part of the detailed bathymetric map generated by this survey is shown in Fig. 3.6.

Similar to the situation south of Java (see seismic line SO137-01, Fig. 3.2) two anticlines are seen in the subsurface of the forearc basin on seismic line SO137-06 (Fig. 3.7). The anticlinal structure closest to the OAH is less developed. The other one lies at a distance of about 25 km from the OAH and shows a disturbed layering in its axial part. It is the south-eastern prolongation of the dextral strike-slip Mentawai Fault. Like the anticline south of Java it forms a ridge. This ridge, named **Semangka Ridge**, divides the fore arc basin into

an elevated and narrower sub-basin in the southwest and a wider, deeper basin in the northeast.

The ridge crest undulates along-strike (Fig. 3.6). To the northwest the ridge becomes narrower and shallower (1811 m). The elevated southern part of the basin also changes its relief. In the southeast it is a small basin, with a central ridge representing the south-westerly compressional structure. To the NW this ridge gets less obvious and terminates in a broad anticline. Other small ridges appear, many of them with indications of faulting in the subsurface. These features merge with the southern margin of the FAB. The floor of this sub-basin rises in northwesterly directions from 2038 m to about 1840 m. Beside gradual changes in slope angle there are places where steep escarpments separate basin and ridge.

PARASOUND records show that the slope of the OAH is dissected by small valleys. The FAB just in front of the OAH is filled with a well stratified sedimentary sequence. In places contourites are visible in the PS records (Fig. 3.8). At the toe of the OAH slope slumps occur.

3.4.2 Accretionary Wedge

The **accretionary wedge** (AW) can be divided into hydro-acoustic type sections. Following the rise from the trench floor the slope shows steps, presumably caused by individual thrust sheets. While in the lower part no major sedimentary cover above the thrust sheets can be observed, many graben-like features are seen at the middle and upper slope. Irregular troughs and ridges dominate the bathymetry of the accretionary wedge. Halfgrabens and grabens are situated between steeply rising ridges. On the lower, steeper part of the AW almost no internal reflection signals were observed.
The grabens and halfgrabens are filled with sediment. In the upper, northeastern part of the wedge slope they become 1.5 seconds (two-way-travel time) thick.

The generation of the present morphology of the AW took mainly place in Late Miocene, when compression increased and the uplift of the thrusted sediments accelerated.

The surface of the youngest part of the AW – the toe and the first thrust sheet - is dissected in a very irregular manner. Narrow troughs alternate with small ridges. Depressions with up to 2 km width with only minor sedimentary fill were observed. Slumps in the basinal areas are common.

3.4.2.1 Accretionary wedge south of West Java

A representative example of the lower part of the sediment covered sections of the AW is shown in Fig. 3.9. Ridges and troughs of variegated size and fill are common. Remains of slumps are situated at the toe of the next ridge. In the northern part a small trough with regular and flat sediments occurs.

3.4.2.2 Accretionary wedge south of southeastern Sumatra

To investigate the nature of the outcropping rocks of the high rising OAH a densely spaced survey (line SO139-85a) was run northwest of the island of **Enggano**, parallel to seismic line SO137-09A (Fig. 3.10) The PS data reveal an undulating seafloor at water depths between 700 to 800 m with irregular small ridges and troughs (Fig. 3.11). The seafloor reflector is thin but strong, presumably representing a hard layer. It is underlain by an

acoustically transparent zone. Only below the transparent zone bedding is indicated, partly inclined. Testing by gravity coring identified this topmost layer to be a hardened layer of fossiliferous calcareous sandstone.

Again as is the case south of Java the accretionary wedge shows a rather dissected appearance in cross-section. Troughs form graben-like features with a sedimentary fill of substantial thickness in the upper part whereas depressions are reduced in number in the lower part and lack a sediment fill.

The front of the accretionary wedge is very irregularly shaped, with many canyons, probably due to faults which are striking more or less perpendicular to the deformation front. Many slopes are steep and the stepwise descent of the wedge indicates structures with block rotational movement.

3.4.3 Sunda Trench

The water depth of the trench floor is more than 6500 m S of Java and more than 6000 m SW of Sumatra. The trench floor is undulated. At the trench floor penetration of PS signals is often more than 50 m.

3.4.4 The Krakatau in the Sunda Strait

In water depths of 40 to 60 m the PARASOUND system delivered clear images of the rough sea bottom as well as the incoherent stratification of the uppermost 20 to 30 m of the sedimentary section. A cut-and-fill seismo-stratigraphic system prevails, indicating sea level fluctuations during the drowning of the Sunda shelf after deglaciation. Off the volcano **Krakatau** the rugged seabed suggests the presence of volcanic debris and flows (Fig. 3.12).

Tab. 3.1 Bathymetric Maps			Cruise SO-139	
No	**Region**	**Area**	**Scale**	**Contour Interval**
	S of W-Java			
1	"	GINCO3-East	1:750.000	50 & 100 m
2	"	Drift	1:100.000	10 m
3	"	Forearc Ridge	1:100.000	10 m
4	"	Accretionary Wedge	1:150.000	10 m
5	OFOS 30 FS	Snails and Mussels Hill	1:20.000	10 m
6	OFOS 84 FS	Snails and Mussels Hill	1:20.000	10 m
7	OFOS 89 FS	Snails and Mussels Hill	1:20.000	10 m
	S of SE-Sumatra			
8	"	GINCO3-West	1:750.000	50 & 100 m
9	OFOS 48 FS	Forearc Basin	1:50.000	10 m
10	OFOS 57 FS	Forearc Basin	1:50.000	10 m
12	OFOS 75 FS	Forearc Basin	1:50.000	10 m

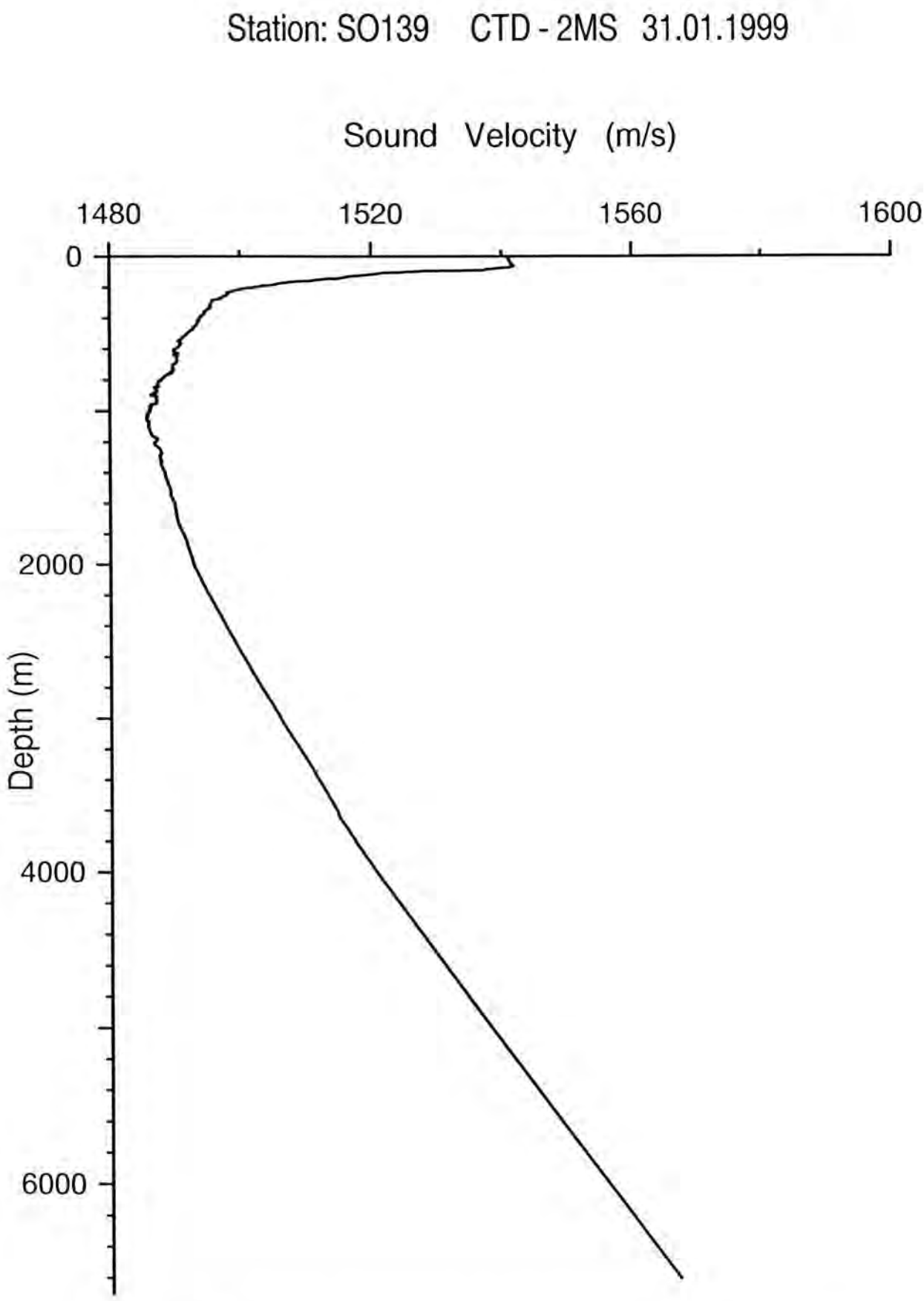

Fig. 3.1 Velocity determination for HYDROSWEEP data acquisition

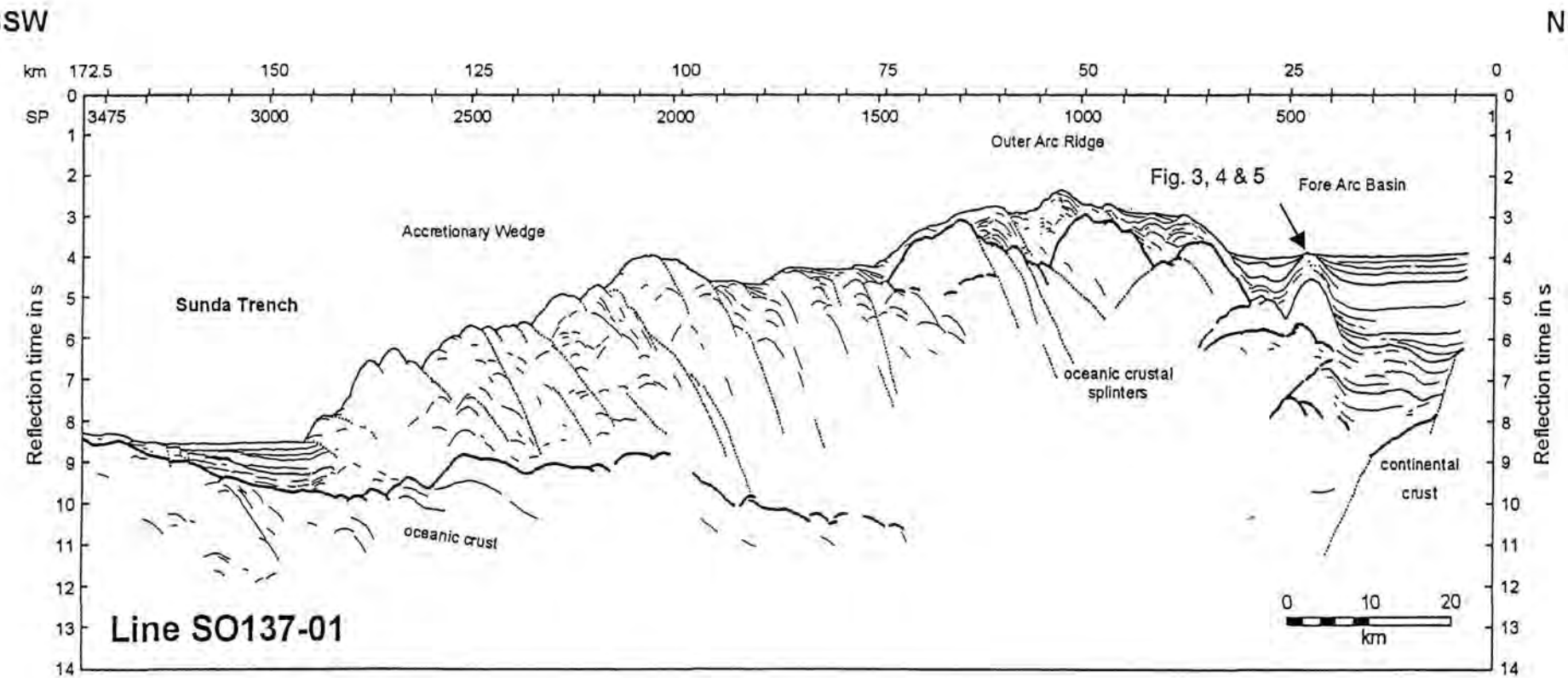

Fig. 3.2 Line drawing of seismic line SO137-01, south of W-Java, showing a transect from the forearc basin in the north, the accretionary wedge with outer arc high in the central part and the Sunda Trench in the south

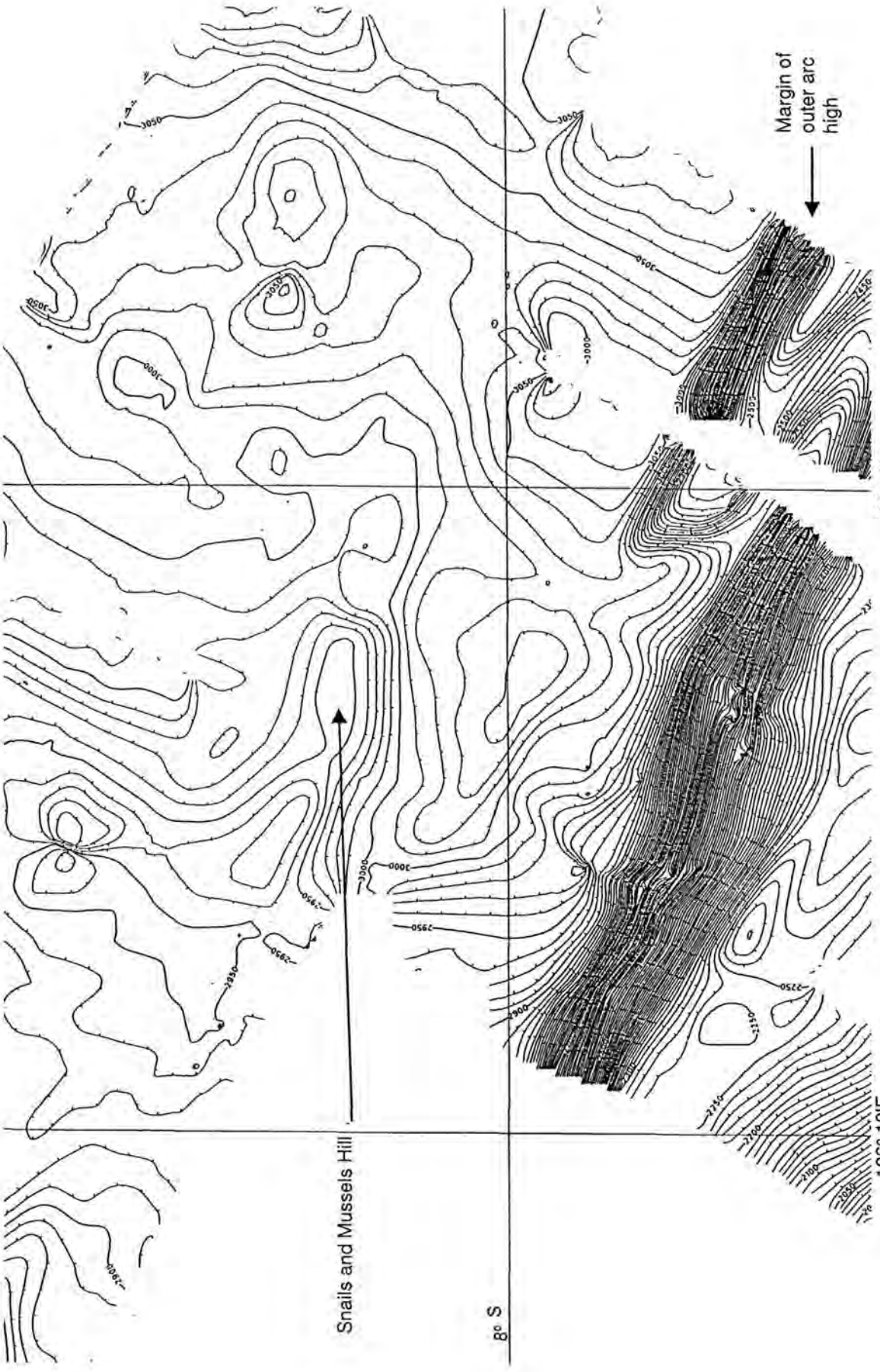

Fig. 3.3 Bathymetric chart of a part of the forearc basin south of W-Java (C.I. 10 m)

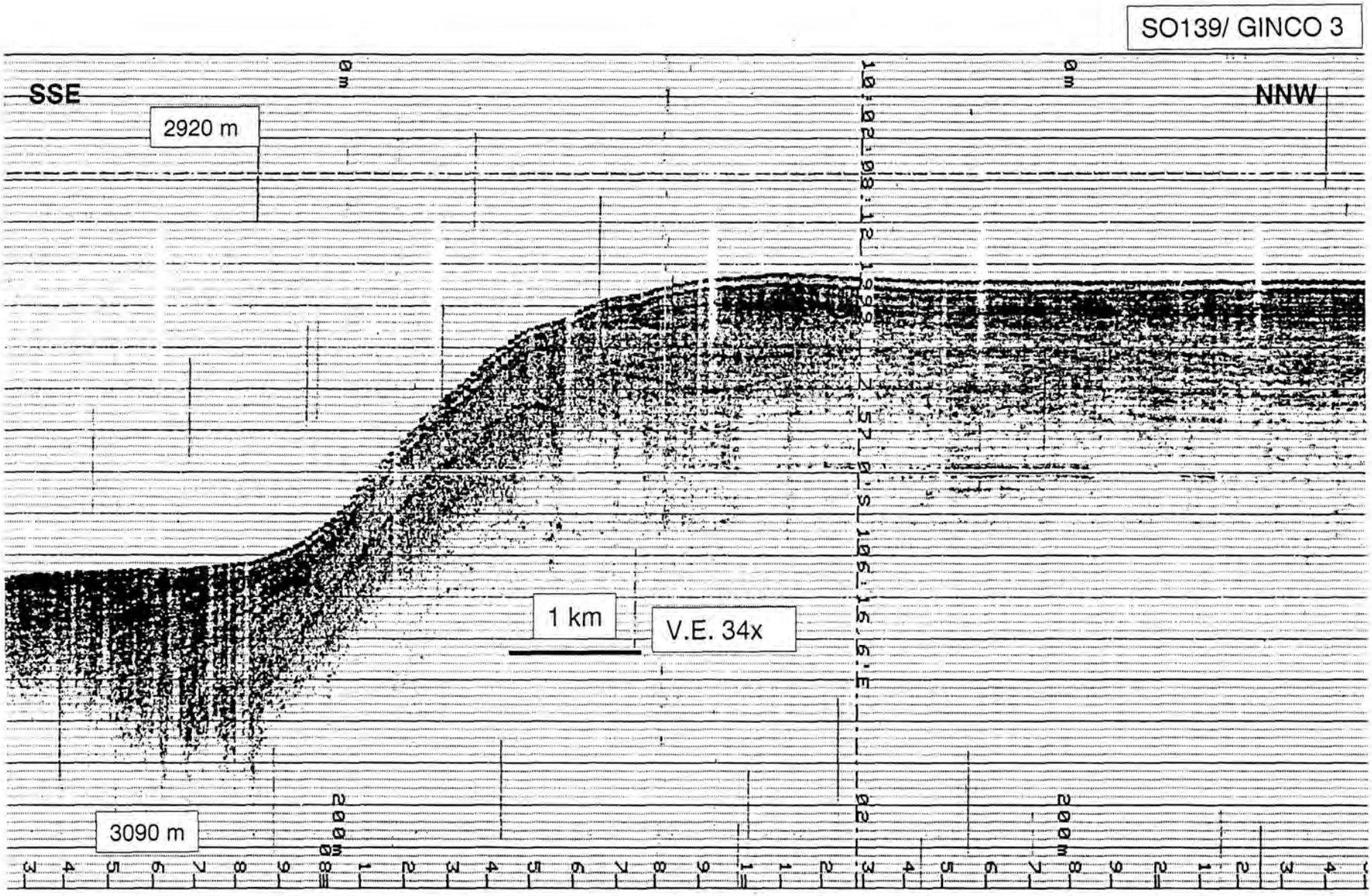

Fig. 3.4 Step in the sea bottom, erosional surface and fault in the sub-surface. Near Snails and Mussels Hill in the forearc basin south of W-Java

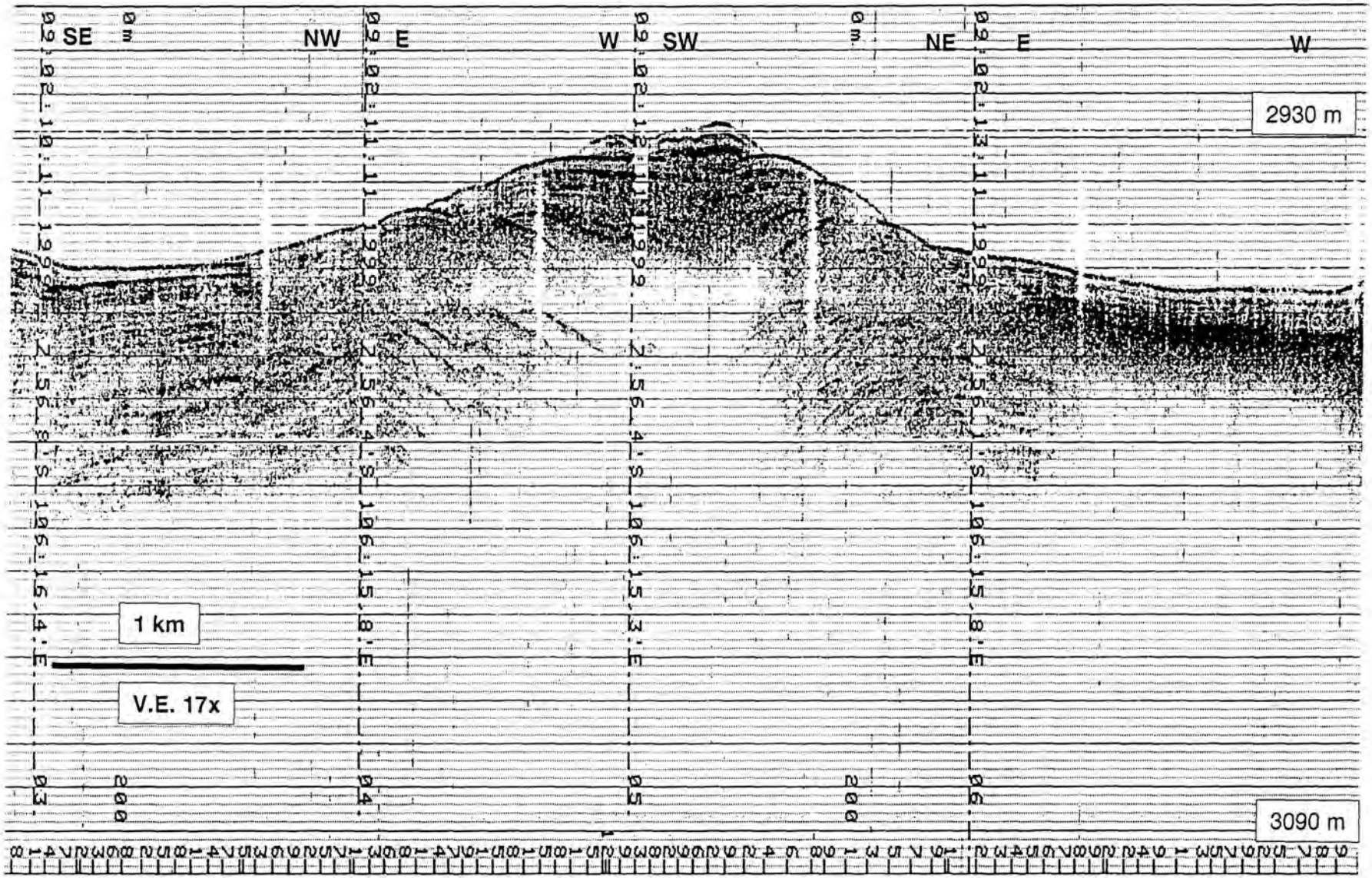

Fig. 3.5 Snails and Mussels Hill in the southern part of the forearc basin south of W-Java, with strongly faulted axial part

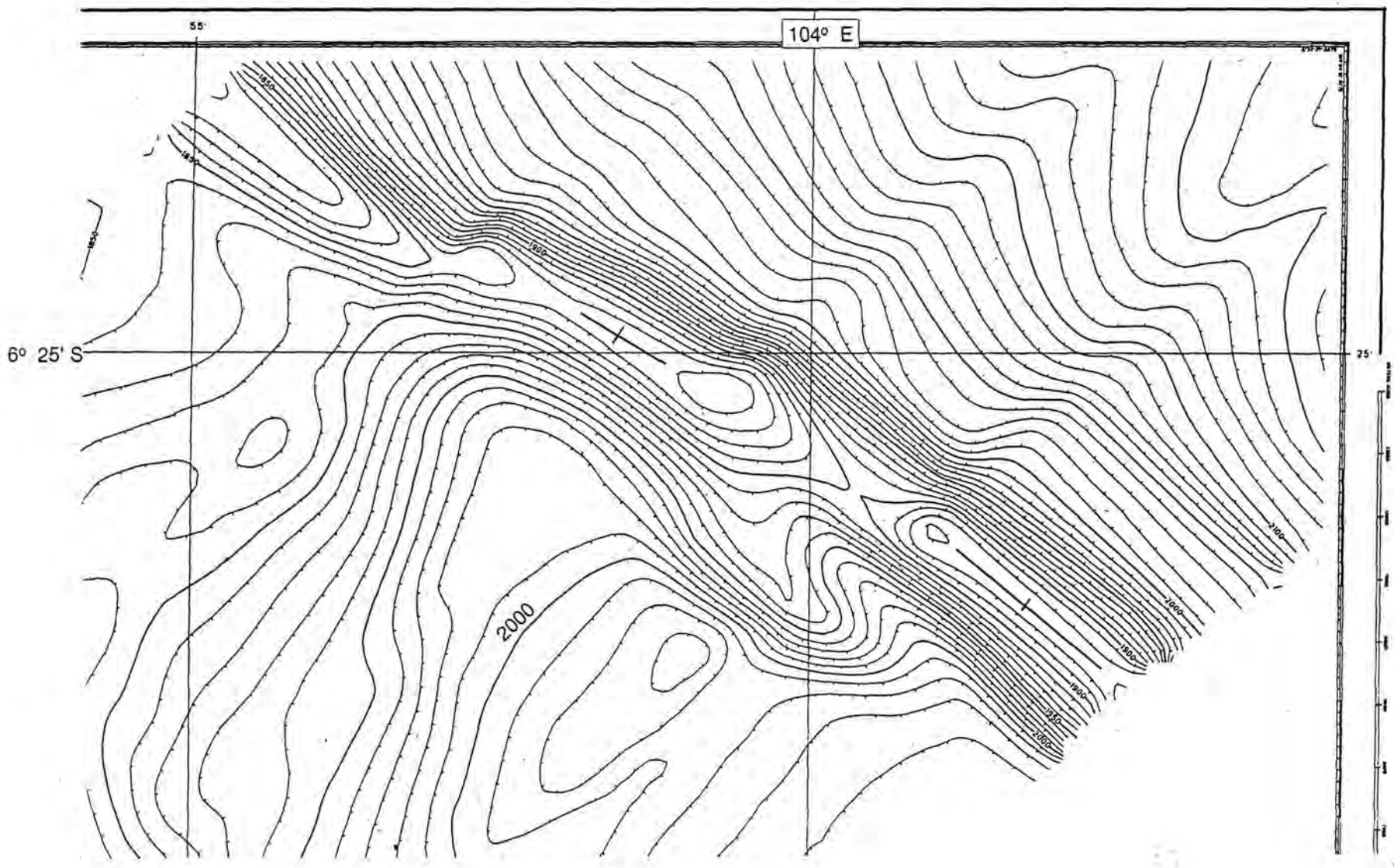

Fig. 3.6 Bathymetric chart of the Semangka Ridge in the southern part of the forearc basin, south of SE-Sumatra (C.I. 10 m)

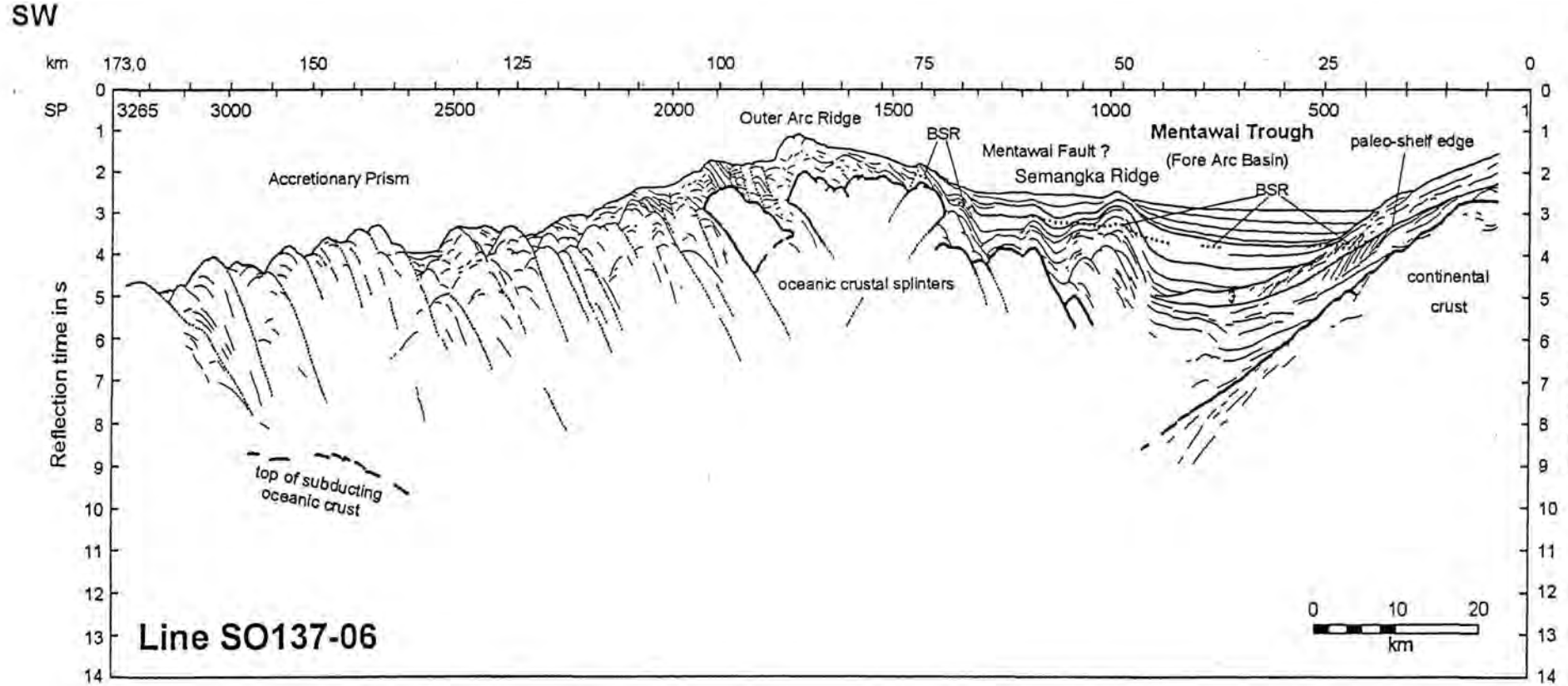

Fig. 3.7 Line drawing of seismic line SO137-06, south of SE-Sumatra, with Semangka Ridge in the southern part of the forearc basin

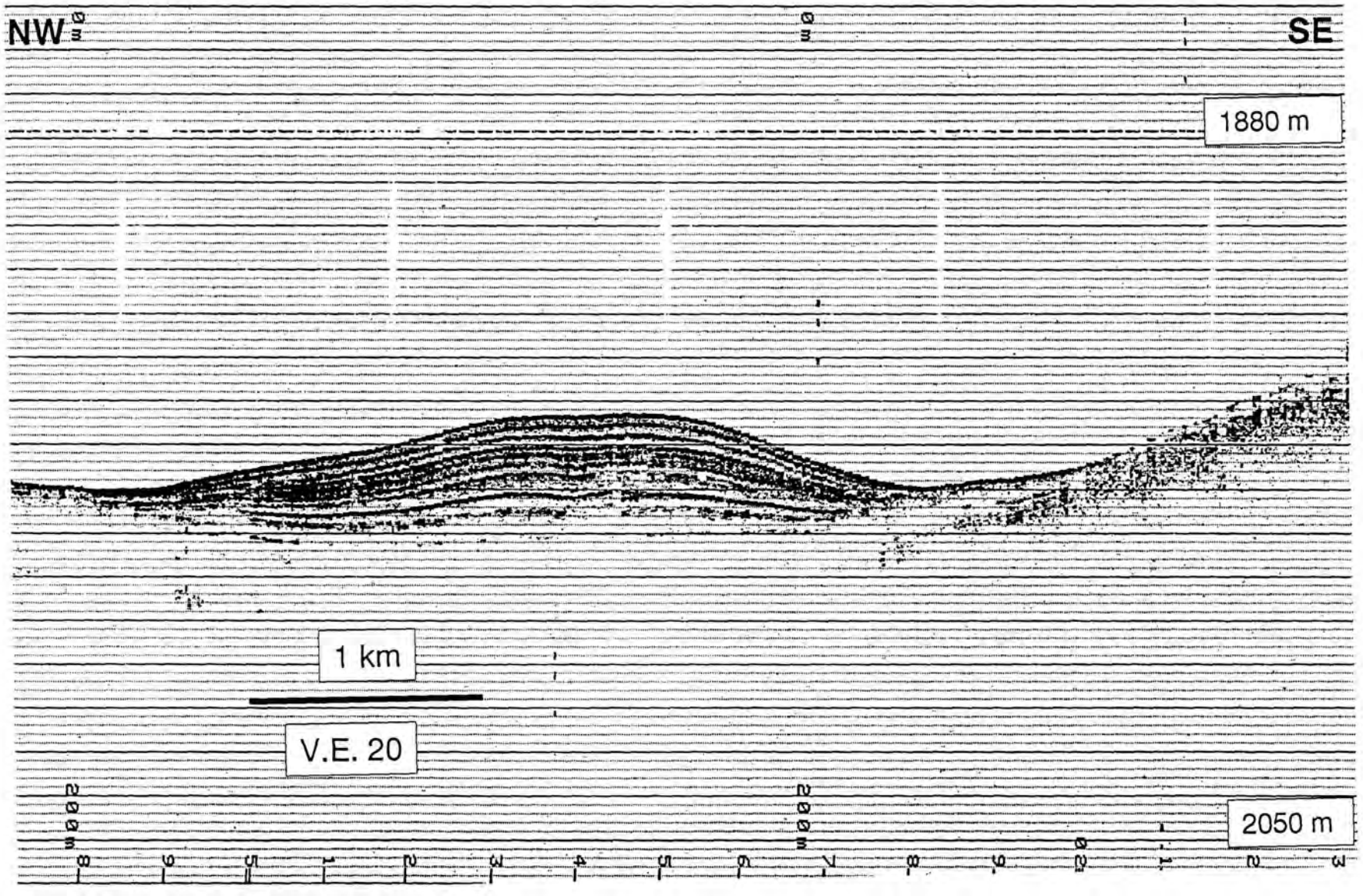

Fig. 3.8 Contourite in the forearc basin south of SE-Sumatra

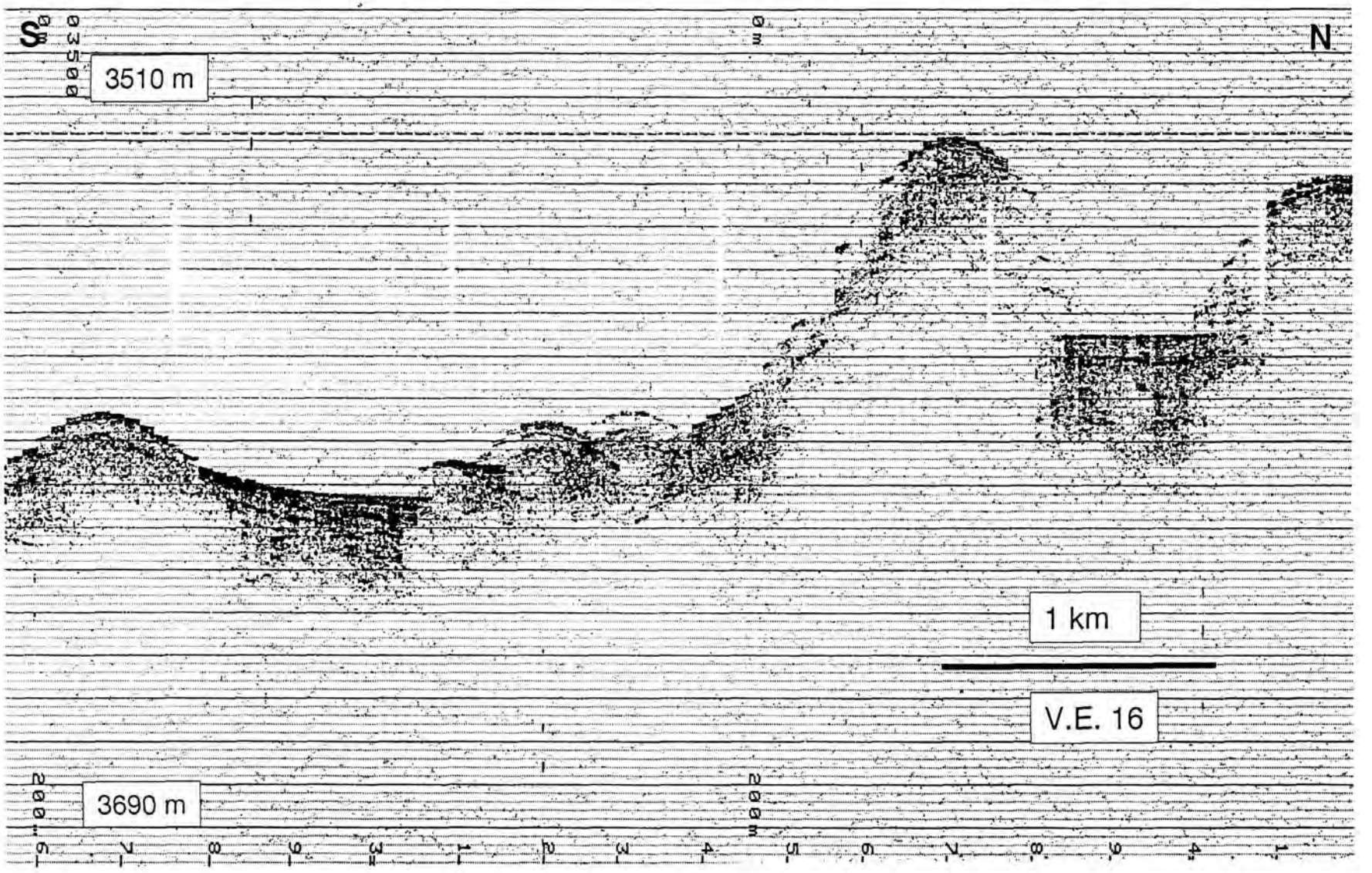

Fig. 3.9 Ridges and troughs in the southern, lower part of the accretionary wedge south of W-Java. Flat bottom in the northernmost trough and a halfgraben in the south, with slumps.

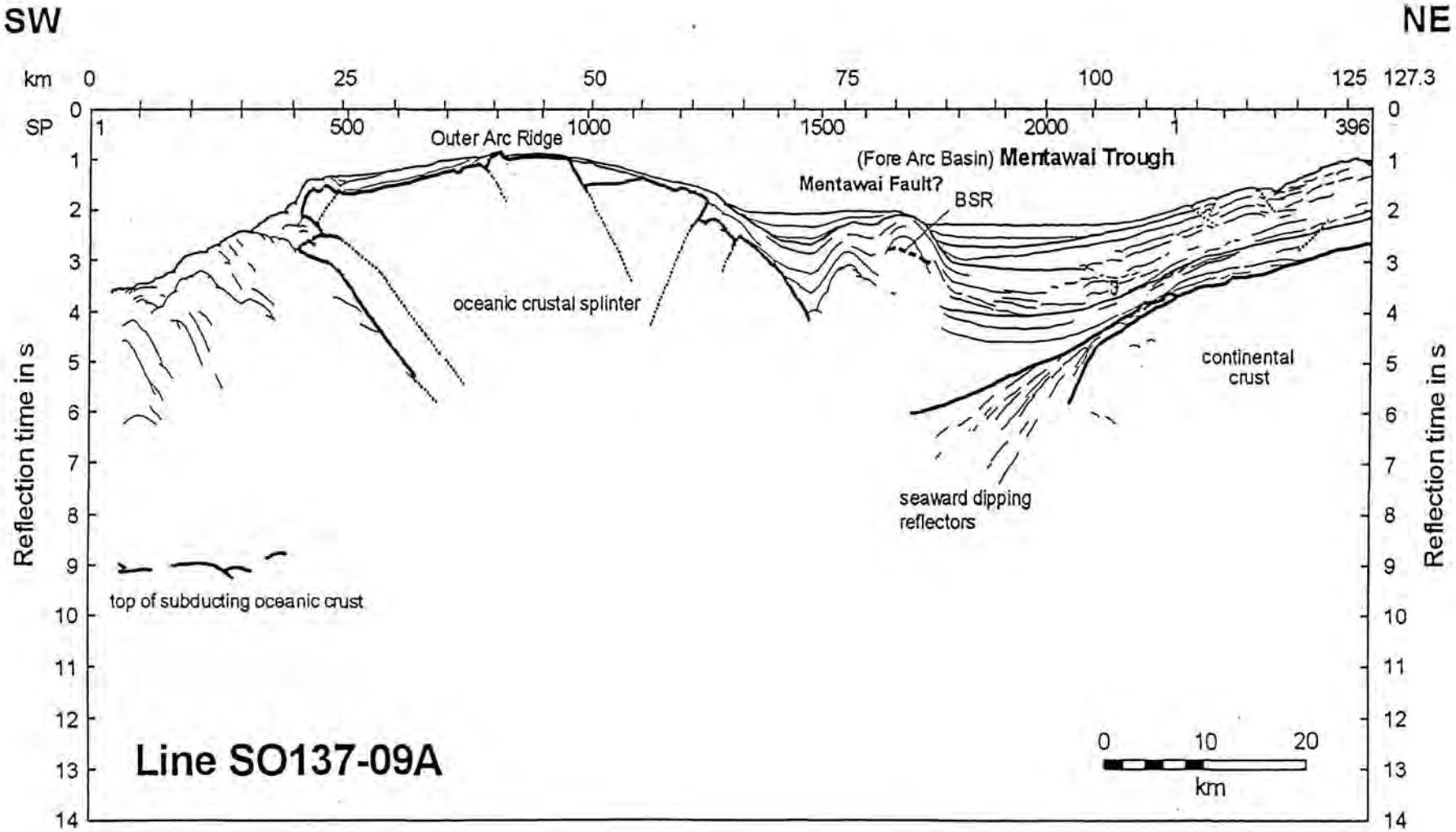

Fig. 3.10 Line drawing of seismic line SO137-09A, south of SE-Sumatra, north-west of Enggano

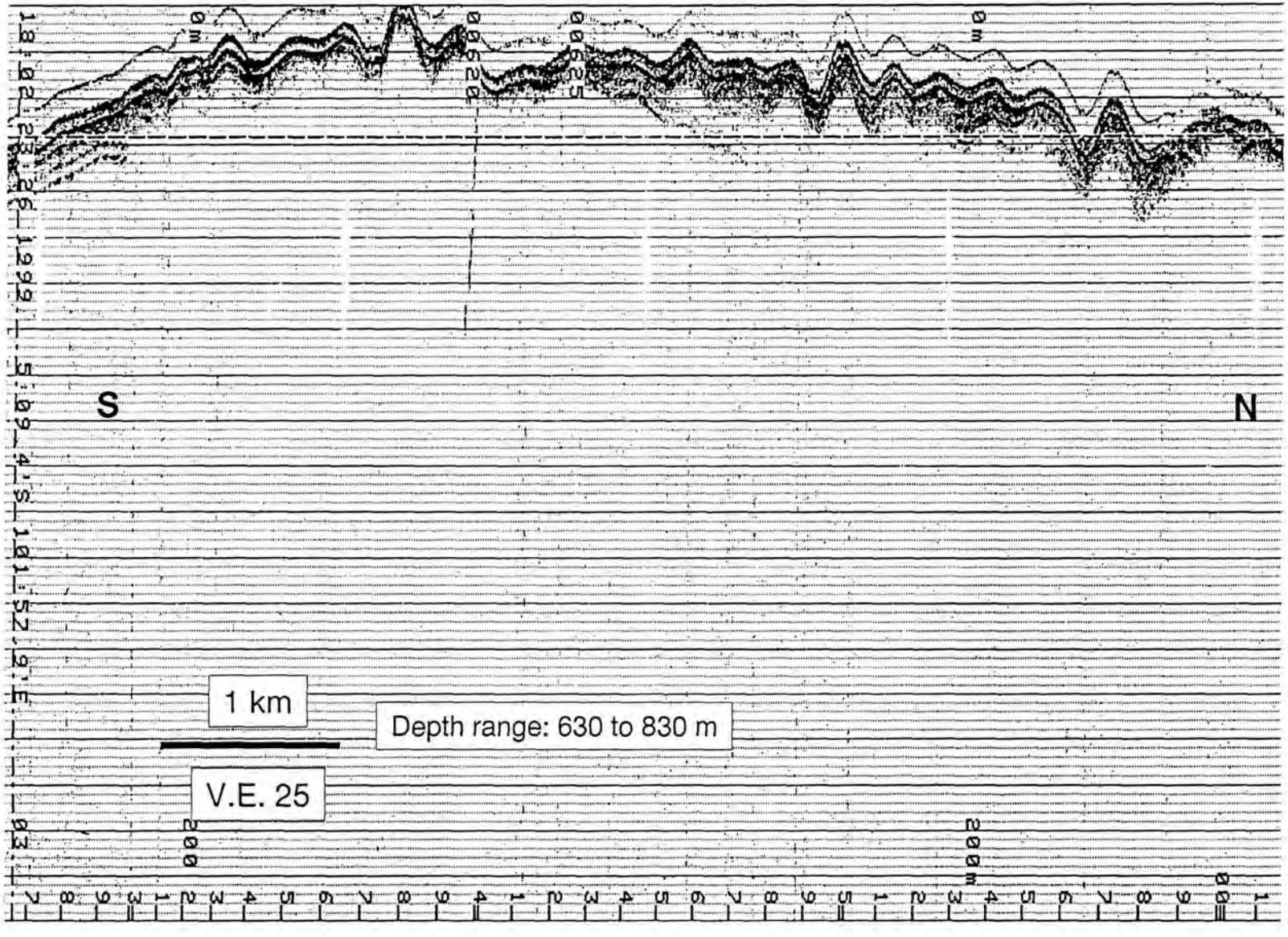

Fig. 3.11 Rough sea bed morphology and inclined beds in the subsurface on the culmination of the outer arc high, north-west of Enggano

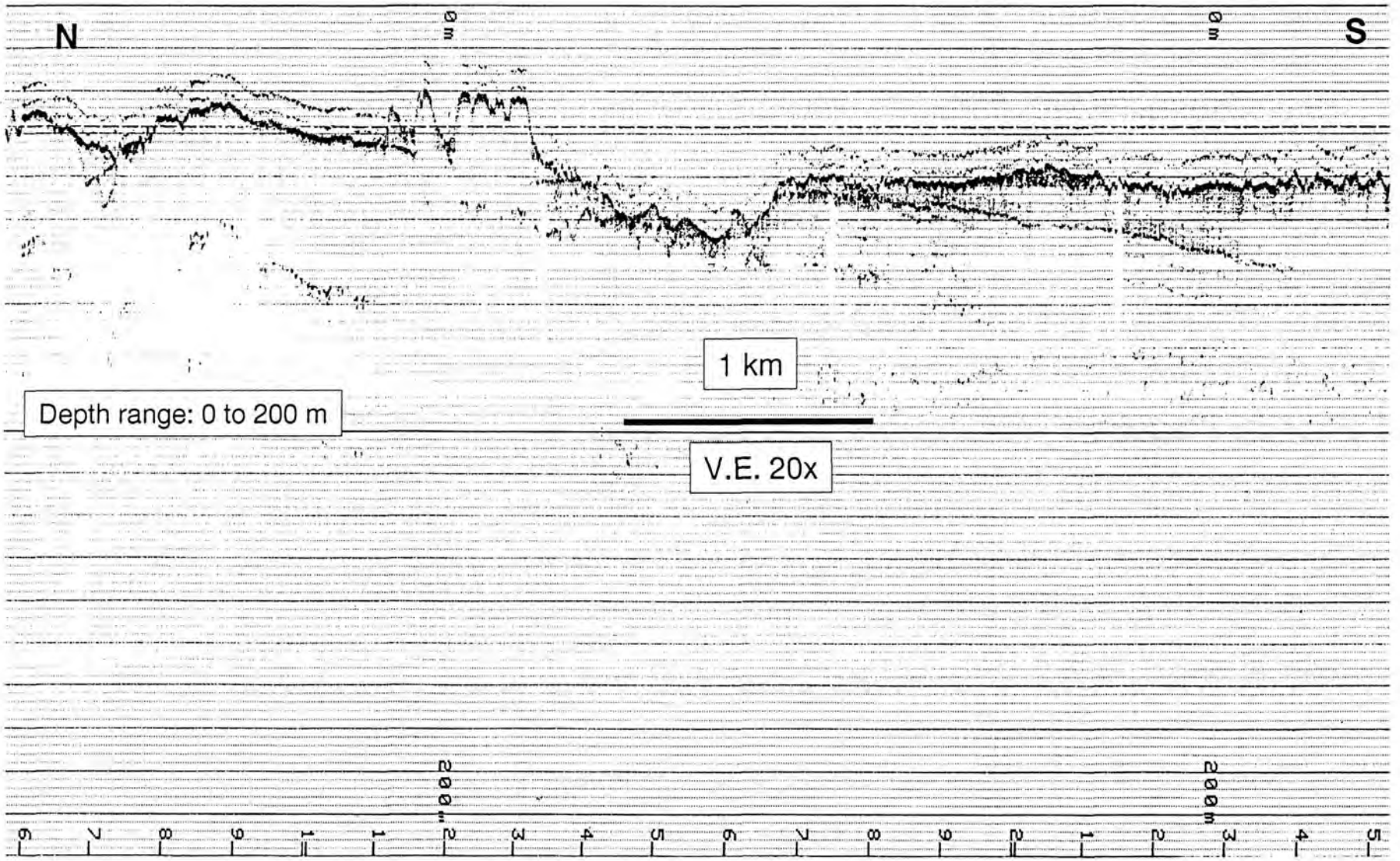

Fig. 3.12 Rugged sea bottom with indication of tilted beds (flows?) in the the Sunda Strait near Krakatau volcano

4. Geothermal measurements

G. Delisle, M. Zeibig

4.1 Introduction

Geothermal measurements were carried out in sediments in the Sunda Strait as well as along the reflection-seismic profiles SO-137-01 and SO-137-06 across the accretionary and forearc basin complexes off the southern coasts of Sumatra and Java. Surprisingly, these as the other seismic profiles measured by SO-137 in the area had shown only isolated occurrences of bottom simulating reflectors (BSR). Heat flow through the accretionary wedges can be calculated with good accuracy from BSR-depth and the use of phase diagrams of gas hydrates. The lack of bottom simulating reflectors, however, required the use of conventional methods to obtain a first conceptual understanding of the geothermal field of these accretionary wedges.

4.2 Methods

During SO-139, a new marine heat flow probe of BGR was employed, built according to the so-called violin bow concept. A glass fibre rod of 4.20 m length is used to stabilise the penetrating part of the probe. A hollow steel rod with a diameter of 13 mm is placed at a distance of 10 cm and parallel to the fibre glass rod, housing 6 thermistors (type Omega 44033), spaced 50 cm apart. The thermal gradient in the sediments is measured continuously in the sediments for a typical time period of about eight minutes, until the frictional heat component caused by the penetration of the probe into the sediments has completely decayed. In addition, the metallic rod houses a heating wire, which is used to determine the in-situ thermal conductivity of sediments after the thermal gradient measurement. This assembly is mounted below a 1.4 t weight, which houses a steel cylinder with the electronic unit for the control of all measurements. All data are transferred via a coax-cable online to a laptop-PC on board.

Description of the electronic unit

Methodology of measurements: To achieve an accuracy of measurement within ~0.002 K, the following approach was chosen. Measured thermal values are recorded, stored, digitised and monitored by a so-called "intelligent sensor module (ISM)", which is installed in a pressure vessel within the 1.4 t weight. This technology enables us to further improve the accuracy of measurement due to the fact that measured values are sent already in digitised form to the memory.

The functions of the ISM-module are defined by the configurations, which are downloaded via PC. The following configuration was used:

a) 7 analogue inputs to measure electrical resistance

	Accuracy	
Range of measurement 20 K-Ohm	0.01% = 2 Ohm	(1)
Resolution/noise	0.003%	(1)
Linearity	0.01%	(2)
T-drift	22 ppm/°C	(2)

(1) values for T = 20°C
(2) data according to company specifications

b) 1 digitised output to monitor the electric power of the heated wire unit necessary for the measurement of the in-situ thermal conductivity

c) 1 analogue input for the measurement of the tilt of the heat flow probe after penetration of sediments (tilt meter).

All analogue recorded values are sent to an analogue-multiplexer and then to a 16-bit-A/D-transformer. The high accuracy and linearity during the A/D-transformation is guaranteed by the application of the sigma-delta-method. To further improve the accuracy of measurement, an arithmetic mean of 20 consecutive measurements per sensor is formed and then accepted as one single measured value.

All specific modules, which control the configuration, linearisation and scaling data in the ISM-module, are stored in an EPROM. Storage and display of the measured data is done via a special computer code, stored on a PC.

To achieve optimum thermistor calibration , the heat flow probe is stopped about 50 m above seafloor, until thermal stabilisation within ~0.001K is obtained. The probe is then lowered with a velocity of 0.3 m sec^{-1}, until full penetration into the sediments reached. It is assumed that the thermistors measure identical sea water temperatures immediately prior to sediment penetration. Recalibration of all thermistors is achieved by using one thermistor as the master thermistor, whose measured value is used to correct the data measured by the other thermistors.

Temperature gradients

During SO-139, 24 heat flow measurements were carried out in total. The geographic co-ordinates of the probing points, their water depths and the measured mean thermal gradients are listed in Table 4.1. The thermal gradients are based on putting a linear trend line across the measured values. All thermal gradients are shown in Figure 4.1, with a uniform sea water-sediment interface temperature normalised to 0° for the purpose of comparison. With the exception of four measurements, the determined thermal gradients are highly linear.

Thermal conductivity

In-situ thermal conductivity values λ have been determined on the basis of the heating curves obtained after completion of the temperature gradient measurements. A constant electrical power output of 3,2 W was applied to the heating wire in the probe. Since the heating current became unstable after 180 seconds due to malfunction of the instrument, the following approach to obtain λ-values was chosen: The response of the temperature sensors to heating was measured in sea water. For each sensor, a characteristic heating curve was obtained. In a second step, this information was used to obtain the exact position of each sensor with respect to the heating wire and the metal rod, which houses sensors and heating wire. This reconstruction was achieved by a computer code, which simulates numerically the thermal behaviour of the probe, when placed in sea water. From this code, characteristic heating curves were then calculated by assuming the probe to rest in material of low thermal conductivity, which is typical for marine sediments. Values of 0.6, to 1.2 W m^{-1} K^{-1} were considered. Figure 4.2 shows as typical example the calculated thermal response of sensor 2 to heating in different thermal environments and Figure 4.3 a summary of all thermal responses of sensor 2 at all heat flow stations of the cruise. The 6 λ-values (6 sensors) obtained by this way for each station show deviations of typically less than 15%. Therefore, the values were accepted and for each station a mean value was derived.(Table

4.1). Instrument failure (non-constant heating power as function of time) was observed at stations 26HF, 62HF, 76HF an 97HF. In these cases, a mean value of 0.95 W m^{-1} K^{-1} is assumed.

Heat flow q was calculated according to the thermal resistance method (see BULLARD, 1939). q is calculated as the slope of a temperature versus thermal resistance plot for an arbitrary depth interval.

$$q = (T-To)/R(z) \quad (1)$$

where
To is the topmost measured temperature (uppermost sensor)
T = temperature
R(z)= thermal resistance, defined by

$$R(z) = \sum d(z)/\lambda \quad (2)$$

with
d = vertical distance z
λ = thermal conductivity.

All q-values and their mean standard deviations are presented in Table 4.1.

4.3 Results

Transect SO-137-06: A complete coverage of this profile with heat flow values was measured from the deformation front to the inshore part of the Bengkulu (forearc) basin. Heat flow is slightly reduced landward of the deformation front with typical values close to 50 mWm^{-2} along the outer arc ridge (see also Figure 4.4). Heat flow drops substantially across the forearc basin. This result is backed by the short segments of BSR shown on the seismic profile SO-137-06. At the north-eastern termination of the Forearc ridge, the BSR is located at about 0.3 s (TWT) below sea floor, implying a heat flow of about 40 mWm^{-2} in close agreement with the probe measurements. The BSR is lowered to 1.0 s (TWT) in the central and north-eastern part of the forearc basin, indicating low heat flow values between 35 – 22 mWm^{-2} (BSR-derived q-values are shown in brackets in Figure 4.4). The thermal gradients of two q-measurements (77HF and 78HF) in the north-eastern sector of the forearc basin show nearly isothermal conditions below 3 m depth below sea floor. It is tentatively proposed that an unidentified geochemical process causes a small disturbance of the temperature field of the surficial sediment layer. Since the Bullard method (see above) brakes down under such circumstances, q was estimated on the basis of the product of the thermal gradient (calculated by linear trend analysis) and λ. BSR-derived q-values in the central and north-eastern sector of the forearc basin tend to be somewhat lower than the values from the heat flow probe. Conceivably are the q-values of heat flow probe influenced by upward migration of fluids (an effect, thermally most prevalent near the sea floor), while the BSR-derived values demonstrate in general a low heat flow due to rapid sedimentation (piling up of cold material). The cooling effect of the subducting oceanic plate may also play a role in reducing heat flow across the forearc basin along SO-137-06.

Transect SO-137-01: The general heat flow trend of this profile differs in detail from the previous line. Heat flow (60 mWm^{-2}) over the forearc-ridge tends to be slightly higher than at the other transect. The highest heat flow values were found in the forearc basin in the area of the South Java Basin fault, where also a methane vent field was discovered during the cruise. The area of active venting yielded the highest values (94,9 and 153,6 mWm^{-2}). However, in close vicinity also low values down to 30 mWm^{-2} were observed. If this strong heat flow contrast is caused by strong lateral sea water circulation in the sediments or is

rather the expression of high local heat flow due to locally high discharge rates of pore water fluids in an area of generally low heat flow needs to be analysed further.

The heat flow profiles across both transects differ slightly from the ones of other accretionary wedges (see e.g. the example of the Celebes Sea accretionary complex. DELISLE et al., 1998). The heat flow profile appears to be more uniform landward of the accretionary front toward the forearc basin. This result implies an only moderate thermal influence of ascending fluid flow. If frictional heating at the contact between the base of the accretionary complex and the fast moving oceanic crust (7 cm a^{-1}) plays a significant role, heatflow must be evaluated by numerical modelling of the whole complex. The top of the outer arc ridges show little evidence of recent to subrecent sedimentation, but rather widespread erosion. Large segments of the outer arc ridge show hard ground which is unsuitable for piston corer penetration. The outer arc ridges apparently undergo widespread uplift and consist presumably mostly of well compacted siltsones and clays.

REFERENCES

BULLARD, E.C., 1939. Heat flow in South Africa. Proceedings of the Royal Society of London. Series A, 173, 474-502.

DELISLE, G., BEIERSDORF, H., NEBEN, S. & STEINMANN, D. , 1998: The geothermal field of the North Sulawesi accretionary wedge and a model on BSR-migration in unstable depositional environments. - In: Henriet, J.-P., Mienert, J. (eds), Gas hydrates: Relevance to World Margin Stability and Climate Change. Geol. Soc. Special Publ. 137, 267-274.

Station / Shotpoint / Profile	Latitude S	Longitude E	Water Depth (m)	Gradient (K/m)+	λ (W m^{-1} K^{-1})	q mW m^{-2}	q_{dev} mW m^{-2}
25HF 620 -01	8°01.606	106°16.115	2998	0,07	1,22	98,0	23,3
26HF 566 -01	8°00.292	106°16.732	3039	0,07	0,95	57,7	15,4
27HF 460 -01	7°57.67	106°17.98	3000	0,068 *	1,07	94,9 122,7	1,4 55,4
35HF 524 -01	7°59.26	106°17.22	3021	0,05 **	1,03	30,9	39,5
36HF ~ 580 -01	7°57.6	106°16.58	2950	0,049	0,99	34,6	9,9
38HF 1719 -03	8°34.0	106°36.471	2246	0,058	1,03	60,2	2,9
39HF 1197 -03	8°46.8	106°30.236	3367	0,047	1,09	63,9	16,4
41HF ~ 1557 -01	8°24.64	106°5.648	3181	0,051	0,89	35,4	10,9
46HF 955 -06	6°24.094	103°58.922	2007	0,03	0,88	32,4	6,6
47HF 1020 -06	6°25.566	103°57.401	1980	0,039	0,81	22,0	9,3
51HF 1165 -06	6°28.49	103°54.41	1910	0,055	0,68	44,6	5,5
52HF 1372 -06	6°32.65	103°50.12	1691	0,060	0,75	48,6	5,2
53HF 1581 -06	6°37.03	103°45.77	1120	0,061	0,78	47,2	5,0
60HF 2320 -06	6°51.87	103°30.08	2653	0,07	1,02	68,0	6,0
62HF 2592 -06	6°57.48	103°24.29	2950	0,039	0,95	49,1	11,6
64HF 1148 - 06a	7°39.86	102°40.06	5945	0,051	0,99	64,2	11,3
69HF	4°59.27	102°07.69	1569	hard ground**	0,95	39,1?	25,6?
76HF 430 -06	6°13.932	104°9.505	2201	0,035	0,95	45,6	11,4
77HF 610 -06	6°17.43	104°05.784	2187	0,04 ***	1,12	44,8	
78HF 745 -06	6°19.967	104°03.018	2171	0,029 ***	0,93	27,0	
85HF ~460 -01	7°57.72	106°17.223	2966	0,042	0,96	55,4	15,0
86HF ~454 -01	7°57.5	106°17.79	2935	0,220	0,76	153,6	12,3
97HF Sunda Strait	6°33.97	104°53.99	1892	0,111	0,95	104,2	4,8
98HF Sunda Strait	6°25.87	104°51.86	1840	hard ground		no value	
99HF Sunda Strait	6°23.559	104°57.976	1398	0,092	0,98	83,3	12,3

+ based on linear transgression curve through all measured temperature values of each station

* apparently only partial penetration; preferred heat flow value (top) is based on 4 lowermost temperature sensors - second value (bottom) is calculated from 5 lowermost sensors of heat flow probe.

** highly non-linear temperature increase with depth in sediments, probably only 3 lowermost sensors in ground.

*** isothermal conditions below 3,15 m depth below sea floor, representing possibly evidence of exo- or endothermal geochemical reactions in sediments. Unlike at other points of measurement, heat flow was calculated by multiplying the temperature gradient (as given by the linear transgression curve) with λ (see further discussion in text).

Table 4.1: Geothermal stations of SO-139

Figure 4.1: Summary of all thermal gradients measured by the heat flow probe. Temperature at sea water-sediment-interface normalised to 0°C.

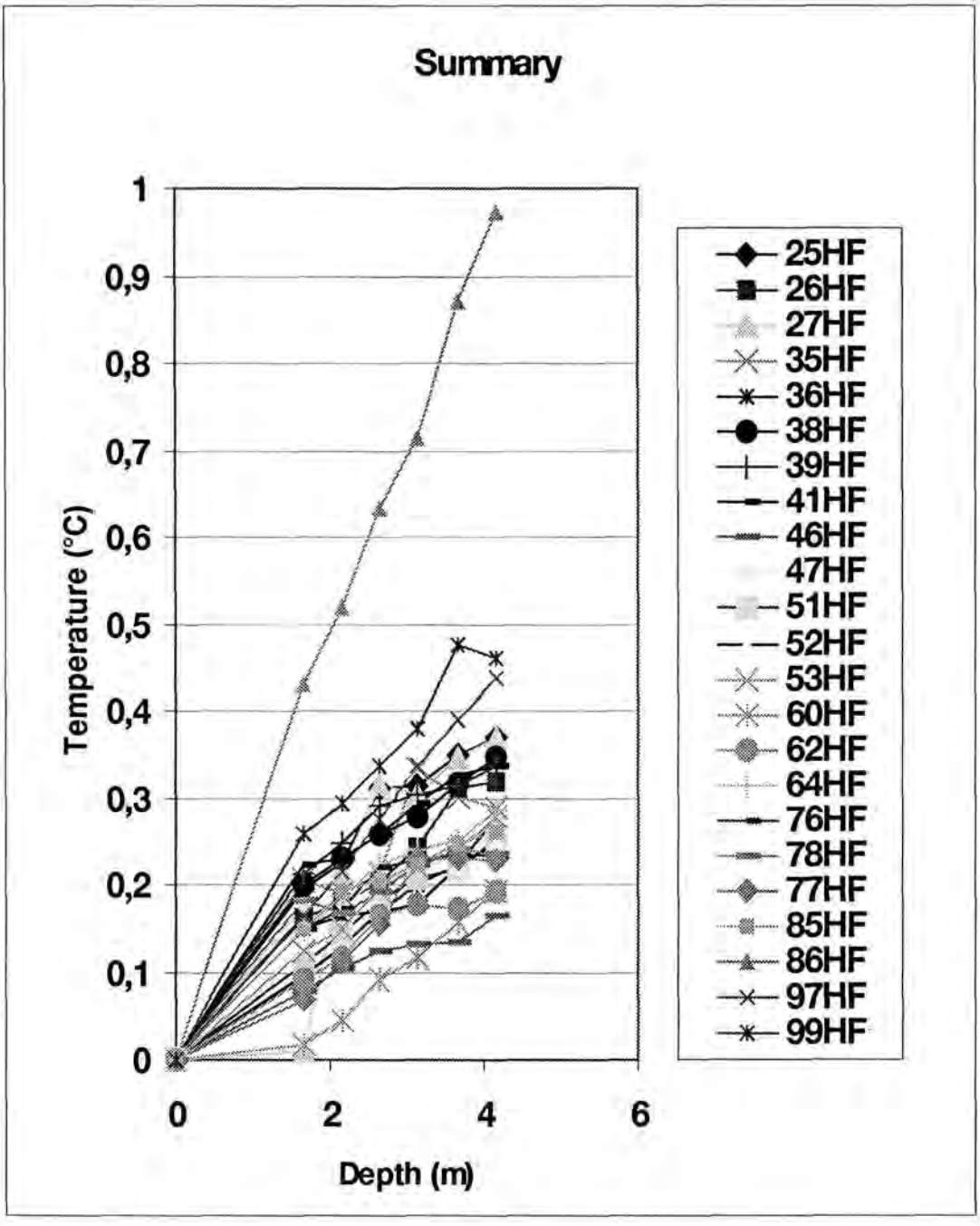

Figure 4.2: Temperature increase measured by sensor 2 of heat flow probe 150 seconds after begin of heating as function of thermal conductivity of penetrated sediment.

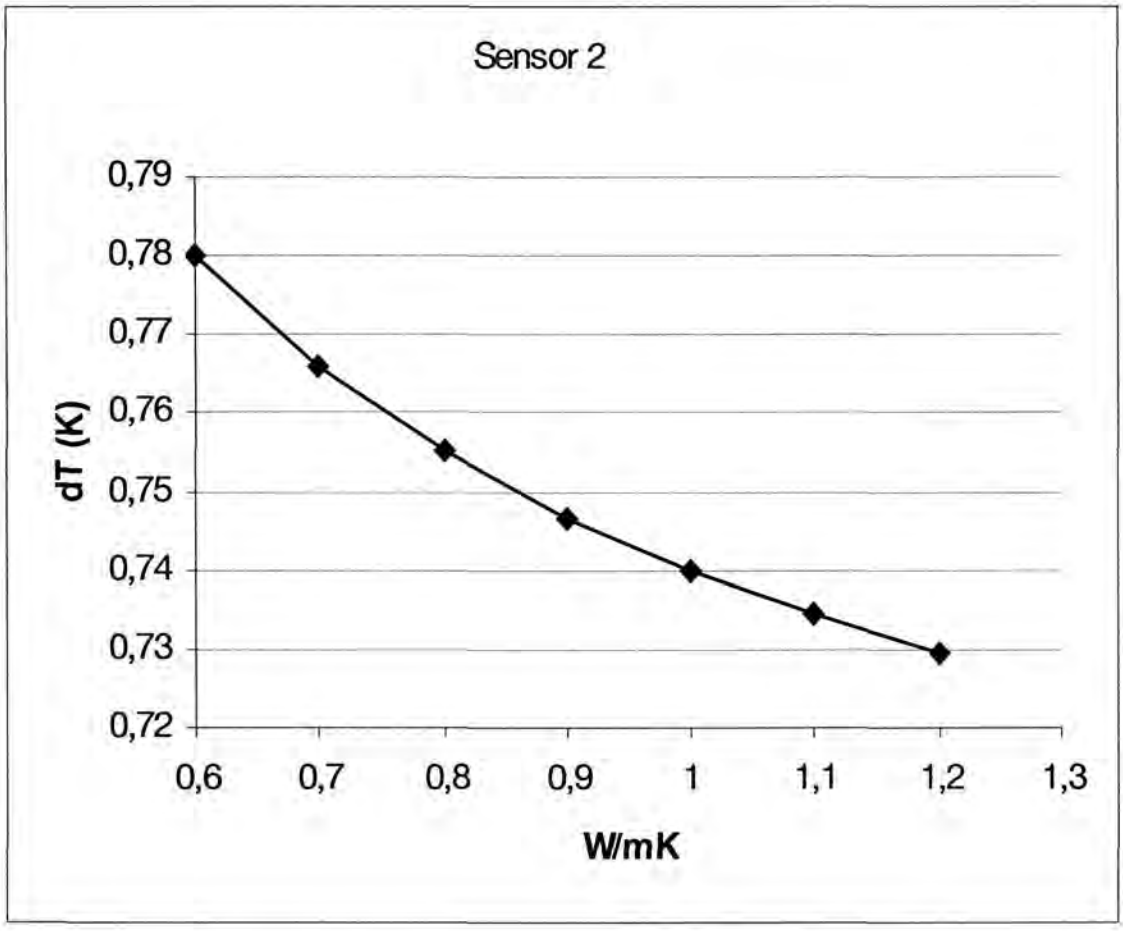

Figure 4.3: Summary of measured temperature increases by sensor 2 for all heat flow stations.

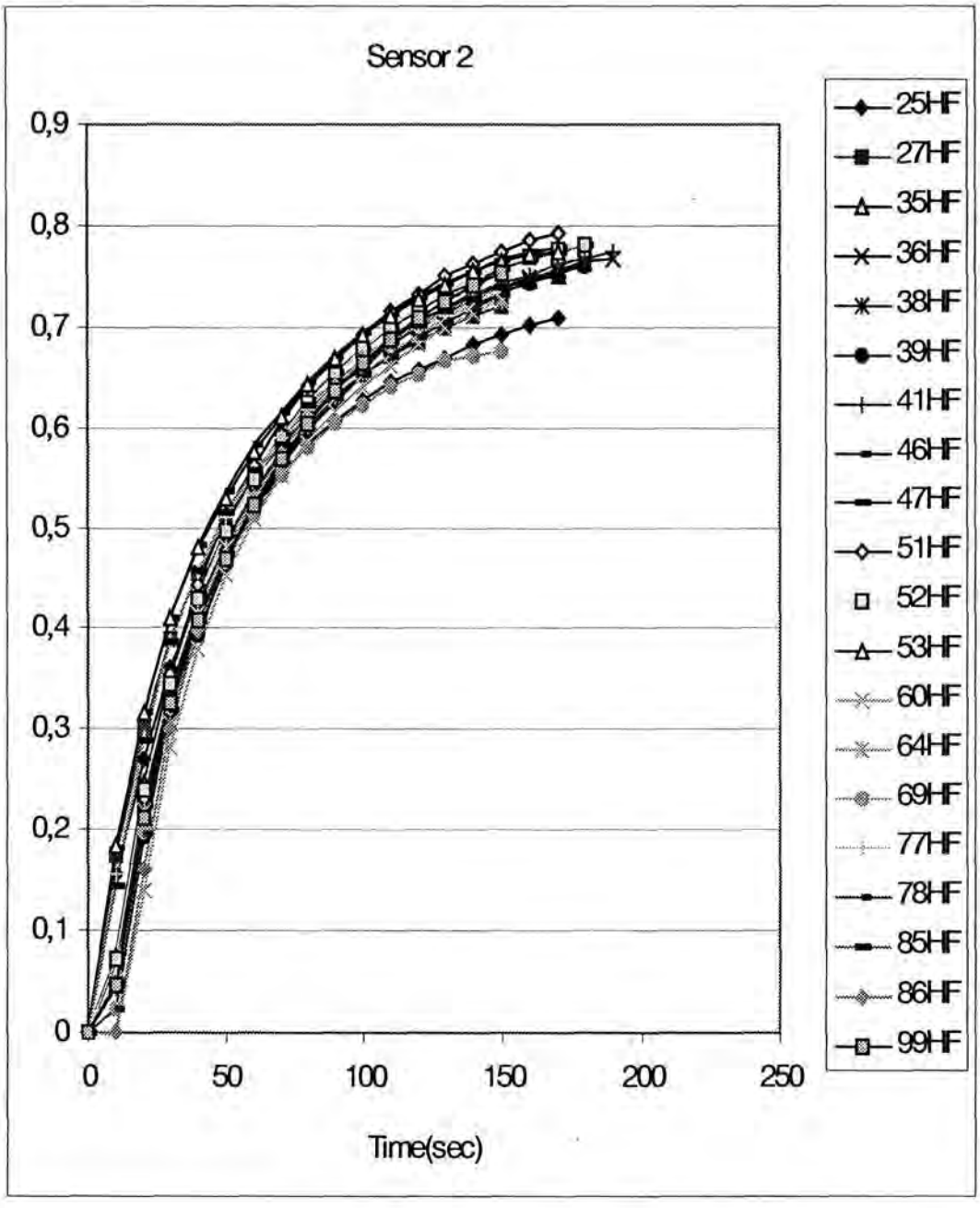

Figure 4.4: Line drawings of the seismic transects SO137-1 and SO137-06. Positions of heat flow stations are shown. Heat flow values are given in mW m^{-2}.

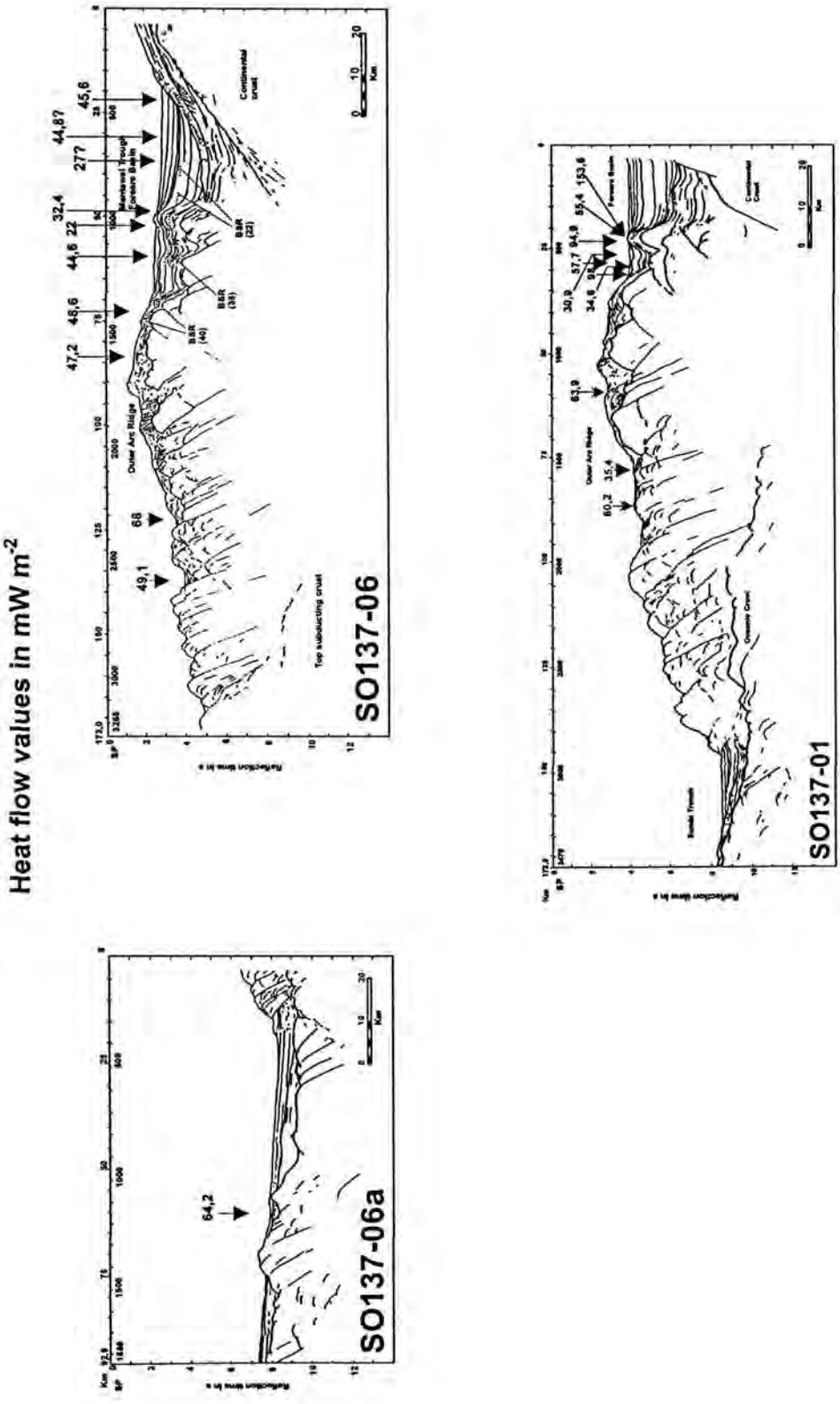

5. Sediments: Cores, TV-grab, and dredge samples

H. Andruleit, M. Wiedicke, W. Weiss, Udrekh, Haryadi Permada, and D. Steinmann

Coring, TV-grab sampling, and dredging played a substantial role during Cruise SO-139 in ground-truthing geophysical findings and developing strategies for an assessment of the hydrocarbon potential as well as locating methane-laden fluid seeps and associated typical lifeforms.

5.1 Geological sampling and core logging

M. Wiedicke, W. Weiss, Udrekh, Haryadi Permada, and D. Steinmann

Geological sampling during cruise SO-139 had to serve several purposes the most important of which were:

- Define nature and age of acousto-stratigraphic sequences where accessible for sampling devices (ground-truthing of seismic results);
- Provide sediment cores for gas analyses of near-surface sediments (in search of seeps) and for pore water analyses;
- Acquire sediment cores from different parts of the accretionary complex for stratigraphic and sedimentological analyses;
- Test seafloor properties in view of a subsequent deployment of the heat-flow probe.
- Assist the search for communities of lifeforms associated with fluid seeps.

5.1.1 Sediment and hard-rock sampling

5.1.1.1 Introduction

We based our work on the information provided by the seismic profiling of the previous SONNE cruises SO-137 and SO-138. Sampling, however, concentrated on selected seismic lines (see Fig. 5.1.1):

- south of Java: lines 137-03 and 137-01,
- south of Sumatra: line 137-06,
- northwest of Pulau Enggano: line 137-09
- south of Sunda Strait: line 137-25

This approach allowed sampling and data acquisition from the deep-sea trench to the forearc basin and base these on coherent structural information which resulted from the previous cruises. Figure 5.1.2 illustrates this concept by presenting two simplified cross sections with the positions of sampling sites (projected) at different structural units - one section south of Java, and the second one south of Sumatra.

5.1.1.2 Sampling methods:

We have used three types of instruments for sea-floor sampling: a) piston corer [Kullenberg-type corer] and gravity corer, b) dredge, c) TV-controlled grab.

a) Two piston corers (KL) with different diameters were deployed during the cruise: an instrument with 90 mm tube diameter and a lead weight of 1.0 tons was used for coring

at sites 3KL - 34KL, in most cases with a barrel length of 15 m. After the loss of the instrument our second piston corer with a tube diameter of 125 mm, a lead weight of about 3 tons, and with barrel length of commonly 20 m was deployed (sites 37KL-96KL). At sites with potential hard rock outcrops we used the large-sized corer as 10 m long gravity corer (SL)(NW of Pulau Enggano, and at the vent site south of Java).

b) For hard-rock sampling we used a 1m-long chain-bag dredge (KD) which was deployed via the A-frame of RV SONNE. Constant recording of ship's position, water depth, cable length and (pronounced) pulls at the cable allow a sufficiently accurate reconstruction of the sampling position.

c) The TV-guided battery-powered hydraulic grab (GA) of RV SONNE was used for small sampling targets and for recovery of large quantities of near-surface sediment (e.g. at the vent site called 'Snails and Mussel Hill').

5.1.1.3 Sampling results

Cores: Core recovery in general was very good. Except for two sites at the accretionary front our corers - with a barrel length of 15m (resp. 20 m) - recovered 12-13 m (resp.17-18 m) of sediment core (Table 5.1.1). Figure 5.1.3 presents simplified core lithologies for all cores. Biostratigraphically determined preliminary ages of the base of sediment cores can be found in Chapter 5.2.

Despite a generally good core recovery marked differences exist between sampling areas depending on their structural position:

- Sediment at **forearc basin** sites could all be easily cored; it consists of turbidite-dominated grey olive-coloured muddy sequences; sandy turbidite layers contain black volcanic debris and in some cases are rich in plant debris (wood);
- Sites at the **outer arc high** (upper accretionary wedge) had to be carefully chosen, as a soft sediment cover doesn't persist everywhere. Cores were taken from local depressions and show a bioturbated hemipelagic foram-rich sediment sequence with some (local) turbiditic intercalations.
- Coring at the **deeper part of the accretionary wedge** appeared difficult as this area exposes an irregular topography lacking a sufficiently thick continuous sediment cover. In few locations within small piggy-back basins cores could be recovered with a hemipelagic sequence including some volcanic ash layers.
- The **accretionary front** is located directly in front of a long steep slope marking the begin of the outcropping youngest thrust sheet of the accretionary complex. Coring at shoulder positions of this first ridge and on the sediment bulge in front of the slope led to damage at the coring device and showed partly consolidated mud, fragments of mudstone and dm-thick medium to coarse sandy layers rich in mica. The mica is considered of continental origin.
- Volcanic ash layers were found in most cores. In turbidite-dominated forearc basin cores ash layers are less frequent (except for cores at the southern basin slope) than in cores taken at the outer-arc high. In general, cores south of Sumatra appear to contain more ash layers than cores taken further east.
- The sediment core from the Semangka graben south of the Sunda Strait encountered an impressive turbidite layer of approximately 14 m thickness. Parasound records prove that this deposit covers vast areas of the graben floor.

- CaCO3 contents of two cores from the Bengkulu basin (south of Sumatra) show a pattern different from that of cores from the South Java Sea basin (Fig. 5.1.4).

Dredges: Except for two hauls our dredge was successfully deployed (see Table 5.1.1). Selected interesting dredge results shall be briefly discussed below:

- Dredging near the accretionary front recovered mudstone, chert fragments and consolidated mud, indicating the presence of indurated and diagenetically altered sediments at the sea-floor surface within the youngest tectonic thrust sheet of the accretionary wedge. Veins within a few mudstone fragments indicate tectonisation and subsequent mineralisation.
- Calcareous arenites (probably of Pleistocene age) were dredged north of Pulau Enggano at shallow but steep escarpments. However, this lithology doesn't represent the expected basement rocks which according to airgun seismic and Parasound records should crop out at the seafloor. Basement is obviously covered by a thin calcareous sediment sequence.
- Basement was sampled south of the Sunda Strait at the northern flank of the Semangka Graben; the recovery of Miocene siltsone, platy sandstone, andesitic (?) volcanites, metamorphic rocks and others indicate the presence of continental basement. Interestingly, one dredge recovered a highly specialised tubeworm (Vestimentifera), the finding of which argues for the existence of vents in the immediate vicinity.
- Dredging across the crest of an anticline within the forearc basin south of Java recovered two shells of vent clams, leading to a focussed and successful search to locate the vent site.

TV-controlled grab: The grab was mainly deployed for the detailed search of vent indications at sites previously surveyed with other instruments.

Efforts concentrated on the so-called 'snail-and-mussel' hill located at a transpressional ridge within the forearc basin south of Java. Six deployments of the grab addressed surface sediment, precipitates and vent organisms at that structure. At the vent site sediments consist of dark olive mud with strong H2S- odour and lack an oxidised surface layer. The sediment surface is covered with scattered clam shells and (living) tube worms; a few living specimen of the clam genus Acharax sp. were sampled. The olive mud of several grab sites contains irregularly shaped carbonate slabs of 10 to 30 cm length. Carbonates are considered in situ precipitates which formed at or near the sediment surface due to emanation (and oxidation) of methane. Tubeworms partially cemented by carbonate support this interpretation.

A more detailed account on observations and biological results of our newly discovered vent site is presented in Chapters 6 (bottom observations) and 7 (geochemistry).

Figure 5.1.1: Working area of cruise SO-139 (GINCO3) with geological sampling sites (KL/SL: coring sites; GA: grab samples; KD: dredge samples)

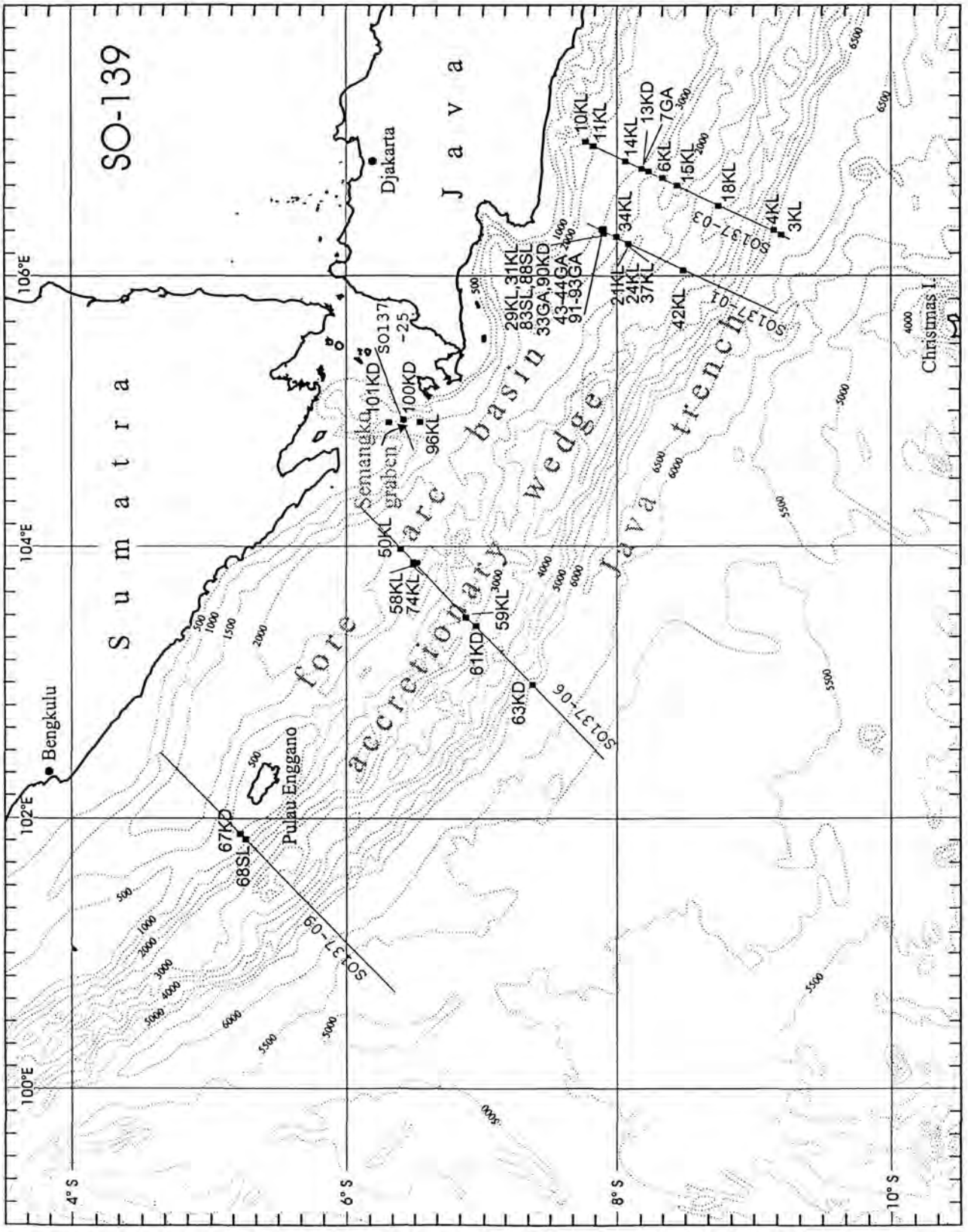

Figure 5.1.2:

Simplified structural profile across the accretionary complex off Java (for details see cruise report SO-137) with the projected position of sampling sites of cruise SO-139.

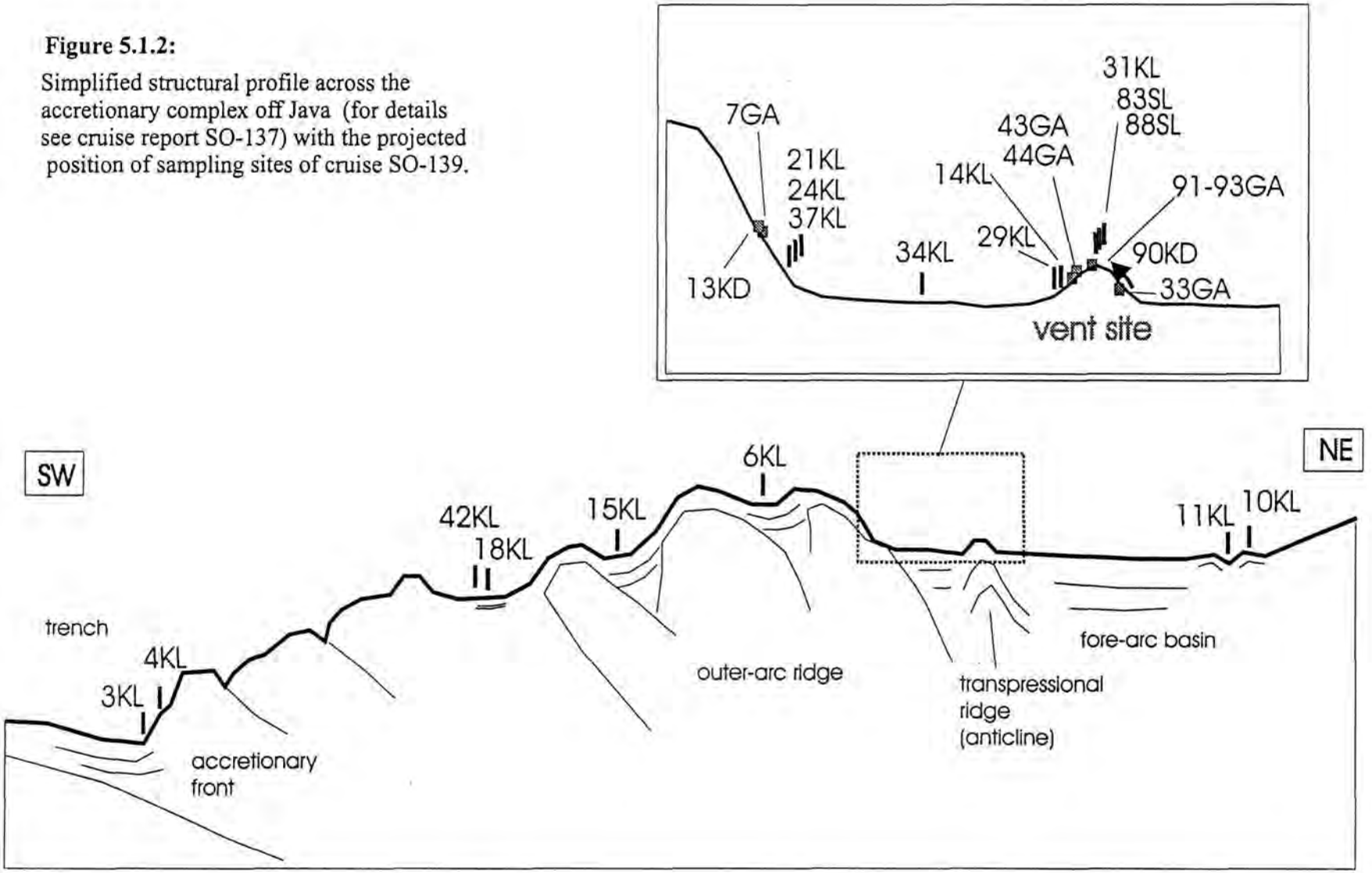

Figure 5.1.2: Part 2: Profiles southwest of Sumatra and off Sunda Strait.

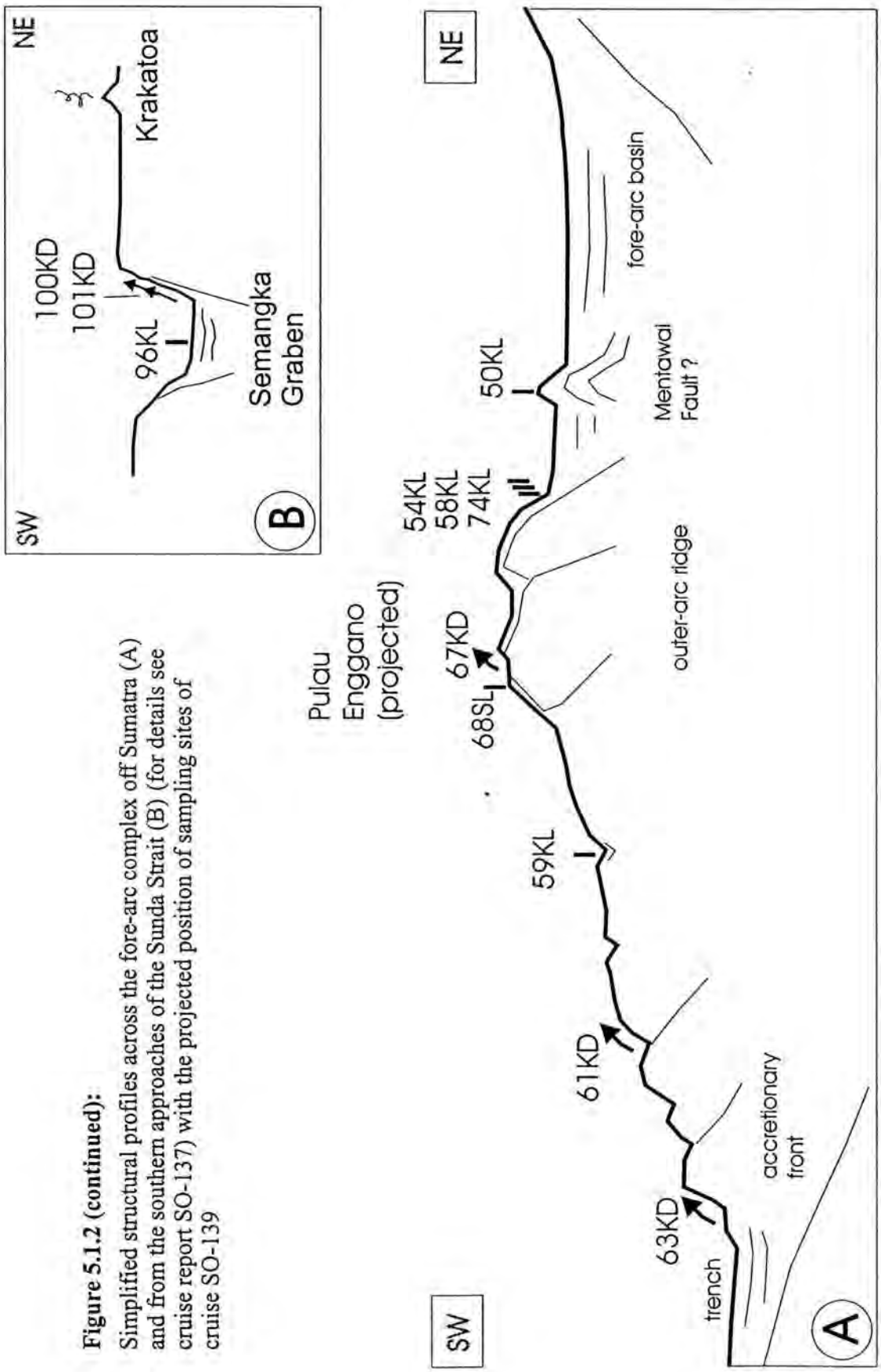

Figure 5.1.2 (continued):
Simplified structural profiles across the fore-arc complex off Sumatra (A) and from the southern approaches of the Sunda Strait (B) (for details see cruise report SO-137) with the projected position of sampling sites of cruise SO-139

Figure 5.1.3: Simplified core lithology of SO-139 cores (part 1: 3KL-31KL)

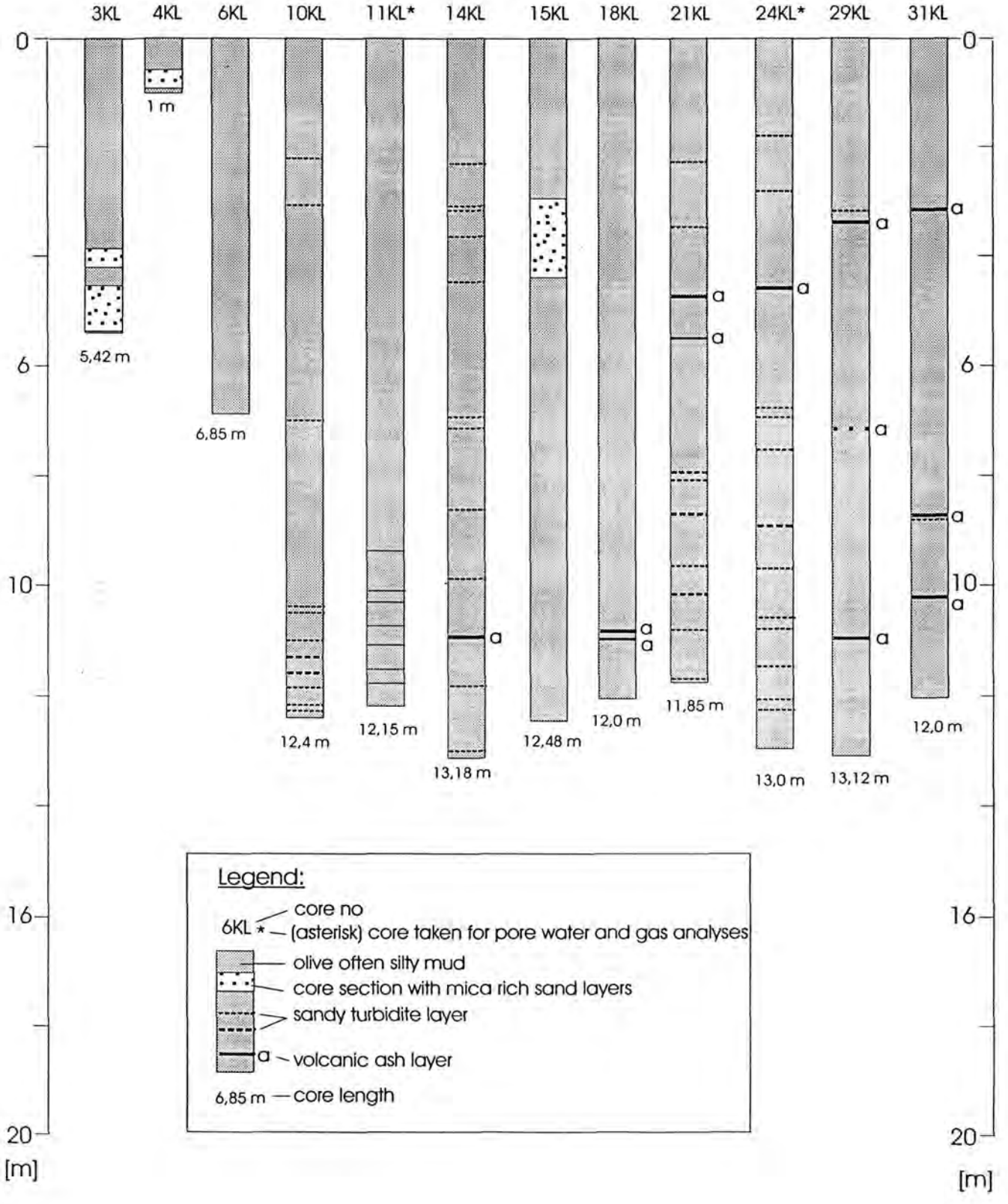

Figure 5.1.3 (continued): Simplified core lithology of SO-139 cores (part 2: 34KL - 96KL)

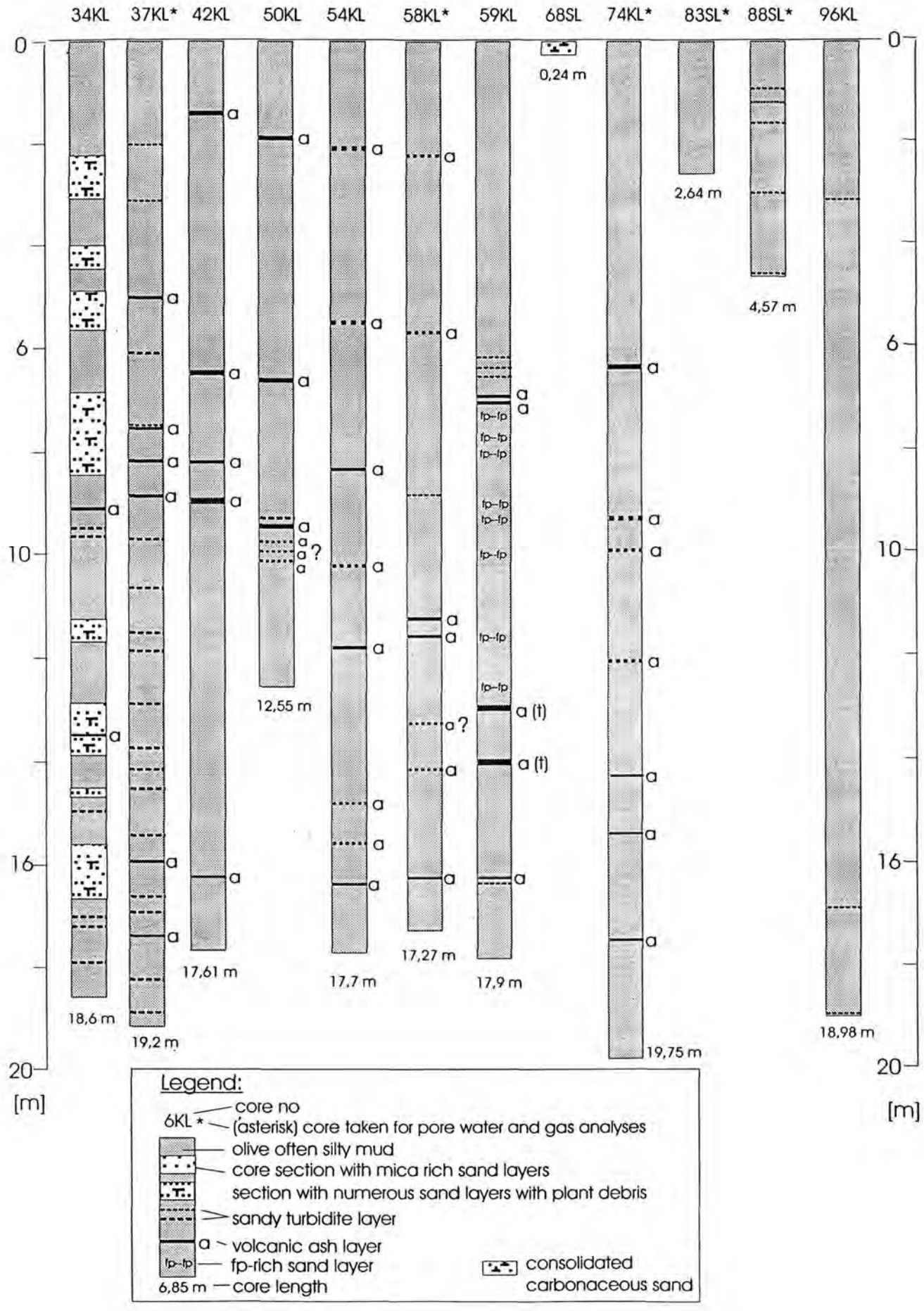

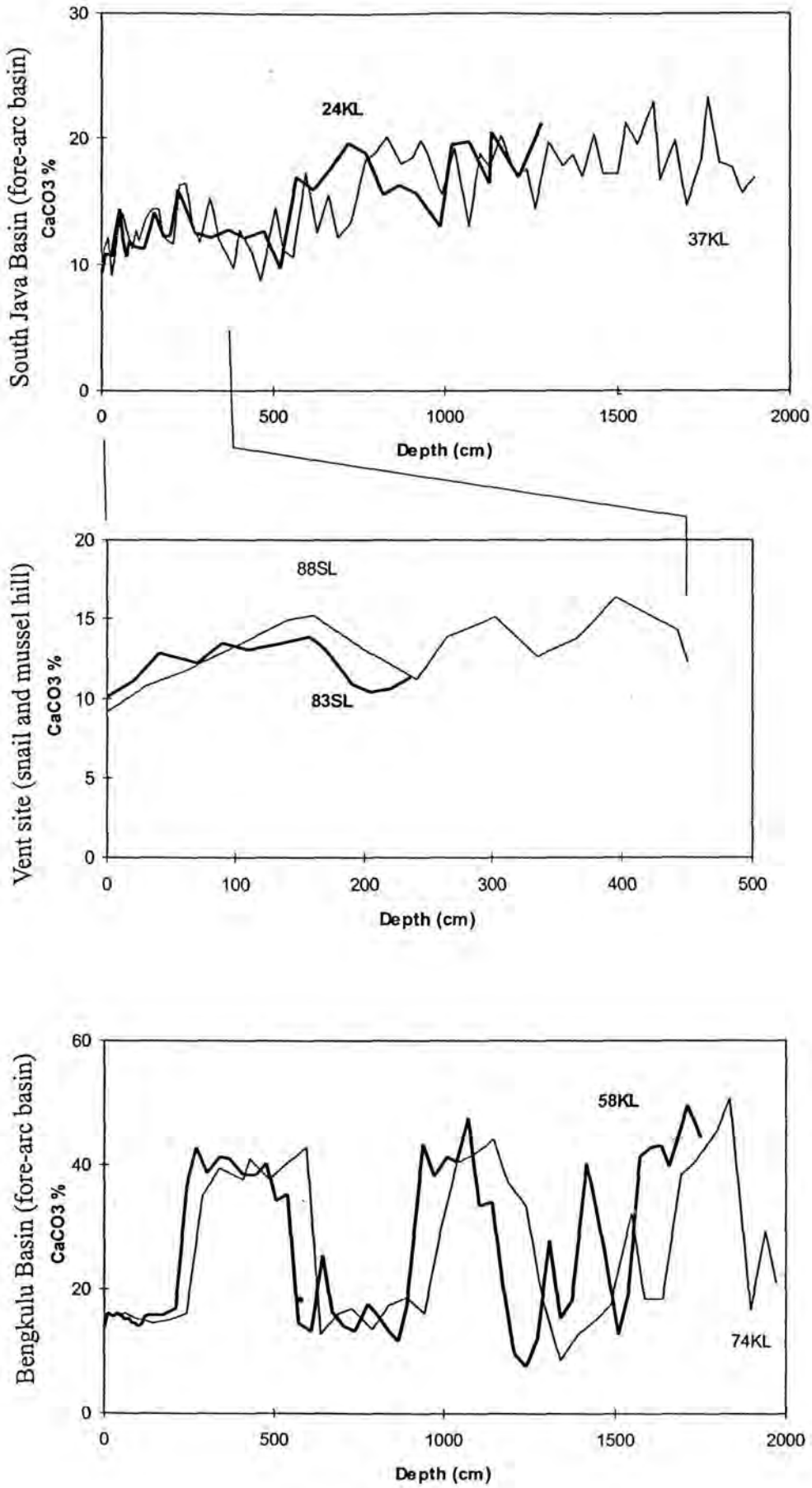

Figure 5.1.4:
Carbonate contents of selected sediment cores of cruise SO-139; $CaCO_3$ content is calculated from CaO as determined by XRF (see Chapter 7.3.1). 24KL and 37KL were taken at the same position with the intention to acquire a longer core for pore-water extraction. Similarly 74KL 'duplicates' core 58KL. Note the general fit of data from the short SL cores at the vent-hill location (83SL, 88SL) with the neighbouring long cores from the foot of the slope of the outer-arc high. Core 74KL has a slightly larger sedimentation rate than 58KL ! Both cores were taken in the Bengkulu basin south of Sumatra. Note, that that the latter two cores display a completely different carbonate distribution pattern than all cores south of Java.

Table 5.1.1: SO-139, Leg 1, geological sampling stations (KL, GA, KD)

Lokation	Recovery (KD=kg;KL=m)	trigger-corer (cm)	Structural setting	WD (m)	Lat (S)	Long (E)	Seismic Line
3KL	ca. 5,42	40	accretionary front, foot of slope	6338	9°11,10'	106°19,01'	3
4KL	ca. 1	25	accretionary front, 100 m above foot of slope	6274	9°10,88'	106°19,10'	3
6KL	6,85	65	small slope basin at outer arc high (OAH)	2139	8°22,04'	106°42,13'	3
10KL	12,4	5	northern margin of fore-arc basin, drift? sediments	2726	7°49,10'	106°57,62'	3
11KL	12,15	80	northern margin of fore-arc basin, drift? sediments	2798	7°56,75'	106°56,75'	3
14KL	13,19	93	ridge within fore-arc basin, crest of hill	3000	8°09,15'	106°48,15'	3
15KL	12,48	69	small slope basin at outer-arc high	2246	8°34,0'	106°36,48'	3
18KL	12	32	central accr. Wedge, small slope basin	3374	8°46,79'	106°30,26'	3
21KL	11,85	87	fore arc basin, close to southern margin	2994	8°01,60'	106°16,13'	1
24KL	13	100	fore arc basin, close to southern margin	2989	8°01,6'	106°16,09'	1
29KL	13,12	/	ridge within fore-arc basin, foot of vent hill	2995	7°57,66'	106°18,00'	1
31KL	12	91	ridge within fore-arc basin, top of hill	2952	7°57,00'	106°16,55'	1
34KL	18,6	65	fore-arc basin, south of vent hill	3021	7°59,25'	106°17,22'	1
37KL	19,2	/	fore-arc basin, close to southern margin (24KL)	2990	8°01,60'	106°16,09'	1
42KL	17,64	/	middle part of accretionary wedge, small basin	3182	8°24,64'	106°05,65'	1
7GA	stiff fp-mud, few rock frags	/	slope between fore-arc basin and outer-arc high	2954	8°16,66'	106°44,54'	3
33GA	mud, 1 x clam	/	ridge within fore-arc basin, light colored sediment patch at base of hill	2989	7°57,79'	106°17,20'	1
43GA	olive mud, carbonate	/	ridge within fore-arc basin, vent location	2930	7°57,44'	106°17,62'	1
44GA	olive mud, carbonate	/	ridge within fore-arc basin, vent location	2900	7°57,45'	106°17,71'	1
13KD	200 kg consol. sed.	/	slope between fore-arc basin and outer-arc high	ca. 2600	ca. 8°20,03'	106°47,2'	3
16KD	empty	/	2nd morphological step of accretionary front	4570	9°02,06'	105°22,28'	3
28KD	concretions, 2 vent clams	/	ridge within fore-arc basin, vent location	ca. 2946	7°56,66'	106°15,85	1

Table 5.1.1 (continued): SO-139, Leg 2, geological sampling stations (KL, KD, GA)

Lokation	Recovery (KD=kg;KL=m)	Structural setting	WD (m)	Lat (S)	Long (E)	Seismic Line
50KL	12,55	crest of ridge within fore-arc basin	1875	6°24.64'	103°58.39'	6
54KL	17,70	slope between fore-arc basin and outer-arc high	1699	6°32,64'	103°50,13'	6
58KL	17,27	slope between fore-arc basin and outer-arc high	1696	6°32,58'	103°50,02'	6
59KL	17,90	small slope basin at central part of accretionary wedge	2655	6°51,87'	103°30,08'	6
68SL	24 cm porous arenitic limestone, with hardground	outer-arc high, with basement outcrops	698	5°11,60'	101°54,89'	9A
74KL	19,75	slope between fore-arc basin and outer-arc high (site 54KL)	1690	6°32,58'	103°50,02'	6
83SL	2,64	ridge within fore-arc basin, vent locatiion, W-side of hill top	2945	7°57,44'	106°17,61	1
88SL	4,57	ridge within fore-arc basin, vent location, N-NE of hill top	2939	7°57,42'	106°17,66	1
96KL	18,22	Semangko graben, southwest of Sunda Strait	1891	6°34,09'	104°54,08'	near 42
61KD	50kg, fp-rich mud, stiff mud, mudstone frags, chert	central part of accretionary wedge, steep slope	ca. 2800	6°55,91'	103°25,93'	6
63KD	mud and mudstone	front of accretionary wedge, steep slope near canyon	ca. 5800	7°21,47'	102°56,67'	6
67KD	pooorly cemented calcareous sands, crusts	outer arc high with basement outcrops, W of Pulau Enggano	627	5°11,33'	101°55,50'	9A
67-2 KD	porous arenitic limestone, with hardground	s.a.	635	5°11,02'	101°55,47'	9A
90KD	2 small rock fragments	ridge within fore-arc basin, E slope of vent hill	2961	7°57,63'	106°17,45'	1
100KD	stiff mud, 1x tube worm	northern flank of Semangko graben near Sunda Straits	1557	6°24,91'	104°49,24'	near 25
101KD	various basement rocks	northern flank of Semangko graben near Sunda Straits	1450	6°12,91'	104°51,78'	near 25
91GA	olive mud with pogos, clams, few shells	vent area, near hill top (ridge within fore-arc basin)	2963	7°57,40'	106°17,90'	1
92GA	olive mud with pogos, few clam shells	vent area, near hill top (ridge within fore-arc basin)	2934	7°57,45'	106°17,81'	1
93GA	olive mud	vent area, near hill top (ridge within fore-arc basin)	2952	7°57,43'	106°17,58'	1

5.1.2 Core logging

M. Wiedicke, W. Weiss, Udrekh, Haryadi Permada, and D. Steinmann

5.1.2.1 Introduction

As a standard procedure we have logged our cores before opening and further sampling. Logging provides a non destructive method for achieving high-resolution records of physical properties which in turn allow derivation of lithologic character and changes.

5.1.2.2 Method:

Before sediment cores were logged we stored them in the ship's lab for at least 8 hours to adjust to room temperature (about 20°C); only cores of uniform temperature give proper logging results . Sediment sections of 1 m were then logged with the Multi-Sensor-Core-Logger (MSCL) of GEOTEK (P. Schultheiss, Surrey, UK). The logging device (see Fig. 5.1.5) is about 4 m long and is capable of logging cores of 1,25 m length and 12,5 cm diameter.The MSCL is automated (PC based) and designed for non-destructive logging; it allows to determine P-wave velocity, bulk density and magnetic susceptibility by measuring p-wave travel time, gamma ray attenuation, and susceptibility. A step motor pushes the core incrementally (during our cruise in steps of 1 cm) ahead thus transporting the core along its three probes:

(a) P-wave sensor: A pair of spring-loaded compressional wave transducers to measure the P-wave travelling time through the core and liner. To get high quality data a good acoustic coupling between the sediment and the liner and between the transducers and the liner is required. The latter was ensured by regularly dropping some water between the liner and the transducers. The recorded signal amplitude, which is very sensitive to acoustic coupling indicates the quality of the required data. The P-wave probe requires repeated and ongoing calibrations for accurate sound velocity calculations.

(b) A gamma-ray probe: A 10 milli-curie caesium-137 gamma source and a detector are mounted on opposite sites of the core track to allow measurements of the attenuation of gamma rays through the core. The small CsCl capsule is securely housed in a 150 mm diameter lead shield with an interchangeable collimator or safety plug. The determination of density is based on the attenuation of gamma rays by a sediment filled liner. The attenuation is measured by a scintillation detector and expressed as counts per time (gamma counts). For the calibration of the gamma probe several standards were prepared (aluminium, graphite, plexiglas), which were run through the logger every day. Also, at the beginning of the logging record of each new core, the instrument records gamma counts through air, which can be used as an inherent standard.

(c) A magnetic susceptibility sensor: to determine the amount of magnetic particles in the sediment. The Bartington loop sensor (MS2B) is located on a central plastic assembly which lies between the two main aluminium box sections. Its position ensures a maximum distance to metal parts of the device which could affect the sensor loop. The inner loop diameter is 100 resp. 130 mm.

Additional aspects of importance to logging are briefly listed below:

- The continuity of the measurements along core is slightly interrupted at the ends of the 1m sections despite the fact that the following 1m-section is already in place for logging. The magnetic susceptibility probe, which integrates over a core length of about 15 cm, therefore produces somewhat low values in the top 8 cm and basal 8 cm of each core section.
- The starting point of each 1m section for logging is manually defined. Therefore, depth accuracy of logging data is limited (+ 2-3 cm) despite the fact that the step motor is working with very high precision.
- The cutting procedure tends to cause mechanical disturbances of the sediment core at both section ends which sometimes influences the quality of gamma-attenuation and P-wave data in the basal and topmost few centimetres. This is particularly true for many of the lowermost 0.5 m sections of the cores, used for immediate ‚gas' samples.
- Additionally, the high gas content of several of the sediment cores of this cruise also affected the gamma counts and occasionally led to a flawed p-wave record.

5.1.2.3 Logging results

Core-log results are graphically presented in Figure 5.1.6; curves represent raw data with false individual data points manually deleted. Log data shall be calibrated and converted to show P-wave velocity and bulk density of the cores.
We logged all piston and gravity cores except for the 'geochemical/pore water cores'(11KL, 24KL, 37KL, 58KL, 74KL, 83SL and 88SL). which had to be opened immediately.

Gamma counts and P-wave traveltime show a positive correlation in all measured cores. Coarser material appears to be denser than finer material and absorbs more acoustic energy than fine-grained material. The highest values of gamma counts and P-wave traveltime were observed in basal sandy layers of turbidites. In areas with high terrigenous input variations of both parameters can be largely explained as a function of grain size and porosity.

Most peaks of the magnetic susceptibility are positive correlated with the gamma counts and p-wave traveltime curves. However, the amplitudes often differ, and not all gamma-count peaks have an equivalent in susceptibility. This could be explained by a commonly higher susceptibility of the coarser grain-size fraction which often incorporates volcanic debris (=>magnetite); pelagic turbidites don't show this signal.
In addition, in many cores the magnetic susceptibility has a low frequency signal (e.g. at 2 m depth of 6KL, upper 2m of 10KL and 15KL), which cannot be found in the records of the two other probes. It is thought to indicate local input of volcanic debris, probably due to volcanic activity of one of the nearby active volcanoes of the island arc.

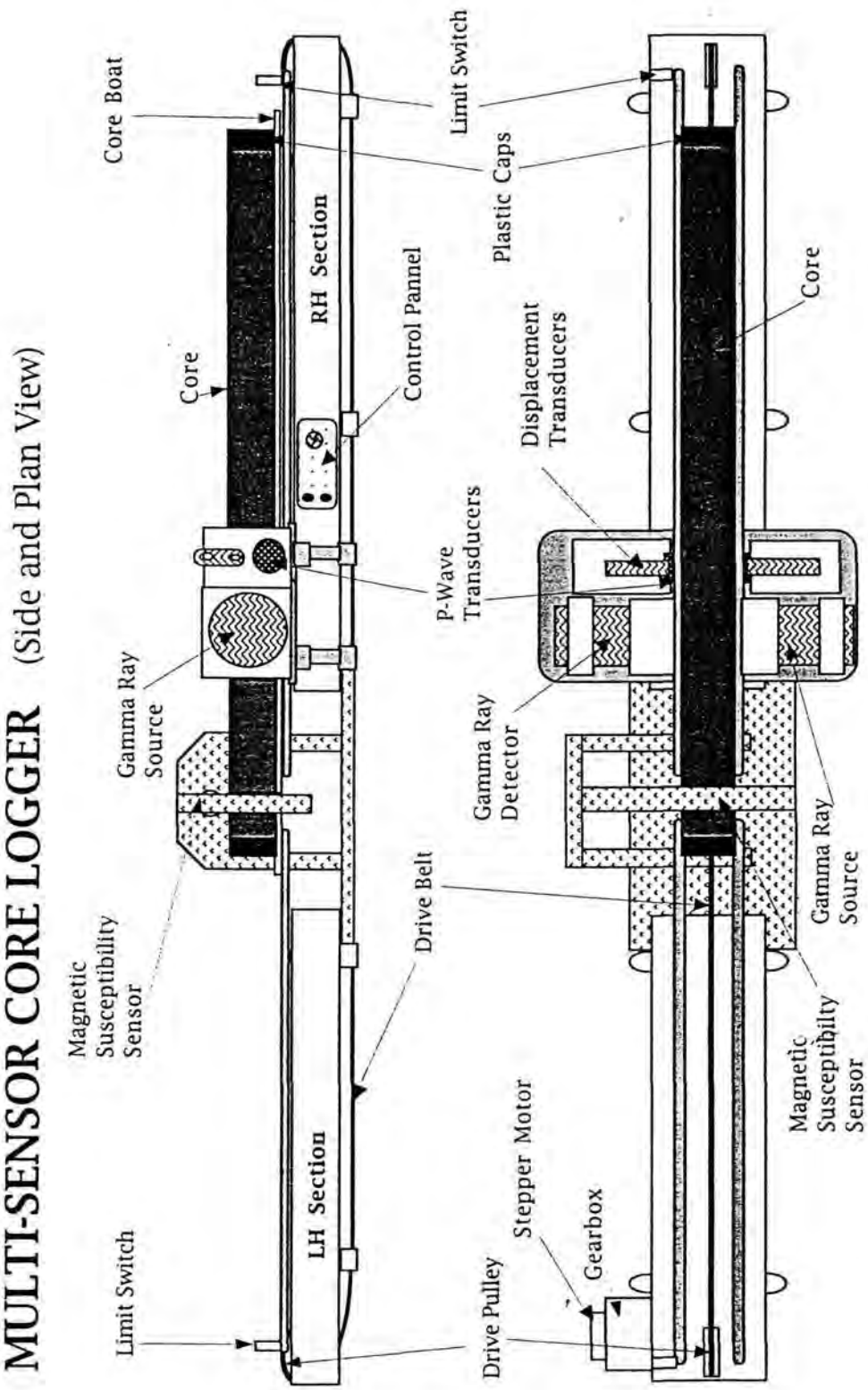

Figure 5.1.5: Sketch of the multi-sensor core-logger (MSCL) used during cruise SO-139

Figure 5.1.6: Results of core logging of 15 cores using the MSCL (3KL, 6KL, 10KL, 14KL, 15KL, 18KL, 21KL, 29KL, 31KL, 34KL, 42KL, 50KL, 54KL, 59KL, 96KL).

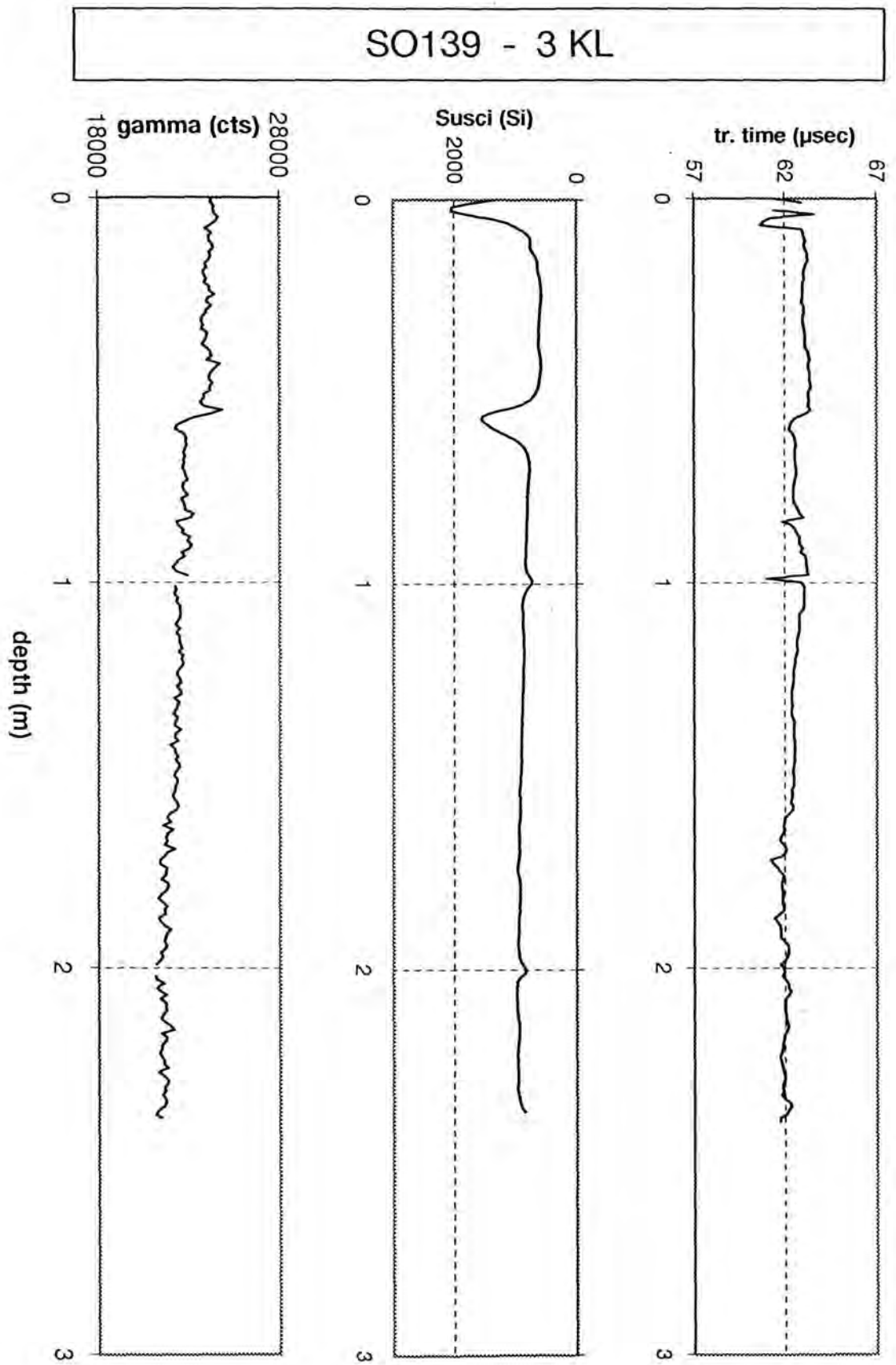

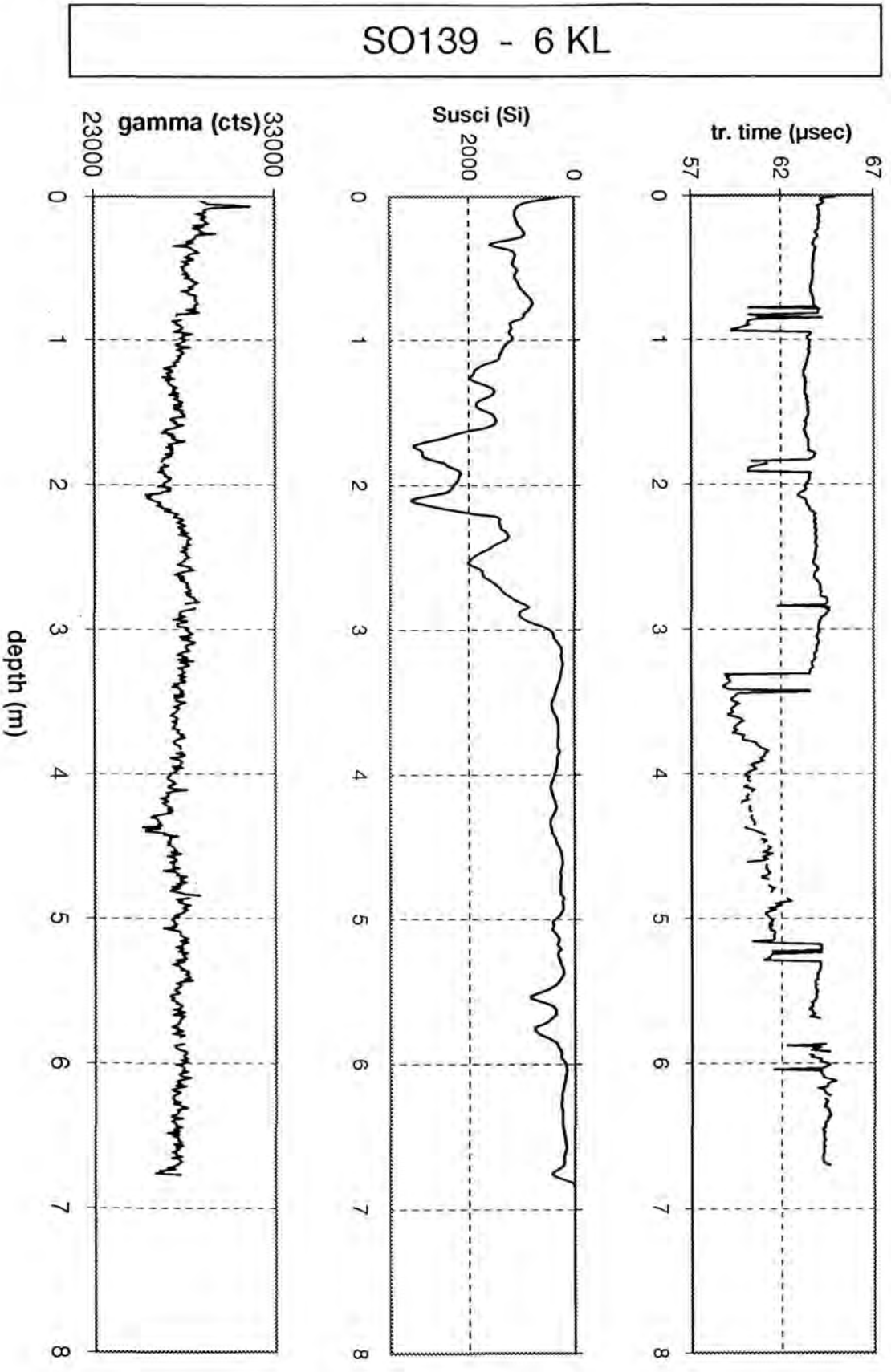
SO139 - 6 KL
gamma (cts)
23000
33000
Susci (Si)
2000
0
tr. time (µsec)
57
62
67
depth (m)
0
1
2
3
4
5
6
7
8

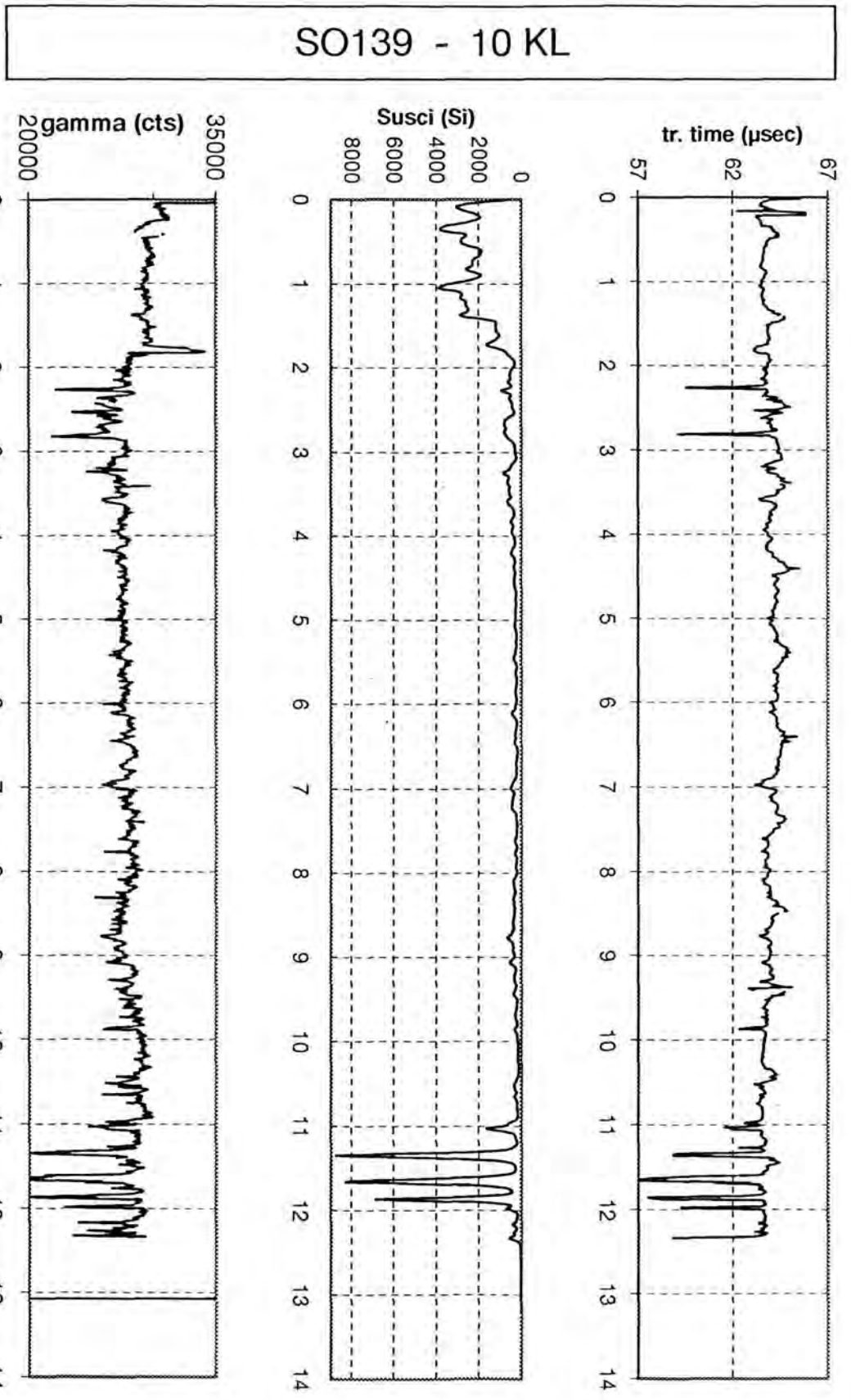
SO139 - 10 KL
tr. time (µsec)
57
62
67
Susci (Si)
0
2000
4000
6000
8000
gamma (cts)
20000
35000
depth (m)
0
1
2
3
4
5
6
7
8
9
10
11
12
13
14

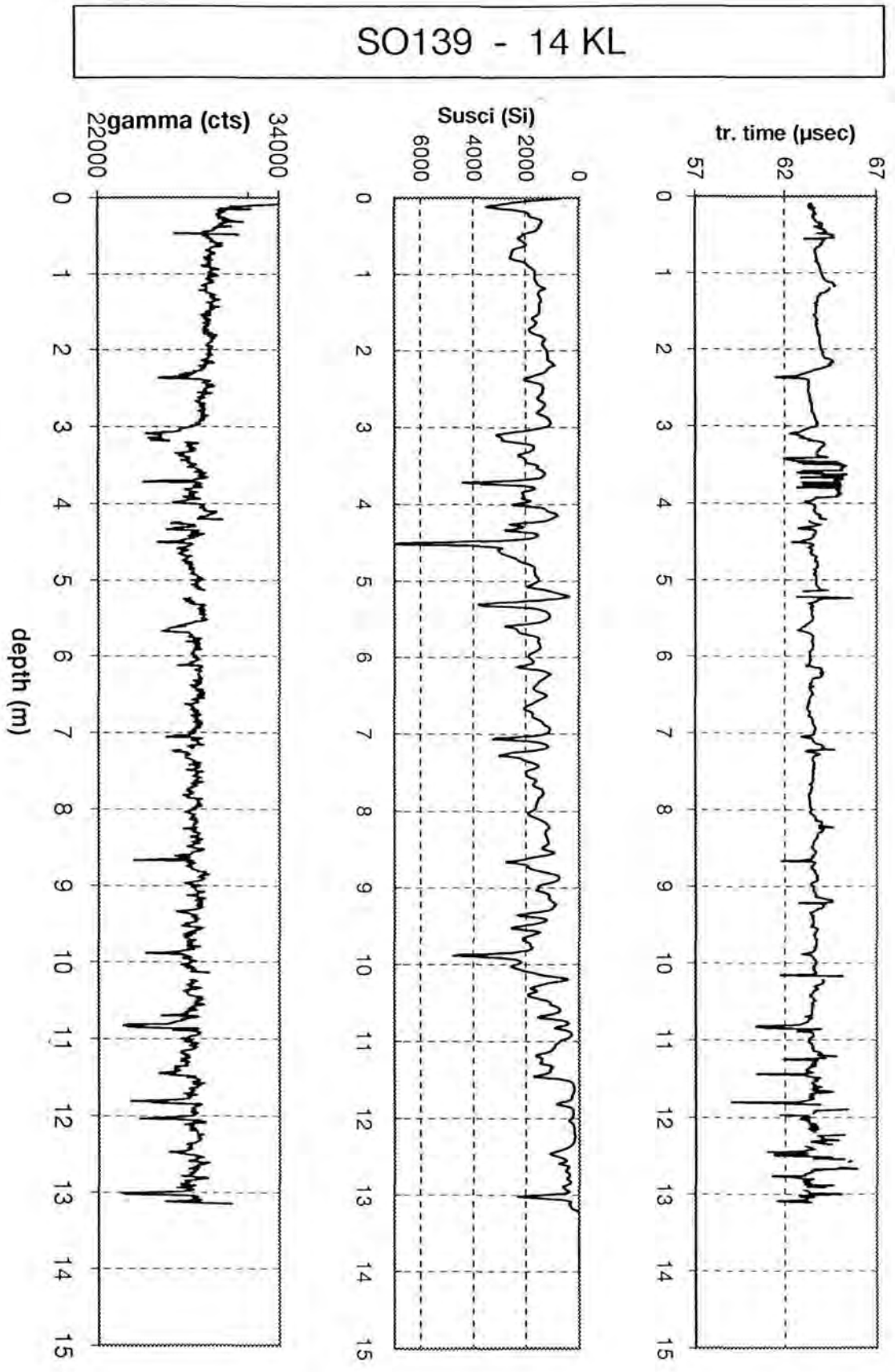
SO139 - 14 KL
tr. time (µsec)
57
62
67
Susci (Si)
0
2000
4000
6000
gamma (cts)
22000
34000
depth (m)
0
1
2
3
4
5
6
7
8
9
10
11
12
13
14
15

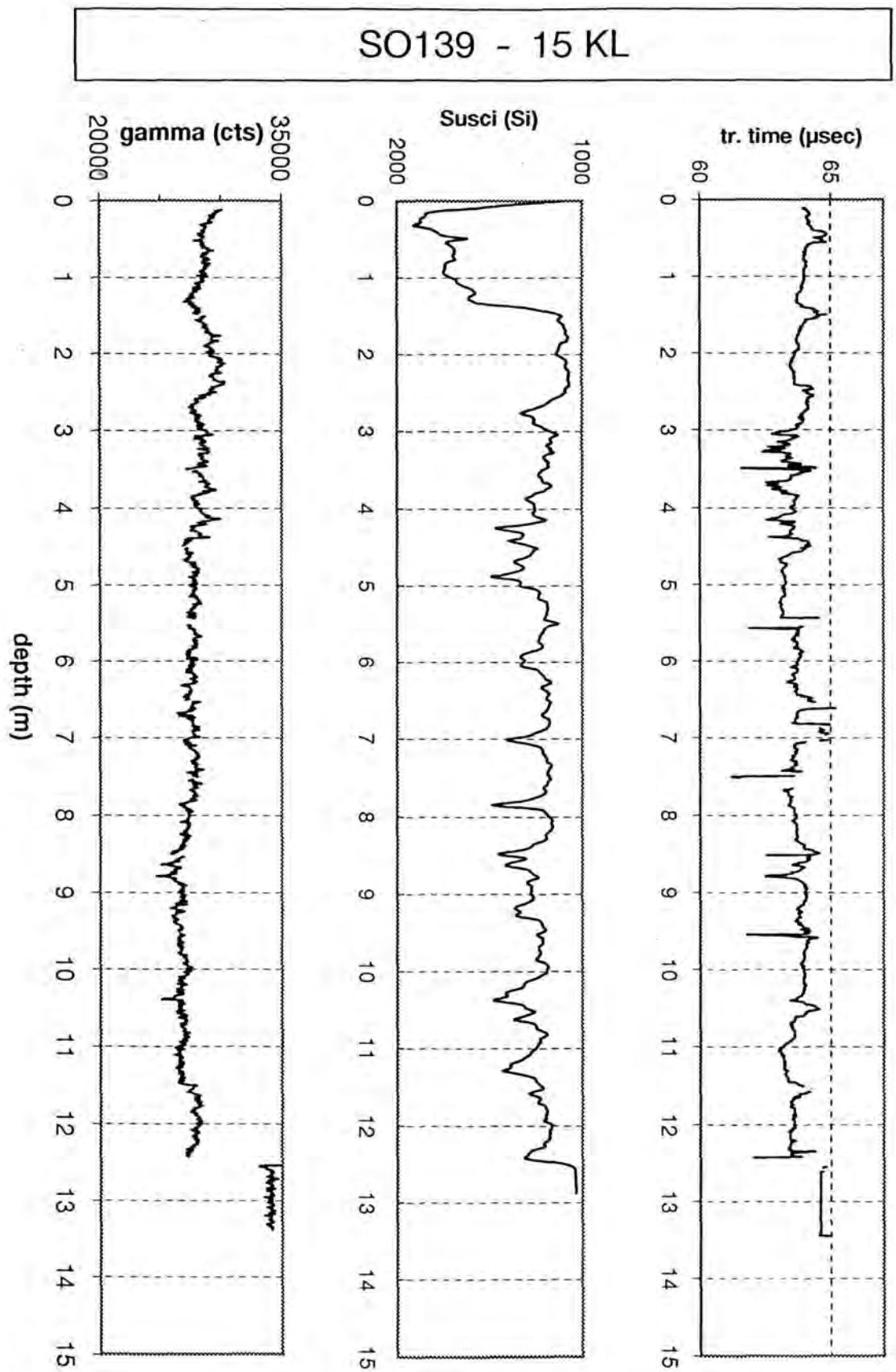
SO139 - 15 KL
tr. time (µsec)
60
65
Susci (Si)
2000
1000
gamma (cts)
20000
35000
depth (m)
0
1
2
3
4
5
6
7
8
9
10
11
12
13
14
15

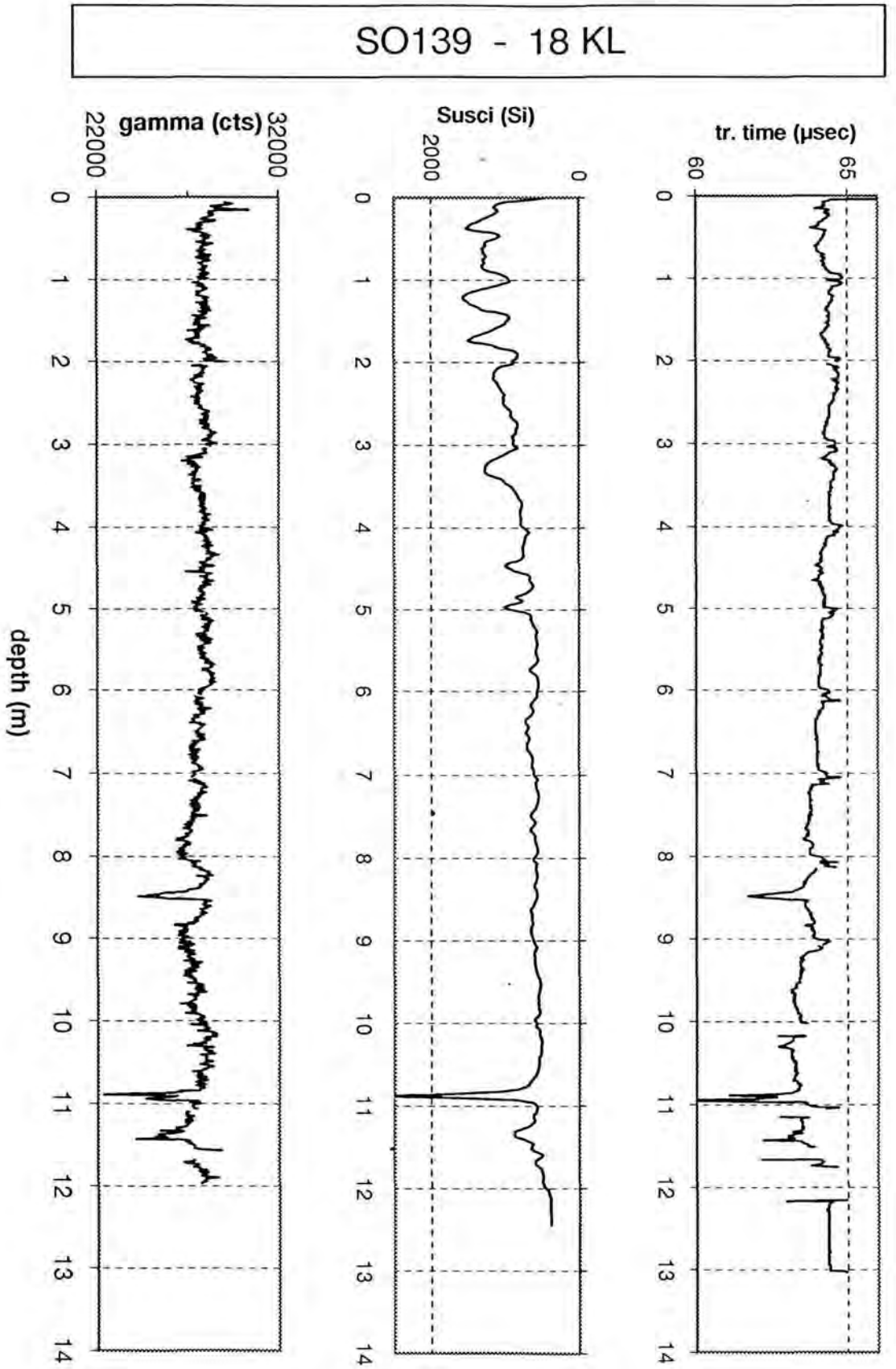
SO139 - 18 KL
tr. time (µsec)
60
65
Susci (Si)
2000
0
gamma (cts)
22000
32000
depth (m)
0
1
2
3
4
5
6
7
8
9
10
11
12
13
14

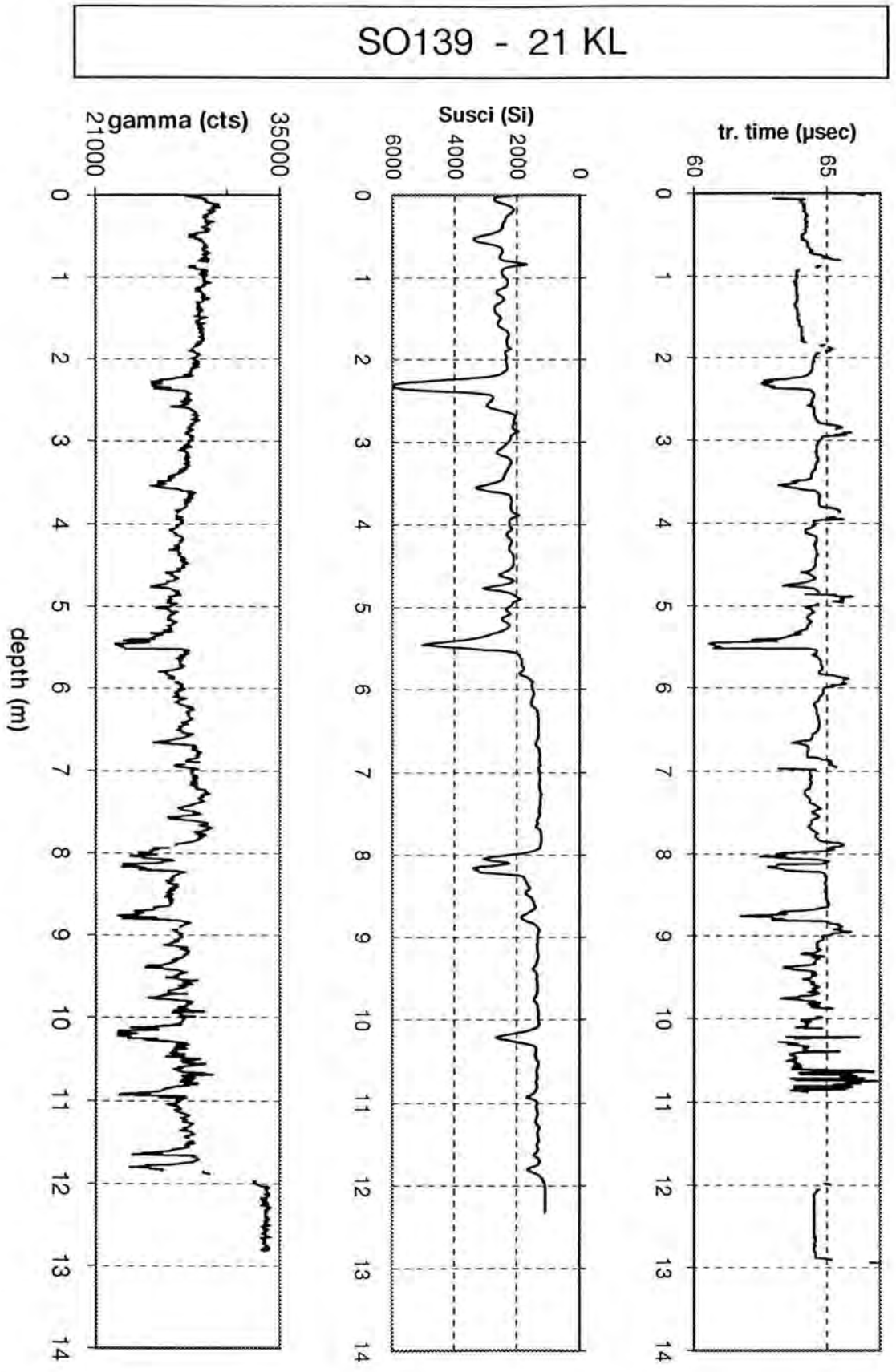
SO139 - 21 KL
tr. time (µsec)
60
65
Susci (Si)
6000
4000
2000
0
gamma (cts)
21000
35000
depth (m)
0
1
2
3
4
5
6
7
8
9
10
11
12
13
14

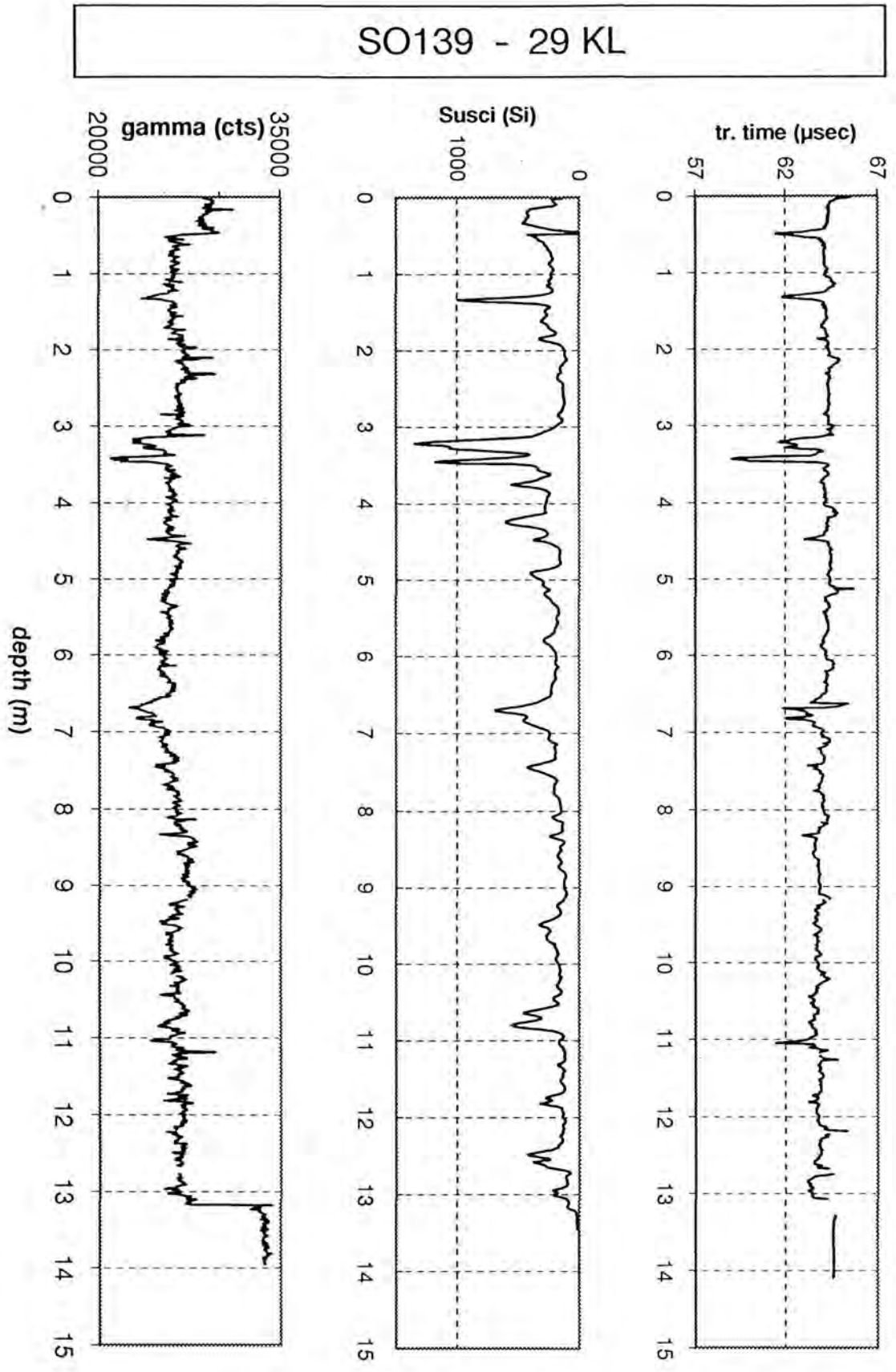
SO139 - 29 KL
tr. time (µsec)
57
62
67
Susci (Si)
1000
0
gamma (cts)
20000
35000
depth (m)
0
1
2
3
4
5
6
7
8
9
10
11
12
13
14
15

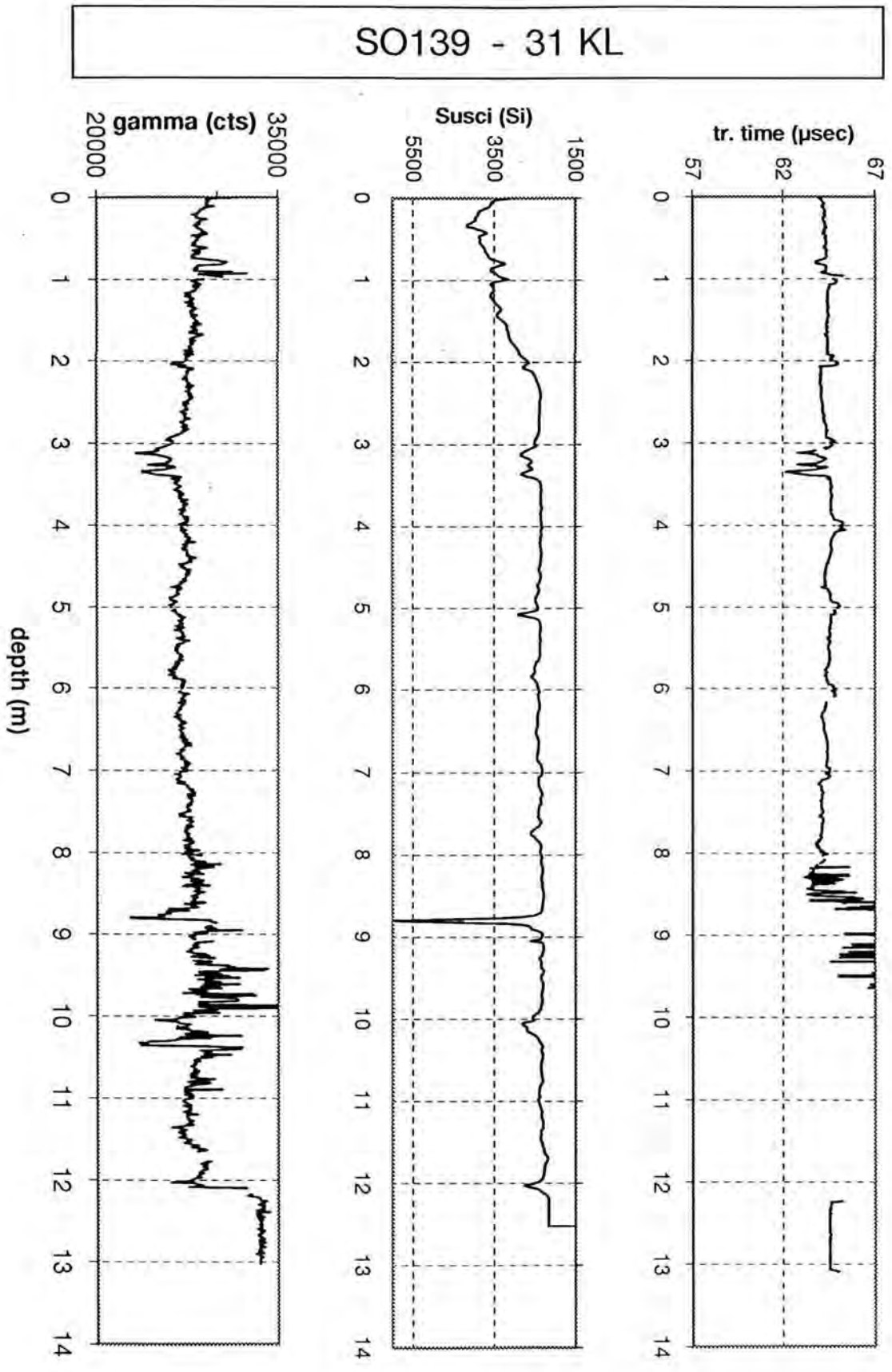
SO139 - 31 KL
tr. time (µsec)
57
62
67
Susci (Si)
5500
3500
1500
gamma (cts)
20000
35000
depth (m)
0
1
2
3
4
5
6
7
8
9
10
11
12
13
14

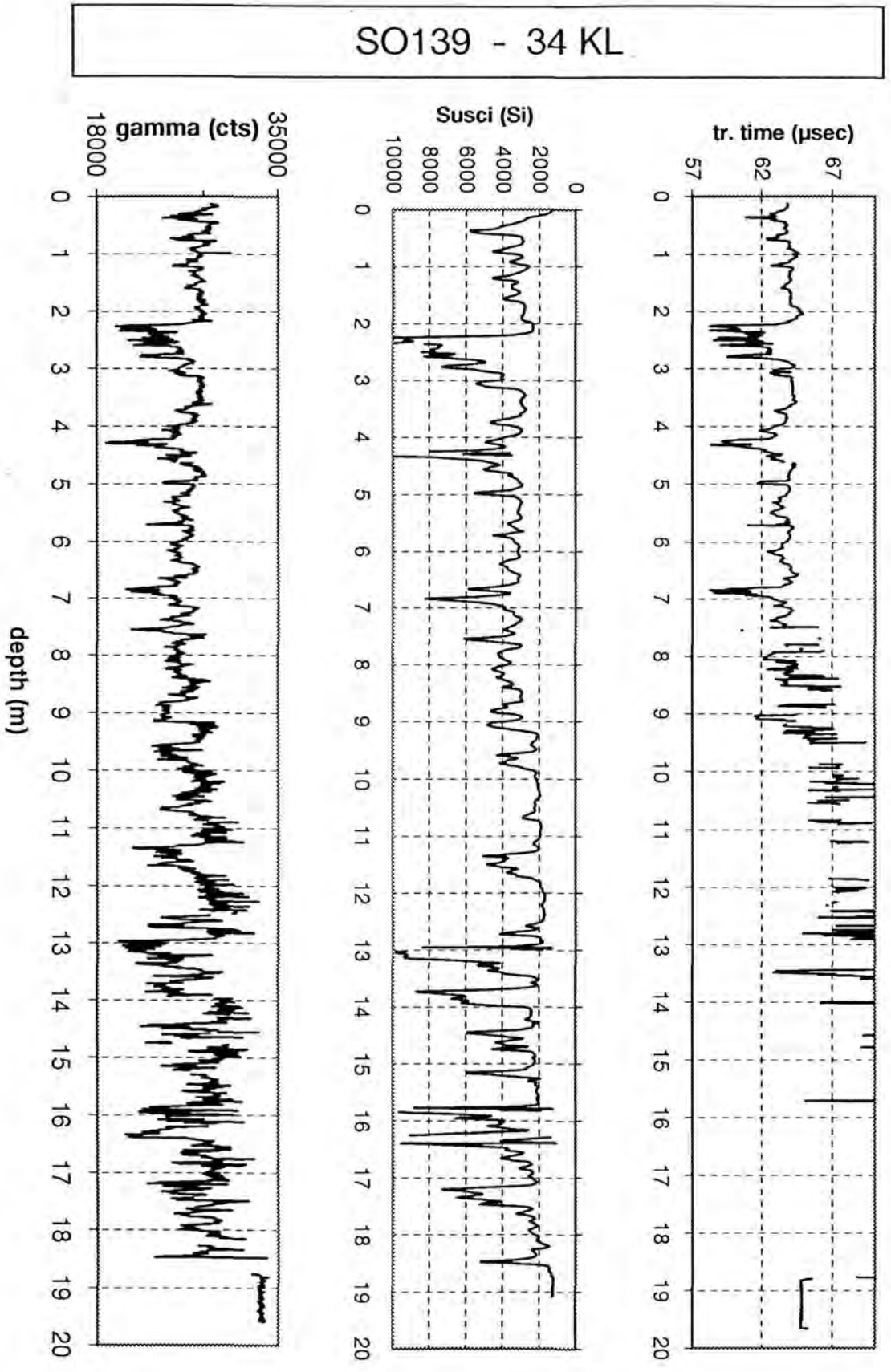
SO139 - 34 KL
tr. time (µsec)
57
62
67
Susci (Si)
0
2000
4000
6000
8000
10000
gamma (cts)
18000
35000
depth (m)
0 1 2 3 4 5 6 7 8 9 10 11 12 13 14 15 16 17 18 19 20

SO139 - 42 KL

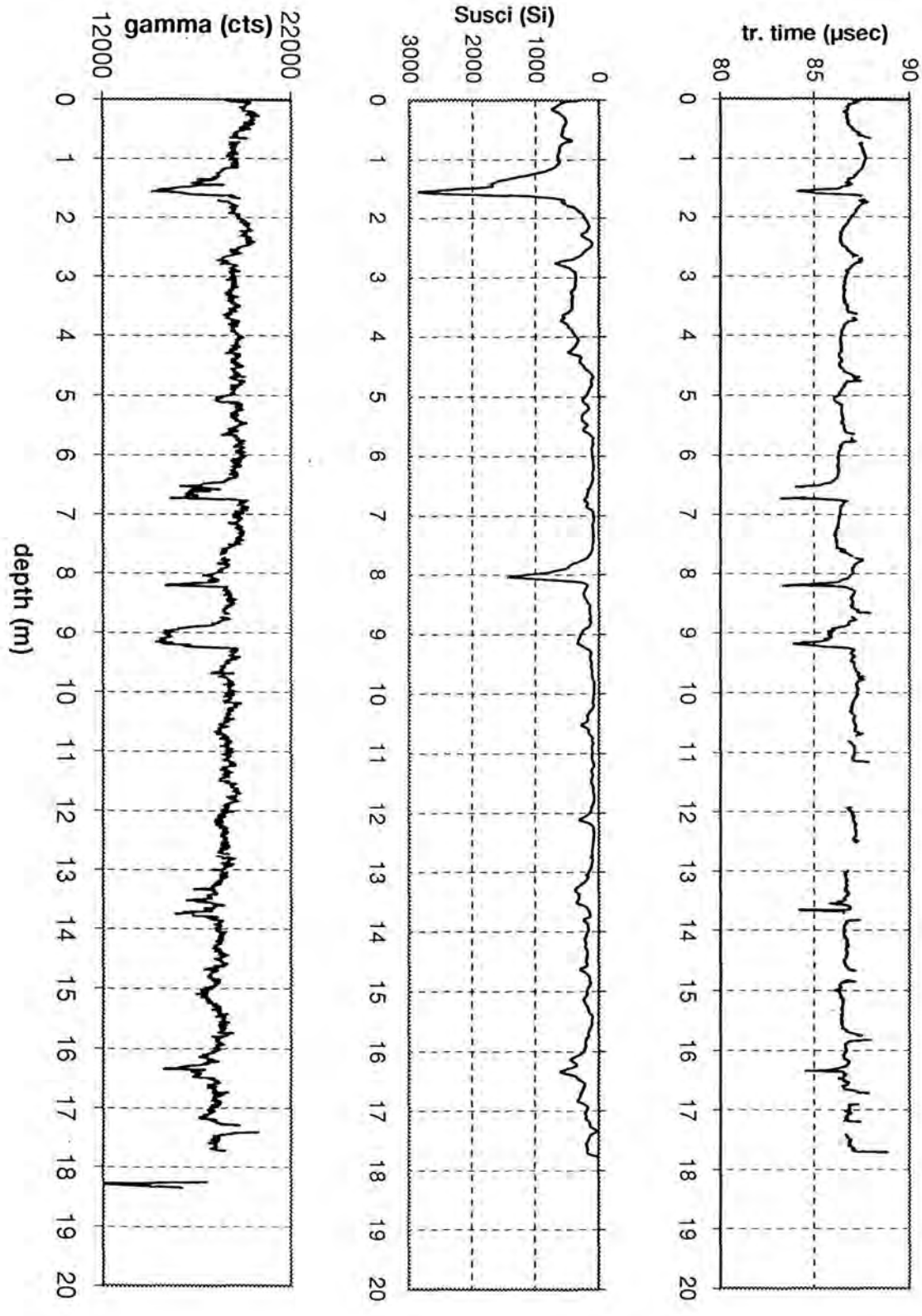
tr. time (µsec)
80
85
90
Susci (Si)
3000
2000
1000
0
gamma (cts)
12000
22000
depth (m)
0
1
2
3
4
5
6
7
8
9
10
11
12
13
14
15
16
17
18
19
20

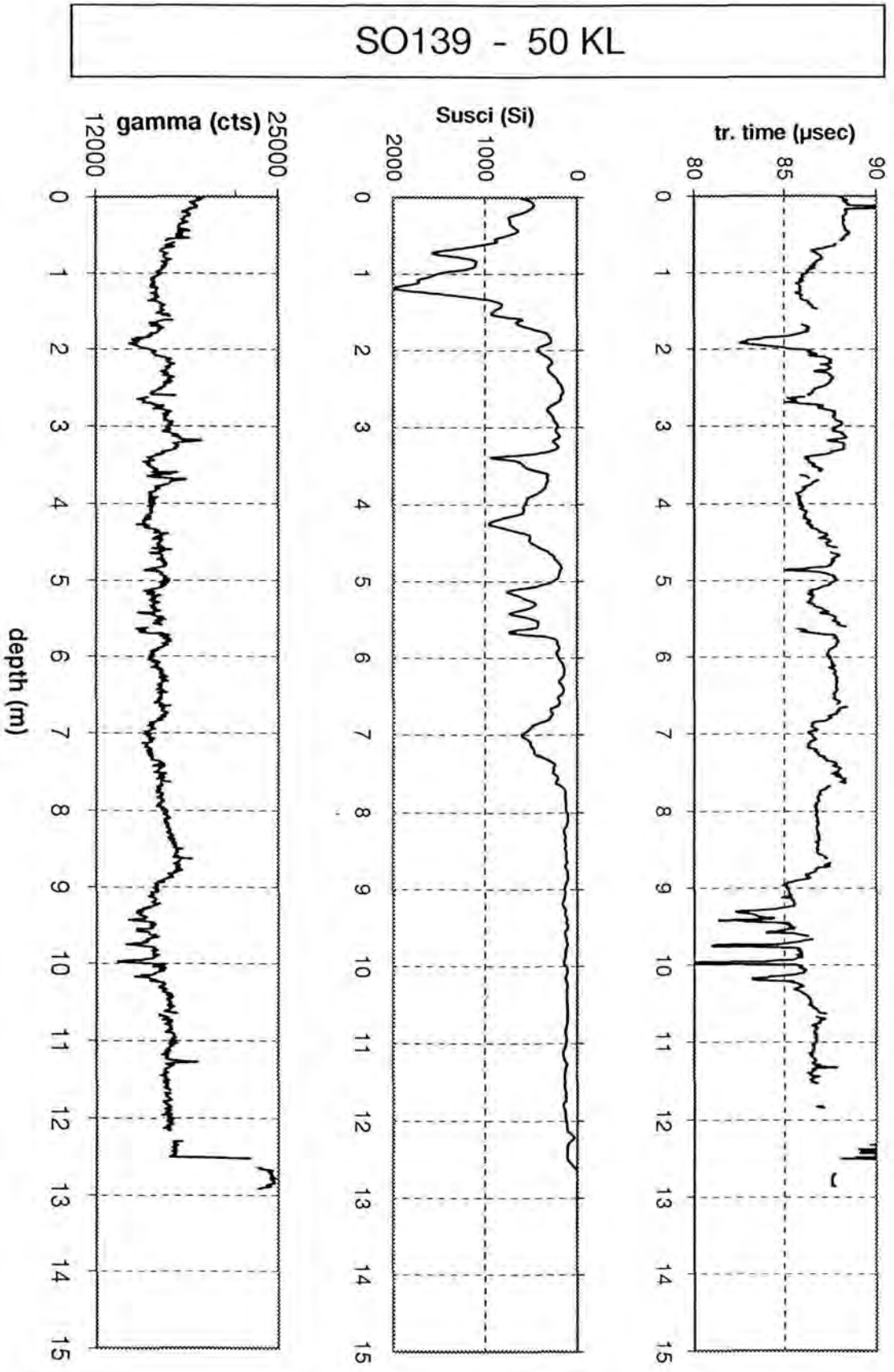
SO139 - 50 KL
tr. time (µsec)
80
85
90
Susci (Si)
2000
1000
0
gamma (cts)
12000
25000
0 1 2 3 4 5 6 7 8 9 10 11 12 13 14 15
depth (m)

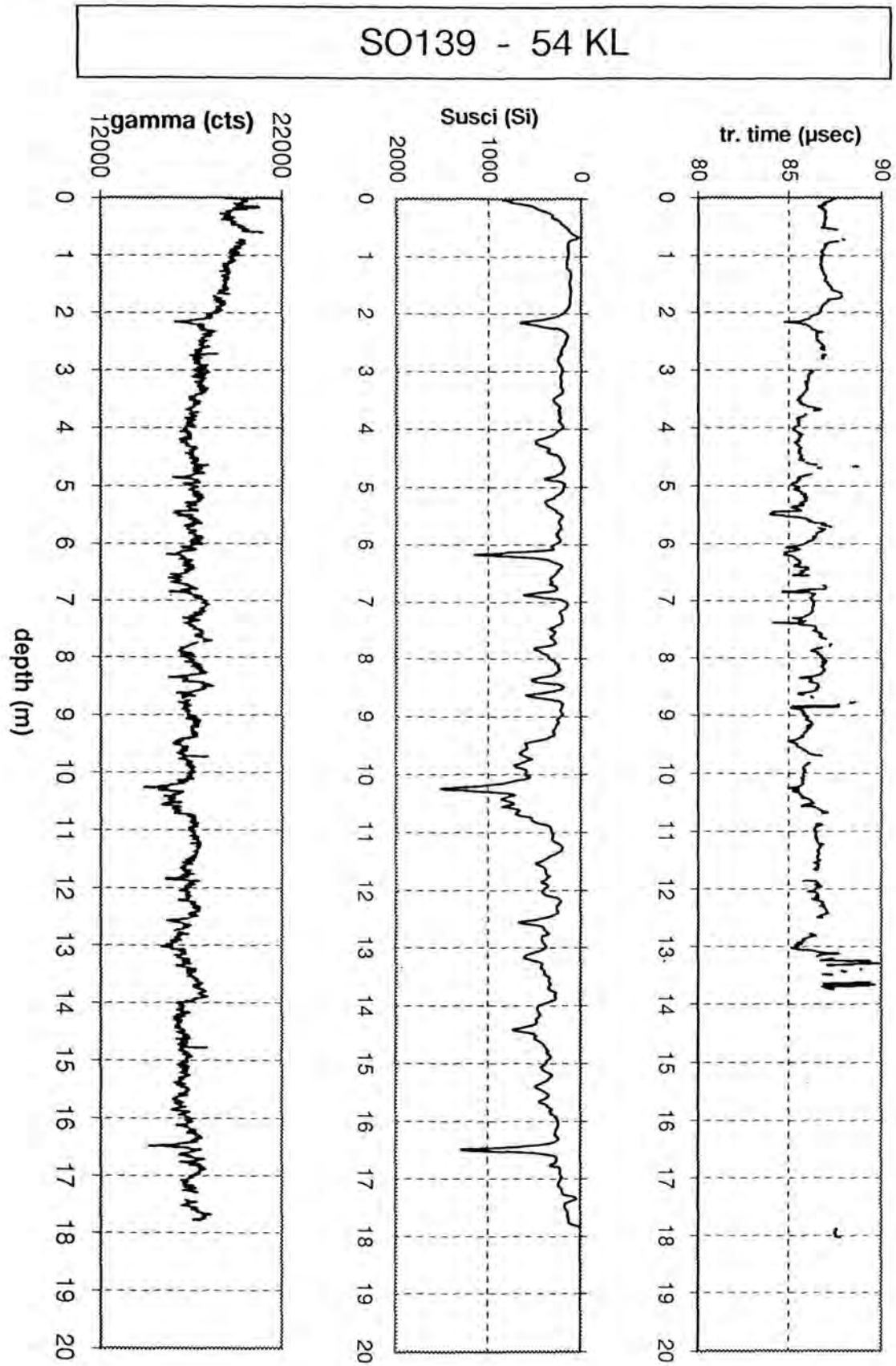
SO139 - 54 KL
tr. time (µsec)
80
85
90
Susci (Si)
2000
1000
0
gamma (cts)
12000
22000
depth (m)
0 1 2 3 4 5 6 7 8 9 10 11 12 13 14 15 16 17 18 19 20

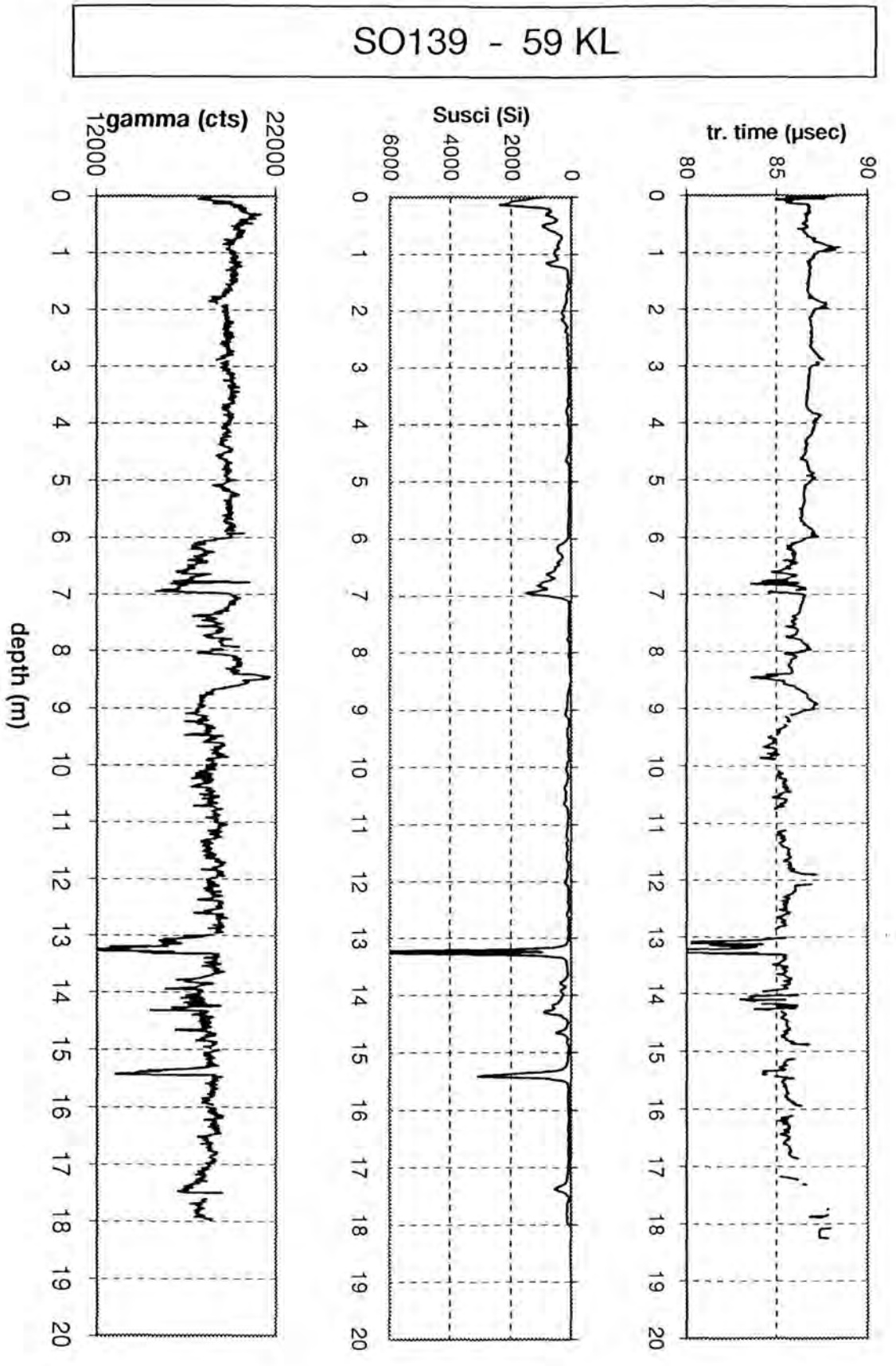
SO139 - 59 KL
tr. time (µsec)
80
85
90
Susci (Si)
6000
4000
2000
0
gamma (cts)
12000
22000
depth (m)
0
1
2
3
4
5
6
7
8
9
10
11
12
13
14
15
16
17
18
19
20

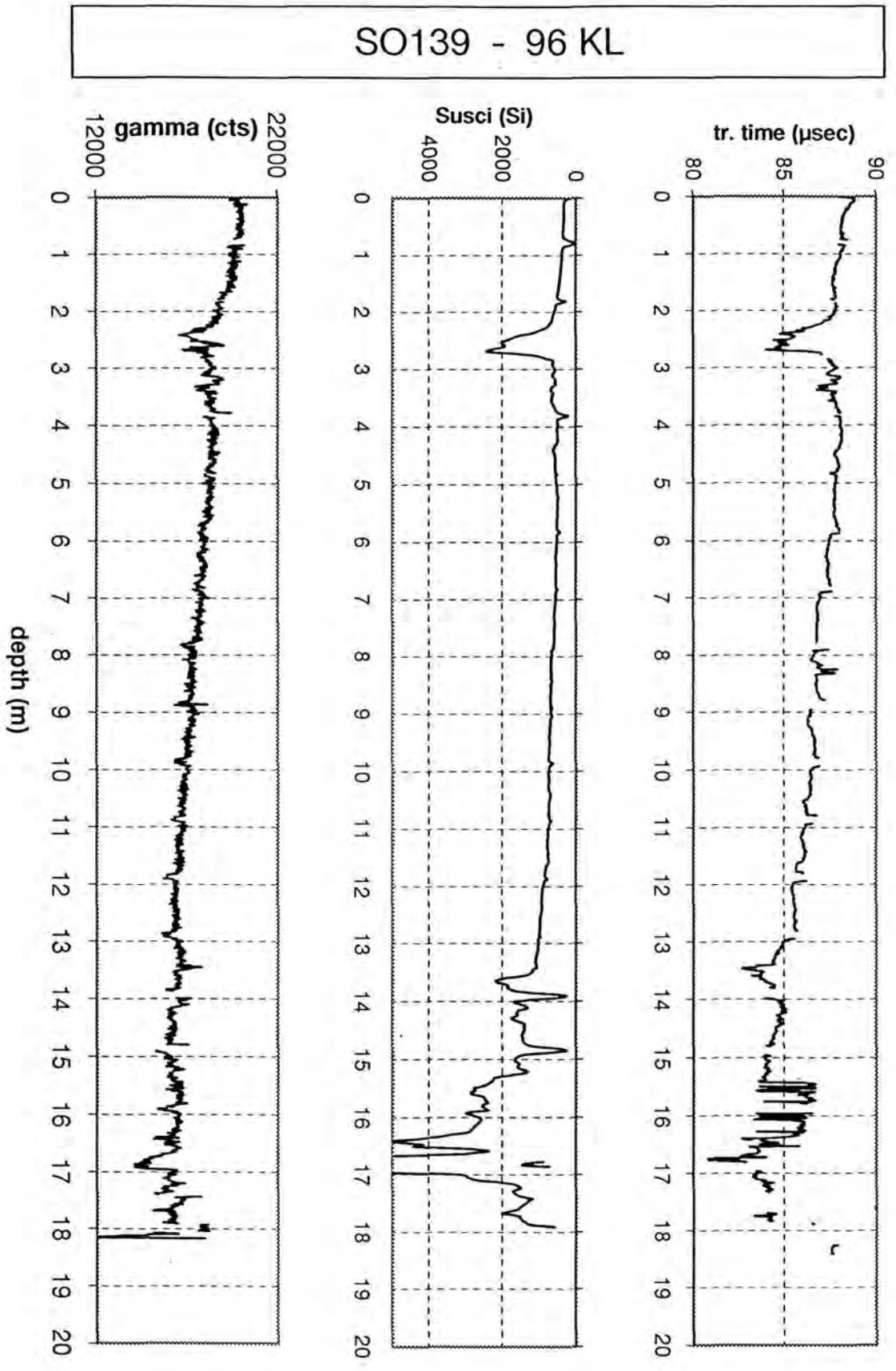
SO139 - 96 KL
tr. time (µsec)
80
85
90
Susci (Si)
0
2000
4000
gamma (cts)
12000
22000
depth (m)
0
1
2
3
4
5
6
7
8
9
10
11
12
13
14
15
16
17
18
19
20

5.2 Paleontological investigations

H. Andruleit and W. Weiss

The paleontological work onboard SONNE aimed at an early assessment of sediment and rock ages and paleoenvironmental data. These data were used in the interpretation of geophysical data, especially of PARASOUND and multi-channel reflection seismic records. Plankton sampling at carefully selected sites was carried out to assist the paleo-environmental interpretation in relation to nutrient supply and interactions with atmospheric and paleoceanographic conditions. Moreover the data from plankton samples of this little sampled region will contribute to a better understanding of the role of the coccolithophores in the carbon cycle, biological pump, and carbonate pump.

5.2.1 Calcareous nannoplankton

H. Andruleit

5.2.1.1 Living coccolithophores from watersamples

Coccolithophores are a major group of marine, unicellular phytoplankton. Their cell surfaces are covered by minute external calcite scales (=coccoliths) which form an important part of fine-grained deep-sea sediments and, therefore, are extensively used in paleoecological and paleoceanographical studies (WINTER and SIESSER, 1994). Recently, cocco-lithophores have gained increased attention as they play a unique role in the global carbon cycle and are peculiar because of their combined effects on both, the biological and the carbonate pump. Because of their optical (albedo - masses of detached coccoliths substantially reflect incoming light) and biochemical (dimethylsulfide - which act as a source molecule for cloud nucleation) effects they likely produce additional feedback to climate change (WESTBROEK et al., 1993).

There are, however, only limited studies available which deal with the biogeographic occurrence of living coccolithophores in the world oceans. Also, relatively little work has been done on absolute abundances of single species according to ecological parameters in modern communities. This is in contrast to extensive geological studies which have used coccolith assemblage changes as indicators of shifts in paleoceanographic conditions (GARD, 1988; GARD and BACKMAN, 1990; BAUMANN and MATTHIESSEN; ANDRULEIT and BAUMANN, 1998). The observed distribution patterns of living coccolithophore communities seem to be reflected in bottom sediments rather well (McINTYRE and BÉ, 1967) although, a fossil assemblage is not a direct image of the former living community. Therefore, this investigation is done with regard to the spatial and seasonal occurrence of geologically important species, e.g. of *Emiliania huxleyi* and *Gephyrocapsa oceanica*. This in turn is essential for a better understanding of the relationship between living communities and accumulated coccolith assemblages in sediments.

At cruise SO-139 the focus of research was on the horizontal and vertical sampling of the surface waters of the eastern Indian Ocean off Indonesia. At a total of seven stations (Tab. 5.2.1.1) water samples were taken at several depth intervals with a rosette sampler according to previous CTD profiling. It was aimed to sample the mixed surface water layer, above, at, and below the thermocline and at the bottom of the photic zone approximately at 200 m water depth. Therefore, at each station six to seven waterdepths were sampled (Fig. 5.2.1.1). The water (5 litres) from each depth was filtered immediately without further treatment through Millipore filters (0.45 µm pore width) using a vacuum pump. Without further washing, rinsing or chemical conservation the filters were dried at 50°C for at least four hours. The filters were then stored in plastic Petri dishes, and kept dry with silica gel.

Due to the lack of a scanning electron microscope coccolithophore numbers were not investigated on bord. Nevertheless an indication as to whether there are sufficient specimens is related to the staining of the filters. All filters from the surface samples show a promising staining, with a approximate maximum around 40 to 80 m, whereas the samples from below the thermocline often seem to have only very low plankton numbers.

Table 5.2.1: Data of the water samples for coccolithophore investigations

Station No:	Date	Sample depths (m)	Position Latitude:	Position Longitude:	Water depth (m)
2 MS	31.01.99	1, 12, 37, 63, 100, 150, 200	S 9:13,7046	E 106:17,6154	6465
9 MS	02.02.99	1, 25, 50, 75, 150, 199	S 7:45,7788	E 106:52,5978	2666
56 MS	15.02.99	1, 25, 50, 70, 100, 140, 200	S 6:32,0310	E 103:49,6878	1704
65 MS	17.02.99	1, 22, 50, 80, 134, 160, 201	S 7:39,8622	E 102:39,9570	5957
70 MS	19.02.99	8, 47, 88, 112, 132, 157, 202	S 4:54,220	E 102:12,793	1740
94 MS	25.02.99	14, 49, 79, 101, 124, 200	S 7:10,026	E 105:38,972	1892
95 MS	25.02.99	10, 50, 84, 100, 114, 202	S 6:34,027	E 104:53,996	1892

Fig. 5.2.1: Typical temperature and salinity profile with depths of water samples

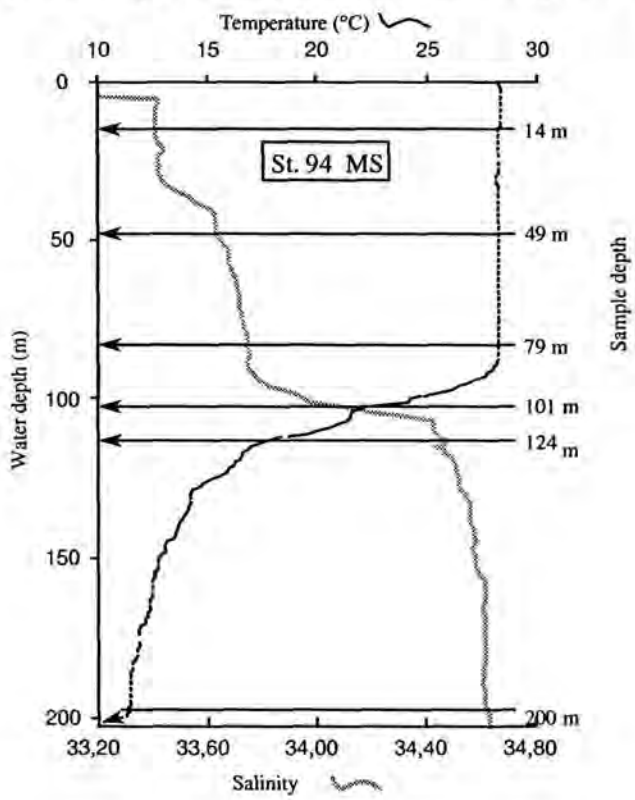

5.2.1.2 Age determinations according to calcareous nannoplankton stratigraphy

(For core characteristics see Chapter 5.1)

Stratigraphic age determinations mainly were performed on down-most core samples and dredge samples to define maximum ages of recovered sediments. Smear slides were prepared after routine standards and analysed with the light microscope. The stratigraphies of Young (1998) for the Neogene, of Hine and Weaver (1998) for the Quaternary, and of Martini (1971) for the entire Cenozoic (presented and modified in Perch-Nielsen (1985)) were used for this study.

Species lists are only shown for selected samples and may not cover all taxa. For locations see station list in the according chapter.
The absence or the presence of *Emiliania huxleyi* could not be unambiguously determined in most samples. Only in one surface sample (15 KL, 0.02 m) *E. huxleyi* was identified with high confidence. Therefore, the nannoplankton zone NN21 was not differentiated in this study.

Table 5.2.2: Results of calcareous nannoplankton stratigraphy

Sample	Age (after Young, 1998)	
3 KL, core catcher	no calcareous nannoplankton found	
6 KL, core catcher	upper Pleistocene to Holocene (NN20 to NN21)	< 0.506 Ma
13 KD, light mudstone	lower Pliocene (Interval G, NN12 to NN15)	5.6 – 3.8 Ma
13 KD, dark mudstone	lower Pliocene (Interval G, NN12 to NN 15)	5.6 – 3.8 Ma
14 KL, core catcher	lower Pleistocene (NN19)	2 – 0.506 Ma
15 KL, 0.02 m	upper Pleistocene to Holocene (NN21)	< 0.294 Ma
15 KL, 12.40 m	upper Pleistocene to Holocene (NN20 to NN21)	< 0.506 Ma
21 KL, core catcher	upper Pleistocene to Holocene (NN20 to NN21)	< 0.506 Ma
28 KD, gray carbonate	no calcareous nannoplankton found	
28 KD, stiff mud	lower Pleistocene (NN19)	2 – 0.506 Ma
34 KL, core catcher	upper Pleistocene to Holocene (NN20 to NN21)	< 0.506 Ma
42 KL, core catcher	upper Pleistocene to Holocene (NN20 to NN21)	< 0.506 Ma
50 KL, core catcher	upper Pleistocene to Holocene (NN20 to NN21)	< 0.506 Ma
58 KL, core catcher	upper Pleistocene to Holocene (NN20 to NN21)	< 0.506 Ma
61 KD-1	no calcareous nannoplankton found	
61 KD-2	Neogene	
61 KD-3	lower Pleistocene (NN19)	2 – 0.506 Ma
61 KD-4	lower Pleistocene (NN19)	2 – 0.506 Ma
61 KD-6	no calcareous nannoplankton found	
61 KD-7	no calcareous nannoplankton found	
63 KD-3	no calcareous nannoplankton found	
63 KD-4	no calcareous nannoplankton found	
67 KD, white sandstone	Neogene (?)	
68 SL, base	Neogene (?)	
74 KL, core catcher	upper Pleistocene to Holocene (NN20 to NN21)	< 0.506 Ma
83 SL, core catcher	upper Pleistocene to Holocene (NN20 to NN21)	< 0.506 Ma
90 KD, mudstone	no calcareous nannoplankton found	
96 KL, 18.22 m	upper Pleistocene to Holocene (NN20 to NN21)	< 0.506 Ma
101 KD-4	Paleogene to Miocene (Paleogene to NN7)	

Explanations

6 KL, core catcher: Absence of *Pseudoemiliania lacunosa* and presence of *Gephyrocapsa oceanica.*

13 KD, light mudstone: Absence of *Discoaster quinqueramus* and presence of *Reticulofenestra pseudoumbilicus.* Observed species: *Calcidiscus leptoporus, Calcidiscus macintyrei, Ceratolithus* sp., *Coccolithus pelagicus, Discoaster brouweri, Discoaster pentaradiatus, Discoaster surculus, Discoaster variabilis, Helicosphaera carteri, Pontosphaera discopora, Pontosphaera multipora, Rhabdosphaera* sp., *Reticulofenestra pseudoumbilicus, Sphenolithus abies.*

13 KD, dark mudstone: (same as 13 KD, light mudstone)

14 KL, core catcher: Presense of *Pseudoemiliania lacunosa* and absence of *Discoaster brouweri.*

15 KL, 0.02 m: Presense of *Emiliania huxleyi.* Observed species: *Calcidiscus leptoporus, Florisphaera profunda, Gephyrocapsa oceanica, Helicosphaera carteri, Rhabdosphaera clavigera, Syracosphaera* sp., *Umbellosphaera* sp., *Umbilicosphaera sibogae.*

15 KL, 12.40 m: (same as 6 KL)

21 KL, core catcher: (same as 6 KL)

28 KD, stiff mud: (same as 14 KL)

34 KL, core catcher: (same as 6 KL)

42 KL, core catcher: (same as 6 KL)

50 KL, core catcher: (same as 6 KL)

58 KL, core catcher: (same as 6 KL)

61 KD-2: Only rare occurrence of taxa of Prinsiaceae.

61 KD-3: (same as 14 KL)

61 KD-4: (same as 14 KL)

67 KD, white sandstone: Only rare occurrence of corroded calcareous nannoplankton. Probably older than Quaternary. Observed species: One 5-armed *Discoaster*, one big *Coccolithus pelagicus*, Prinsiaceae.

68 SL, base: Probably same age as sample 67 KD (same material) but only Prinsiaceae could be observed.

74 KL, core catcher: (same as 6 KL)

83 SL, core catcher: (same as 6 KL)

96 KL, 18.22 m: (same as 6 KL)

101 KD-4: The calcareous nannoplankton assemblage is of low diversity and severely recrystallised. Observed taxa are: *Cyclicargolithus floridanus, Discoaster deflandrei* Prinsiaceae, *Sphenolithus moriformis, Sphenolithus* sp. Therefore, only an minimum age of 10.9 Ma can be deduced. The absence of *Sphenolithus heteromorphus* (and other species) might be interpreted as an indication of a maximum age of middle Miocene. However, this cannot unambiguously be proven.

REFERENCES

ANDRULEIT, H. and BAUMANN, K.-H., 1998: History of the Last Deglaciation and Holocene in the Nordic Seas as revealed by coccolithophore assemblages.- Mar. Micropaleontol., 35: 179-201

BAUMANN, K.-H., and MATTHIESSEN, J., 1992: Variations in surface water mass conditions in the Norwegian Sea: Evidence from Holocene coccolith and dinoflagellate cyst assemblages.- Mar. Micropaleontol., 20: 129-146

GARD, G., 1988: Late Quaternary calcareous nannofossil biozonation, chronology and paleo-oceanography in areas north of the Faeroe-Iceland Ridge.- Quat. Sci. Rev., 7: 65-78

GARD, G, and BACKMAN, J., 1990: Synthesis of Arctic and Sub-Arctic coccolith biochronology and history of North Atlantic drift water influx during the last 500.000 years.- In "Geological history of the polar oceans: Arctic versus Antarctic" (Bleil, U., and Thiede, J., Eds.), Kluwer Academic Publishers, 417-436

HINE, N., and WEAVER, P.P.E., 1998: Quaternary.- in: P. R. Bown "Calcareous Nannofossil Biostratigraphy", Chapman and Hall, 266-283

MARTINI, E. 1971: Standard Tertiary and Quaternary calcareous nannoplankton zonation.- in: A. Farinacci "Proceedings of the Second Planktonic Conference Roma" 1970, 739-785.

McINTYRE, A. and BÉ, A.W.H. 1967: Modern coccolithophoridae of the Atlantic Ocean - I. Placoliths and Cyrtoliths. - Deep-Sea Res., 14, 561-597

PERCH-NIELSEN, K. 1985: Cenozoic calcareous nannofossils.- in: Bolli, H.M., Saunders, J.B. and Perch-Nielsen, K. "Plankton Stratigraphy", 427-554

WESTBROEK, P., BROWN, C. W., van BLEIJSWIJK, J., BROWNLEE, C., BRUMMER, G. J., CONTE, M., EGGE, J., FERNANDEZ, E., JORDAN, R., KNAPPERSBUSCH, M., STEFELS, J., VELDHUIS, M., van der WAL, P., and YOUNG, J., 1993: A model system approach to biological climate forcing. The example of Emiliania huxleyi. Glob. Planet. Change, 8, 27-46

WINTER, A., and SIESSER, W.G., 1994: Coccolithophores.- Cambridge University Press.

YOUNG, J.R. 1998: Neogene.- in: P. R. Bown "Calcareous Nannofossil Biostratigraphy", Chapman and Hall, 225-265.

5.2.2 Planktonic foraminiferal biostratigraphy

W. Weiss

Few biostratigraphic age determinations based on planktonic foraminifers were made, especially on thin sections from dredged limestone/rock samples. The thin sections were prepared after standard procedures and analysed under a Wild photomacroscope M 400. The biostratigraphic age assignments using planktonic foraminifers are based on KENNETT and SRINIVASAN (1983), IKEBE and TSUCHI (1984), BOLLI and SAUNDERS (1985) and BERGGREN *et al.* (1995).

SO 139-7GA (thin section no. 2825)
Seismic line 03, southern margin of the forearc basin
Radiolarian packstone
No age assignment

SO139-13KD-2 (thin section no. 2826)
Seismic line 03, southern margin of the forearc basin
Micritic matrix with planktonic and few benthic forams
Globigerina spp.
Globigerinoides spp.
Globorotalia tumida
Globorotalia menardii
Orbulina universa
Age: Pliocene-Pleistocene

SO139-13KD-3 (thin section no. 2827)
Seismic line 03, southern margin of the forearc basin
Micritic („vermicular") matrix with few benthic and planktonic forams
Globigerina spp.
Globigerinoides spp.
Age: Neogene

SO139-44GA (thin section no. 2828)
Seismic line 01, Snails and Mussels Hill
Micritic matrix with radiolarians, planktonic and few benthic forams
Pulleniatina obliquiloculata
Globorotalia menardii
Globorotalia tosaensis
? *Sphaeroidinellopsis* sp
Globorotalia tumida
Age: Late Pliocene to Early Pleistocene

SO139-44GA-1 (thin section no. 2831)
Seismic line 01, Snails and Mussels Hill
Micritic matrix with planktonic forams
Pulleniatina obliquiloculata
Globorotalia tumida
Age: Pliocene to Recent

SO139-44GA-2 (thin section no. 2832)
Seismic line 01, Snails and Mussels Hill
Micritic matrix with planktonic forams
Globorotalia tosaensis
Globorotalia tumida
Pulleniatina obliquiloculata
Globigerinoides ruber
Globigerinoides conglobatus
Orbulina universa
Globorotalia cf. *truncatulinoides*
Globorotalia menardii
Globorotalia hirsuta
Age: Late Pliocene (probably close to the Pliocene-Pleistocene transition)

SO139-61KD-1 (thin section no. 2829)
Seismic line 06, outer part of the fore arc ridge
Sandy matrix without microfossils

SO139-67KD-2 (thin section no. 2830)
Seismic line 09, top of the fore arc ridge
Microfossil packstone with benthic and planktonic forams, algal and molluscan fragments
Gypsina sp.
? *Amphistegina* sp.
Globigerina spp.
Globigerinoides spp.
? *Sphaeroidinellopsis* sp
Age: Neogene

Remarks: At the „Snails and Mussels Hill" carbonate precipitated in sediments of Late Pliocene to Early Pleistocene age (44GA) according to planktonic foraminifers.

REFERENCES

BERGGREN, W.A., D.V. KENT, C. Swisher III, and M.-P. AUBRY, 1995: A revised Cenozoic geochronology and chronostratigraphy. - In: Berggren, W.A., D.V. Kent, M.-P. Aubry & J. Hardenbol (Eds.): Geochronology, time scales and global stratigraphic correlation, SEPM Special Publ., 54, 129-212; Tulsa

BOLLI, H.M. and SAUNDERS, J.B., 1985: Oligocene to Holocene low latitude planktonic foraminifera. - In Bolli, H.M., Saunders, J.B. and Perch-Nielsen, K. (eds.), Plankton Stratigraphy, 155-262; Cambridge

IKEBE, N. and TSUCHI, R., 1984: Pacific Neogene datum planes. Contributions to biostratigraphy and chronology. – 288p., Tokyo

KENNETT, J.P. and SRINIVASAN, M.S., 1983: Neogene planktonic foraminifera. A phylogenetic atlas. - 265 p.; Stroudsburg/Pennsylvania

6. Biological samples and seafloor observations

H. Sahling

6.1 Seafloor observations with TV-sled OFOS (FS) and TV-grab TVG (GA)

The Ocean Floor Observation System (OFOS), a towed video-sled was used to find active fluid expulsion sites and to map their occurrences as well as their geological surroundings in different settings. Chemoautotrophic communities and precipitates are the main manifestations of fluid venting and can be observed by the video-sled. As the TV-grab yielded information's on venting areas too, the visual observations are included in this chapter.

6.1.1 Methods

The OFOS (German: FS Fotoschlitten) was built 1998 by the RTB GmbH, Germany. It is equipped with a colour camera (*CCD Multi-Sea-Cam 2050, Fa. Deep Sea Power & Light Inc.*, 81° oblique angle), a black-and-white camera (*CCD OE 1390/1391, Fa. Kongsberg [Simrad/Osprey],* 53° oblique angle), two still cameras (*Photosea 5000, Nikkon* 28 mm, 60° oblique angle) in stereo mode and two special lights (*Sea-Arc 2 HMI 400*, each 200 W) as well as two halogen lamps (*Deep-Multi Sea-Lite*, each 250 W). A flash system (*M383-002, Fa. Benthos*) is controlled by an altitude meter (Model: *2110, Benthos*) modifying the flash intensity depending on the distance to the bottom. Due to the amount of time required for the strobe to cycle, a photo image can be made after every 8 seconds with the total number of images restricted to the amount of the film. We used 33.5 m of 400 or 200 ASA *Kodak Ektachrome* film yielding approximately 800 images. A laser system (*Micro-Sea-Laser, Deep Sea Power & Light*) with 3 modules is used, two laser point vertically and parallel in 20 cm distance downward, one laser points oblique to the other. A compass (Fa. *RTB GmbH*), a tool for recording the pitch and roll (*Mark 2, Fa. RTB GmbH*), a not active interface for triggering a water sampler module, a responder (*DHT 163, Fa. Simrad*) corresponding with a board unit (*SSBL HPR 1507, Simrad*) and a CTD (*SBE 9/11, Fa. Seabird*) are used also. The power is supplied via coaxial cable (1000V, max. 1050 W) and the data are transferred by a fibreglass cable, the system is controlled by a board unit allowing a control of the light intensity and taking photos, manually or in regular time intervals. The data are stored in the ships central database and displayed on a PC (Software by *Werum*). Especially the display of the position and the depth profile over time is of good value for additional information.
OFOS is towed at approximately 0.4 to 0.8 knots. Optimal viewing conditions are at 1-3 m altitude which were maintained by continually adjusting the length of cable through a winch operator.
The slides were developed by the physician on board ship to get detailed information and control of the technical function of the sled (Thank you Anke!). The area covered by slides is approximately the same size as the black and white video, also the slides display an area slightly larger relatively to the video screen.
The video signal is recorded on commercial VHS or S-VHS videotapes and will find its final deposition, as well as the slides from camera B, in the archive at BGR, slides from camera A will be analysed and stored at GEOMAR.

Due to the introduction of several new hardware and software modules some problems occurred during this cruise. The digits in the in the data chamber of the still camera cannot be clearly read, the display of time is not working. The data from the CTD, heading, roll, pitch and altitude are stored but cannot be read from the data base. The termination of the transmitter cable does not work reliably in water depth near 6000 m.

6.1.2 Results

6.1.2.1 Accretionary wedge off Java

20 FS
Based on the geophysical profile SO 137-03, the small scale bathymetry and the two CTD-casts MS 2 and 5 (showing week methane anomalies) an OFOS track was planned at the accretionary wedge off Java. One anomaly was found deeper than 6000 m water depth, beyond the depth limit of OFOS, and a second week peak at 5200 m (MS 5). 20 FS was planned to cover the depth range between 4800 m and 6000 m, unfortunately the cable termination broke and OFOS had to be brought up again. During the 1 h deployment close to the seafloor a depth range between approximately 4800 and 5000 m was covered. There were no indications of vents. Only soft sediment was observed with a relativily high abundance of Lebensspuren. Some Xenophyophoracea and cosmopolitan sea-cucumber were seen.

40 FS
For a survey of the accretionary wedge along seismic line SO137-01, a profile was planned to observe a potential interesting site without having information about methane anomalies in this area. Again after 1 hour 10 min on the seafloor the data transfer was interrupted probably due to cable problems at the lower cable termination. We observed many Lebensspuren and relatively few epibenthic animals. In depths near the end of the profile high scarps of consolidated sediments were seen. We found no indication for venting.

6.1.2.2 Forearc basin off Sumatra

The forearc basin in the area of profile SO137-06 was subject of detailed water column surveys and ocean floor observations. Very high methane anomalies were found but no characteristic vent indications could be observed in this area.

48 FS
The ridge-forming Mentawai fault running parallel to the axis of the basin divides it into two sub-basins. A slight methane anomaly at CTD station 45 MS NE of the fault and the findings at the South Java basin fault (continuation of the Mentawai F.) gave reason for an OFOS track along the ridge crest of the fault system. This profile covered two small summits with water depths of 1870 m and 1860 m and reached water depth of about 1980 m when changing the course perpendicular down the ridge in SW direction. No indication for venting could be observed.

57 FS
Based on the finding that at station 49 MS SW at the fault only weak methane anomalies were found the CTD was deployed at station 55 MS at the boundary of the forearc basin with the slope of the outer arc ridge and yielded methane anomalies of very high concentrations in water depth between 1600-1640 m.
This water depth range was the target for 57 FS which was planned to observe the slope of the outer are ridge from 1550 m to 1660 m into northerly a direction. The target depth was crossed three times, no indication for venting could be found. Only a continuous surface of soft sediment was observed along the track. The bottom fauna changed with the water depth and sometimes significantly high abundance's of medusa were found drifting in the near bottom current. At the end of the track some plastic garbage was observed as well as a greyish sediment coloration of unknown origin.

75 FS
The methane anomaly found in 49 MS was confirmed by CTD casts 71 MS, 72 MS and 73 MS located on a profile sub-parallel to the strike of the slope, although their location depth was some tens of meters deeper. Encouraged by this, OFOS was deployed again at the slope at the northern end of 57 FS starting in a northerly direction. Along a first part of the track a depth range between 1500 m and 1755 m was covered before running OFOS uphill in westerly directions to a depth of 1690 m.
No indication for venting could be found. A similar depth-dependent zonation of animals was observed as for 57 FS. Very astonishing was the high abundance of medusa drifting in the bottom water, sometimes 10 of these reddish-brown medusa were seen at a time on the video. The medusa occurred in patches, at least four aggregations were observed. A few times shells of bivalves were visible but they didn't resemble typical vent clams. At some parts the seafloor is covered by very small blocks of greyish colour which looks like consolidated sediment but their origin is not clear.

6.1.2.3 Anticline structure associated with South Java Basin Fault

30 FS
A large anticline marks the South Java Basin fault and is well visible on the reflection seismic profile SO137-01. Subsequent detailed bathymetric mapping revealed that the anticline forms an E-W-striking low undulating ridge which terminates immediately E of seismic profile SO137-01. Here the crestline shows a distinct elevation. OFOS 30 FS track was run somewhat south of and sub-parallel to the crestline. Scattered empty shells of protobranch bivalves (*Acharax* sp. and gen. sp.?) were seen indicating fluid venting in the vicinity. High abundance of buccinid gastropods indicate high numbers of prey and give therefore an indirect evidence for extensive chemoautotrophic communities. Only the surface of soft sediment was seen with variations in colour. The whitish areas and spots were thought to result from a suboxic sediment under the surface.

33 GA
Based on the information from 30 FS and scarce bathymetric information the TV-grab was deployed at station 33 GA at the base of the ridge termination. It grabbed into sediment which was suspicious due to an oval whitish structure of about 3 m in diameter. The grab yielded one *Acharax* sp. alive and 1-2 µM hydrogen sulfide in the subsurface sediments indicating a weak influence of reduced chemical compounds, but the low concentration of nutrients may indicate an inflow of bottom water due to convection on a scale of ten's of meters.

43 GA
Following the first results that chemoautotrophic organisms (*Acharax* sp.) are present in this area we conducted another grabbing attempt. This profile was planned to cover the top of the terminal elevation of the anticline ridge. The discovery was overwhelming: 200 m along track a giant seep with chemoautotrophic organisms and precipitates was observed. First indications for venting on the way up-slope to the hill top were empty bivalve shells and buccinid gastropods on soft sediment. Coming closer to the active vents the sediment surface gets rougher, first single blocks of carbonate precipitates are visible, and scarp-like structures which may be caused by erosion are inhabited by pogonophorans. The very active central venting zone was defined by the occurrence of either pogonophorans, clams, or areas dominated by carbonates with signs of active venting e.g. bacterial mats. It seems like if all over this area subsurface carbonates are present, as thin pogonophorans are. In some areas thick vestimentiferans are visible, covering several square meters. In other areas, tens of meters wide, small shells are scattered around. In one case a cluster of tentatively vesicomyid bivalves of up to 20 cm in length was observed!

One grabbing attempt was made at the beginning of the vent area but the tilt was too strong and therefore the grab did not close. We therefore grabbed in an area were carbonates with bacterial mats, thin pogonophora and single big clam shells were visible as well as two large holes in the sediment surface, up to 5 cm in diameter and of unknown origin. Unfortunately the grab did not close tightly and much of the content washed out during the way to the surface. The grab yielded mainly precipitates and empty shells of *Acharax* sp. and another thyasirid bivalve. No porewater was squeezed from the sediment, hence no information on hydrogen sulphid and methane was obtained.

44 GA
The grab followed the track of 43 GA and grabbing was attempted at the eastern edge of the vent area but too much tilt forced us to continue the profile. Unfortunately the weight hanging below the grab to provide distance control was out of sight and due to a relatively rough sea a correct distance between the grab and the sediment surface was difficult to maintain. From time to time the bottom became visible displaying always vigorous fluid venting in the same vent area found on track 43 GA. We crossed this field and, as no grabbing was conducted we reversed the direction of the track by drifting back with the ship. We grabbed in an area with carbonate crusts, bacterial mats and pogonophora. This grab yielded again precipitates and thin pogonophora, porewater was squeezed out of one subcore and one sediment sample was analysed for methane content.

84 FS
Based on the results from 43 & 44 GA and due to the currents-against-the-wind situation a profile from SE to NW was conducted to map the vent field at the top of the small elevation and to get high-resolution photographs. Surprisingly a clam cluster of approximately 2 m in diameter was observed in a small depression at the eastern base of the terminal elevation. At the top of the elevation a field of scattered clam-shells was found, but living bivalves were not identified on the video. Instead, thin pogonophorans seem to be present along most of the hill top. There was not such vigorous venting observed as before during the grab deployments, e.g. the dark coloured carbonates were not seen again.

89 FS
The track was planned to cross the profile 84 FS perpendicularly but due to the weather and current situation a more East to West transect was conducted. The ship moved along the transect before OFOS reached the bottom when the bottom became visible, we were in the vent field consisting of clams and pogonophorans. Only one indication for some of the darker carbonates was found, however, during most of vent observations of nearly half an hour we saw pogonophorans and scattered clam-shells.

91 GA
The track for this grab was planned from the East to the West as this was the favoured direction for moving the ship at low speed. At the top of the terminal elevation only few areas with scattered clams were observed but no grabbing attempt was made as no indication for active venting was found. Further to the west, still on the ridge crest not even empty shells were found. The ship was turned and we approached the hill now from the west. After over 4 hours of search. The grab was lowered into a field with pogonophorans, some empty clam-shells and holes probably indicative for *Acharax* sp. living in the sediment.

92 GA
The search track for a proper grabbing position was more characterised by a spontaneous adaptation of the ship course according to the bottom observations. In general we crossed the prospective vent area four times heading east or west. At the beginning large areas of scattered clams and some living clusters were observed but the ship moved too fast to allow grabbing. Shortly before passing the hill top again from west to east high turbidity in the water made the seafloor observation nearly impossible, the water became more clear after moving further to the south. The high particle load was caused by the tool deployments over

the preceding hours and days. We grabbed pogonophorans somewhat east of the top.

93 GA
This track was planned to repeat the successful observation tracks of 43 & 44 GA. Not surprisingly we found the impact traces of a former grabbing attempt. Further on we observed shells and pogonophorans but did not see again the dark coloured precipitates. It was tried to grab into sediment with a high number of clam shells scattered around, with the hope that also buried clams could be sampled. Unfortunately, we obviously missed the area by some meters, because only very few shells were seen.

6.1.3 Discussion

The visual observation of the seafloor is the only possibility to search for areas of venting and to map these in order to plan and conduct sampling with the help of tools with or without TV-guidance. Four main investigation areas were selected to search for fluid seepage, the accretionary wedges and the forearc-basins off Sumatra and Java. The results are based on the visual on-line observations and a quick look through the slides developed on board. More information will be gathered by detailed analysis of the photographs.

At the accretionary wedge off Java near the profiles SO 137-01 and 03 the TV-sled due to technical limitations did not reach the prospective water depth at the deformation front were seepage was expected based on slightly elevated methane concentrations in the water column. Therefore we are lacking information on venting and its manifestations. However, methane anomalies are strong indications for venting and new attempts to search for characteristic signs should be undertaken, and necessarily also at depth greater than 6000 m along the deformation front.

As no methane anomaly was found by the CTD/rosette cast (66 MS) at the accretionary wedge off Sumatra at profile SO 137-19 and due to a shortage of time no further attempts were made to find seeps.

In the forearc basin off Sumatra we found no characteristic manifestations for fluid venting although very high methane anomalies were measured in the bottom-near seawater. The occurrence of medusa is suspicious and certainly indicates high organic matter concentration. The variable depth where methane anomalies were measured and the high abundance of benthopelagic plankton may suggest a very variable bottom current transporting its methane load from distant sources. As we do not have information about the particle load a high methane concentration due to bacterial activity in nepheloid layers can not be ruled out.

The large anticline structure in the forearc-basin off Java, marked by a low ridge, was subject of most intensive visual observations and sampling. High activity of venting was discovered at the terminal elevation of the ridge which rises only about 50 m above the surrounding seafloor to a water depth around 2910 m. Venting was indicated by clams, pogonophora, and authigenic precipitates. The venting activity is thought to be highly variable on a spatial scale of some meters as indicated by characteristic animals. Two types of clams which were not recovered alive but were seen on the pictures, probably the genus *Calyptogena* (Bivalvia, Vesicomyidae), well known from hydrothermal vents and cold seeps around the world, and a thyasirid bivalve. These bivalves indicate focused venting and were only seen in small clusters and in small numbers compared to the very high amount of scattered clam-shells observed all over the area. The shells were also observed on the slope of the hill and may indicate erosion. Vestimentiferan ("tube worms") were also seen together with precipitates which appeared dark in colour due to Fe/Mn crusts. This is thought to be the most active area as also indicated by the porewater analysis of the TV-grab sample 44 GV.

Another sign for venting is a thin pogonophora found in nearly all grabs as well as the bivalve *Acharax* sp. The pogonophora were observed most widespread in the area and a mapping of this species based on all TV observations will give in idea of the extension of a zone of diffusive venting.

6.1.4 Conclusion

The occurrence of organisms characteristic for fluid venting in the forearc basin off Java is the second finding of this kind in the Indian Ocean. Although no visual evidence of fluid expulsion at the other three investigation areas could be gathered the very high methane anomalies found in the forearc basin off Sumatra is a strong evidence. The significant methane anomalies at the accretionary wedge off Java gives also hope for discovering more cold seeps in this region. Fluid venting seems to be much more widespread along the subduction zone off Java as previously expected.

6.2 Biological samples and TV-grab sampling

Chemoautotrophic organisms and authigenic precipitates are often the only visual manifestation of fluid venting. The occurrence of characteristic communities at sites with high hydrogen sulfide or methane supply is well known from different geological settings, e.g. at cold seeps in compressional wedges in subduction zones or hydrothermal vents at mid oceanic ridges or back-arc spreading centers. The fauna described in this areas consists mainly of two systematic groups, the molluscs with gastropods and bivalves and pogonophorans. These organisms have in common that their nutrition is dependent on symbiotic bacteria harboured in specialised tissue. The bacteria are able to gain energy from the oxidation of reduced chemical compounds (e.g. methane or hydrogen sulfide) and use this to fix inorganic carbon. The host is to a variable degree dependent on this autotrophically fixed organic carbon.

The observed distribution of closely related species world wide is of major interest for understanding the biogeography of this organisms which are restricted to active venting zones and therefore does only propagate along a two dimensional system. The biogeography of this organism is highly dependent on the chemical and physical characteristics of the discharging fluids.

One aspect of this study must be a complete inventory of chemoautotrophic organisms by taxonomists and evaluation of their dependence on fluids by means of stable isotopic composition, electron microscopy and genetic investigations. The small scale geochemical characterisation will help to explain the distribution patterns of the different vent animals.
With the use of the ship-owned TV-guided grab the question of small scale geochemical and biological heterogeneity will be answered.

6.2.1 Methods

The TV-guided grab A (GA) aboard RV SONNE is capable of sampling an area of 1.82 m^2 (1.06 x 1.72 m) up to 40 cm deep when it is fully open when lowered on the surface. The grab is equipped with a colour camera (*CCD Multi-Sea-Cam 2050, Fa. Deep Sea Power & Light Inc.*, 81° oblique angle), a black-and-white camera (*CCD OE 1390/1391, Fa. Kongsberg [Simrad/Osprey]*, 53° oblique angle), four halogen lamps (*ROS*), and the power is supplied by two deep sea batteries (32 Ah) allowing about 3 hours of observation and three grabbing attempts. An instrument is warning if the grab has too much tilt to be closed after touching the seafloor. The data are transferred by a fibreglass cable.

Before sampling the grab is towed 2 - 3 meter above ground. The winch operator manually adjusts the cable length to keep this distance. The camera looks through the jaws and objects of interest can be grabbed by settling the grab and closing the jaws hydraulically. Commands come from the board unit.

Biological and geological samples were recovered with a chain bag dredge (KD, Kettensack- Dredge) designed by the BGR. It has a mouth opening 0.94 m wide and 0.35 m high. Within a chain bag with 6 cm holes a nylon net holds back objects larger than 2 cm and collects them in the 1 m long bag.

Animals collected with one of the above described tools are selected by hand and transferred to the cold storage room (+4 °C) immediately. Sediment is sieved through a mesh with a 0.5 cm grid and also hand-picked from gravel. The animals are sorted by the taxonomic group and fixed for systematic determination in 8 % formaldehyde in seawater or 70 % ethanol. Tissue for electron microscopy is fixed in 2 % 0.2 µm filtered Glutaraldehyde in seawater. Tissue for stable isotope measurements are washed in pure water and is frozen at -20 °C, tissue for genetic studies is washed in 0.45 µm filtered seawater and is frozen also at -20 °C.

6.2.2 Results

6.2.2.1 Anticline structure associated with the South Java Basin fault

33 GA
The grab was lowered on an oval area of about 2 m in diameter with whitish sediment coloration, shortly after the seafloor became visible. It came on deck full of sediment, which overflowed through the lids of the grab. One subsample was collected for pore water analysis, another one out of the open grab was analysed for methane concentration.
After opening and sieving one *Acharax* sp. (Bivalvia) alive was recovered, tissue frozen for stable isotope analysis and genetics, the rest was fixed for taxonomy.

43 GA
On the top of the terminal elevation we observed chemoautotrophic communities with overwhelming abundance as well as precipitates. Grabing was attempted at the very beginning of the field but the tilt was too much, and search was continued. We grabbed in an area where 2 big holes of unknown origin were visible, carbonates and thin pogonophora. In direct vicinity a shell of an up to 20 cm long clam (*Calyptogena* sp.?) was seen as well as bacterial mats.
Shortly before we reached the surface waters we turned on all lights (not only one) and saw that the grab was not tightly closed. We closed it again and, thus, stopped the washing out process.
The grab was only filled to 1/3 because of the washing out in the water column.
In two areas the pogonophora abundance was higher. The first impression was, that the whole grab was filled with this semi-liquid sediment containing half of the volume carbonate precipitates. No pore water was squeezed.
After the opening two sediment layers were found: one muddy sediment layer with a very strong smell of hydrogen sulfide and one layer of more sticky sediment without this smell.

The grab sample was dominated by pogonophora within about 30 specimens all alive, characterised by very thin tubes (1 mm) of up to 50 cm length, many individuals penetrated through carbonates suggesting that pogonophora started growing before precipitation.
Only 1 Ophiuroidae and 1 Sipunculida were recovered beside empty shells of some bivalves and gastropods.
No porewater was squeezed.

44 GA
The grab was lowered in an area where carbonates and bacterial mats as well as pogonophora were visible. 1 buccinid gastropod and 1 holothuria were also seen but could not be found in the grab. However, the occurrence of epifauna indicate only weak influence of hydrogen sulfide on the sediment surface.
On deck the grab was full, with sediment pressed to the very top of the jaws. A liquid sediment was mixed to equal parts with carbonates. Only in the deeper layers (below about 20 cm) the sediment was less liquid but still contained carbonates.

Pushing the sub sample boxes into the sediment was quite difficult and only two boxes out of the same hatch were pressed for gaining pore water. Core 1 was orientated closer to the outer edge of the jaw while core 2 was more in the middle. Both boxes had the same distance of about 20 cm to an area with relatively denser pogonophora community (about 15) at the outer edge of the jaw. The sample for methane analysis was taken from the hatch in the other jaw but at the same side, in a distance of about 1.3 m to the pore water boxes.

The sieved fraction yielded again the thin pogonophora, about 50 specimens all alive. Only one tube worm tentatively identified as a Vestimentifera and some empty tubes of this species were recovered. One *Acharax* sp. was recovered alive but many shell fragments and only few whole pairs of shells, about 12 individuals in total, were found. Unfortunately only shells (five) of Thyasirid bivalves were recovered. Some small gastropod and bivalve shells probably representing the seafloor community off the vent sites as well as 1 Ophiuroidae and 3 Sipunculida. At least four species of Polychaeta were found.

90 KD
The dredge was towed over the prospective vent area but only two rock fragments were dredged.

91 GA
The grab jaws were partly closed before setting the grab on the seafloor, slightly more open then the viewing angle of the camera, to avoid sinking of the grab to deeply into the soft sediment. After more then 4 hours of search the grab was lowered on a field of pogonophora in which some white shells were visible and holes may indicate the occurrence of *Acharax* sp.
The grab was full of sediment pressed up to the very top of the jaws and the space in between. Beside the thin pogonophorans in abundance similar to samples 43 GA or 44 GA and without aggregation no other animal was seen on the surface. Two subcores for pore water were taken, core 1 next to the core were methane was measured and core 2 in a distance of about 50 cm. Three *Acharax* sp. were found alive in the grab with commensale polychaets in the mantle cavity, some empty shells and two free living polychaets.

92 GA
The grab touched the sediment with pogonophora visible on the surface after over 4 hours of search for a vent field to be sampled. The grab must have fallen on the side or grabbed the sediment in a very oblique angle, as only half of the grab was full of sediment while the other side was less filled and more strongly eroded due to travelling through the water column.

The sediment surface protected by the lid of the grab had a brownish layer. About 50 thin pogonophorans were concentrated in the middle of the grab, 2 *Acharax* sp. were found alive, and only some more empty shells completed the. No pore water was squeezed, but methane from sediment was analysed.

93 GA
Along the track of 43 GA and 44 GA also with this grab deployment we failed to re-discover the most active vent fields with precipitates. We therefore lowered the grab at a position

where a dense aggregation of clams was visible. Unfortunately we missed this area and grabbed sediments with only few shells on top. On deck the grab was full of homogenous very sticky greyish-green mud without any species alive. Only some shell pieces were recovered. One subcore was squeezed and one methane sample taken.
The thin pogonophorans recovered belong to the genera *Lamellisabella* and maybe *Oligobrachia* (pers. comm. E. C. Southward).

6.2.2.2 Vestimentifera in 100 KD

The graben marking the southern extension of the Sumatra fault was sampled for bedrocks with the geological dredge. Beside the rocks two pieces of Vestimentifera were recovered. One tube was about 20 cm long, up to 1 cm in diameter and had around every centimetre a trumpet-like opening which was overgrown by a new smaller tube which opened the same way again. Only the lower part of the animal was missing, obturatum, vestimentum and some cm of the trophosom were intact. The second piece contained only the vestimentum and some part of the trophosom.
The recovered specimens is similar to the vestimentiferans recovered during SO 133 cruise at Edison Seamount, Lihir; the genus is new, related to *Escarpia* and will be described soon (pers. comm., E. C. Southward).

6.2.3 Discussion

The discovery of fluid venting in the area of the South Java Basin fault is proven by the occurrence of characteristic vent fauna and authigenic carbonates. The bivalve *Acharax* sp. and the whole group of pogonophora is well known from sites of fluid seepage and reducing environments e.g. at sewage outfalls. Both groups depend on the chemoautotrophic endosymbionts which oxidise reduced sulfur to gain energy. Thyasirid bivalves occur but were only recovered as shells. Within the group of Thyasirids many species live in symbiosis with either methane or sulfur oxidising bacteria, or both. A third clam was observed but not sampled, probably the genus *Calyptogena*, well known from active venting sites, but the determination of both bivalve species will remain open until living samples will be recovered.

In all grabs from the vent site we found *Acharax* sp. and thin pogonophorans, indicating that these animals, which are hardly seen on the video, are very widely distributed in this area.

The vestimentifera from the lower wall of the eastern flank of the graben marking the southern extension of the Sumatra fault does strongly indicate fluid flow. This group of tube worm is known from cold seeps off Oregon and Japan as well as the hydrocarbon seeps in the Gulf of Mexico.

Taking into account the very small sampling area covered by the dredge and the size of this animal vigorous venting can be expected.

6.2.4 Conclusion

The finding of chemoautotrophic organisms in the subduction zone off Java renders very important information in the geological context as it proves fluid venting. The animals themselves will give, after detailed taxonomic investigations, valuable information about the biogeography of these animals.

7. Geochemical Analyses - Methane in Water and Sediments

E. Faber, Haryadi Permada, , B. Harazim, H.S. Koesnadi, V. Marchig, N. von Mirbach, J. Poggenburg, and W. Stahl

Gases from water and sediment samples were analysed for the concentration of hydrocarbons. The data on methane and heavier hydrocarbon (hc) components in the sediments give information on the existence of hydrocarbons in the shallow samples, their formation by microbial processes at moderate depth and/or their formation by thermal degradation of organic matter at greater depth and higher temperatures and migration into the shallow sediments. If thermal hydrocarbons are present the data, especially the isotope data still to be determined in the land based laboratory, give information on the hydrocarbon potential in the survey area. In case of high methane concentrations, methane hydrate occurrence may be indicated in the survey area by the geochemical data.

7.1 CTD Measurements (p, t, salinity, oxygen)

E. Faber, J. Poggenburg, W. Stahl

The hydrographic parameters (temperature, pressure, salinity, sound velocity and dissolved oxygen) were measured using a CTD Seabird SBE Model 11 plus (SEA-Bird Electronics Inc.) combined with a 24 bottle (10 litre) rosette water sampler (Niskin bottles). Depth profiles were run to within about 9 m of the bottom. Data of all CTD-runs are stored in the Seabird computer and are also available on CD. The CTD (including oxygen sensor) and the water sampling system were working properly without problems. However, due to problems with the winch lowering and hoisting often took quite a long time and the CTD data should be used with care in case of data evaluation for oceanographic purpose.

7.1.1 Results

CTD data of all multiprobe stations are stored on CD. As an example representing the data from other stations, sound velocity, salinity, oxygen content and water temperature only of station 87 MS are plotted in Fig. 7.1 relative to the water depth.

The general depth trends of these parameters are:

The sound velocity is about 1540 m/sec in the uppermost 100 m, decreases rapidly down to 1495 m/sec at the depth of ca. 200 m where it lowers the slope with depth and decreases down to a minimum value of 1485 m/sec at 1000 m. Downwards below 1000 m it increases up to 1505 m/sec at the final depth. Between ca. 100 and 1400 m sound velocity curve is very rough.

The salinity is about 33.4 ‰ at the surface, increases rapidly up to 34.5 ‰ at a depth of ca. 100 m where it lowers the slope with depth and increases to about 34.7 ‰ at 400 m. At the final depth it has nearly the same value. Between ca. 100 and 1400 m salinity variations are higher than in the depth interval of 1400 m to the final depth.

At the surface oxygen has the highest concentration of ~6 mg/l which is only slightly lower at 100 m. At 400 m oxygen has the lowest reading 2.4 mg/l. Below 400 m oxygen increases up to 43.7 mg/l at 2800 m but decreases slightly to the final depth. Strong and well defined variations with depth are found in the interval 200 to 1400 m.

Temperature in the uppermost 100 m is about 28.2 °C but rapidly falls to 12 °C at 200 m. The temperature continuously decreases downwards and has its minimum of 1.8 °C at the

lowermost depth. Like with the other parameters the temperature curve is rough between 200 and 1400 m.

Scales of Fig. 7.1 don't resolve that very small variations were observed in the lowermost part of the water column which form individual layers of constant temperature and/or salinity (better density). Whether these data can be used to trace fairly constant methane concentrations within specific layers and to locate or map active methane vent sites needs further investigations.

7.2 Water samples

E. Faber, J. Poggenburg, W. Stahl

7.2.1 Methods

For extraction of dissolved gases from the water samples (collected using the CTD-rosette system) the vacuum/ultrasonic technique, modified after Schmitt et al. (1991), was used (Fig. 7.2). Equilibrium between the (pre-) evacuated headspace of the degassing unit and the water is established rapidly by the application of ultrasonic energy to the water sample (one litre) for about 10 minutes. An aliquot (0.5 ml) of the extracted gas is injected into a gas chromatograph (Shimadzu Mini 3 equipped with a FID and a 2 m x 1/8"column packed with Porapaq Q) for methane analyses aboard. Methane concentration is given as nano (10^{-9}) litres of methane per litre of water (nl/l).

The large fraction of the water gases not used for analysis aboard were stored in evacuated glass vessels. Stable carbon isotope ratios on the methane and on the carbon dioxide will be determined in the laboratory at the BGR in Hannover for gas genetic interpretations.

7.2.2 Results

Results of methane in the water samples are given in Table 7.1 or on CD, respectively. Data is given in Figures 7.3 to 7.8. In each of theses figures stations are summarised according to the different sampling areas like in the vicinity of seismic lines SO-137-03, SO-137-01, SO-137-06 and stations in deep water (max. depth > 5000 m).

Methane concentration of stations in the first sampling area, according to seismic line SO-137-03 are given in Fig. 7.3. Methane in the uppermost samples of stations 2 MS and 8 MS is around 40 nl/l which is very close to the equilibrium concentration with atmospheric methane. For the other stations the concentrations are lower. This may be interpreted in the sense that the surface water in the areas of the latter stations represents sinks for atmospheric methane. At about 50 m depth a relative minimum in methane concentrations (< 30 nl/l) is observed. Stations 8 MS and 17 MS show elevated concentrations between 100 and 200 m depth. These maxima are related to biological activity which was described previously (FABER et al., 1998). Below 300 m methane concentrations are lower than < 20 nl/l, characterising ocean water background concentrations. Only for stations 8 MS and 12 MS concentrations are slightly elevated indicating methane input into the bottom water. Input locations could not be localised as methane concentrations are only slightly elevated suggesting distant input, hence difficult to find. Deep water stations 2 MS, 17 MS and 19 MS are discussed later.

In the sampling area of seismic line SO137–01 methane distribution in the water column is quite different from that near line SO137–03. Concentration in the surface samples is below atmospheric equilibrium value (Fig 7.4). Biogenic activity within the first hundred meters is not indicated, as methane values are in the range of background concentrations down to ca.

2500 m. Below 2500 m methane increases and reaches a maximum of 5028 nl/l at 2900 m (station 80 MS). This values is the highest methane concentration found throughout the whole cruise SO 139. The high methane concentrations are related to methane input from the sub-bottom into the bottom water through active vent system(s).

Stations 80 to 87 MS were sampled during re-visiting the survey area of seismic line SO137-03 with the intention to locate the active vent sites using the methane concentrations in the water samples as guiding tool. Therefore, at these stations samples were taken only below 2500 m where methane concentrations were expected to be elevated due to vent emanations. Fig. 7.5 shows the methane concentration in the depth range from 2500 to nearly 3000 m. Values near background were found down to about 2780 m. In the deeper water column down to 3000 m methane concentrations were elevated at all stations (except at 22 MS) and showed one or more maxima. Mapping the maxima did not allow to definitely locate the active vent site(s) during shipboard operation because of the low number of CTD-stations. It was mentioned above that strong variations of CTD-data in the distribution curves were observed. Variations are also detectable in the lowermost hundreds of meters, as is shown for example in Fig. 7.6 for station 80 MS, where the scales of the CTD-data were spread to detect small variations. Sound velocity continuously increases with depth while temperature and salinity decreases. Oxygen is relatively stable but decreases slightly downwards. Interestingly, layering is detectable most pronounced in the temperature distribution, but also in the oxygen curve. In the salinity trace the layers are much more difficult to observe. Obviously temperature does mostly determine the density and consequently the stability of individual water layers even at the depth close to the bottom. As can be seen in Fig. 7.6, the correlation between individual layers and the methane concentrations may allow to locate active methane vent sites if related to bathymetric data. Vent site location may possibly be easier by just running CTD-stations without water sampling and related methane concentration determination for all stations and all depth.

In the survey area west of southern Sumatra at seismic line SO-137–06 methane concentrations remained near background down to about 1500 m but increase below. At 1640 m the maximum concentration found in this area was about 2112 nl/l at station 55 MS (Fig. 7.7). This high value indicates methane input into the deep water from vents as discussed for the area at seismic line SO137–01. The low number of locations did not allow to localise a vent site.

As methane is a non-conservative component it suffers bacterial oxidation in the sediment when sulphate or oxygen is available. As can be seen from the CTD-data oxygen is present all over the water column. Therefore, methane oxidation starts immediately after the methane enters the ocean water. As oxidation causes isotopic fractionation, there will be a shift in the $^{13}C/^{12}C$-ratios of the methane increasing with distance from the vents. This trend may help to determine direction and distance to the vent site(s).

Deep water stations were located ocean-ward of the accretionary wedge where water was more than 6000 m deep. As can be seen in Fig. 7.8 methane was enriched in the uppermost 200 m as discussed above for stations 2 MS and 17 MS. Down to nearly 5000 m methane concentrations have background values only. Below 5000 m the concentrations increased and reached the maximum value of 122 nl/l at 6002 m at station 2 MS. These relatively high concentrations are indicative for methane input from the wedge. However, as the maximum concentrations were much lower compared to the high values mentioned above, the distance to the vent sites was great or methane concentrations in the vent(s) are low. Because of the lack of time for extended vent-searching no detailed search for the active vents at the foot of the accretionary wedge was undertaken.

Table 7.1: Methane concentrations in water samples of CTD-stations for water sampling

Station	Depth m	GC No.	Gas ml	CH4 nl/l
2MS	6467	28	14	9
2MS	6002	29	13	122
2MS	5002	30	14	10
2MS	3999	31	13	9
2MS	3000	32	16	10
2MS	1999	33	16	13
2MS	1000	34	10	19
2MS	0	35	11	43
5MS	6327	38	11	92
5MS	6300	39	9	74
5MS	6250	41	14	75
5MS	6199	40	23	85
5MS	6150	48	17	90
5MS	6100	42	14	107
5MS	6050	46	11	63
5MS	5999	43	11	61
5MS	5800	44	10	60
5MS	5599	45	10	21
5MS	5199	46	15	42
5MS	3999	49	15	15
5MS	2000	50	18	18
5MS	1000	51	12	12
5MS	500	52	5	6
5MS	2	53	8	26
8MS	2723	56	13	35
8MS	2720	57	11	25
8MS	2700	58	10	22
8MS	2600	59	12	31
8MS	2500	60	12	39
8MS	2000	61	11	32
8MS	1599	62	14	44
8MS	999	63	7	13
8MS	500	64	6	12
8MS	100	65	12	44
8MS	50	66	7	23
8MS	0	67	9	41
12MS	2605	68	12	40
12MS	2589	69	9	30
12MS	2559	70	9	37
12MS	2518	71	10	45
12MS	2298	72	7	14
12MS	1799	73	9	18
12MS	1200	74	7	8
12MS	499	75	4	6
12MS	200	76	7	26
12MS	100	77	6	18
12MS	50	78	8	26
12MS	2	79	8	30

Table 7.1, Page 2

Station	Depth m	GC No.	Gas ml	CH4 nl/l
17MS	6403	86	14	118
17MS	6298	87	15	119
17MS	6200	88	15	105
17MS	5999	89	14	79
17MS	5800	90	13	78
17MS	5601	91	16	71
17MS	5399	92	15	44
17MS	4999	93	10	17
17MS	4000	94	12	7
17MS	3000	95	10	7
17MS	999	96	9	7
17MS	500	100	7	10
17MS	200	97	9	41
17MS	100	98	8	63
17MS	2	99	8	27
19MS	5540	102	13	24
19MS	5500	103	5	7
19MS	5450	104	9	16
19MS	5399	109	18	48
19MS	5350	107	15	33
19MS	5300	105	10	16
19MS	5200	106	13	27
19MS	5099	108	15	28
19MS	5001	110	16	27
19MS	4799	111	18	34
19MS	4600	112	11	16
19MS	3000	113	14	14
19MS	2000	114	11	8
19MS	200	115	8	37
19MS	76	116	7	22
19MS	2	117	8	28
22MS	2977	121	9	25
22MS	2960	123	6	14
22MS	2939	122	9	29
22MS	2919	124	9	32
22MS	2788	125	13	32
22MS	2601	126	12	12
22MS	2400	127	10	24
22MS	2201	128	12	22
22MS	1700	129	8	6
22MS	1001	130	10	23
22MS	199	131	7	15
22MS	99	132	7	23
22MS	50	133	10	33
22MS	12	134	6	17

Table 7.1, Page 3

Station	Depth m	GC No.	Gas ml	CH4 nl/l
23MS	2972	135	9	38
23MS	2959	136	6	20
23MS	2950	137	8	24
23MS	2931	138	15	58
23MS	2910	139	17	67
23MS	2800	140	12	45
23MS	2600	141	10	35
23MS	2100	142	9	8
23MS	1000	143	2	7
23MS	201	144	5	18
23MS	100	145	5	12
23MS	50	146	7	25
23MS	10	147	6	21
32MS	2986	155	10	41
32MS	2980	156	5	15
32MS	2960	157	9	44
32MS	2940	158	8	54
32MS	2920	160	11	168
32MS	2900	159	9	165
32MS	2800	162	15	77
32MS	2499	161	11	15
32MS	1500	163	9	10
32MS	1000	164	7	30
32MS	200	165	7	25
32MS	49	166	5	12
32MS	10	167	7	24
45MS	1989	182	10	20
45MS	1980	183	6	9
45MS	1920	184	9	16
45MS	1890	197	13	23
45MS	1860	185	9	14
45MS	1829	186	10	17
45MS	1815	188	13	34
45MS	1800	187	14	30
45MS	1748	189	9	21
45MS	1699	190	5	16
45MS	1650	193	12	73
45MS	1600	191	9	64
45MS	1550	194	11	60
45MS	1500	192	8	14
45MS	79	195	7	22
45MS	10	196	9	30

Table 7.1, Page 4

Station	Depth m	GC No.	Gas ml	CH4 nl/l
49MS	2008	199	8	11
49MS	1999	200	6	8
49MS	1958	201	6	9
49MS	1920	202	8	13
49MS	1880	203	13	26
49MS	1840	204	7	11
49MS	1800	207	7	12
49MS	1700	206	8	27
49MS	1660	208	9	48
49MS	1640	211	20	67
49MS	1620	209	14	43
49MS	1549	210	7	8
49MS	1348	213	6	13
55MS	1673	220	12	329
55MS	1660	221	8	835
55MS	1649	232	5	530
55MS	1640	222	9	2112
55MS	1620	223	9	1329
55MS	1601	223	9	938
55MS	1560	225	10	92
55MS	1520	224	8	48
55MS	1449	226	6	36
55MS	1350	227	7	12
55MS	1200	228	8	11
55MS	400	229	4	7
55MS	100	230	6	21
55MS	0	231	7	25
66MS	6175	239	13	41
66MS	6099	240	7	5
66MS	6050	241	9	9
66MS	5950	242	10	8
66MS	5849	243	13	11
66MS	5749	244	10	8
66MS	5450	247	11	10
66MS	5300	248	10	8
66MS	4000	249	8	6
66MS	2001	250	8	5
66MS	2	251	6	19
71MS	1680	256	11	553
71MS	1659	258	6	115
71MS	1650	259	7	86
71MS	1640	257	7	64
71MS	1640	263	7	62
71MS	1619	260	11	98
71MS	1599	261	7	50
71MS	1559	262	7	70

Table 7.1, Page 5

Station	Depth m	GC No.	Gas ml	CH4 nl/l
72MS	1725	264	11	1961
72MS	1720	265	5	987
72MS	1699	267	6	523
72MS	1680	268	7	93
72MS	1659	269	10	91
72MS	1639	266	6	65
72MS	1597	271	5	37
72MS	1519	270	7	16
73MS	1718	272	11	935
73MS	1710	273	4	387
73MS	1701	274	6	437
73MS	1679	275	6	189
73MS	1660	276	8	47
73MS	1640	277	6	58
73MS	1620	278	6	53
73MS	1600	279	7	53
73MS	1560	281	3	30
73MS	1520	280	5	92
79MS	1872	283	18	38
79MS	1840	284	8	12
79MS	1761	285	14	38
79MS	1720	286	15	49
79MS	1680	289	12	35
79MS	1640	288	5	22
79MS	1600	290	10	40
79MS	1560	291	5	11
79MS	1521	292	5	6
79MS	1480	293	5	5
79MS	1400	294	6	7
79MS	1000	295	6	8
80MS	2933	297	8	407
80MS	2919	298	3	171
80MS	2910	299	4	1770
80MS	2900	306	9	5028
80MS	2880	300	8	1767
80MS	2840	301	10	1674
80MS	2800	302	7	21
80MS	2760	303	7	26
80MS	2620	305	7	10
80MS	2519	304	3	4

Table 7.1, Page 6

Station	Depth m	GC No.	Gas ml	CH4 nl/l
81MS	2966	307	12	223
81MS	2950	311	3	48
81MS	2940	308	8	111
81MS	2930	314	8	105
81MS	2910	310	9	164
81MS	2910	315	7	111
81MS	2900	309	6	68
81MS	2848	312	5	10
81MS	2801	313	7	19
81MS	2660	316	5	7
82MS	2914	317	13	364
82MS	2909	324	3	73
82MS	2899	318	10	114
82MS	2889	326	7	136
82MS	2879	319	11	99
82MS	2870	325	6	51
82MS	2861	323	12	237
82MS	2850	320	8	200
82MS	2830	321	8	18
82MS	2809	322	4	7
87MS	2922	329	12	338
87MS	2918	334	4	121
87MS	2910	330	8	124
87MS	2900	331	8	59
87MS	2889	337	10	28
87MS	2880	332	9	44
87MS	2870	333	5	8
87MS	2861	335	11	23
87MS	2850	336	13	29
87MS	2835	338	9	24
87MS	2820	345	9	107
87MS	2809	339	9	569
87MS	2800	346	16	404
87MS	2780	340	6	18
87MS	2774	341	6	67
87MS	2650	342	9	20
87MS	2600	343	8	9

Fig. 7.1: Depth trends of CTD data (sound velocity, salinity, oxygen and temperature) from station 87 MS

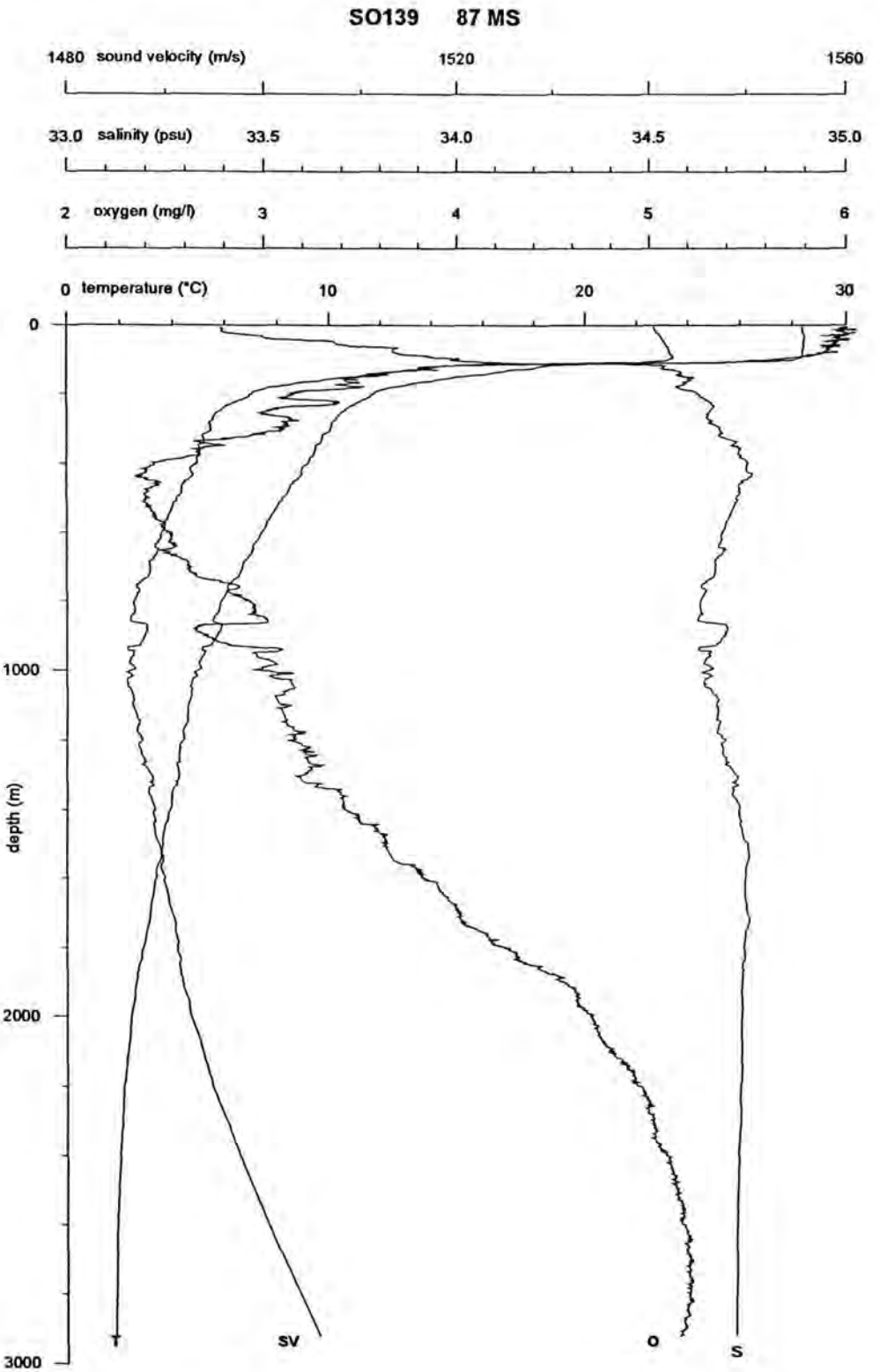

Fig. 7.2: Mobile apparatus for the extraction of gases from water samples by the application of ultrasonic energy to the water (1 litre)

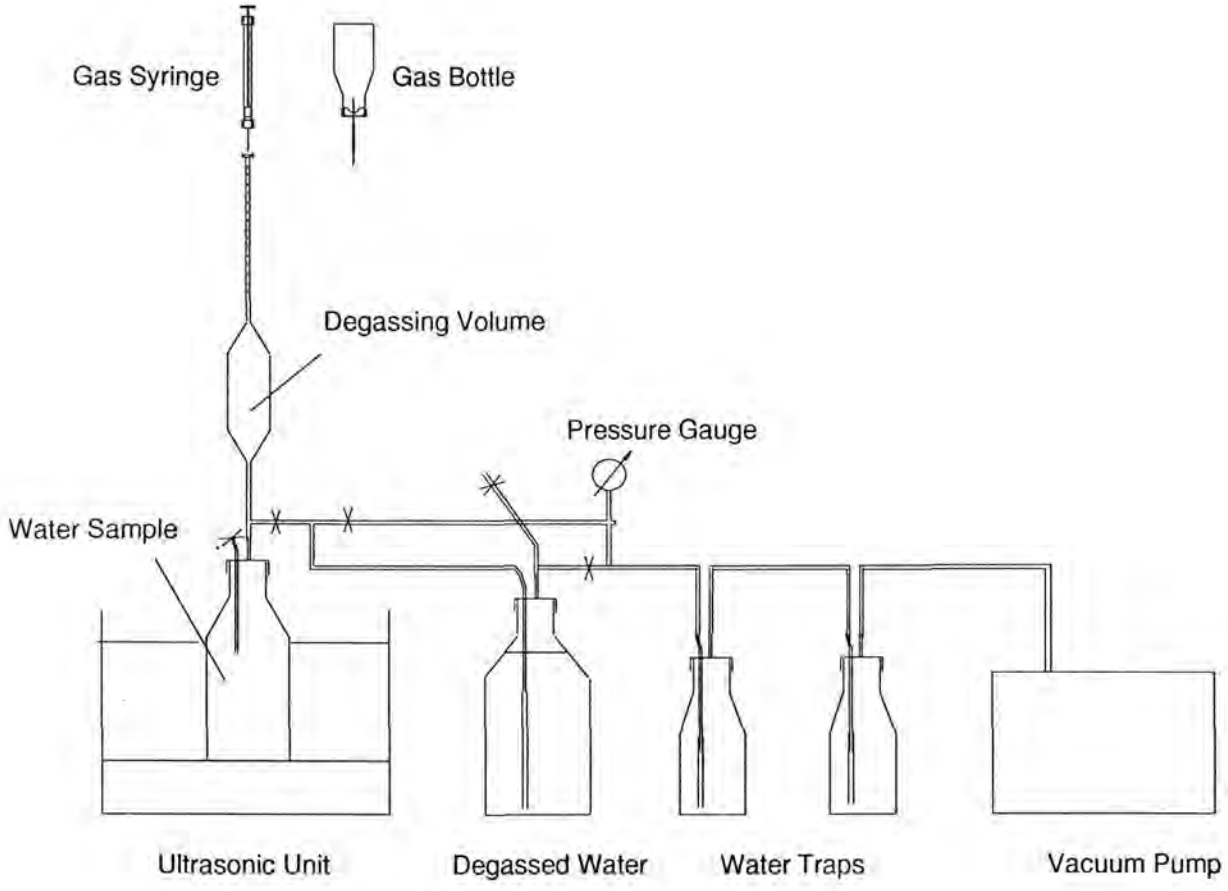

Fig. 7.3: Methane concentration in water samples plotted versus sampling depth from stations 2 MS, 5 MS, 8 MS, 12 MS, 17 MS and 19 MS aligned around seismic line SO 137-03

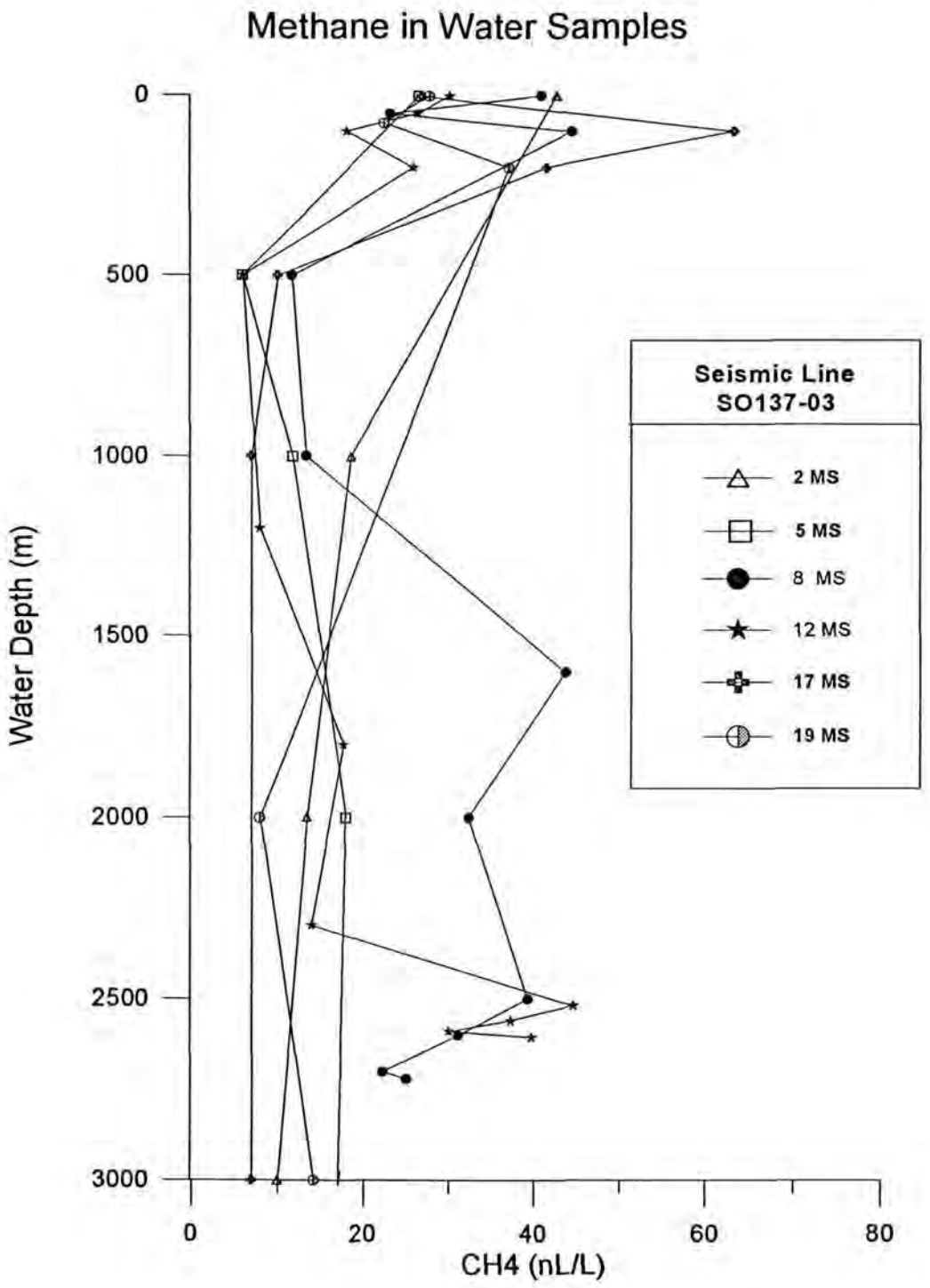

Fig. 7.4: Methane concentration in water samples plotted versus sampling depth from stations 22 MS, 23 MS, 32 MS, 80 MS, 81 MS, 82 MS and 87 MS aligned around seismic line SO 137-01

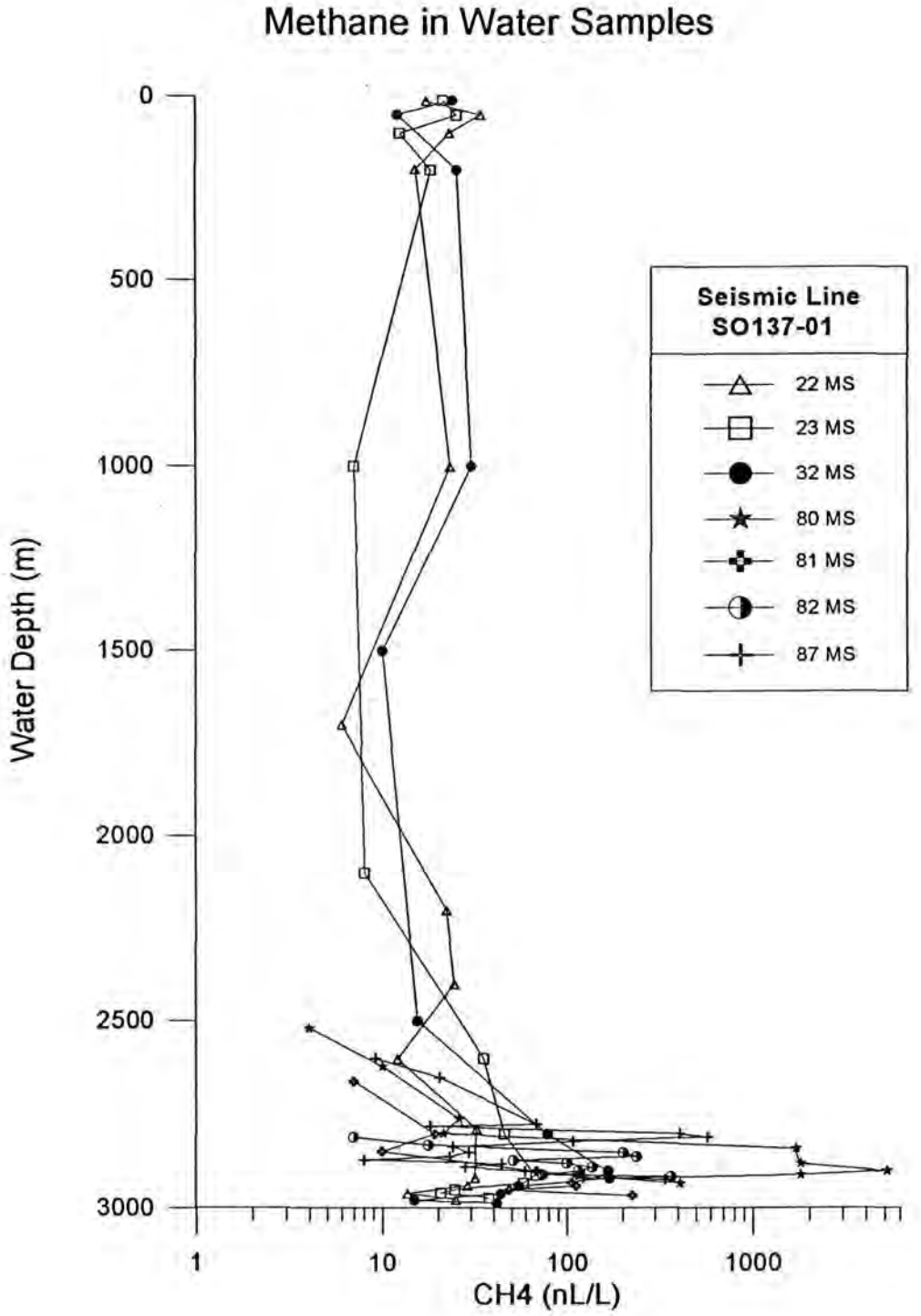

Fig. 7.5: Methane concentration in water samples plotted versus sampling depth from stations as in Fig. 4 but focussed to the depth 2500 to 3000 m

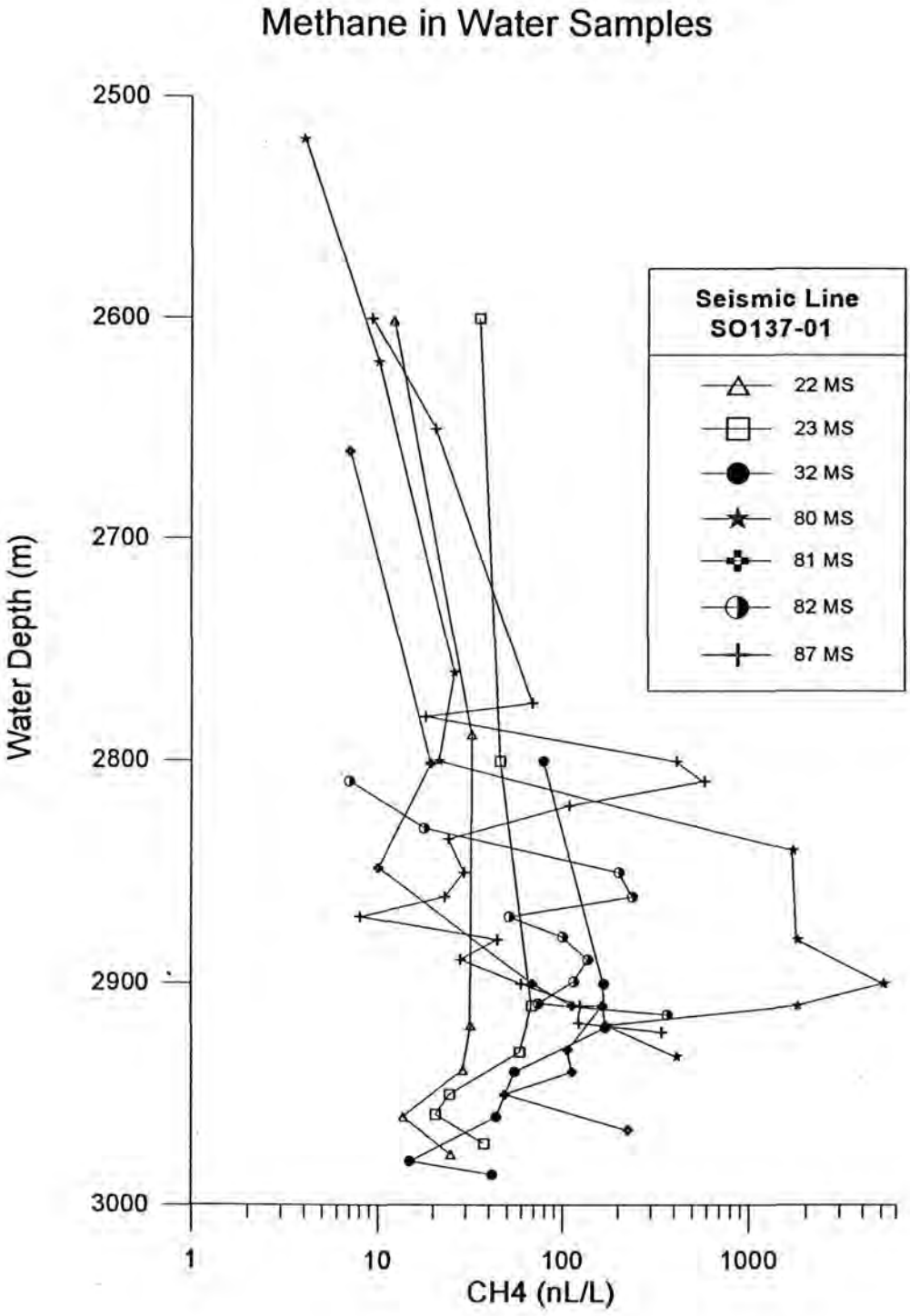

Fig. 7.6: CTD-data (sound velocity, salinity, oxygen and temperature) and methane concentration of station 80 MS plotted versus water depth between 2600 and 3000 m

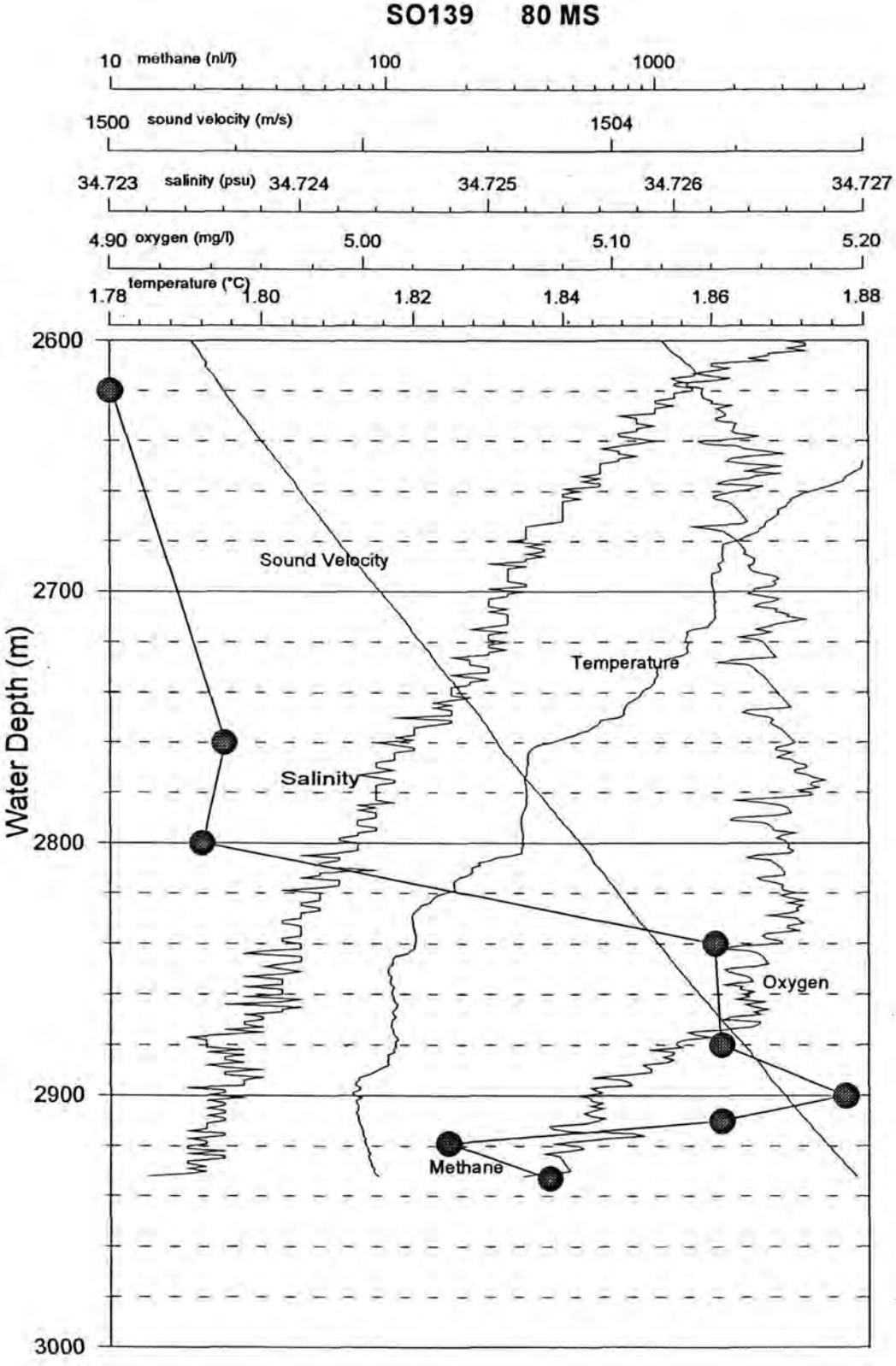

Fig. 7.7: Methane concentration in water samples plotted versus sampling depth from stations 45 MS, 49 MS, 55 MS, 71 MS, 72 MS, 73 MS and 79 MS aligned around seismic line SO 137-06

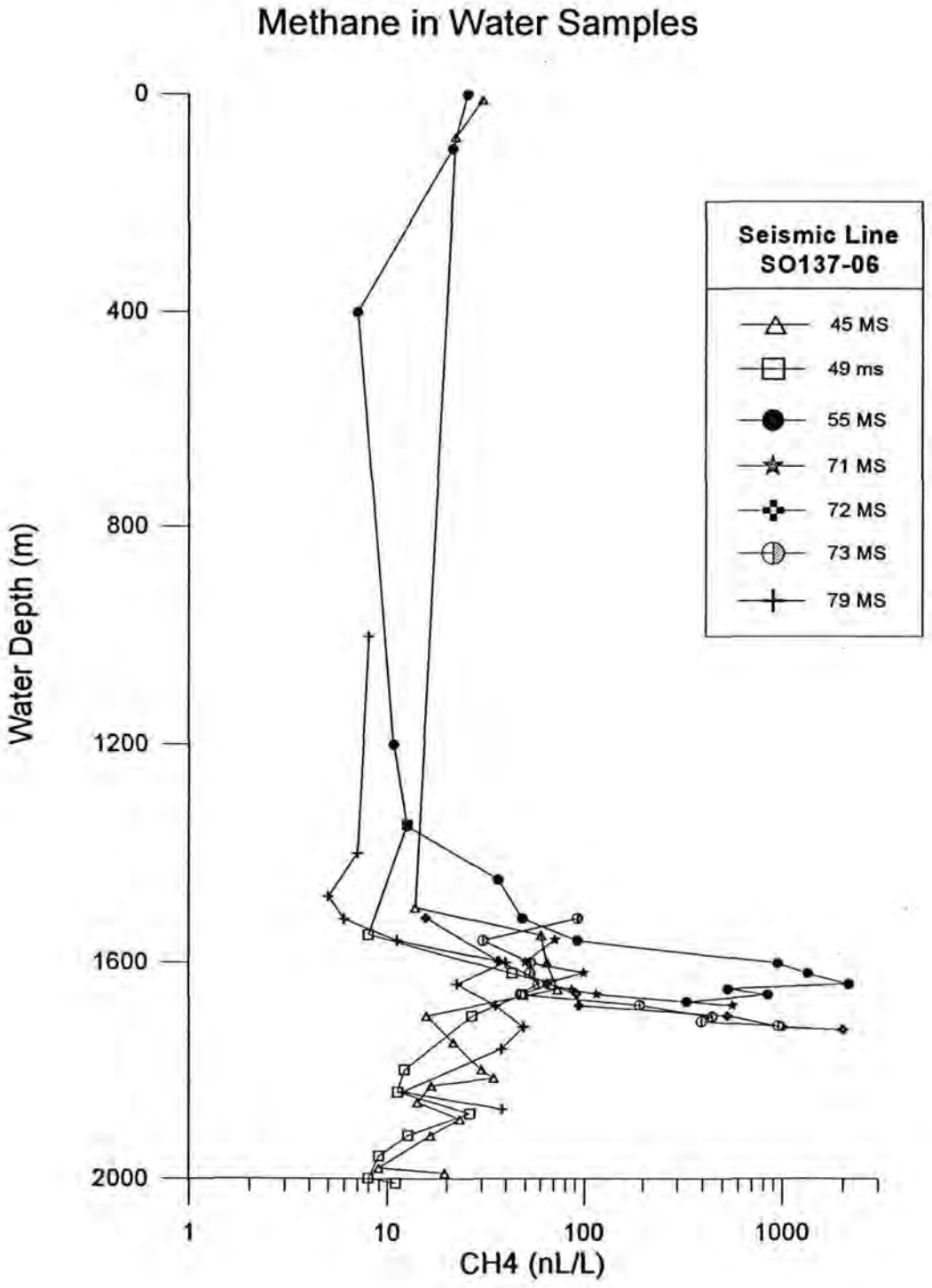

Fig. 7.8: Methane concentrations in water samples versus sampling depth from deep water stations 5 MS, 2 MS, 17 MS, 19 MS and 66 MS

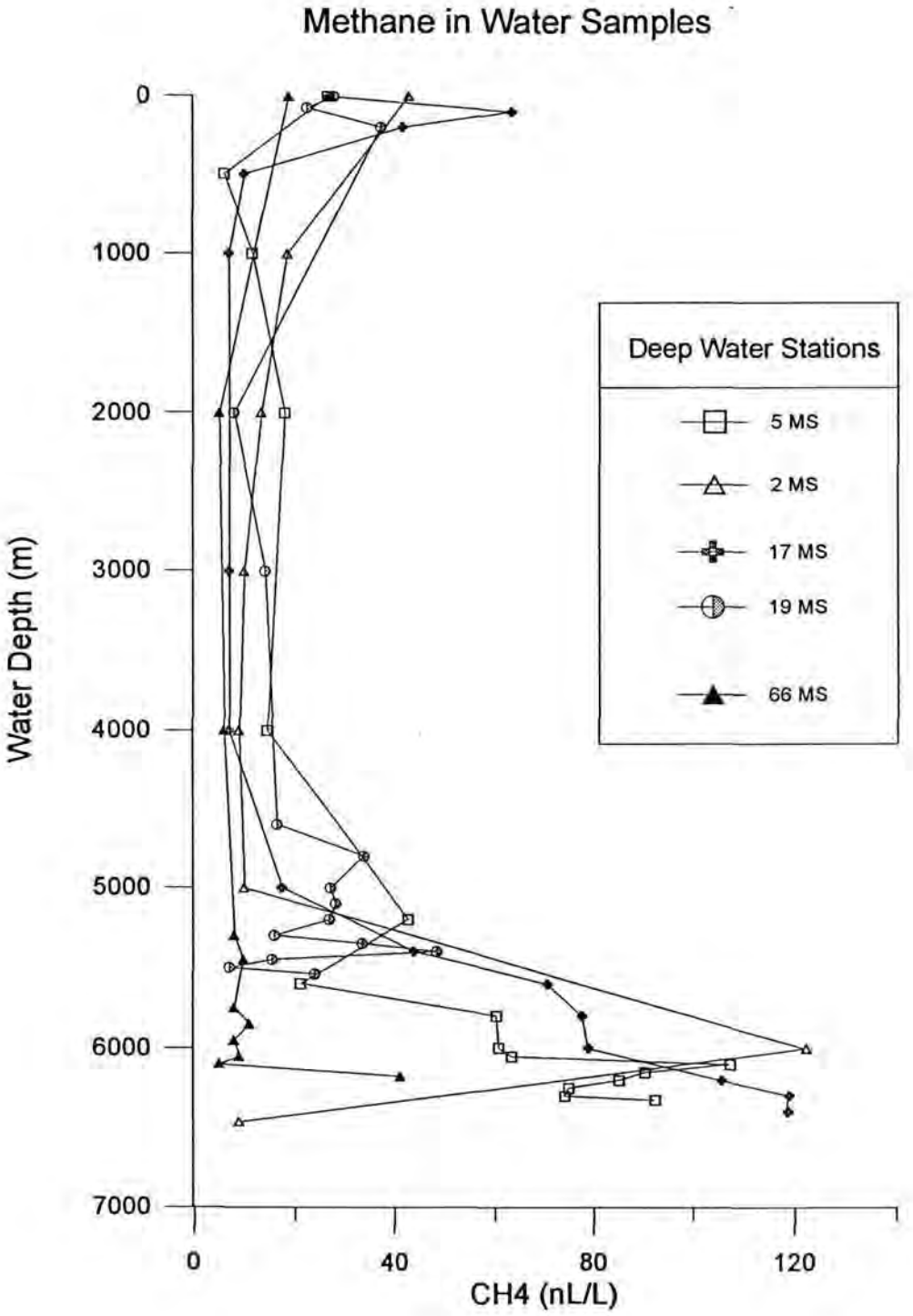

7.3 Pore water analyses of piston and gravity cores

B. Harazim, V. Marchig, Haryadi Permada, and H.S. Koesnadi

The aim of the investigation is to decipher the early diagenetic processes within the sediments in the area where bottom simulating seismic reflectors were observed and may indicate the lower boundary of gas hydrates. The top of the layer is not defined in the seismic records. The stability field for gas hydrates concerning temperature and pressure is reaching the sea floor, but the concentration of methane even in deepest parts of investigated cores (20 m bsf) does not reach the level which is needed for formation of gas hydrates. It is assumed that gas hydrate disintegrates under rising temperature and falling pressure. The disintegration of gas hydrate horizon in the sediment frees fresh water and methane which both try to migrate upwards through the sediment, react with sediments and change the composition of pore water.

7.3.1 Methods of pore water extraction from sediments and pore water analyses

During Cruise SO 139 interstitial water samples (pore water) were extracted from sediments with a pore water press newly designed by BGR.
Compact PTFE sample vessels with a maximum volume of 125 ccm, Tefzel LUER LOCK outlets for the sample water and self-locking sea-waterproof V4A-stainless steel inertgas-valves guaranteed a contamination-free sample preparation procedure. Also a newly designed quicklook support and a miniaturised pressure gas distribution-block improved the handling of great amounts of samples (350).

For geochemical analyses the cores were cut into 1m-sections and caried immediately to the cold storage at a temperature around 4° C. After the whole core (up to 20 m) was cut into 1 m sections each section was split in half-core segments. One half was used for stratigraphic analyses. The other half was used for the extraction of porewater. Special sections of 5 or 8 cm were marked by a geologist or geochemist. Samples of up to 125 ccm solid material from marked sections were transferred into the sample vessels. After covering the sample with parafilm and a NBR-rubbermat the vessels were mounted in the porewater press stand. Extraction time was 30 minutes and a pressure of 2 to 4 bar (Argon) was applied. Depending on the composition of the sediment 20 ccm to 50 ccm of pore water were gained. The sample was filtered through a „Sartorius" cellulose nitrate filter 0.45µm type 11306-100-N and directly collected in 25 ccm storage containers.

The following tools were used for pore water shipboard analyses:

Determination of **pH**
SCHOTT pH-meter CG 837, temperature compensated
Electrode SCHOTT N 1042 A

Determination of **Eh**
SCHOTT pH-meter CG 837, temperature compensated
Electrode SCHOTT Pt 61 (Pt-Ag/AgCl)

Determination of **conductivity** and **salinity**
WTW Conductivity Meter LF 323
Electrode WTW Tetra Con 325 (851228041)

Determination of **oxygen**

Picoamperemeter with
O_2-microsensor for probe systems, in situ determination
Eletrode No. 17099802

Determination of **H_2S / Sulfide**

Picoamperemeter with
H_2S-microsensor for probe systems, in situ determination
Eletrode No. 17099804 - 3 mg/L
Eletrode No. 17099803 - 10 mg/L
Eletrode No. 17099801 - 50 mg/L

The new amperometric microsensor has been developed for the in situ determination of dissolved H_2S /Sulfide in natural waters. Because of the partial pressure of the gaseous H_2S, the analyte is separated by penetration through the membrane. Inside the sensor the hydrogen sulfide reacts with a redox mediator. The reoxidation at the working electrode causes a current corresponding to the concentration of the dissolved molecular H_2S amount. The sensor has a very short response time of down to 200 milliseconds and streaming as with Clark-type oxygen-sensors is not necessary, so that profiling with high resolution is possible. The sensor works highly selectively and there are no signal equivalents to CO, CO_2, H_2O-vapour, CH_4 nor NH_3. Both salt concentrations of up to 40 g/L and turbid or coloured solutions do not interfere with the signal. For measuring the total sulfide concentration from pH 5 to pH 8,5 the sensor was combined with a pH electrode and in each case with a temperature measurement.

The pH-ranged from 7.2 to 8.5. To adjust the pH below pH 3, the sample was mixed in a reaction-coil of 1 m with 0.05 n-H_2SO_4 (1:1) and pumped through a closed measuring-cell (flowrate 1.8 ml/min.). Total sulfide was calculated with to following to terms:

$$C_{H^+} = 10^{-pH} \qquad (Gl.\ 1)$$

$$C_{totalsulfide} = C_{H2\,S} \times [C^2_{H+} + (C_{H+} \times 1{,}205 \times 10^{-7}) + 4{,}7861 \times 10^{-21}] / C^2_{H+} \qquad (Gl.\ 2)$$

Planned shore based analyses

Determination of following anions in the pore water:

Cl^-
SO_4^{2-}
Br^-
PO_4^{3-}

Determination of following cations in the pore water:

Fe
Mn
alkaline metals and earth alkaline metals
heavy metals

Verification of the decrease of total salinity as observed in 58 KL, 74 KL, 44 TVG, 91 TVG & 93 TVG.

Determination of the following parameter in the squeeze cakes

Fe
Mn
alkaline metals and earth alkaline metals
heavy metals
Trace elements (all by XRF)

$C_{org.}$
S

7.3.2 Results; piston cores from forearc basins

Sampling took place in the South Java Basin and in the Bengkulu Basin, on positions where methane enrichment in sea water was indicating methane venting or venting with characteristic vent fauna was observed.

The sampling strategy was to core for stratigraphic purposes on every position, followed by retrieving one or several cores for pore water analyses. The stratigraphic core provided information about physical properties of sediment and about sedimentation rate in the location. It was not used for pore water extraction because it was already warmed during processing in the laboratory.

Core 21KL was sampled on the position in South Java Basin where tectonic disturbance of deeper sediments suggested leaking of methane from the assumed gas hydrate layer. Twelve meters of sediment were recovered of which the bottom part contained, as expected, enrichment of methane (max. 22251 ppb CH_4 , see FABER et al., this volume). This core was used for stratigraphic studies exclusively.

At the same position two other sediment cores were recovered: 24KL (12.9 m) and 37KL (19.06 m). From these cores pore water was extracted.

In the Bengkulu Basin methane enrichment in sea water was indicating methane venting, but no active vent was observed. Core 54KL (17.7 m) was sampled for stratigraphic purposes. It was placed over the fault system in deeper layers of the sedimentary basin. Its bottom part showed an increased methane concentration (24 816 ppb CH_4 , see FABER et al., this volume). At the same position two other cores were recovered for pore water extraction, 58KL (17.5 m) and 74KL (19.7 m).

Fig. 7.9 shows the methane concentration in the sediment for two cores taken for pore water investigations (see FABER et al., this volume). The maximum concentrations were found in the deepest parts of cores exceeding 30 000 ppb CH_4. As already mentioned these methane concentrations, although very high for the sediment, still are too low for the formation of gas hydrates. That means that the gas hydrate layer, if present must have its top deeper than 20 m below the sea floor. The concentrations of methane are decreasing towards sea floor; the important difference between the two positions is, that the background values of methane are reached 7 m under the sea floor in the South Java Basin cores and at 13 m under the sea floor in the Bengkulu Basin cores.

Fig. 7.10 shows the composition of pore water for two South Java Basin cores, as determined on board. The depth in the core in which methane in the sediment decreased to the background values is characterised with a decrease of Eh, an increase of sulfide, and, less pronounced, a decrease of salinity and an increase of pH.

The same qualitative statement applies to the changes in composition of pore water in the two Bengkulu Basin cores (see Fig. 7.11), but quantitative changes are higher in the order of magnitude and they also do not reach back to the initial levels in the deeper parts of the two cores.

Composition of pore water from gravity cores sampled on vent positions in the South Java Basin

The re-precipitation of calcite at the vent position (Snails and Mussels Hill) is forming Carbonate crusts which partly cover the surrounding of vents. For precaution, sediment was sampled with the less vulnerable short gravity corer or TV-controlled grab. The composition of pore water from the grab sampler is described by SAHLING and v. MIRBACH (this volume). The composition of pore water from two gravity cores is shown in Fig. 7.12. Gravity core 88SL shows the decrease of Eh and increase of sulfide already in depth in the sediment of only 2m. The other core, 83SL , is probably too short and does not reach the depth in which the electronegativity starts. Both cores have strong decrease of salinity in their pore water with depth.

The methane concentrations in both gravity cores show only background values (FABER et al., this volume) but the enrichment of methane in the sediment could not be expected in these two cores as they are both not long enough to reach the layers under the redox boundary in which the methane enrichment can be found.

On the same plot the same parameters from a „background" core 11KL are shown.This was sampled in a part of the South Java Basin without any methane anomaly (10KL was the stratigraphic core for this background location, see WIEDICKE et al., this volume). The pore water profile from the core 11KL shows a weak decrease of Eh, but this is not enough to initiate reduction of sulphate to sulfide. Salinity is also not changing systematically with depth in the core.

The salinity problem

Both gravity cores from the vent position as well as the short (40cm) core taken from the TV-controlled grab sampler of the same position show a strong decrease in salinity of pore water[1] beginning directly below the sediment surface (see Fig. 7.12 and SAHLIG and v. MIRBACH, this volume),. The two piston cores from Bengkulu Basin also reveal a decrease in their pore water salinity, but in these cores the decrease is initiated at the redox boundary and not starting directly below the sediment surface.

Part of the salinity decrease could be caused by the reduction of sulphate to sulfide and precipitation of pyrite. Both processes are lowering the electric conductivity of pore water. The other reason for lowering of the salinity is the dilution of pore water with the salt-free water from decaying gas hydrate. Further investigations in the shore based laboratories will help to evaluate the influence of the two factors in the salinity decrease in pore water.

---

[1]) the subsequent increase of salinity in two deepest samples of core **88SL** is, to our opinion, based on dilution with sea water, because gravity coring is apt to sucking more sea water during sampling than the piston coring.

Figure 7.9: Methane content in the sediment cores from South Java Basin and Bengkulu basin; changes of content with depth in the cores (data from FABER et al., this volume)

South Java Basin

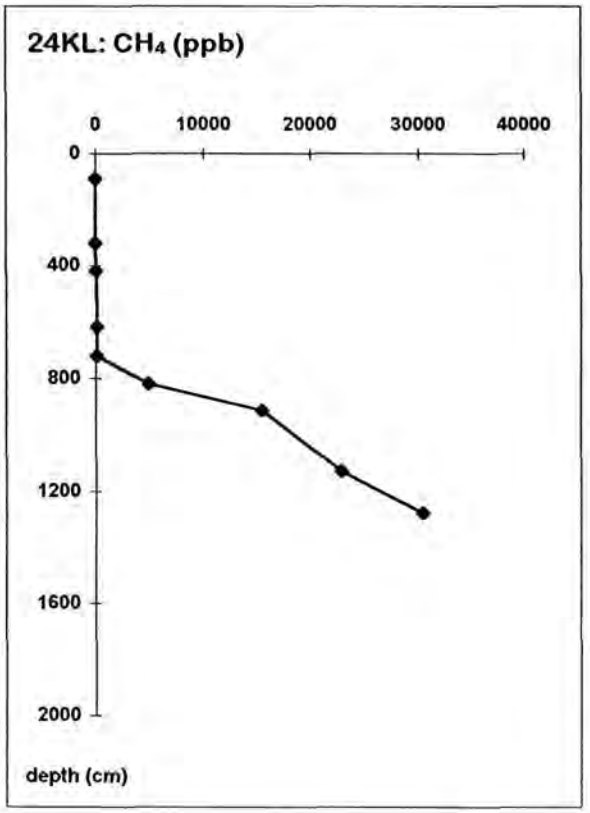

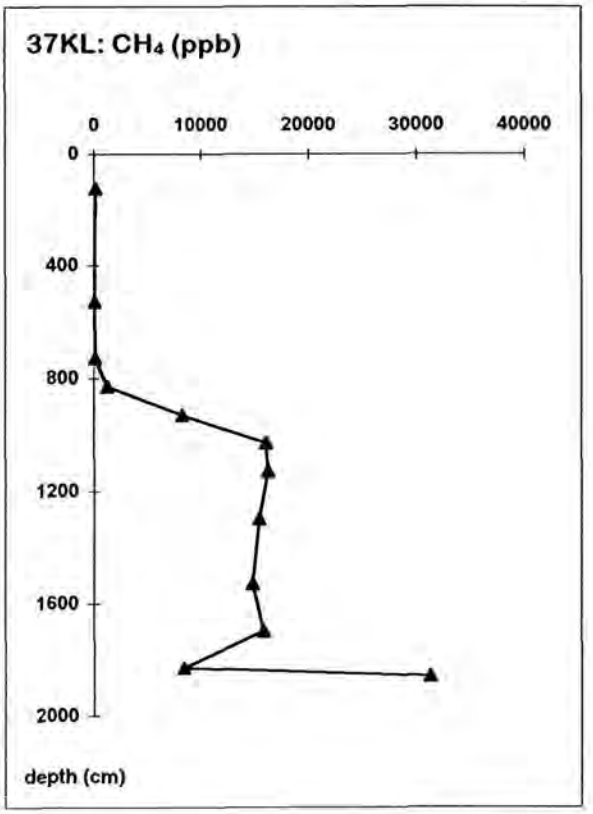

BENGKULU BASIN

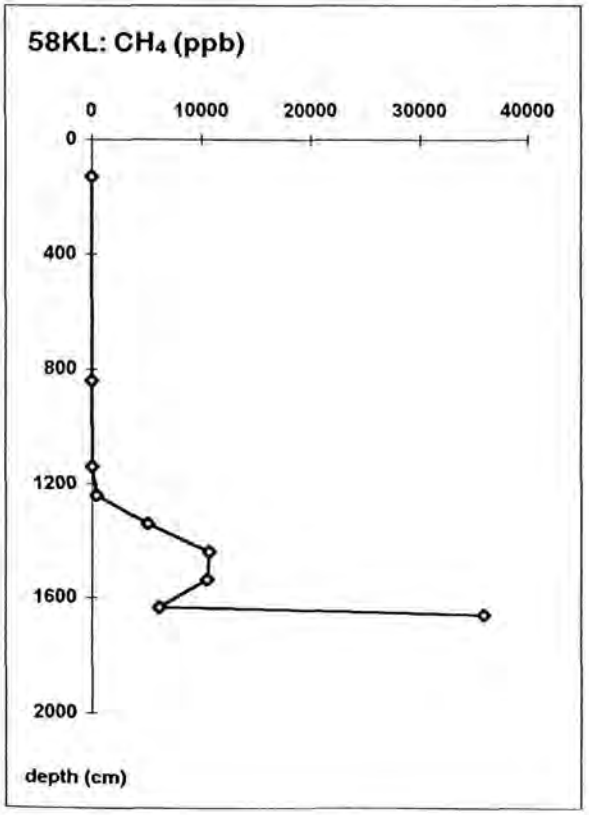

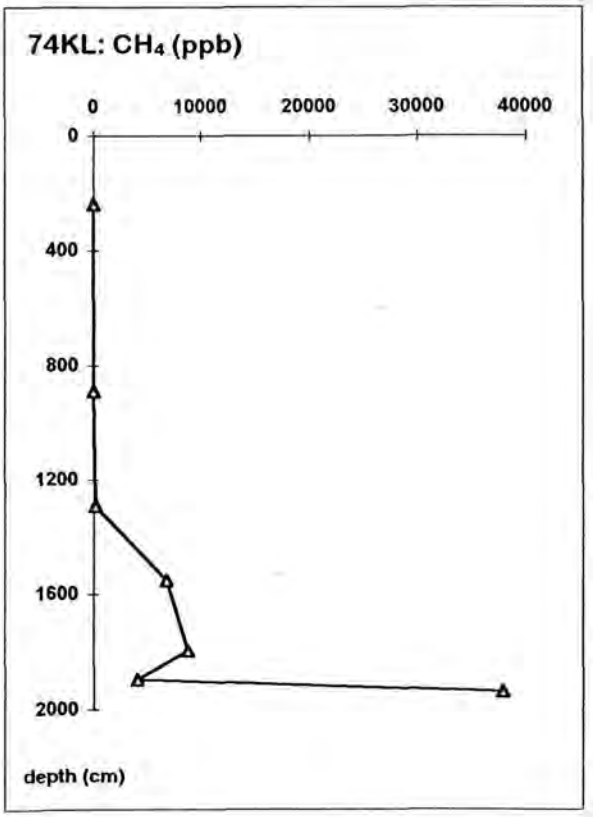

Figure 7.10: Results of shipboard analyses of pore water in sediment cores from South Java Basin; changes in salinity and pH with depth in the cores

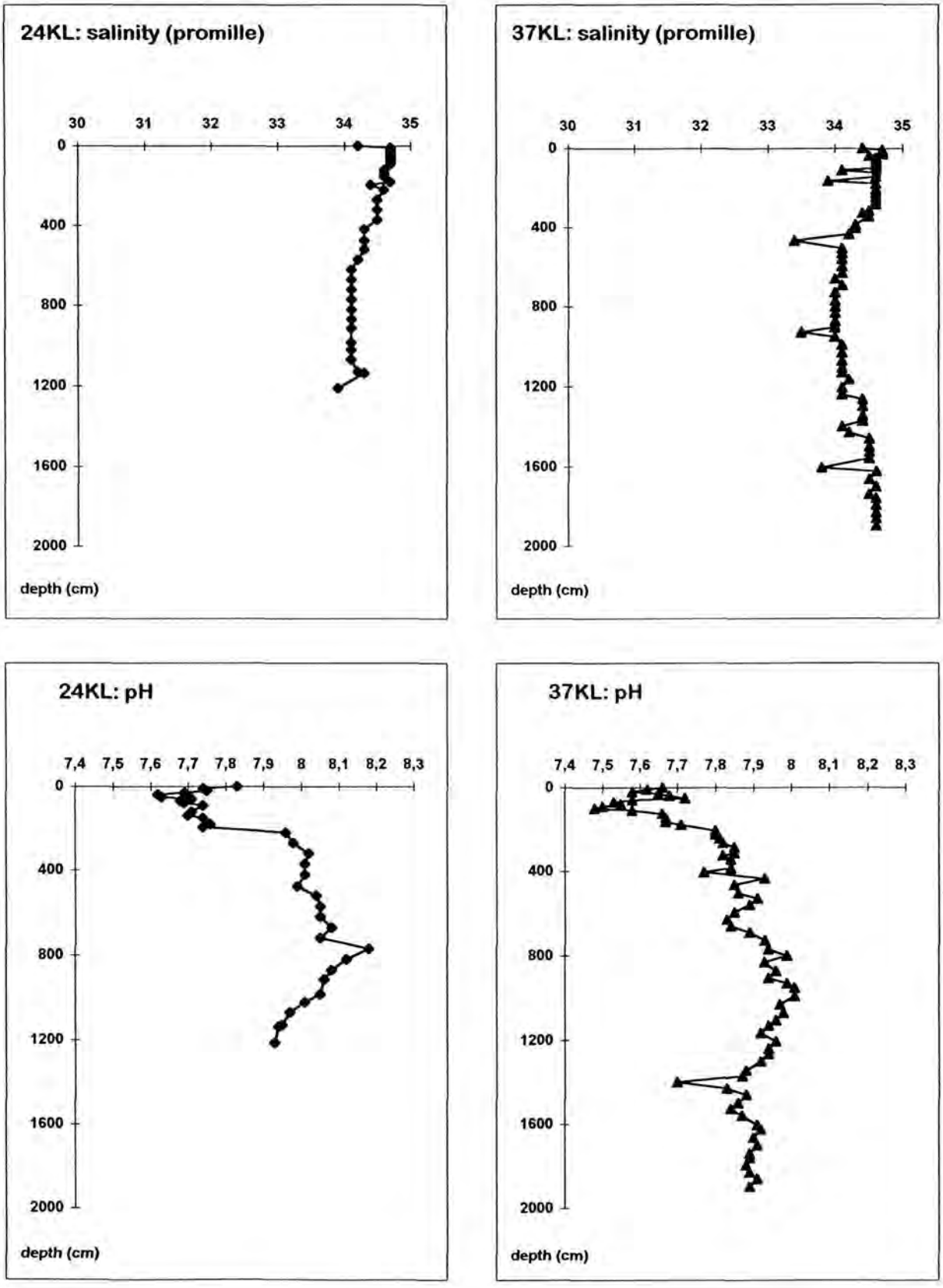

Figure 7.10 (continued):
Results of shipboard analyses of pore water in sediment cores from South Java Basin; changes in Eh and sulfide content with depth in the cores.

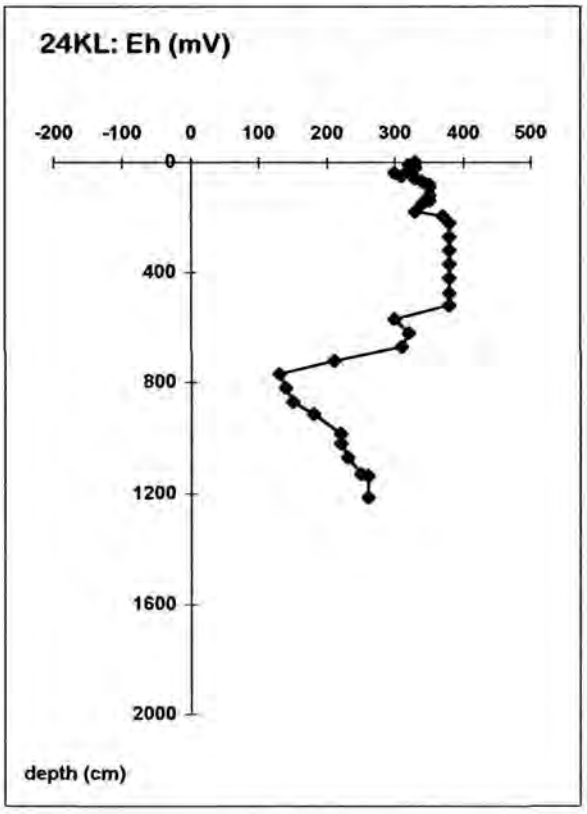

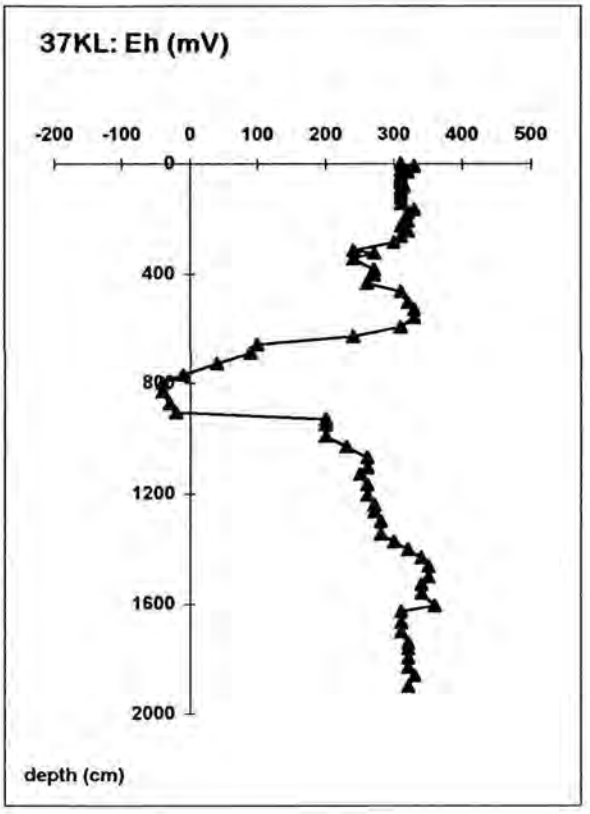

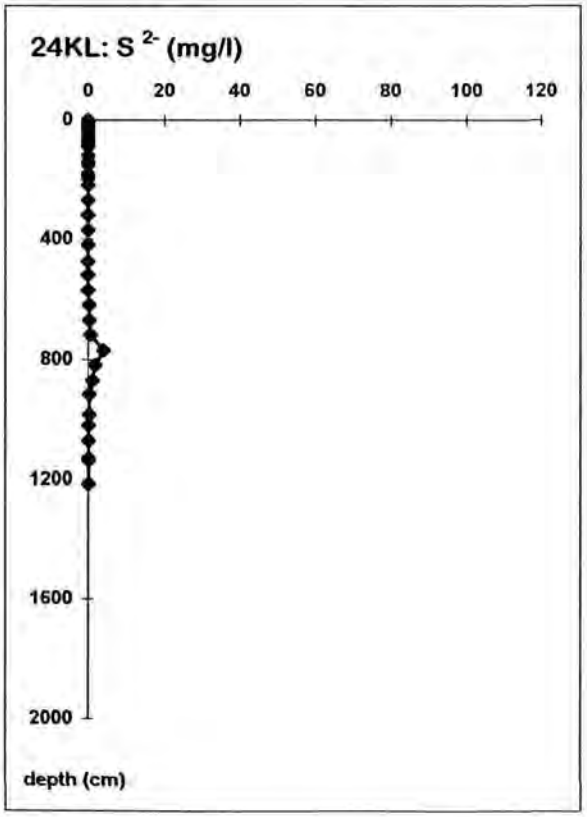

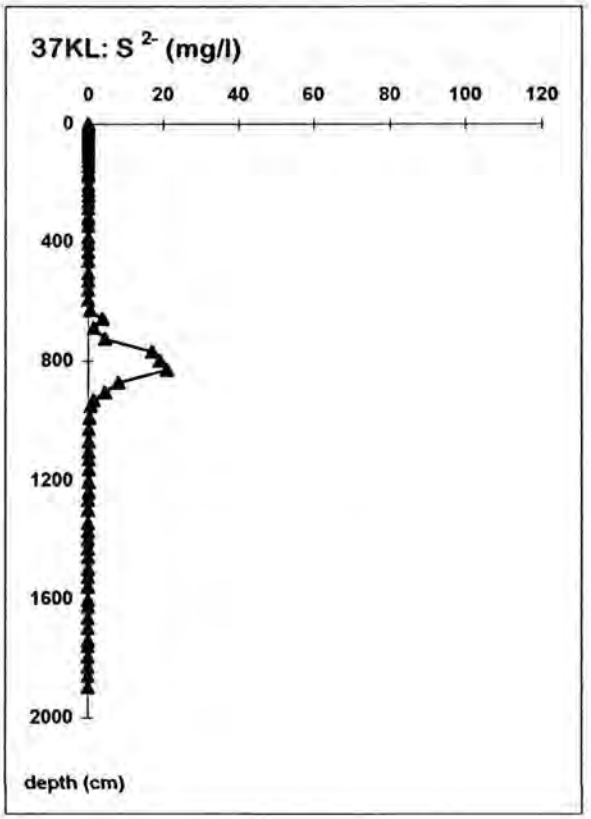

Figure 7.11: Results of shipboard analyses of pore water in sediment cores from Bengkulu Basin: changes in salinity and pH with depth in the cores

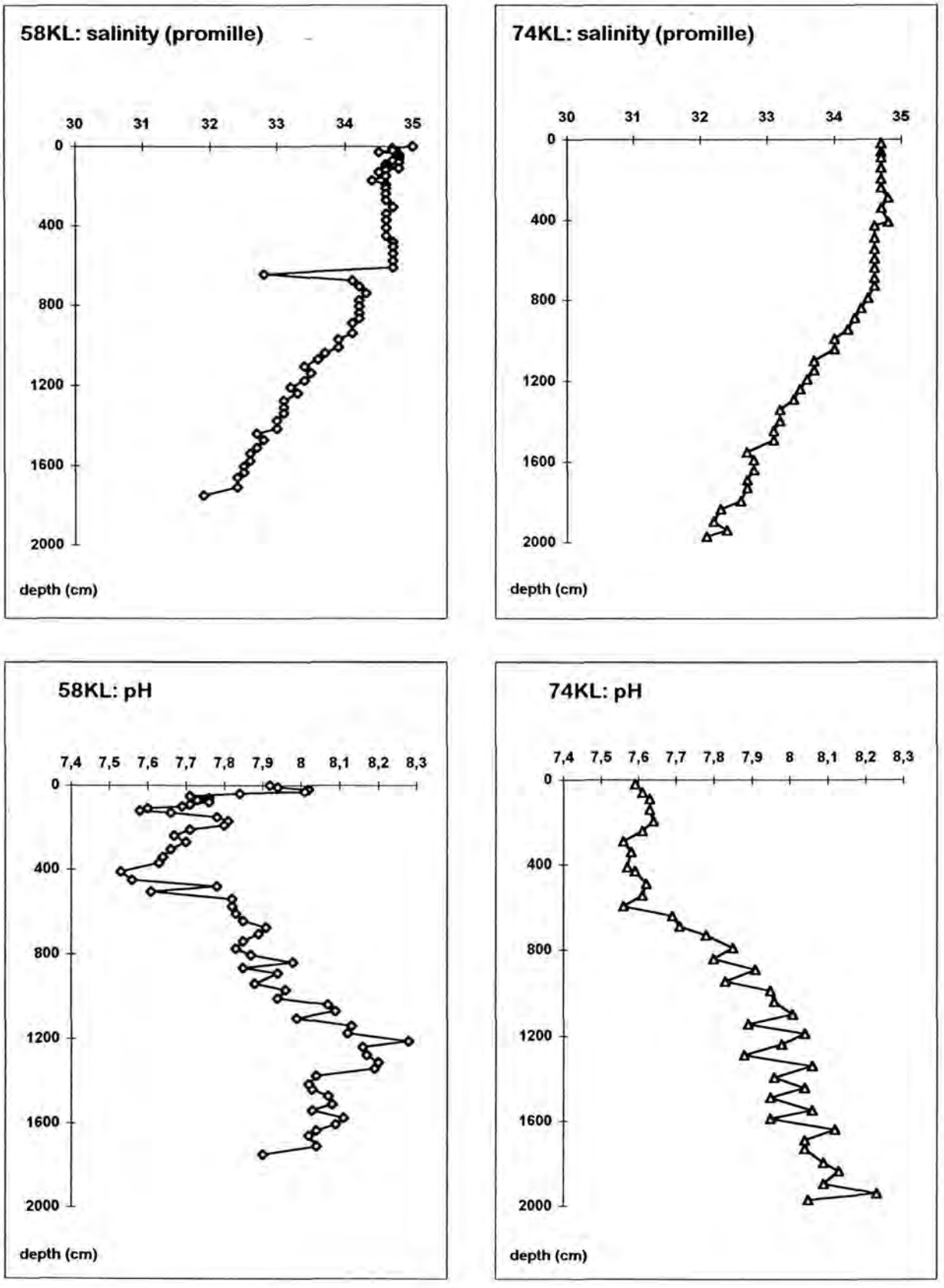

Figure 7.11 (continued):
Results of shipboard analyses of pore water in sediment cores from Bengkulu Basin: changes in Eh and sulfide with depth in the cores

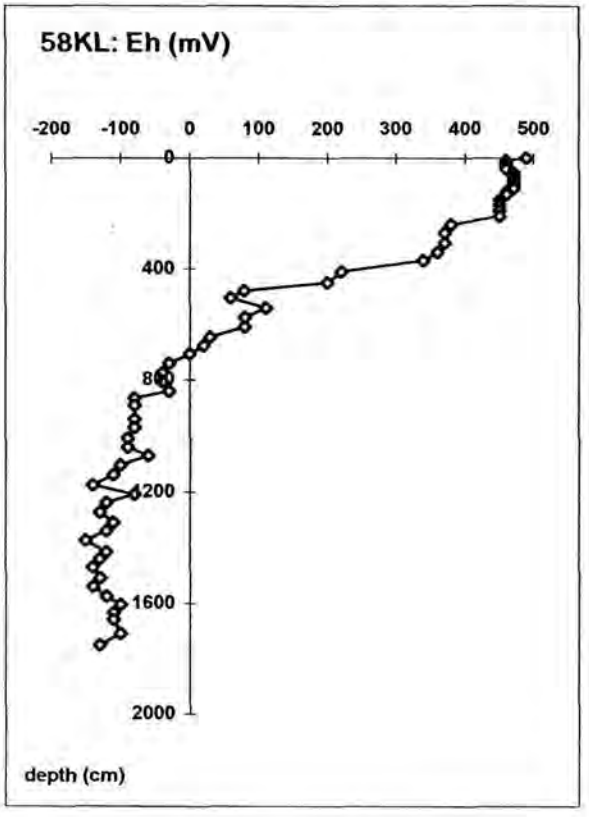

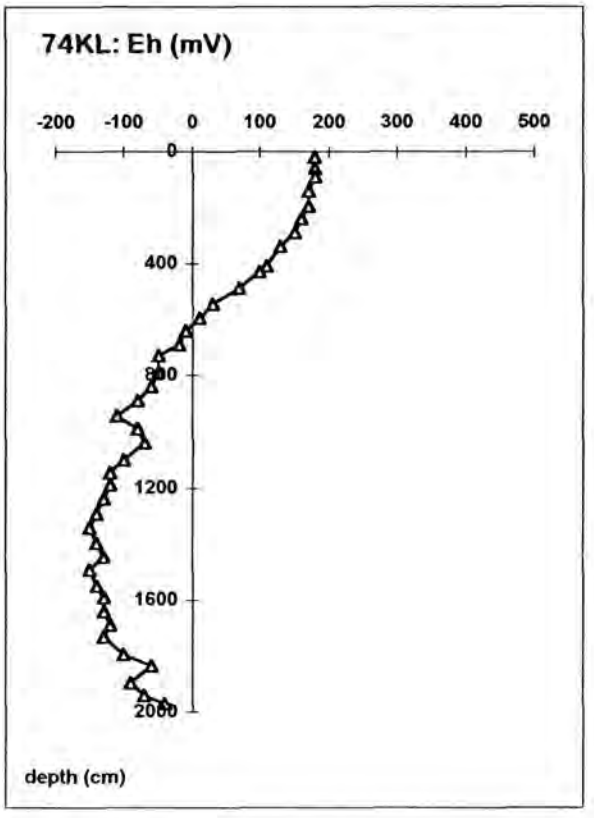

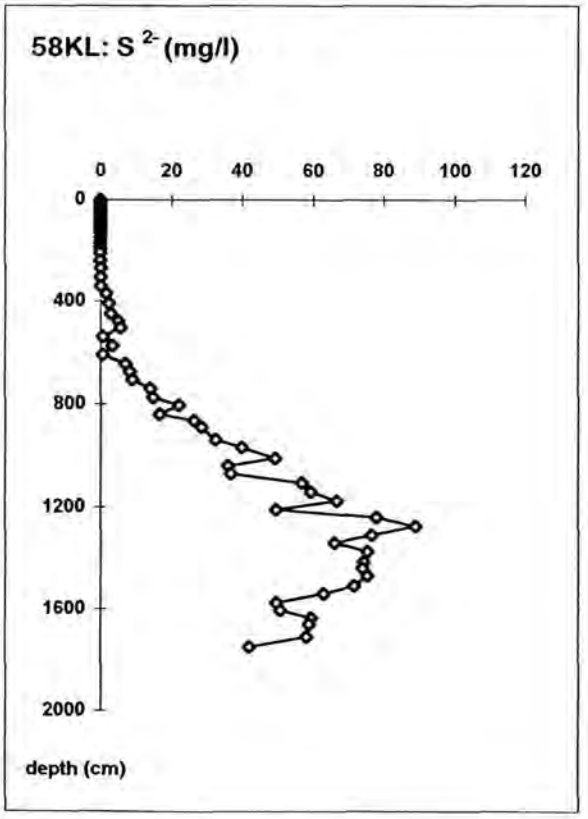

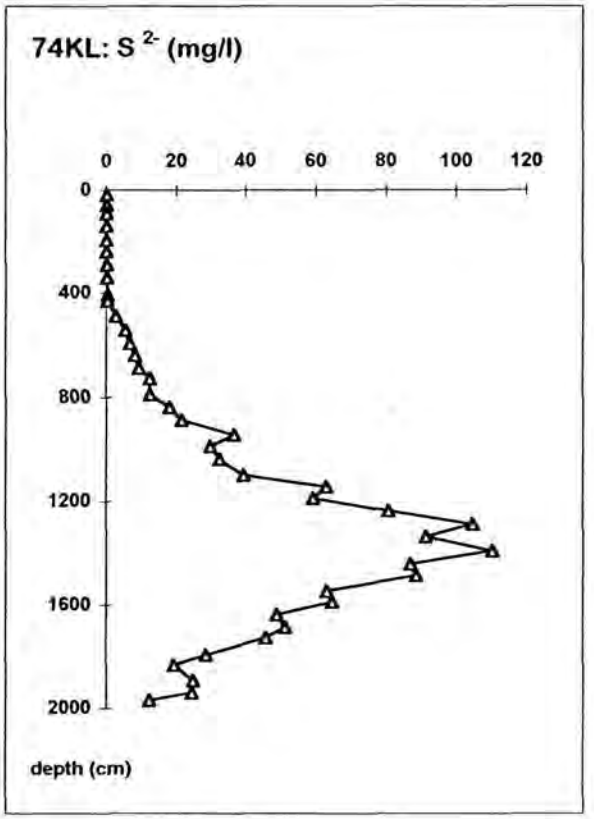

Figure 7.12: Results of shipboard analyses of pore water in sediment cores from vent position in South Java Basin; changes in salinity and pH with depth in the cores

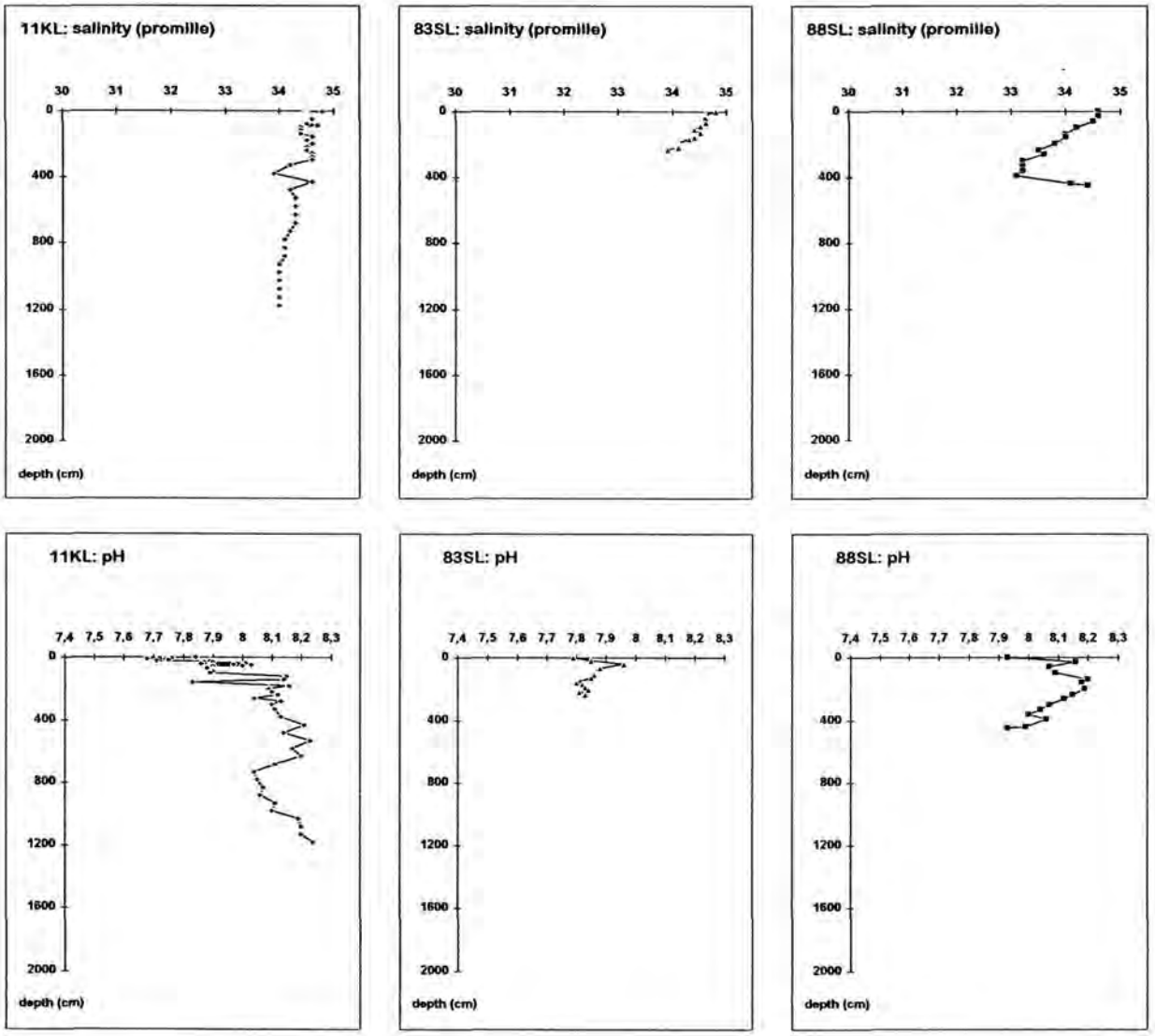

Figure 7.12 (continued):
Results of shipboard analyses of pore water in sediment cores from vent position in South Java Basin; changes in Eh and sulfide content with depth in the cores

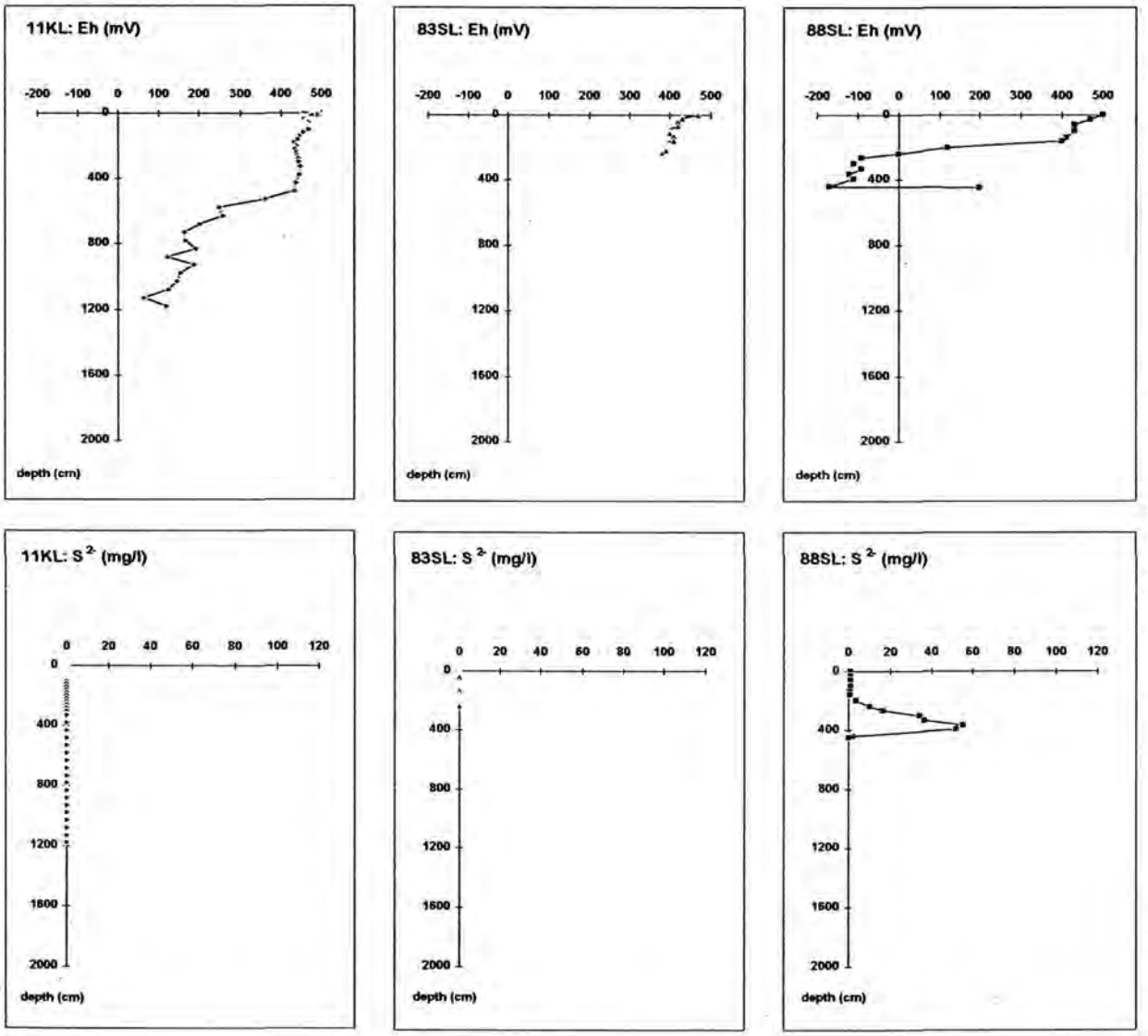

7.4 Pore water analyses of cores from TV-grab

N. von Mirbach

7.4.1 Method

To subsample the TV grab for pore water analyses plastic boxes were pushed into the sediment from the top where the surface appeared to be least disturbed. The boxes were immediately segmented in the cold room (+ 4 °C) and pore water was collected with a polypropylene squeezer pressurised by argon and fitted with 0.45 µm cellulose acetate membrane filters. The sediment was cut in slices of different thickness depending on the core length.

The analytical procedures were based on "Methods of Seawater Analysis" (GRASSHOFF et al. 1983). The alkalinity and the sulfide concentrations of the pore water were measured as soon as possible after collecting the samples. Subsequently, the pore water was analysed for silicate and ammonia. Silicate, ammonia and sulfide were measured with photometric methods.

Alkalinity
The total alkalinity (TA) was calculated from a single point titration of 1.0 ml pore water. Buffers for calibration were prepared from 0.01 N HCl (Titrisol) in 70% (v/v) artificial sea water. To obtain an exact pH of 3.00 and 3.52 an additional amount of acid has to be added to compensate the alkalinity of salt impurities. This amount is calculated from a Gran titration of 100 ml artificial sea water (STUMM and MORGAN, 1996). The total alkalinity is calculated from the excess of acid after the addition of 0.3 up to several ml of 0.01 N HCl, resulting in a voltage corresponding to a pH of between 3.00 and 3.52. This method is established for small amounts of pore water with an alkalinity of about 2 to 3 mM. Data that exceed this value by a factor of 10 may not be quite reliable, because the ionic strength is reduced significantly by the addition of greater amounts of acid. In this case the pore water samples were titrated with 0.1 N HCl instead of 0.01 N HCl to avoid too much dilution.

Ammonia
Ammonia was analysed by DTT reagent (dichloro isocyanuric acid) and disodium nitropusside in a citrate buffer and measurement at 630 nm.

Silicate
To determine the silicate content of pore water samples ammonium heptamolybdate-tetrahydrate solution in combination with oxalic acid was applied. The absorption of samples were measured at 810 nm. Silicate values are influenced by high sulfide concentrations. To avoid this problem samples with an obvious high sulfide content were stored in open vials in the cold room to remove sulfide. The later conducted measurements were still influenced by the sulfide. Therefore the silicate data are less reliable.

Sulfide
The pore water samples were stabilised by zinc acetate gelatine solution immediately after retrieval. Sulfide was analysed by the N,N- Dimethyl-p-phenylen diamin dihydrochloride method and ferric chloride solution as catalyst. The absorption was measured at 670 nm. This method for sulfide determination described in GRASSHOFF et al. (1983) was adapted to pore water samples with a high sulfide content by elevating the amount of zinc acetate gelatine solution to fix the sulfide (1ml instead of 50µl per 1ml sample volume).

Shore-based laboratory studies
Subsamples were taken for shore-based analyses of sulfate, chloride and bromide (by ion chromatography). Various cations like barium, boron, calcium, lithium, magnesium, manganese, potassium, sodium and strontium will be analysed at GEOMAR by ICP-AES

Method. The squeeze cakes will be analysed for C:N ratio and calcium content.

7.4.2 Results

Results from every single grab

Station: 33 GA
Position: 07° 57.79' S / 106° 17.20' E
Methane by E. Faber: appr. 300 ppb in a closed eye grabbed subsample after opening
Pore water squeezed from sub-box B without relation to fauna.
Pore water characteristics:
The concentration of Si, NH_4, and alkalinity are low compared to 24 KL and the concentration does not increase significantly with depth. Si, NH_4 and alkalinity show values very close to the concentrations in the bottom water. This can be explained by an inflow of bottom water due to a large scale circulation driven by the outflow, so we would be in a recharge area. Hydrogen sulfide concentrations increase with depth but the maximum concentrations of 2 µM at 45 cm are also quite low (Fig. 7.13).

Station: 43 GA
Position: 07° 57.45' S / 106° 17.62' E
Methane by E. Faber: appr. 19,530 ppb in a closed eye grabbed subsample after opening
No pore water was squeezed.

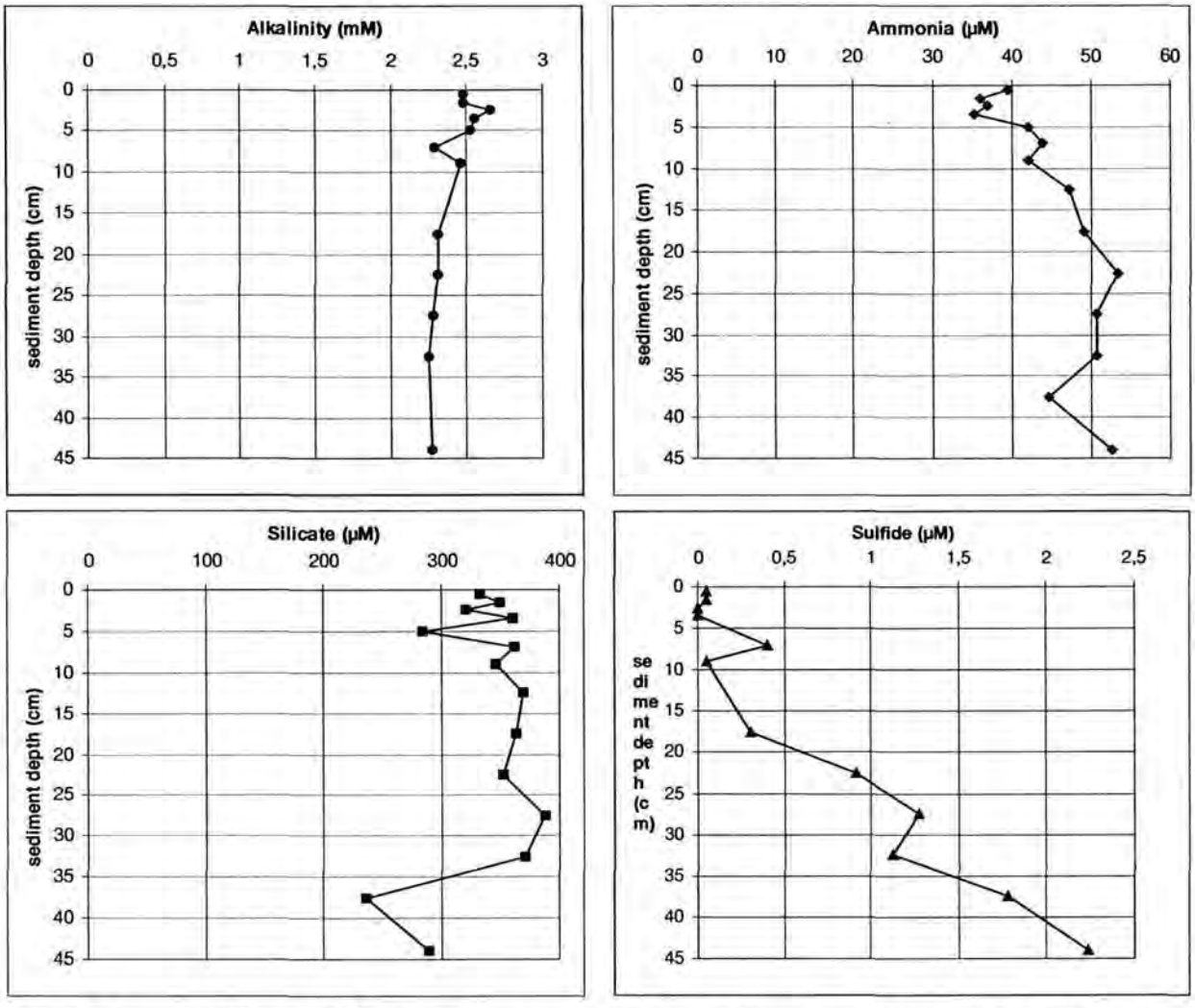

Fig. 7.13: TV Grab 33GA. Pore water profiles of alkalinity, ammonia, silicate and sulfide

Station: 44 GA
Position: 07° 57.45' S / 106° 17.71' E
Pushing the sub sample boxes into the sediment was quite difficult and only two boxes out of the same hatch were pressed for gaining pore water. Core 1 was orientated closer to the outer edge of the jaw while core 2 was more in the middle. Both boxes had the same distance of about 20 cm to an area with relatively more pogonophorans (about 15) at the outer edge of the jaw. The methane sample was taken from the hatch in the other jaw but at the same site, in a distance of about 1.3 m to the pore water boxes.
Methane by E. Faber: 17,616 ppb in the middle of the sediment at about 20-25 cm
Pore water characteristics:
With the 44 GA we sampled a vent field as clearly shown by the chemoautotrophic organism and the strong smell of sulfide. The sub core 1 is strongly influenced by sea water as can be seen in the silicate concentration which show clearly bottom water values up to a depth of 25 cm (Fig. 7.14).

Alkalinity was not measured

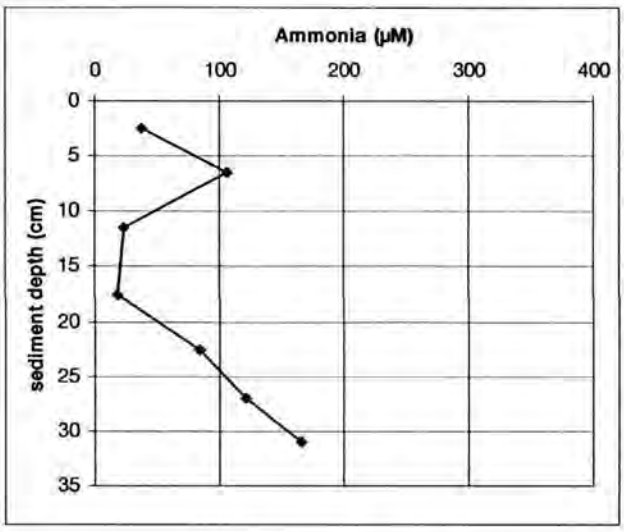

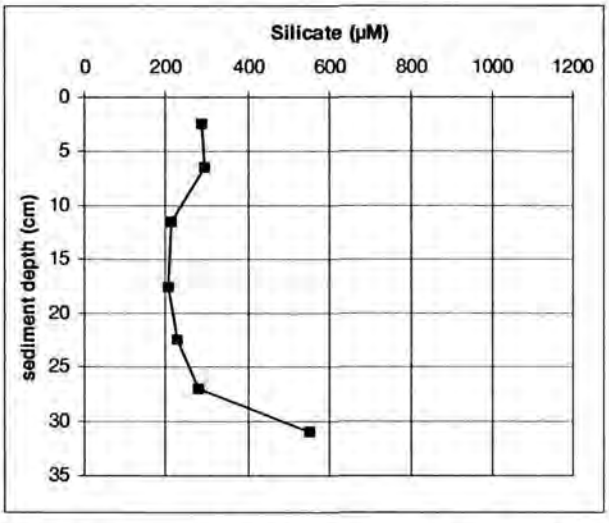

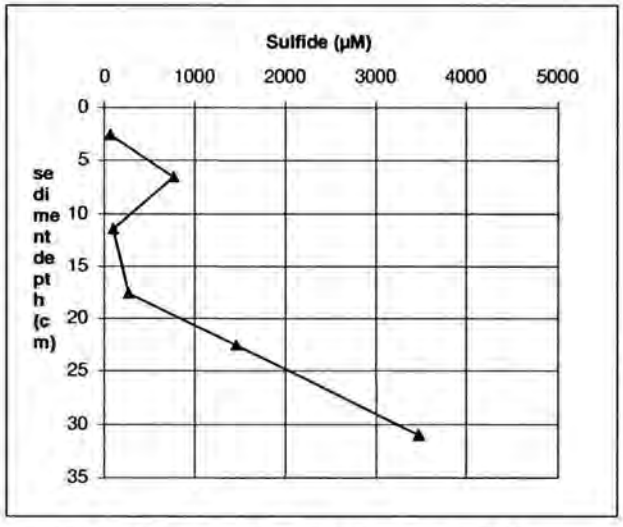

Fig. 7.14: TV Grab 44GA core 1. Pore water profiles of ammonia, silicate and sulfide

The core was taken close to the jaw in the grab below the hatch front opening and therefore a stronger mixing with sea water is reasonable.
The silicate concentration in core 2 increases significantly in a nearly linear way as does the salinity (compare Marchig-Chapter) indicating a nearly undisturbed pore water chemistry (Fig. 7.15). Ammonia increases with depth to a concentration up to 300 µM which is a factor 3 higher then in a normal diagenetic situation as found in 24 KL.

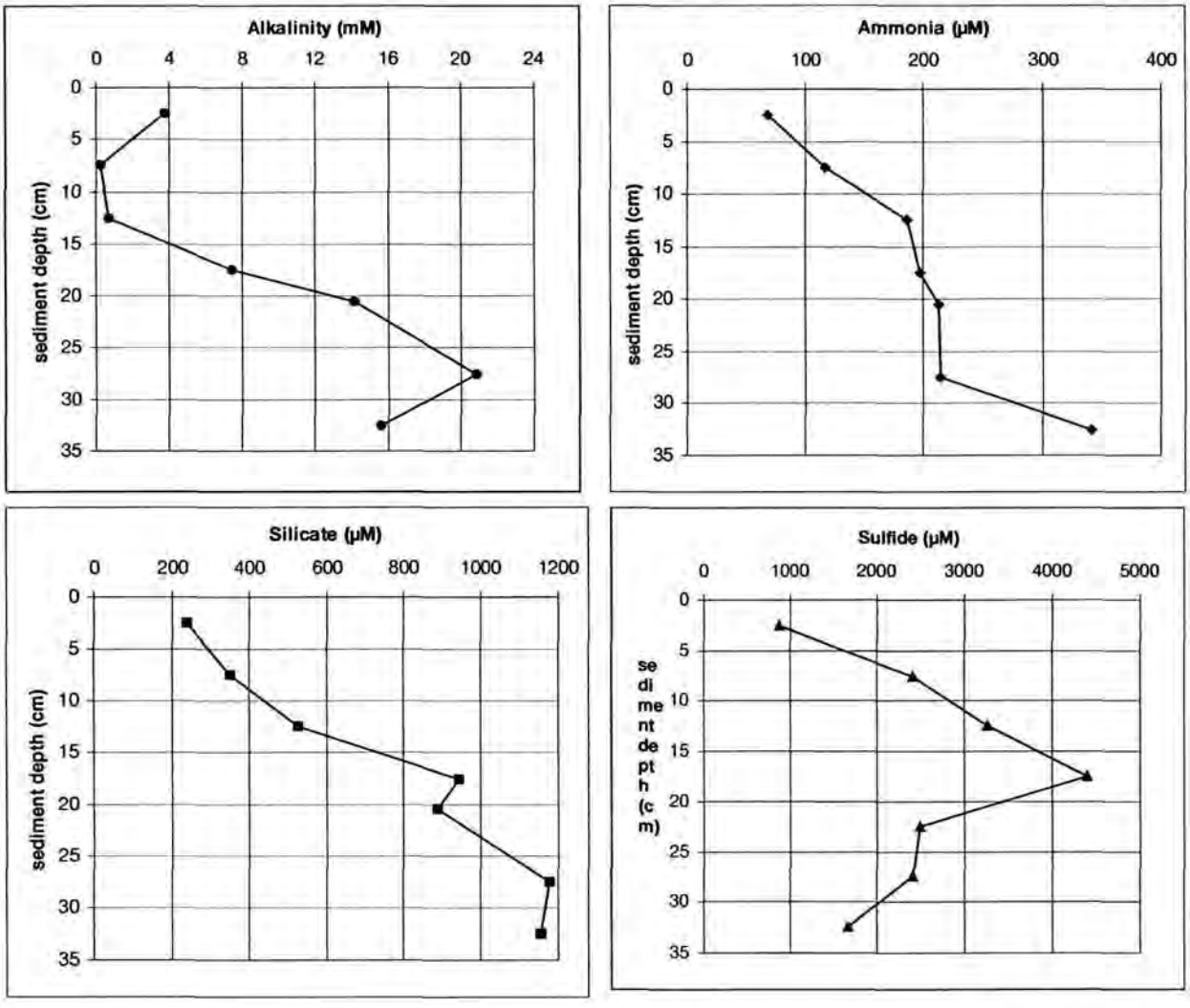

Fig. 7.15: TV Grab 44GA core 2. Pore water profiles of alkalinity, ammonia, silicate and sulfide

The alkalinity deeper than 15 cm increases to a maximum of 20 mM in 27 cm sediment depth, which is 10 cm deeper than the sulfide maximum with over 4 mM. If we take a significant increase in alkalinity as a first approximation for the amount methane oxidised, the zone of methane oxidation is reached in this shallow grab. Unfortunately, we have only measured one methane concentration and not a depth profile. The ratio between the alkalinity and ammonia reflects the C to N ratios and shows with values of 13 in 24 KL a typical redfield based diagenesis of organic matter, while C:N ratios of over 70 in 44 GA indicate a significant amount of oxidised methane in the fluids.

Station: 91 GA
Position: 07° 57.40' S / 106° 17.90' E
Two cores were squeezed: core 1 was sampled next to the location where methane was measured. Core 2 was approx. 50 cm apart of core 1. Albeit the jaws of the grab were partly closed at the beginning of the deployment the grab was completely full. Pogonophorans were present at the surface and three *Acharax* species were found in the grab.
Pore water characteristics:
In grab 91 GA the highest sulfide concentrations of the cruise were detected (Fig.7.16). These high values of 11 mM (11,000 µM) were found in the upper core at 5 cm. Propagating deeper in the sediment a decline down to 2 mM were measured at 45 cm. The alkalinity shows a different slope, low values of 4 mM at the sediment surface rise very moderate up

to 8 mM at 35 cm. The sharp decrease at 37 cm is supposed to a mistake in analytical procedure and therefore not realistic. The ammonia concentrations were too low for the photometic method. This fact is unusual, high sulfide concentrations are normally linked to high ammonia levels. Probably the nitrogen supply in this sediment area are very low. The C_{org} measurements will elucidate the content of organic matter in this sediment area.

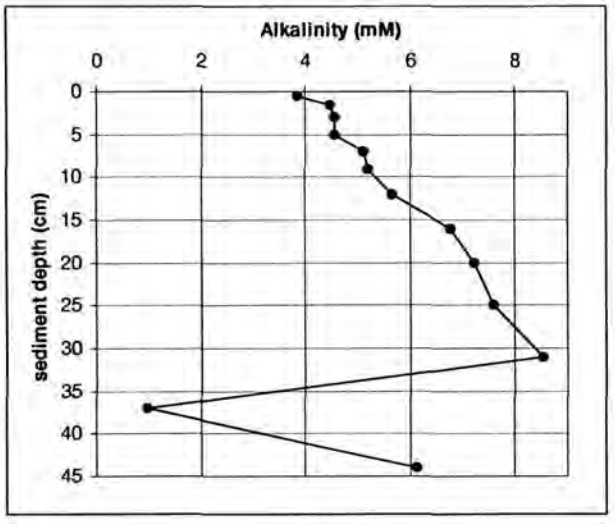

Ammonia: below detection limit of 20 µM

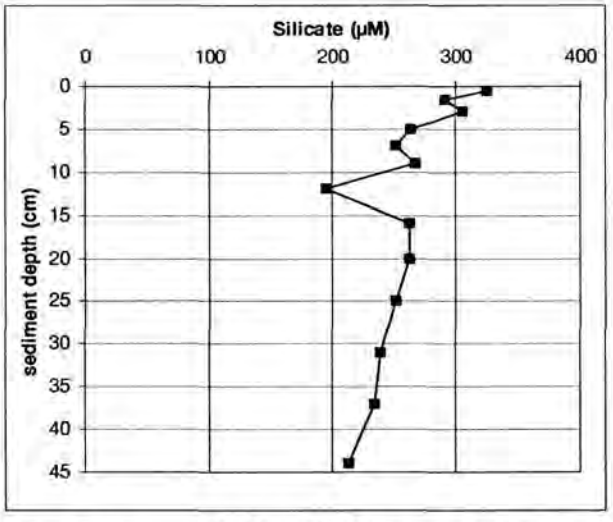

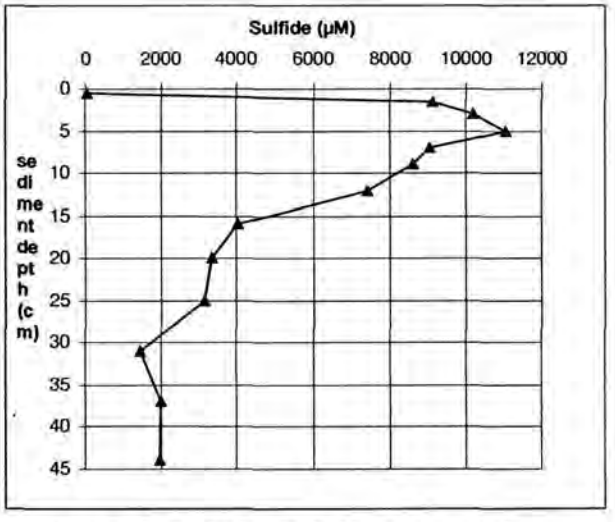

Fig. 7.16: TV Grab 91GA core 1. Pore water profiles of alkalinity, silicate and sulfide.

Core 2 was only 50 cm apart of the first core and the C_{org} content seems to be as low as in the first core in respect to the absence of ammonia (Fig.7.17). The alkalinity and silicate profiles are comparable to the first core. Only the sulfide shows different concentrations. The sharp increase in the uppermost sediment to a mM level is absent. The concentration of sulfide in core no. 2 increases to a level of 300 µM. Deeper in the sediment the sulfide content varies but no decline was detected like in the first one.
Comparing the two cores shows the heterogeneity of seeping areas. The first core probably hit the focused outflow and the second core was sampled in the vicinity influenced by diffusive horizontal transport processes in the sediment.

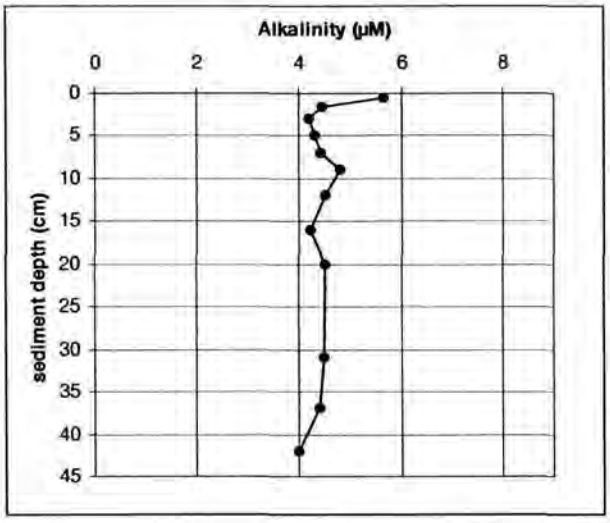

Ammonia: below detection limit of 20 µM

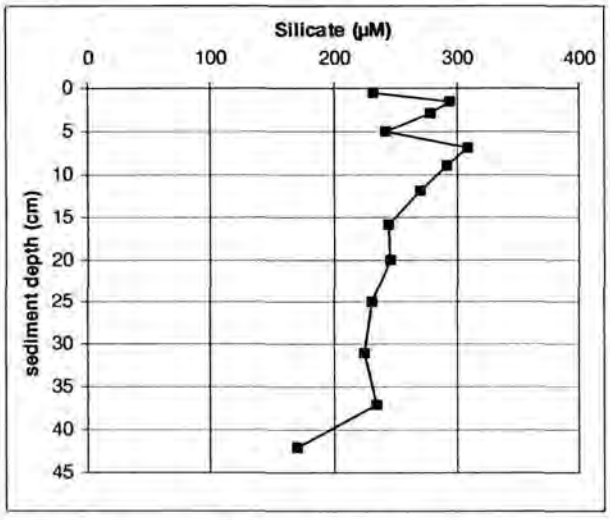

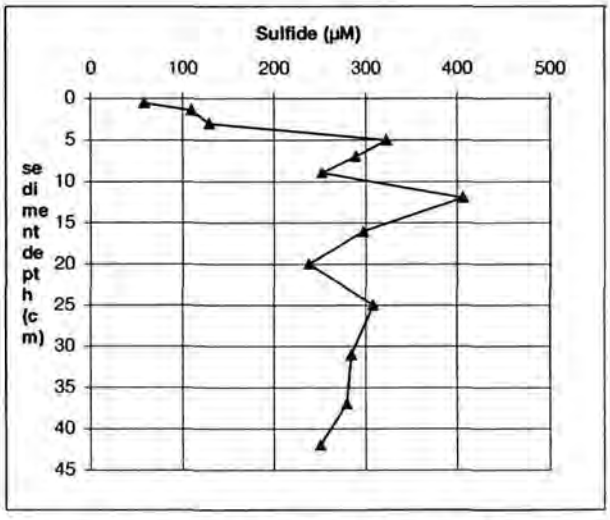

Fig. 7.17: TV Grab 91GA core 2. Pore water profiles of alkalinity, silicate and sulfide.

Station: 92GA
Position: 07° 57.45' S / 106° 17.81' E
Methane: by E. Faber
No pore water was squeezed because of oblique penetration of grab into the sediment. Therefore the grab was only partly filled.

Station 93GA
Position: 07° 57.44' S / 106° 17.59' E
Methane by E. Faber
No macro fauna only some shells on the sediment surface very sticky sediment (see chapter 6.2)
Pore water characteristics:
Despite no macro fauna this core shows similar results with the cores from station 91 GA. The alkalinity varies between 4 and 5.5 mM (Fig. 7.18), ammonia was not detectable and the amount and variation of silicate concentration are typical for pore water chemistry. Again the sulfide concentration deviates. Moderate concentrations at the surface rise over 1 mM at 15 cm sediment depth following by a decline to sediment water interface values from around 500 µM.

This general pattern was noticed also at the other TV grab stations and can be explained by sulfate reduction going on in these sediment depth. This reduction is coupled with methane oxidation.

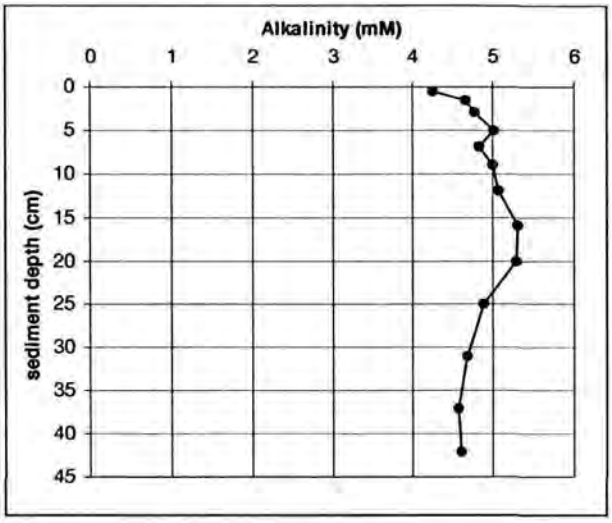

Ammonia: below detection limit of 20 µM

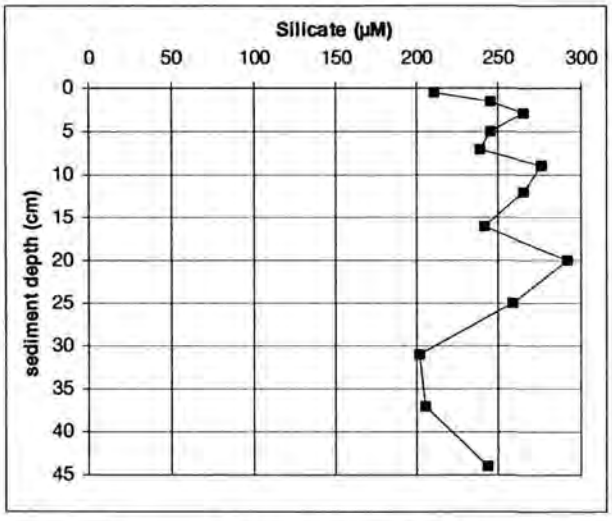

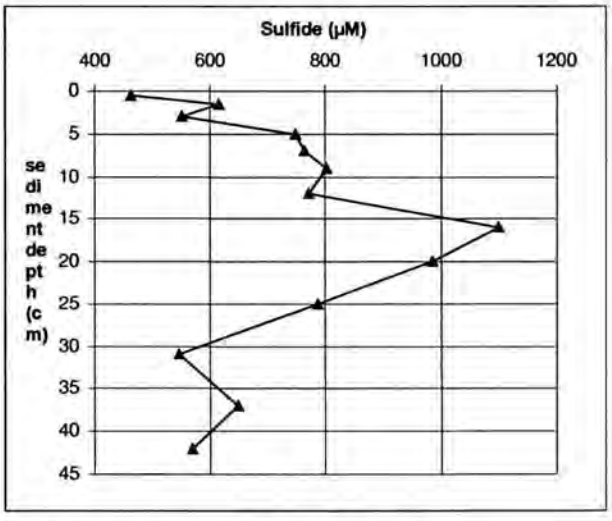

Fig. 7.18: TV Grab 93GA. Pore water profiles of alkalinity, silicate and sulfide.

REFERENCES

GRASSHOFF, K., EHRHARDT, M., and KREMLING K., 1983: Methods of seawater analysis, VCH, Weinheim.

STUMM, W., and MORGAN J.J., 1996: Aquatic Chemistry, Wiley, New York

7.5 Gas concentrations in sediments

E. Faber, J. Poggenburg, and W. Stahl

7.5.1 Methods

Sediment samples were degassed aboard according to the technique described by FABER and STAHL (1983). About 100 to 150 g of wet sediments were heated in a vacuum apparatus up to more than 90°C while phosphoric acid was added to the stirred sample. The carbon dioxide liberated was fixed in a KOH-solution. Methane through butane were measured injecting 1 ml of the extracted gas into a gas chromatograph (Shimadzu Mini 3 equipped with a FID and a 2 m x 1/8"column packed with Porapaq Q) running a temperature program. Concentrations of hydrocarbons are given in nano (10^{-9}) gram hc per gram of wet sediment (ppbw).

The large fraction of the sediment gases not used for analysis aboard were stored in evacuated glass vessels. Stable carbon isotope ratios on the hydrocarbons and on the carbon dioxide will be determined in the laboratory at the BGR in Hannover for gas genetic interpretations.

7.5.2 Results

According to the degassing procedure described above, total or combined gases (FABER et al., 1997) are extracted from the sediment samples. These gases should contain both, bacterial and thermal gases. The bacterial gases can be generated by methanogenesis from the organic precursors if present in sufficient quantity, and if oxygen and sulfate in the sediment is depleted. Thermal gases (methane, heavier hydrocarbons) originate from mature organic sediments which are dependent on the local geothermal gradient generally found in the depth of some hundreds to thousands of meters. In the shallow sediments they are present only after migration into the surface. However, as heavier hydrocarbons are found only in background concentrations in most of the samples, the existence of a source rock in the survey areas, which is in the maturity stage of the oil window, is highly unlikely. Therefore the methane found is of bacterial origin or comes from a deep overcooked source rock. The $^{13}C/^{12}C$-data of methane (to be measured) will show the genetic origin of the methane.

Fig. 7.19 shows the methane concentrations for stations in the survey area aligned along the seismic line SO-137–03. Down to 12 m methane concentrations are below 100 ppbw, most of these samples have methane contents of less than ca. 50 ppbw, which is considered to represent background values. The deepest samples from cores 14 KI and 15 KL have methane concentrations higher than 800 ppbw. This increase of methane with depth is related to methanogenesis due to sulfate depletion at sediment depth below ca. 12 m. Again, the bacterial origin of the methane has to be shown by isotope analysis. Due to the sediment type along seismic line SO-137–03 the maximum core length is restricted to about 13.20 m – methane concentrations in the deeper sediment sections are not known. However, as the concentrations at 13.20 m is not higher than ca. 12000 ppbw and is the lowest of the three areas sampled, the relative low methane in the sediment mirrors the low methane concentrations in the water samples in this area.

Methane data in the survey area of seismic line SO-137–01 is shown in Fig. 7.20. For the piston cores (KL) the concentrations are low down to ca. 8 m. Below this depth there is a sharp increase, at least for stations 24 KL and 37 KL. At ca. 8.5 m data stabilises and below is more or less constant down to the final depth. As sulfate is exhausted below the depth of 8 m bacterial methane formation is most likely and explains the high methane concentrations. This holds true also for stations 21 KL, 31 KL and 34 KL. The depth trends

of the methane concentrations of stations 24 KL and 37 KL look like textbook-trends for methanogenesis in sediments.

In the "Snails and Mussels Hill" survey area (bacterial) methane concentrations in the surface sediments are high, as are the methane values in the bottom near water layers in this area. Methane escaping from the sediments most likely explains this situation. At the stations 43 GA/TVG and 44 GA/TVG high methane concentrations (>17000 ppbw) were found in the grab samples, where sediments were taken from very shallow depth (< 1 m). These grab samplers where located very close, if not at active vent locations, otherwise the high values at the sediment surface could not be explained. When grab sampler 44 GA/TVD was launched aboard, a gas sample was taken using a syringe and extracting gas from the very surface of the grab's sediment. The methane concentration in this "air"-sample was 50 ppmv (Table 7.2, 44 GA H), which is by about 30 times the atmospheric methane concentration. It shows that, although the grab was heaved to the water surface and part of the methane may have been lost, the large quantity of methane extracted from the grab's sediment does confirm the active vent situation.

The results of the survey area of seismic line SO-137–06 are shown in Fig. 7.21. The situation is similar to area of seismic line SO-137–01: There are low methane concentrations in the surface sediments, including the grab samples 91 to 93 GA/TVG. Below 12 m the concentrations increase and stabilise between 13 and 14 m with values around 10000 ppbw. Maximum concentrations are around 30000 ppbw. The methane concentrations are as high, but found 4 m deeper as in the area of line SO-137–01. At active vent sites this methane can be transported to the sediment surface, and, expelled into the water, can explain the high methane values in the in area SO 137 – 06 at and below 1600 m water depth.

Finally, it should be mentioned that although the methane concentrations in the sediments are high concentrations are not high enough for methane hydrate formation and hydrates have not been observed in the cores. It has to be admitted that during recovery of the samples aboard and core treatment unknown quantities of methane may have been lost.

REFERENCES

FABER, E. and STAHL, W.J., 1983: Analytical procedure and results of an isotope geochemical surface survey in an area of the British North Sea. - Petrol. Geochem. and Expl. of Europe. Geol. Soc. London Spec. Publ, Blackwell (ed: Brooks J), 51-63.

FABER, E., BERNER, U., HOLLERBACH, A., and GERLING, P., 1997: Isotope geochemistry in surface exploration for hydrocarbons. - Geol. Jb. D103, 103-127.

FABER, E., BOTZ, R., POGGENBURG, J., SCHMIDT, M., STOFFERS, P., and HARTMANN, M., 1998: Methane in Red Sea brines. - Organic Geochemistry Vol. 29, 1-3, 363-379.

SCHMITT, M., FABER, E., BOTZ R., and STOFFERS, P., 1991:Extraction of methane from seawater using ultrasonic vacuum degassing. - Anal. Chemistry 63, 5, 529-532.

Table 7.2: Hydrocarbon compositions and –concentrations in the sediment samples taken with piston corer, gravity corer and grab sampler

Station	Teufe m	GC No.	CH4 %	C2H4 %	C2H6 %	C3H6 %	C3H8 %	CH4 ppb	C2H4 ppb	C2H6 ppb	C3H6 ppb	C3H8 ppb
3KL	3.00	008D	97.74	0.30	1.09	0.59	0.27	18	0	0	0	0
3KL	5.50	012D	96.53	0.52	2.34	0.00	0.60	32	0	1	0	1
4KL	0.00	013D	96.93	0.99	2.08	0.00	0.00	28	0	1	0	0
6KL	5.55	007E	94.21	0.00	5.79	0.00	0.00	13	0	2	0	0
6KL	5.85	004E	90.47	0.00	6.86	0.00	2.68	16	0	2	0	1
6KL	6.85	003E	97.68	0.00	2.32	0.00	0.00	14	0	1	0	0
7TVG	0.30	006E	80.48	2.37	12.12	5.04	0.00	6	0	2	1	0
10KL	12.35	008E	91.00	0.00	6.52	0.00	2.48	12	0	2	0	1
11KL	2.25	011E	88.29	0.90	7.97	0.00	2.84	7	0	1	0	1
11KL	7.15	010E	96.70	0.42	2.88	0.00	0.00	15	0	1	0	0
11KL	12.15	009E	98.23	0.00	1.33	0.00	0.44	32	0	1	0	0
14KL	5.19	016E	92.57	0.00	5.17	0.00	2.26	9	0	1	0	1
14KL	10.19	015E	99.48	0.00	0.39	0.00	0.12	93	0	1	0	0
14KL	13.19	012E	99.92	0.00	0.06	0.00	0.02	21290	2	0	1	
14KL	13.19	013E	99.98	0.00	0.01	0.00	0.00	10615	0	2	0	1
14KL	13.19	014E	99.99	0.00	0.01	0.00	0.00	11948	0	2	0	1
15KL	5.48	021E	98.67	0.00	1.21	0.00	0.12	98	0	2	0	0
15KL	5.48	022E	98.77	0.00	1.23	0.00	0.00	92	0	2	0	0
15KL	12.48	020E	98.88	0.00	1.05	0.00	0.07	879	0	17	0	2
18KI	11.85	023E	100.00	0.00	0.00	0.00	0.00	8	0	0	0	0
21KL	11.35	024E	100.00	0.00	0.00	0.00	0.00	22251	0	1	0	1
21KL	11.85	025E	99.99	0.00	0.01	0.00	0.00	7387	0	1	0	0
	0.00											
24KL	1.00	031E	94.60	0.00	4.14	0.00	1.26	10	0	1	0	0
24KL	3.00	030E	96.67	0.00	2.45	0.00	0.87	20	0	1	0	1
24KL	4.00	033E	97.20	0.00	2.02	0.00	0.77	57	0	2	0	1
24KL	6.00	029E	99.42	0.00	0.42	0.00	0.16	127	0	1	0	1
24KL	7.00	034E	94.73	0.00	3.77	0.00	1.50	97	0	7	0	4
24KL	8.00	028E	99.98	0.00	0.01	0.00	0.00	4942	0	1	0	1
24KL	9.00	032E	99.99	0.00	0.01	0.00	0.00	15457	0	2	0	1
24KL	11.00	027E	99.99	0.00	0.00	0.00	0.00	22937	0	2	0	1
24KL	12.50	026E	100.00	0.00	0.00	0.00	0.00	30446	0	2	0	1
29KL	12.62	035E	95.70	0.00	3.17	0.00	1.13	91	0	6	0	3
31KL	11.50	036E	100.00	0.00	0.00	0.00	0.00	14035	0	0	0	0
33GA	0.01	003F	99.86	0.00	0.14	0.00	0.00	321	0	1	0	0
34KL	18.10	004F	99.93	0.00	0.05	0.00	0.02	7358	0	7	0	4
34KL	17.60	005F	100.00	0.00	0.00	0.00	0.00	4178	0	0	0	0

Table 7.2, Page 2

Station	Teufe m	GC No.	CH4 %	C2H4 %	C2H6 %	C3H6 %	C3H8 %	CH4 ppb	C2H4 ppb	C2H6 ppb	C3H6 ppb	C3H8 ppb	
37KL	1.20	042F	99.36	0.00	0.46	0.00	0.18	160	0	1	0	1	
37KL	5.20	020F	96.55	0.00	2.46	0.00	0.99	44	0	2	0	1	
37KI	7.20	022F	99.49	0.00	0.38	0.00	0.12	125	0	1	0	0	
37KL	8.20	018F	99.69	0.00	0.22	0.00	0.09	1267	0	5	0	3	
37KL	9.20	021F	99.98	0.00	0.01	0.00	0.01	8292	0	2	0	2	
37KL	10.20	017F	99.99	0.00	0.00	0.00	0.00	16136	0	1	0	1	
37KL	11.20	016F	99.99	0.00	0.00	0.00	0.00	16214	0	1	0	1	
37KL	13.20	014F	100.00	0.00	0.00	0.00	0.00	15469	0	1	0	1	
37KL	15.20	012F	99.99	0.00	0.01	0.00	0.00	14888	0	2	0	1	
37KL	17.20	007F	99.99	0.00	0.01	0.00	0.00	15868	0	2	0	1	
37KL	18.20	023F	99.98	0.00	0.01	0.00	0.01	8400	0	1	0	1	
37KL	18.20	026F	99.99	0.00	0.01	0.00	0.00	11140	0	1	0	1	
37KL	18.70	006F	100.00	0.00	0.00	0.00	0.00	31264	0	1	0	1	
42KL	17.20	025F	99.62	0.00	0.29	0.00	0.09	466	0	3	0	1	
43GA	0.50	027F	99.88	0.00	0.12	0.00	0.00	19532	0	43	0	1	
44GA	0.50	028F	99.58	0.00	0.42	0.00	0.00	17616	0	139	0	1	
44GA Headspace				100.00	0.00	0.00	0.00	0.00	50	0	0	0	0
50KL	12.15	029F	99.98	0.00	0.01	0.00	0.00	18914	0	4	0	2	
50KL-Pressling	12.15	030F	99.96	0.00	0.03	0.00	0.01	3920	0	2	0	1	
54KL	17.26	031F	99.96	0.00	0.04	0.00	0.00	24816	0	18	0	0	
58KL	1.27	037F	95.50	0.94	2.62	0.00	0.93	9	0	0	0	0	
58KL	8.25	035F	95.51	0.00	3.52	0.00	0.97	19	0	1	0	1	
58KL	11.30	034F	94.58	0.00	4.51	0.00	0.91	46	0	4	0	1	
58KL	12.30	039F	98.89	0.00	0.95	0.00	0.16	410	0	7	0	2	
58KL	13.30	041F	99.91	0.00	0.08	0.00	0.01	5123	0	8	0	2	
58KL	14.30	033F	99.93	0.00	0.05	0.00	0.01	10661	0	11	0	4	
58KL	15.27	038F	99.95	0.00	0.04	0.00	0.01	10484	0	9	0	3	
58KL	16.30	040F	99.89	0.00	0.08	0.00	0.03	6125	0	9	0	5	
58KL	16.80	032F	99.96	0.00	0.03	0.00	0.00	35872	0	23	0	5	
59KL	17.40	036F	99.75	0.00	0.10	0.00	0.15	1731	0	3	0	7	
74KL	2.75	053F	96.16	1.25	2.60	0.00	0.00	13	0	1	0	0	
74KL	8.75	054F	83.00	0.43	3.33	0.52	12.72	18	0	1	0	8	
74KL	12.75	051F	98.56	0.00	1.21	0.00	0.23	208	0	5	0	1	
74KL	15.75	050F	99.94	0.00	0.05	0.00	0.01	6800	0	7	0	2	
74KL	17.75	049F	99.93	0.00	0.05	0.00	0.02	8822	0	9	0	4	
74KL	18.75	052F	99.89	0.00	0.08	0.00	0.03	4050	0	6	0	3	
74KL	19.30	046F	99.96	0.00	0.03	0.00	0.01	37794	0	21	0	5	

Table 7.2, Page 3

Station	Teufe m	GC No.	CH4 %	C2H4 %	C2H6 %	C3H6 %	C3H8 %	CH4 ppb	C2H4 ppb	C2H6 ppb	C3H6 ppb	C3H8 ppb
83SL	2.20	055F	85.67	1.35	6.75	3.65	2.58	11	0	2	1	1
88SL	4.10	056F	92.05	0.65	5.12	1.04	1.14	11	0	1	0	0
88SL	2.60	057F	95.75	0.19	3.04	0.00	1.01	52	0	3	0	1
91GA	0.30	058F	96.98	0.23	1.63	0.91	0.25	44	0	1	1	0
91GA	0.10	059F	97.49	0.22	1.63	0.00	0.67	43	0	1	0	1
92GA	0.15	060F	97.26	0.30	1.71	0.00	0.73	24	0	1	0	0
93GA	0.40	061F	97.10	0.40	1.58	0.36	0.56	36	0	1	0	1
98KL	0.44	062F	90.54	0.62	3.57	3.59	1.67	6	0	0	1	0

Fig. 7.19: Methane concentration in sediment samples plotted versus sediment depth from stations 3 KL, 4 KL, 6 KL, 7 GA, 10 KL, 11 KL, 14 KL, 15 KL and 18 KL aligned around seismic line SO 137-03

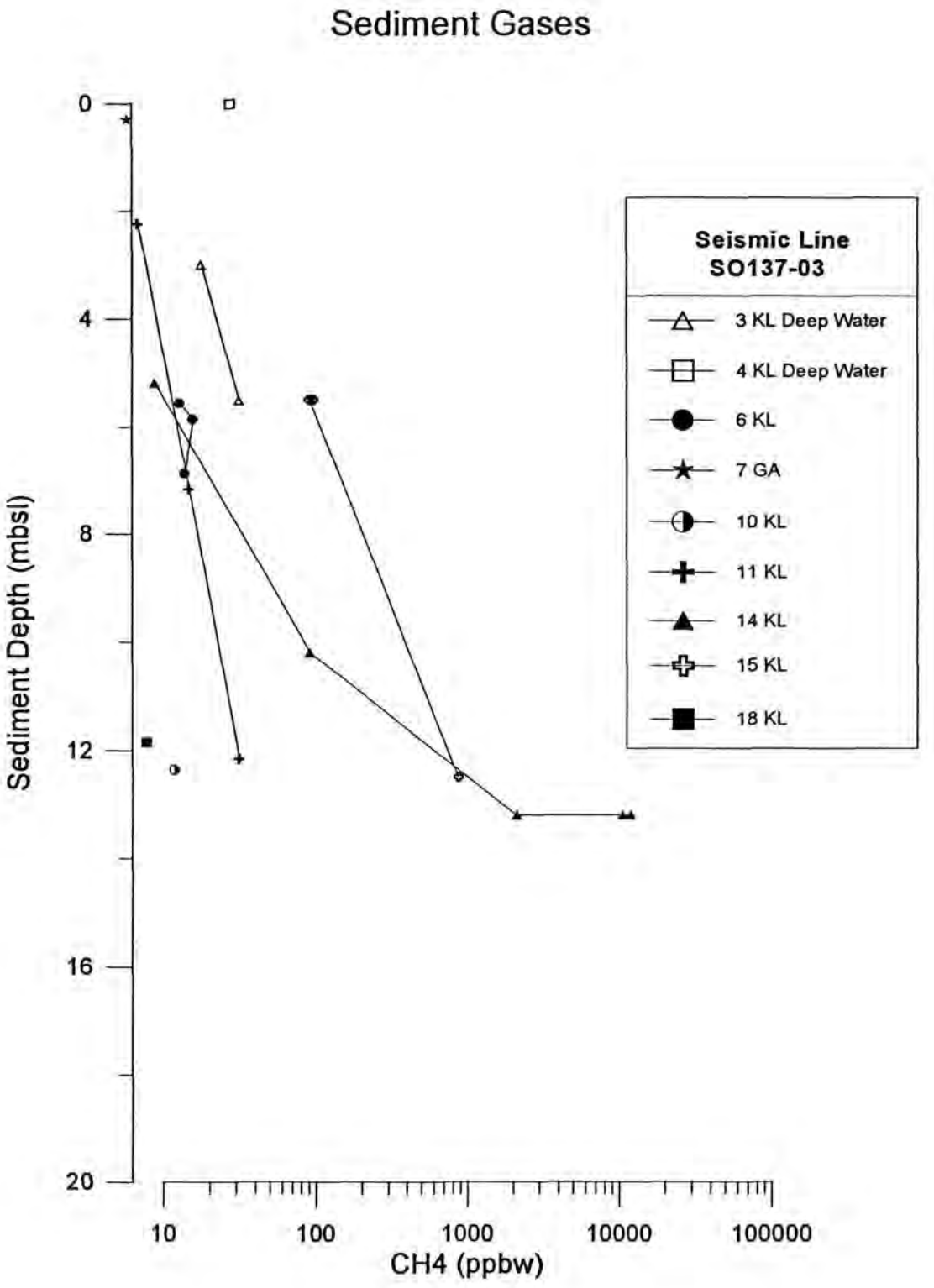

Fig. 7.20: Methane concentration in sediment samples plotted versus sediment depth from stations 21 KL, 24 KL, 29 KL, 31 GA, 33 GA/TVG, 34 KL, 37 KL, 42 KL, 43 GA/TVG and 44GA/TVG KL aligned around seismic line SO 137-01

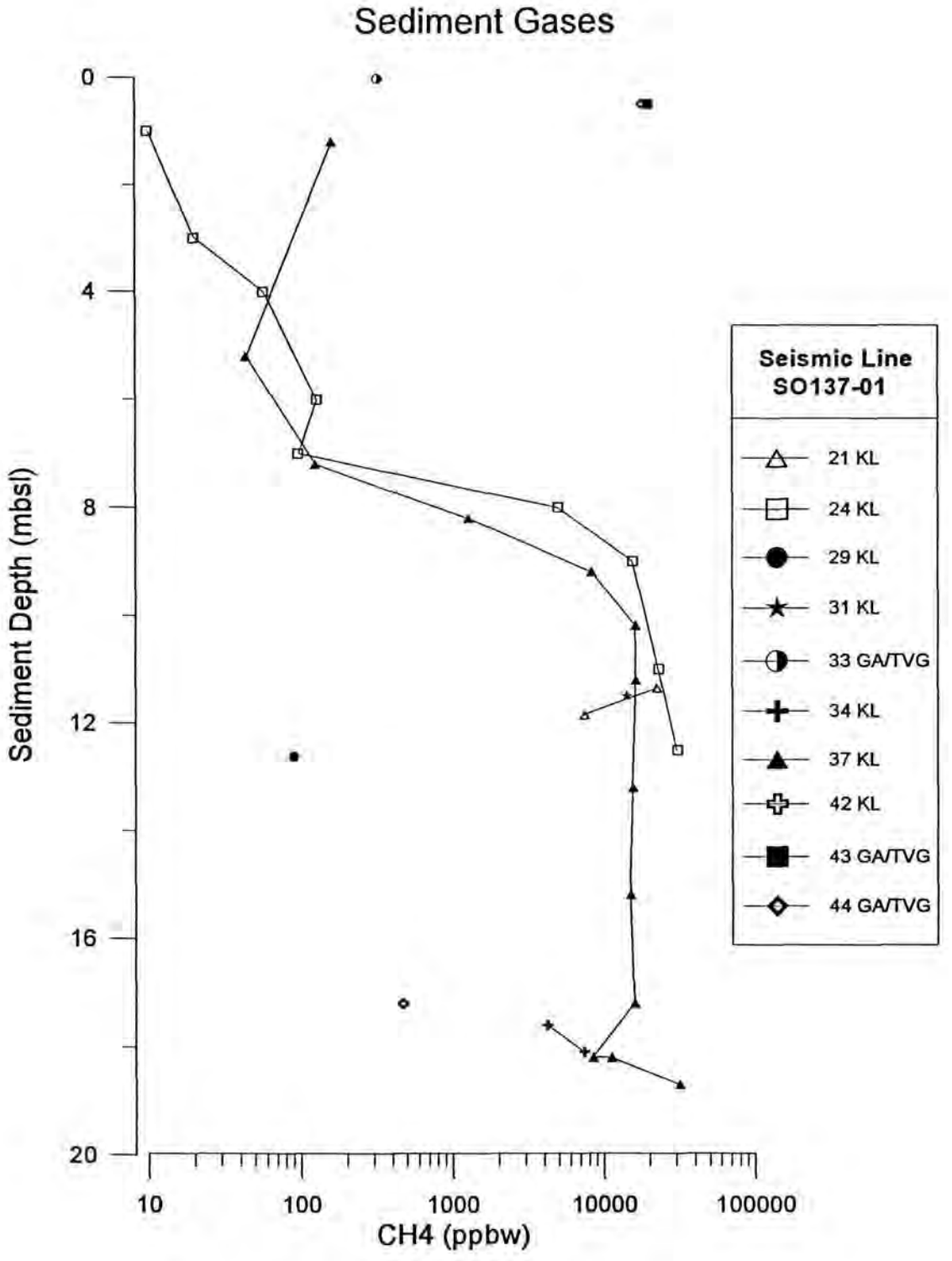

Fig. 7.21: Methane concentration in sediment samples plotted versus sediment depth from stations 50 KL, 54 KL, 58 KL, 59 KL, 74 KL, 83 SL, 88 SL, 91 GA/TVG, 92 GA/TVG and 93GA/TVG KL aligned around seismic line SO 137-06

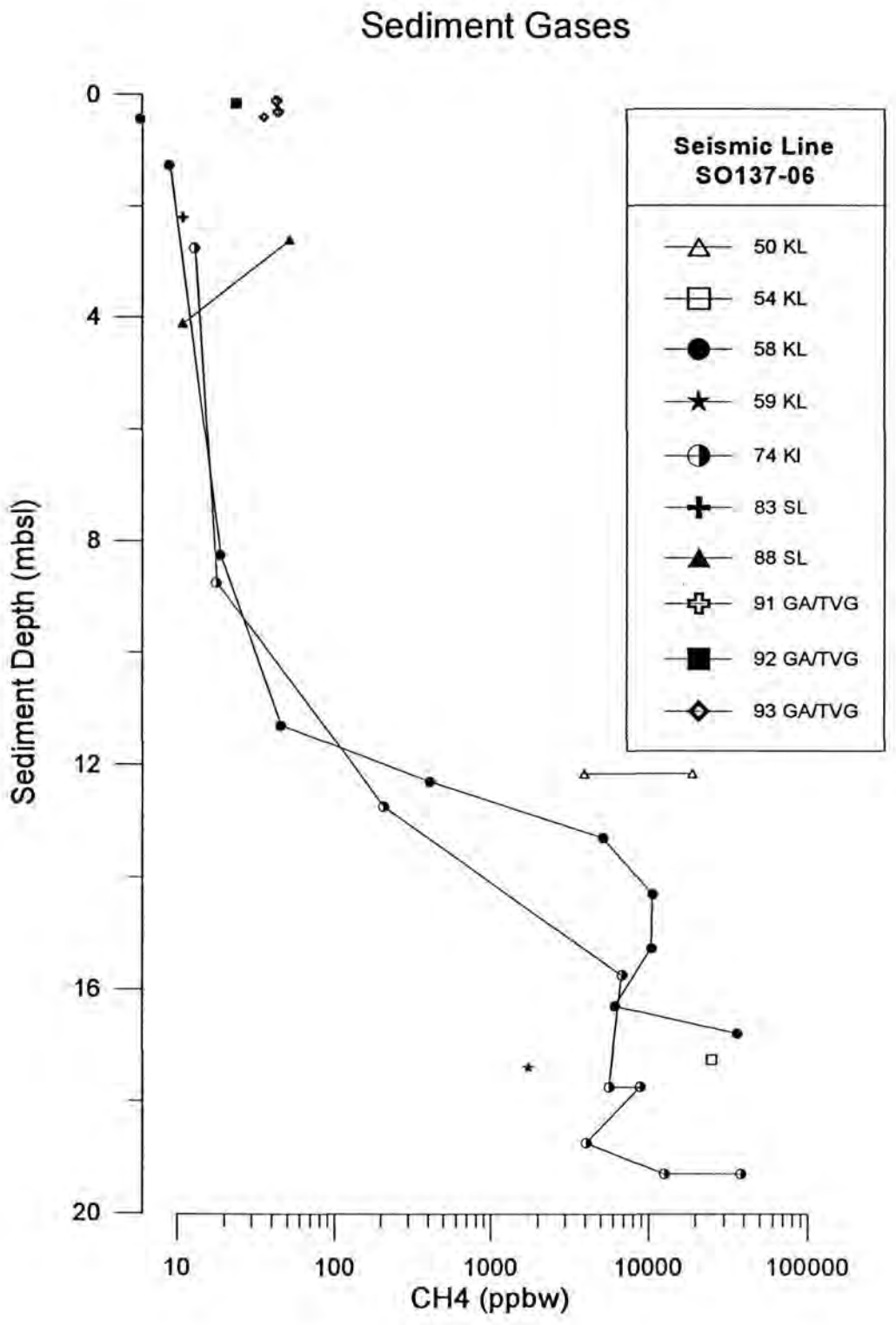

8. Conclusions

H. Beiersdorf

Cruise SO-139 has achieved its main goals, namely the calibration of a number of reflection seismic features and the detection of methane-laden fluid seeps in the forearc realm.

Methane anomalies, fluid venting and vent-related biota

Faint methane anomalies in the water column were located at the deformation front off southern Sumatra as well as off West Java. Although no active vent field was discovered, this observation suggests that venting may occur in this environment.

The low heat flow in the accretionary complex (see below) may be an indication of little heat transport by fluids migrating upwards along thrust faults. This is supported by the lack of significant methane concentrations in the sediment cover of the complex. The exceptionally increased methane concentration in one of the intra-slope basins may indicate in-situ methane generation within the basin fill.

The only active vent site in the survey area was discovered at the eastern termination of the large anticline structure ("Snails and Mussels Hill") in the South Java Basin. It is the first of its kind found in a forearc basin without volcanic activity, and the second vent site reported from the Indian Ocean. The venting is indicated by a typical fauna (i.e. clams, pogonophora) and authigenic precipitates.

Methane concentrations of surface sediments at the vent site are generally high, obviously caused by upward-migrating methane-laden fluids. The "methane profile" of piston cores in the immediate vicinity of the vent site shows concentrations below 1000 ppbw in the upper 8 m. Significantly higher concentrations up to around 10 000 ppbw are observed below this depth. In the South Java Basin away from the vent site the level of increased methane concentrations is lowered to 12 to 14 m. The same observation was made in cores from the Bengkulu Basin. the deviation of the methane concentration curve near the vent site from the other curves may be due to an intensified lateral methane supply to the sediments from the vents. The methane concentrations measured are too low for a formation of gas hydrates in the sediments for which the analyses were carried out.

An interesting observation was the correlation of high methane concentrations in the water column with layers of constant water temperatures. In future vent exploration this may be used for locating vent areas without time-consuming analyses of water samples for methane concentrations.

The finding of a specimen of *Vestimentifera sp.* in sediments from the offshore extension of the Semangka Graben in conjunction with the high heat flow (see below) may be an indication for active vents in the graben, perhaps associated with faults providing conduits for methane laden fluids from methane generating levels.

Calibration of reflection seismic features

The lithologies of rocks recovered from the accretionary complex suggest that the complex is build up mainly by mudstone which has suffered tectonic stress resulting in cleavage and fracturing followed by a vein-filling mineralisation. The origin of the mudstone is predominantly hemipelagic. However, some input from the Ganges-Brahmaputra fluviatile sediment shedding into the Sunda Trench cannot be ruled out at least for the youngest thrust sheet.

To a great extent the accretionary complex is thinly covered by hemipelagic sediments which reach thicker accumulations in small intra-slope basins only. The uppermost meters of the sedimentary sequences are represented by olive gray Pliocene/Pleistocene muds. Intercalated turbiditic layers hint at sporadic sediment shedding most likely caused by mobilisation of older sediment when thrust blocks underwent tectonic motions, i.e. uplift in particular. Frequent intercalated volcanic ash layers are reflecting volcanic eruption phases of the neighbouring Sunda Arc.

Some Pliocene parts of the sediment blanket of the accretionary wedge were slightly indurated by compaction, as can be judged from samples dredged at the South Java (forearc) Ridge.

The same olive gray muds as found in the sediment cover of the accretionary complex were cored in the South Java and Bengkulu (forearc) basins. Turbiditic layers in these muds can be attributed either to sporadic sediment shedding from the forearc ridge following tectonic motions (see above), or they originated from sporadic sediment shedding from the slope of the Sunda Arc.

The large anticlinal structure which runs from seismic profile BGR137-01 in westerly directions, subdivides the fore arc basins into a northern and a southern sub-basin. Its eastern termination coincides with the onset of oblique subduction under West Java, hence may be caused by transpressive tectonic forces. Along the crest of the anticline vents expelling methane-laden fluids may be common, as active venting at the "Snails and Mussels Hill" as well as methane anomalies in the water column suggest (see above). Below the crest of the anticline the reflection seismic pattern indicates an intense disturbance of the layered basinal sedimentary sequence. This probably is due to the transpressive tectonic deformation. The disturbance of strata in turn may have created conduits for upward migrating fluids and formation of vents.

From bathymetric and reflection seismic records it became clear that the Semangka Graben, which is associated to the Central Sumatra Fault, extends into the forearc complex south of the Sunda Strait. Sampling at the walls of the graben revealed that at least the eastern wall is formed by continental rocks. At the southern wall, these rocks may be covered by young mud.

The forearc ridge northwest of Enggano is underlain by hardened calcareous sand and sandstone which are responsible for the acoustically "hard" seafloor reflections seen in the reflection seismic as well as in the PARASOUND records. The hard sediments were sampled with the gravity corer only. Dredging attempts within a narrow, several tens of meters deep valley following the ridge crest did not provide rocks, but high pulls at the dredging wire and finally a complete anchoring by the dredge suggest instead, that the seafloor is rugged and hard at least for much of the northern slope of the valley.

Heat flow across the Sunda Trench and the forearc complex

The heat flow of around 64 mW/m^2 measured in the sediment cover of the Indo-Australian Plate just in front of the Sunda Trench off southern Sumatra supports the plate tectonic model of the region which suggests that Cretaceous oceanic crust is arriving at the subduction zone.

Heat flow across the accretionary complexes off southern Sumatra and western Java varies between 35 and 64 mW/m^2. The accretionary wedge off Sumatra seems to be slightly cooler. This difference applies also to the forearc basins: The Bengkulu Basin (22 - 49 mW/m^2) is cooler than the South Java Basin (30 - 153 mW/m^2). The different heat flow regimes seem to be related to the difference between a higher subduction rate at the Java fore arc complex in comparison to that off southern Sumatra. In addition the low heat flow in the Bengkulu Basin is in agreement with the deep level of bottom simulating reflectors which are considered to be the expression of the lower boundary of gas hydrates.

The high heat flow (83 -104 mW/m^2) and the indication of fluid vents at the southward extension of the Semangka Graben may be related to active faults tapping a heat source (Krakatau magma chamber?) and a methane-generating zone within the graben fill.

ACKNOWLEDGEMENTS

We are grateful to the Government of the Republic of Indonesia for granting permission to work in Indonesia's Exclusive Economic Zone. We would like to thank BPP Teknologi (Agency for the Assessment and Application of Technology), Jakarta, especially Dr. Soesilo Indroyono (Head of the Natural Resources Division), Dipl.Ing. Basri Gani, and Cpt. Gustav Mueller for their effective assistance during the preparatory phase and during Cruise SO-139. Our special thanks go to Dr. H. Keune of the Embassy of the Federal Republic of Germany for his help around the SONNE port activities in conjunction with the TECHNOGERMA and in achieving the research licence. Captain Henning Papenhagen and his crew with stamina and energy helped tremendously to make the cruise a success. Therefore, our sincere thanks also go to them.

Cruise SO-139 was carried out with grant 03G0139A of the Bundesministerium für Bildung und Forschung (BMBF). This support is gratefully acknowledged. We also like to thank the Projektträger BEO for their effective processing this grant.

BUNDESANSTALT FÜR GEOWISSENSCHAFTEN UND ROHSTOFFE
Hannover, den 17. Juni 1999

Leiter der Abteilung Geophysik,
Meeres- und Polarforschung:

(Dr. B. Buttkus)
- Direktor und Professor -

Projektleiter:

(Prof. Dr. H. Beiersdorf)
- Direktor und Professor -

Bundesanstalt für Geowissenschaften und Rohstoffe
Hannover
Germany

According to the Implementation Arrangement
between the
Bundesanstalt für Geowissenschaften und Rohstoffe (BGR)
and the
Agency for the Assessment and Application of Technology (BPPT)/Jakarta
concerning

Geoscientific Investigations along the Convergence Zone between the Eastern Eurasian and Indo-Australian Plates off Indonesia

the following data and samples were left to

***Mr. Udrekh* of BPPT**

on the occasion of his disembarkation from RV SONNE in the port of Jakarta/Java on February 27, 1999:

1)Bathymetric maps
Area East 1:750 000 50m contour intervals
Area East 1:750 000 100m contour intervals
Area West 1:750 000 50m contour intervals
Area West 1:750 000 100m contour intervals
Forearc Ridge 1:100 000
Drifts 1:100 000
OFOS Track 30FS 1:20 000
OFOS Track 84FS 1:20 000
OFOS Track 89FS 1:20 000
OFOS Track 48FS 1:50 000
OFOS Track 57FS 1:50 000
OFOS Track 75FS 1:50 000
2) Samples
Split halves of all cores except for core 96KL which was not opened, and all cores which were completely used up by geochemists for gas and porewater analyses.
3) Draft Cruise Report SO139 with Cruise Timetable, List of Stations and HYDROSWEEP/PARASOUND Profiles, Station Map of Area West, Station Map of Area East, and Track Chart of all HYDROSWEEP/PARASOUND Profiles and Transits.
4) CD with all CTD Data and Data File for all maps mentioned above.

On board RV SONNE, February 20, 1999.

(Udrekh)

(Helmut Beiersdorf)
Chief Scientist Cruise SO139

Embassy of the Federal Republic of GERMANY

Jl. M.H. Thamrin 1
Jakarta 10310
Tel.: 390 1750
Fax: 390 1757
e-mail: Germany @rad.net.id

Press Release

Jakarta, 02.03.1999

Natural gas discovered south of Java

Natural gas in form of gas hydrates which contains considerable amounts of methane has been detected by the recent cruise of the German Research Vessel „Sonne" south of Java.

Gas hydrates are ice-like substances which are formed below the seafloor when temperatures are near freezing point and pressure equals the weight of three to four kilometers water above it. Gas hydrates are considered as one of the future energy resources.

The Federal Institute for Geosciences and Natural Resources BGR (Hannover, Germany) and BPP Teknologi (Jakarta, Indonesia) are jointly carrying out a research project aiming at studying the geological processes which are forming gas hydrates off Indonesia. Under the scope of this project the German research vessel SONNE (97.60 m long, 4 734 tons displacement), one of the largest of its kind in the world, has worked for three months at the continental margin south of Sumatra and Java. The most spectacular finding coming out of the work of Indonesian and German scientists on board is the discovery of gas hydrates in the so-called South Java Basin. The basin is a geological feature which was formed when two gigantic plates of earth crust, the Indo-Australian and the Eurasian plates, collided some tens of millions of years ago. The basin was filled with the remains of ancient micro-organisms and detritus eroded from nearby continents (e.g. Java).

About 100 km south of western Java, in a water depth of 2938 m they discovered an area where methane-laden fluids escape the seafloor. These methane vents have attracted a unique community of marine lifeforms. A TV-guided grab sampler recovered clams, snails and worms dwelling solely on methane and accompanying hydrogen sulfide. The sediment came up with the grab sampler showed not only a high concentration of methance but also a low salinity of water queezed out from the sediment.

It is not the first discovery of gas hydrates in Indonesia's EEZ. In 1994 BGR and BPPT have discovered a huge gas hydrate deposit of the North Arm of Sulawesi.

Results of the recent research cruise will be presented at a press conference which will be held on board of the SONNE on Tuesday, March 2, 1999 at Tanjung Priok Harbour.

Document Control Sheet

1. ISBN or ISSN	2. Type of Report Cruise Report

3a. Report Title
Geoscientific investigations at the active convergence zone between the Eastern Eurasian and Indo-Australian Plates off Indonesia

3b. Title of Publication

4a. Author(s) of the Report (Family Name, First Name(s)) Beiersdorf, H. and cruise participants	5. End of Project 31.12.2000
4b. Author(s) of the Publication (Family Name, First Name(s))	6. Publication Date June 1999
	7. Form of Publication
8. Performing Organization(s) (Name, Address) Bundesanstalt für Geowissenschaften und Rohstoffe Stilleweg 2 30655 Hannover Post Box 51 01 53 30631 Hannover Germany	9. Originator's Report No. Archive No.:118.878 10. Reference No. 03G 0139A 11a. No. of Pages Report 154 11b. No. of Pages Publication
13. Sponsoring Agency (Name, Address) Bundesministerium für Bildung und Forschung (BMBF) 53170 Bonn	12. No. of References 31 14. No. of Tables 12 15. No. of Figures 49

16. Supplementary Notes
Cruise Report of Research Cruise SO139 GINCO3 with RV SONNE (January 29 - March 04, 1999)

17. Presented at (Title, Place, Date)
Forschungszentrum Jülich, BEO, Rostock-Warnemünde

18. Abstract
Cruise SO139 GINCO3 investigated the accretionary complex at the Sunda arc off southern Sumatra and western Java; geological, geochemical, geothermal, and biological methods were applied (3000 km profiling with swath mapping and sediment echosounding systems; 101 sampling and probing stations). The accretionary complex (AC) consists of partially tectonised mudstones. The youngest thrust sheet showed silty mic-rich claystones and soft mud. From the thin sediment cover of the AC we sampled Pliocene/Pleistocene to recent muddy sediments with volcanic ash and turbiditic intercalations. Similar sequences were encountered in the forearc basin (FAB). Heat flow at the AC off Sumatra and Java is 35 - 64 mW/m^2. In the Bengkulu Basin (FAB) it ranges between 22 - 45 mW/m^2 and in the South Java Basin (FAB) between 30 - 153 mW/m^2. At the prolongation of the Semangka graben heat flow is 83 - 104 mW/m^2. At the northern graben shoulder we sampled rocks of continental provenance (Miocene claystone, greenstone, diabas, andesite, Quarzite). From the same structure we recovered Vestimentifer sp., a tubeworm specialised to vent areas. At a transversal fault (associated with a large anticline structure) within the FAB off Java we samples additional vent fauna (Acharax sp., pogonoferan tubeworms). These faunal elements are all indicative for methane venting and were found associated with carbonate slabs and methane anomalies in the overlying water column. The vent site also exhibited the highest heat flow (153mW/m^2). This vent site is the first one discovered in a forearc basin without known active volcanism. Additional methane anomalies were found at the southern margins of the forearc basin (at the foot of the steep slope to the outer arc high). These findings combined with the recording of bottom simulating reflectors argue for the existance of gas hydrates and active fluid migration in the forearc basin.

19. Keywords
Indonesia, accretionary complex, forearc basin, methane, cold seeps, vent fauna

20. Publisher	21. Price

Berichtsblatt

1. ISBN or ISSN	2. Berichtsart Fahrtbericht

3a. Titel des Berichts
Geowissenschaftliche Untersuchungen an der aktiven Konvergenzzone zwischen der ost-eurasischen und indisch-australischen Platte im Bereich Indonesiens

3b. Titel der Publikation

4a. Autoren des Berichts (Name, Vorname(n))
Beiersdorf, H. und Fahrtteilnehmer

4b. Autoren der Publikation (Name, Vorname(n))

5. Abschlußdatum des Vorhabens
31.12.2000

6. Veröffentlichungsdatum
Juni 1999

7. Form der Publikation

8. Durchführende Institution(en) (Name, Adresse)

Bundesanstalt für Geowissenschaften und Rohstoffe
Stilleweg 2
30655 Hannover

Postfach 51 01 53
30631 Hannover

9. Ber.Nr. Durchführende Institution
118.878

10. Förderkennzeichen *)
03G 0139A

11a. Seitenzahl Bericht
154

11b. Seitenzahl Publikation

13. Fördernde Institution (Name, Adresse)

Bundesministerium für Bildung
und Forschung (BMBF)

53170 Bonn

12. Literaturangaben
31

14. Tabellen
12

15. Abbildungen
49

16. Zusätzliche Angaben
Fahrtbericht SO139 GINCO3 mit FS SONNE (29. Januar - 04.März 1999)

17. Vorgelegt bei (Titel, Ort, Datum)
Forschungszentrum Jülich, BEO, Rostock-Warnemünde

18. Kurzfassung
Auf der Forschungsfahrt SO-139 GINCO 3 wurde der Akkretions-Komplex am Sunda-Bogen vor Süd-Sumatra und West-Java geologisch, geochemisch, geothermisch und biologisch untersucht (ca. 3000 km Vermessung mit Fächerecholot und Sedimentecholot; 101 Meß- und Probenahmestationen). Nach geologischen Befunden besteht der Akkretionskeil (AK) aus z.T. geklüfteten und tektonisierten Tonsteinen. In der jüngsten Schuppe wurden auch siltige glimmerhaltige Tonsteine und Schlämme angetroffen. Die dünne Abdeckung des AK besteht in ihrem jüngsten Teil aus Plio-/Pleistozän- bis Rezentsedimenten mit vulkanischen Aschen- und Turbiditlagen. Sie bilden auch im Forearc-Becken (FAB) die jüngsten Sedimente. Der Wärmefluß am AK vor Sumatra und Java liegt zwischen 35 - 64 mW/m^2. Im Bengkulu- (FAB) Becken liegt er zwischen 22 und 45 mW/m^2 und im Süd-Java- (FAB) Becken zwischen 30 und 153 mW/m^2. In der Verlängerung des Semangka-Grabens wurden 83 - 104 mW/m^2 gemessen. An der N-Schulter des Grabens wurde kontinentales Grundgebirge gedredscht (miozäne Tonsteine, Grünstein, Diabas Andesit, Quarzit). Im Graben wurde Vestimentifera sp., ein Anzeiger für "Methan-Venting" gefunden. An einer Transversalstörung im FAB, die mit einer großen Antiklinalstruktur verbunden ist, wurden vor West-Java weitere "Vent"-Faunen gefunden (Acharax sp., Pogonophoren). Sie sind mit Methan-Anomalien in den bodennahen Sedimenten, Karbonatabscheidungen und Methan-Anomalien in der Wassersäule verbunden. Im "Vent"-Gebiet wurde auch der höchste Wärmestrom (153 mW/m^2) gemessen. Es ist das erste "Vent"-Feld in einem reinen FAB ohne vulkanische Tätigkeit überhaupt. Weitere Methan-Anomalien wurden an den südlichen Rändern des FAB, am Fuß des "Outer Arc High" gefunden. Sie deuten zusammen mit den Meeresboden simulierenden seismischen Reflektoren im FAB auf Methangas-Bildung in großer Tiefe und Fluidmigration zum Meeresboden hin.

19. Schlagwörter
Indonesien, Akkretionskomplex, 'forearc'-Basin, Methan, kalte Quellen, Vent-Fauna

20. Verlag	21. Preis

*) Auf das Förderkennzeichen des BMBF soll auch in der Veröffentlichung hingewiesen werden.